

Analysis of Smallish function in the  
regulation of actomyosin  
contractility during epithelial  
morphogenesis in *Drosophila  
melanogaster*

Inaugural-Dissertation

zur

Erlangung des Doktorgrades

der Mathematisch-Naturwissenschaftlichen Fakultät

der Universität zu Köln

vorgelegt von

Patrizia Kroll

aus Dormagen

Eingereicht: Oktober 2023

Veröffentlichung: November 2024

Berichtersteller:

Prof. Dr. Andreas Wodarz

Prof. Dr. Siegfried Roth

Tag der mündlichen Prüfung:

17.01.2024

## Table of content

|  |           |
|--|-----------|
| Table of content .....   | I         |
| List of figures .....  | IV        |
| List of supplementary figures .....  | VI        |
| List of tables .....   | VII       |
| List of supplementary tables .....   | VIII      |
| List of abbreviations .....  | IX        |
| Abstract .....   | XVI       |
| <b>1 Introduction.....</b>   | <b>1</b>  |
| 1.1 Establishment of cell polarity in epithelial cells during development.....             | 1         |
| 1.2 Planar cell polarity is established in multicellular tissues.....                      | 7         |
| 1.3 The actomyosin network is regulated by the Rho-associated protein kinase Rok.....      | 11        |
| 1.4 The tight control of actomyosin and AJs is critical for epithelial morphogenesis ..... | 14        |
| 1.5 Smallish regulates actomyosin contractility in epithelial cells .....                  | 19        |
| 1.6 Scope of this thesis .....   | 22        |
| <b>2 Material &amp; Methods.....</b>   | <b>23</b> |
| 2.1 Material.....  | 23        |
| 2.1.1 Fly stocks.....  | 23        |
| 2.1.2 Primary antibodies.....  | 25        |
| 2.1.3 Secondary antibodies.....  | 25        |
| 2.1.4 Other conjugates .....   | 25        |
| 2.1.5 Bacterial strains .....  | 26        |
| 2.1.6 Cell Culture.....  | 26        |
| 2.1.7 Plasmids .....   | 26        |
| 2.1.8 Oligonucleotides .....   | 28        |
| 2.1.9 Kits .....   | 29        |
| 2.1.10 Imaging systems .....   | 30        |
| 2.1.11 Technical devices .....   | 30        |
| 2.1.12 Software.....   | 30        |
| 2.2 Methods.....   | 31        |
| 2.2.1 Fly work.....  | 31        |
| 2.2.1.1 Fly breeding .....   | 31        |
| 2.2.1.2 Fly Food Standard medium (Ashburner 1989) .....                                    | 31        |
| 2.2.1.3 Apple agar plates.....   | 31        |
| 2.2.1.4 Gal4-UAS System .....  | 31        |
| 2.2.1.5 Fly crossing .....   | 32        |
| 2.2.1.6 Injection.....   | 33        |

|         |   |    |
|---------|---|----|
| 2.2.1.7 | Live imaging of embryos.....  | 33 |
| 2.2.2   | Molecular biology .....   | 34 |
| 2.2.3   | Biochemical methods.....  | 37 |
| 2.2.3.1 | Sample preparation for mass spectrometry (MS) .....   | 37 |
| 2.2.3.2 | Protein extraction from embryos.....  | 37 |
| 2.2.3.3 | Protein extraction from S2 cells .....  | 38 |
| 2.2.3.4 | Determination of protein concentration.....   | 38 |
| 2.2.3.5 | Immunoprecipitation.....  | 38 |
| 2.2.3.6 | SDS-PAGE.....   | 38 |
| 2.2.3.7 | Western blot.....   | 39 |
| 2.2.3.8 | Purification of GST-tagged proteins .....   | 40 |
| 2.2.3.9 | Kinase assay.....   | 41 |
| 2.2.4   | Cell culture.....   | 41 |
| 2.2.4.1 | Cultivation of S2 cells.....  | 41 |
| 2.2.4.2 | Cell transfection.....  | 41 |
| 2.2.5   | Histology .....   | 42 |
| 2.2.5.1 | Formaldehyde (FA) fixation of embryos.....  | 42 |
| 2.2.5.2 | Paraformaldehyde (PFA) fixation of embryos .....  | 42 |
| 2.2.5.3 | Immunofluorescence (IF) staining of embryos.....  | 42 |
| 2.2.5.4 | Diaminobenzidine tetrahydrochloride (DAB) staining of embryos .....   | 43 |
| 2.2.5.5 | Fixation and immunofluorescence staining of ovaries and imaginal discs .....                                    | 43 |
| 2.2.6   | Mass spectrometry data analysis .....   | 44 |
| 3       | Results .....   | 45 |
| 3.1     | <i>smash</i> <sup>Δ35m/z</sup> null allele mutant embryos show early morphogenetic defects.....                 | 45 |
| 3.2     | The phosphorylation of Sqh is strongly reduced upon loss of Smash .....   | 47 |
| 3.3     | Smash does not affect the phosphorylation of Sqh <i>in vitro</i> .....  | 48 |
| 3.4     | The subcellular localization of Smash is dependent on Rok.....  | 49 |
| 3.5     | Investigation of Smash sfGFP knock-in lines.....  | 51 |
| 3.6     | sfGFP:SmashPM resembles the localization pattern of endogenous SmashPM .....                                    | 52 |
| 3.7     | sfGFP:SmashPI is specifically expressed in posterior follicle cells in ovaries.....                             | 57 |
| 3.8     | <i>smash</i> <sup>Δ35m/z</sup> and sfGFP:SmashPI <sup>m/z</sup> embryos show impaired germ band elongation..... | 62 |
| 3.9     | SmashPM N-term has a reduced ability to promote F-actin enrichment.....   | 65 |
| 3.10    | Overexpression of SmashPM and SmashPM N-term induces cell shape changes .....                                   | 73 |
| 3.11    | Identification of novel Smash interaction partners by biotin proximity labeling .....                           | 76 |
| 3.12    | Smash interacts with Ajuba .....  | 84 |
| 3.13    | Smash co-localizes with Lasp in ovaries and embryonic epithelium .....  | 87 |
| 4       | Discussion .....  | 89 |
| 4.1     | Course and objective of the discussion .....  | 89 |
| 4.2     | Description of the <i>smash</i> <sup>Δ35m/z</sup> embryonic phenotype.....                                      | 89 |

---

|     |  |     |
|-----|--|-----|
| 4.3 | A CRISPR/Cas9 approach reveals new insight into Smash function .....               | 93  |
| 4.4 | TurboID proximity labeling assay identifies novel Smash interaction partners ..... | 101 |
| 4.5 | Conclusion.....  | 111 |
|     | References.....  | 113 |
|     | Supplementary material.....  | 127 |
|     | Acknowledgements .....   | 155 |
|     | Erklärung zur Dissertation .....   | 156 |

## List of figures

|   |    |
|---|----|
| Figure 1: Comparison of <i>Drosophila</i> and vertebrate epithelial cells.....  | 2  |
| Figure 2: Organization of the ZA in epithelial cells in vertebrates. ....   | 3  |
| Figure 3: Cellularization during <i>Drosophila</i> embryogenesis.....   | 4  |
| Figure 4: Establishment of apicobasal polarity in <i>Drosophila</i> epithelial cells. ....  | 6  |
| Figure 5: Core PCP and Fat-Dachsous pathway in <i>Drosophila</i> . ....   | 9  |
| Figure 6: Canonical and non-canonical Wnt signaling pathway in vertebrates. ....  | 10 |
| Figure 7: Rok activates Myosin II and drives actomyosin filament assembly. ....   | 12 |
| Figure 8: The Fog signaling pathway regulates Rok kinase activity.....  | 13 |
| Figure 9: Apical constriction leads to a reduction of the apical cell perimeter, which is important for gastrulation. ....                            | 15 |
| Figure 10: Cell intercalation causes local cell rearrangements.....   | 16 |
| Figure 11: Proteins are localized in a planar polarized fashion during germ band elongation in <i>Drosophila</i> embryos. ....                        | 18 |
| Figure 12: Protein structure of SmashPM and SmashPI.....  | 19 |
| Figure 13: Scanning electron microscopy of wild-type (WT) and <i>smash</i> <sup>Δ35m/z</sup> embryos at stage 13.....                                 | 20 |
| Figure 14: Cloning procedure for the pU6-chiRNA vector. ....  | 35 |
| Figure 15: Phenotypic analysis of <i>smash</i> <sup>Δ35m/z</sup> mutant embryos. ....   | 46 |
| Figure 16: Phosphomyosin signal is reduced in <i>smash</i> <sup>Δ35m/z</sup> mutant embryos compared to WT.....                                       | 47 |
| Figure 17: Smash does not affect the phosphorylation of Sqh in vitro.....   | 48 |
| Figure 18: Smash planar polarized localization is affected in <i>Rok</i> <sup>2</sup> embryos. ....   | 50 |
| Figure 19: CRISPR/Cas9 strategy to generate sfGFP knock-in lines targeting the <i>smash</i> locus. ....   | 51 |
| Figure 20: Endogenous SmashPM expression in WT ovaries.....   | 53 |
| Figure 21: sfGFP:SmashPM expression in ovaries.....   | 54 |
| Figure 22: Close-up of egg chambers showing endogenous SmashPM and sfGFP:SmashPM localization pattern. ....   | 55 |
| Figure 23: sfGFP:SmashPM expression in embryos. ....  | 56 |
| Figure 24: sfGFP:SmashPI expression in ovaries. ....  | 58 |
| Figure 25: An aberrant signal was detected in sfGFP:SmashPI <sup>m/z</sup> embryos when the antibody against the N-terminus of SmashPM was used. .... | 59 |
| Figure 26: Detection of sfGFP fusion proteins in embryos and ovaries.....   | 60 |
| Figure 27: Phenotypic analysis of sfGFP:SmashPI <sup>m/z</sup> embryos. ....  | 61 |
| Figure 28: Relative germ band elongation in WT, <i>smash</i> <sup>Δ35m/z</sup> , and sfGFP:SmashPI <sup>m/z</sup> embryos. ....                       | 62 |
| Figure 29: Live imaging of WT, <i>smash</i> <sup>Δ35m/z</sup> , and sfGFP:SmashPI <sup>m/z</sup> embryos. ....  | 63 |
| Figure 30: Relative germ band elongation speed in WT, <i>smash</i> <sup>Δ35m/z</sup> , and sfGFP:SmashPI <sup>m/z</sup> embryos.....                  | 64 |

---

|  |     |
|--|-----|
| Figure 31: Overexpression of mCD8:eGFP, eGFP:SmashPM, eGFP:SmashPM N-term, and eGFP:SmashPM mut in the follicle epithelium.....                              | 66  |
| Figure 32: GFP membrane/cytosol ratio in follicle cells.....   | 68  |
| Figure 33: Phalloidin intensity at the apical cell cortex of follicle cells.....   | 69  |
| Figure 34: Correlation between apical GFP and phalloidin signal in follicle cells.....   | 70  |
| Figure 35: Abnormal morphology in eGFP:SmashPM overexpressing ovaries.....   | 71  |
| Figure 36: Determination of embryo length and width.....   | 72  |
| Figure 37: Stochastic overexpression of SmashPM variants in the follicle epithelium.....   | 74  |
| Figure 38: Apical cell area in follicle epithelium upon stochastic overexpression of mCD8:eGFP, eGFP:SmashPM, eGFP:SmashPM N-term, and eGFP:SmashPM mut..... | 75  |
| Figure 39: Workflow of the biotin proximity labeling assay.....  | 76  |
| Figure 40: Expression of TurboID fusion proteins in S2 cells.....  | 77  |
| Figure 41: Efficient biotinylation occurs in S2 cells expressing TurboID fusion proteins.....  | 78  |
| Figure 42: Subcellular localization of fusion proteins in the embryonic epithelium.....  | 78  |
| Figure 43: TurboID efficiently biotinylates proteins in embryos.....   | 80  |
| Figure 44: Proteomic analysis identifies novel, potential Smash-interacting proteins.....  | 81  |
| Figure 45: Myc:Ajuba co-immunoprecipitated with GFP:SmashPM.....   | 84  |
| Figure 46: Nonspecific dots appeared in <i>Jub</i> <sup>54</sup> germline clones when the antibody against the N-terminus of Smash was used.....             | 85  |
| Figure 47: The planar polarity of Smash is unaffected in <i>Jub</i> germline clones compared to WT.....  | 86  |
| Figure 48: sfGFP:SmashPM partially co-localizes with Lasp in ovaries.....  | 87  |
| Figure 49: SmashPM co-localizes with GFP:Lasp in embryonic epithelium.....   | 88  |
| Figure 50: The molecular working mechanism of Smash – Model No. 1.....   | 92  |
| Figure 51: The molecular working mechanism of Smash – Model No. 2.....   | 95  |
| Figure 52: Graphical summary of overexpression experiments in the follicle epithelium.....   | 99  |
| Figure 53: The molecular working mechanism of Smash – Final Model.....   | 110 |

## List of supplementary figures

|  |     |
|--|-----|
| Figure S 1: A weak Smash signal was detected in <i>smash</i> <sup>Δ35</sup> maternal mutant embryos. ....                                      | 128 |
| Figure S 2: Detection of GFP fusion proteins used for the in vitro kinase assay.....   | 129 |
| Figure S 3: Expression pattern of endogenous SmashPM, sfGFP:SmashPM, and sfGFP:SmashPI in wing disc.....                                       | 130 |
| Figure S 4: sfGFP:SmashPI <sup>m/z</sup> is not expressed in embryos.....  | 130 |
| Figure S 5: Comparison of WT and sfGFP:SmashPI ovarian morphology.....   | 131 |
| Figure S 6: Mean GBE in WT, <i>smash</i> <sup>Δ35m/z</sup> , and sfGFP:SmashPI <sup>m/z</sup> embryos.....                                     | 131 |
| Figure S 7: Direct comparison of mean GBE in WT, <i>smash</i> <sup>Δ35m/z</sup> , and sfGFP:SmashPI <sup>m/z</sup> embryos.....                | 132 |
| Figure S 8: Mean GBE speed in WT, <i>smash</i> <sup>Δ35m/z</sup> , and sfGFP:SmashPI <sup>m/z</sup> embryos.....                               | 135 |
| Figure S 9: Direct comparison of mean GBE speed in WT, <i>smash</i> <sup>Δ35m/z</sup> , and sfGFP:SmashPI <sup>m/z</sup> embryos.<br>.....     | 135 |
| Figure S 10: Close-up of phalloidin signal in ovaries overexpressing mCD8:eGFP, eGFP:SmashPM, eGFP:SmashPM N-term, and eGFP:SmashPM mut.....   | 138 |
| Figure S 11: GFP intensity at the apical cell cortex of follicle cells.....  | 139 |
| Figure S 12: GFP intensity in the cytosol of follicle cells. ....  | 140 |
| Figure S 13: Comparison of GFP intensities at the apical cell cortex with GFP intensities in the cytosol of follicle cells. ....               | 141 |
| Figure S 14: Phalloidin intensity in the cytosol of follicle cells.....  | 142 |
| Figure S 15: Comparison of phalloidin intensities at the apical cell cortex with phalloidin intensities in the cytosol of follicle cells. .... | 143 |
| Figure S 16: GO term analysis sorted by molecular function. ....   | 146 |
| Figure S 17: GO term analysis sorted by biological process.....  | 148 |
| Figure S 18: GFP:Smash and Myc:Ajuba co-localize in S2 cells. ....   | 150 |
| Figure S 19: Plasmid map of pUASP-attB-eGFP-rfA_TurboID.....   | 151 |
| Figure S 20: Plasmid map of pUASP-attB-eGFP-rfA_TurboID:SmashPM.....   | 151 |
| Figure S 21: Plasmid map of pUASP-attB-eGFP-rfA_SmashPM.....   | 152 |
| Figure S 22: Plasmid map of pUAST-attB-eGFP-rfA_SmashPM.....   | 152 |
| Figure S 23: Plasmid map of pUAST-attB-eGFP-rfA_SmashPM N-term. ....   | 153 |
| Figure S 24: Plasmid map of pUAST-attB-eGFP-rfA_SmashPM mut. ....  | 153 |
| Figure S 25: Plasmid map of pBluescript_sgRNA3_sfGFP. ....   | 154 |
| Figure S 26: Plasmid map of pScareless-sfGFP-dsRed_HA_sgRNA7.....  | 154 |

---

## List of tables

|  |    |
|--|----|
| Table 1: List of fly stocks.....   | 23 |
| Table 2: List of primary antibodies.....   | 25 |
| Table 3: List of secondary antibodies.....   | 25 |
| Table 4: List of other conjugates.....   | 25 |
| Table 5: List of plasmids.....   | 26 |
| Table 6: List of oligonucleotides.....   | 28 |
| Table 7: Summary mean GBE in WT, <i>smash</i> <sup><math>\Delta 35^{m/z}</math></sup> , and sfGFP:SmashPI <sup><math>m/z</math></sup> embryos..... | 63 |
| Table 8: New Smash-interacting proteins identified by biotin proximity labeling.....   | 82 |

## List of supplementary tables

|   |     |
|---|-----|
| Table S 1: Statistical test to determine the significance of the differences between WT, <i>smash</i> <sup>Δ35m/z</sup> , and sfGFP:SmashPI <sup>m/z</sup> relative GBE.....  | 132 |
| Table S 2: Statistical test to determine the significance of the differences between WT, <i>smash</i> <sup>Δ35m/z</sup> , and sfGFP:SmashPI <sup>m/z</sup> GBE speed.....   | 136 |
| Table S 3: Statistical test to determine the significance of the differences in GFP intensity at the apical cortex of follicle cells between mCD8:eGFP, eGFP:SmashPM, eGFP:SmashPM N-term, and eGFP:SmashPM mut overexpressing ovaries..... | 139 |
| Table S 4: Statistical test to determine the significance of the differences in GFP intensity in the cytosol of follicle cells between mCD8:eGFP, eGFP:SmashPM, eGFP:SmashPM N-term, and eGFP:SmashPM mut overexpressing ovaries.....       | 140 |
| Table S 5: Statistical test to determine the significance of the differences in GFP membrane/cytosol ratio mCD8:eGFP, eGFP:SmashPM, eGFP:SmashPM N-term, and eGFP:SmashPM mut overexpressing ovaries.....                                   | 141 |
| Table S 6: Statistical test to determine the significance of the differences in apical phalloidin intensity between mCD8:eGFP, eGFP:SmashPM, eGFP:SmashPM N-term, and eGFP:SmashPM mut overexpressing ovaries.....                          | 142 |
| Table S 7: Statistical test to determine the significance of the differences in cytosolic phalloidin intensity between mCD8:eGFP, eGFP:SmashPM, eGFP:SmashPM N-term, and eGFP:SmashPM mut overexpressing ovaries.....                       | 143 |
| Table S 8: Statistical test to determine the significance of the differences in cell area between mCD8:eGFP, eGFP:SmashPM, eGFP:SmashPM N-term, and eGFP:SmashPM mut overexpressing ovaries.....  | 144 |
| Table S 9: List of input genes for GO term analysis.....  | 145 |
| Table S 10: Go term molecular function TurboID:eGFP – eGFP:TurboID:SmashPM.....   | 147 |
| Table S 11: Go term molecular function eGFP:SmashPM – eGFP:TurboID:SmashPM.....   | 147 |
| Table S 12: Go term biological process TurboID:eGFP – eGFP:TurboID:SmashPM.....   | 149 |
| Table S 13: Go term biological process eGFP:SmashPM – eGFP:TurboID:SmashPM.....   | 149 |

## List of abbreviations

### Proteins

|              |  |
|--------------|--|
| Ack          | Activated Cdc42 kinase                             |
| Antp         | Antennapedia                                       |
| aPKC         | Atypical protein kinase C                          |
| Arm          | Armadillo  |
| Baz          | Bazooka  |
| Cdc42        | Cell division cycle 42                             |
| CK1          | Casein kinase-1                                    |
| Cno          | Canoe  |
| Crb          | Crumbs   |
| Cta          | Concertina   |
| DECad        | <i>Drosophila</i> E-Cadherin                       |
| Dgn          | Diego  |
| Dlg          | Discs large  |
| Ds           | Dachsous   |
| Dsh/DVL      | Dishevelled  |
| Ex           | Expanded   |
| Fj           | Four-jointed kinase                                |
| Fmi          | Flamingo   |
| Fog          | Folded gastrulation                                |
| Ft           | Fat  |
| Fz           | Frizzled   |
| GSK3 $\beta$ | Glycogen synthase kinase 3 beta                    |
| Jub          | Ajuba  |
| Lgl          | Lethal giant larvae                                |
| LMO7         | Lim domain only 7                                  |
| LRP5/6       | Lipoprotein receptor-related protein 5/6           |
| Moe          | Moesin   |
| Nos          | Nanos  |
| Nup54        | Nucleoporin 54                                     |
| Par6 /Par1   | Partitioning defective 6/ Partitioning defective 1 |

|        |  |
|--------|--|
| PATJ   | Pals1-associated tight junction protein              |
| Pk     | Prickle  |
| Pnut   | Peanut   |
| RhoGEF | Rho Guanine nucleotide exchange factor               |
| Rok    | Rho-associated coiled-coil containing protein kinase |
| Scra   | Scraps   |
| Scrib  | Scribble   |
| Shi    | Shibire  |
| Shrm   | Shroom   |
| Smash  | Smallish   |
| Sqh    | Spaghetti squash                                     |
| Std    | Stardust   |
| Tud    | Tudor  |
| Vang   | Van Gogh   |
| Vas    | Vasa   |
| Wnt    | acronym combining Wingless (Wg)/Integrated (Int)     |
| Yrt    | Yurt   |
| Zip    | Zipper   |

**Protein domains**

|      |  |
|------|--|
| ABD  | Actin binding domain                                   |
| CH   | Calponin homology                                      |
| CRIB | Cdc42/Rac interactive binding domain                   |
| FBM  | FERM domain binding motif                              |
| FERM | 4.1 protein, Ezrin, Radixin, Moesin                    |
| LIM  | Lin-11, Isl-1, Mec-3                                   |
| PBM  | PDZ binding motif                                      |
| PDZ  | Postsynaptic density 95/Discs large/Zonula occludens 1 |
| PH   | Pleckstrin homology                                    |
| SAM  | Sterile $\alpha$ -motif                                |
| SH3  | Src homology 3   |
| SR   | Spectrin repeat  |

---

**Chemicals**

|                               |  |
|-------------------------------|--|
| BSA                           | Bovine serum albumin                       |
| CAA                           | Chloroacetamide                            |
| DAB                           | Diaminobenzidine tetrahydrochloride        |
| DTT                           | Dithiothreitol                             |
| EDTA                          | Ethylene diamine tetraacetic acid          |
| EGTA                          | Ethylene glycol tetraacetic acid           |
| EtOH                          | Ethanol                                    |
| FA                            | Formic acid / Formaldehyde                 |
| FBS                           | Fetal bovine serum                         |
| H <sub>2</sub> O <sub>2</sub> | Hydrogen peroxide                          |
| IPTG                          | Isopropyl- $\beta$ -D-thiogalactopyranosid |
| MeOH                          | Methanol                                   |
| NaCl                          | Sodium chloride                            |
| NHS                           | Normal horse serum                         |
| NP-40                         | Nonidet P-40                               |
| PAGE                          | Polyacrylamide gel electrophoresis         |
| PFA                           | Paraformaldehyde                           |
| SDS                           | Sodium dodecyl sulfate                     |
| Tris HCl                      | Tris-Hydrochloride                         |

**Units**

|     |                       |
|-----|-----------------------|
| °C  | Degree Celsius        |
| µg  | Microgramm            |
| µl  | Microliter            |
| µm  | Micromolar            |
| G   | G force               |
| g   | Gramm                 |
| h   | Hour                  |
| kDa | Kilo Dalton           |
| l   | Liter                 |
| m   | Molar                 |
| ml  | Milliliter            |
| mM  | Millimolar            |
| ng  | Nanogram              |
| pH  | Potential of hydrogen |
| Rpm | Round per minute      |
| s   | Second                |
| V   | Volt                  |

**General terminology**

|          |                                   |
|----------|-----------------------------------|
| A/P      | Anterior/posterior                |
| aa       | Amino acid                        |
| AF       | Alexa Fluor®                      |
| AJ       | Adherens junction                 |
| ALM      | Apicolateral margin               |
| ATP      | Adenosin triphosphate             |
| BJ       | Basal adherens junction           |
| bp       | base pairs                        |
| Chr      | Chromosome                        |
| CLD      | Compact letter code               |
| C-term   | C-terminus                        |
| D/V      | Dorsal/ventral                    |
| DGC      | Dystrophin glycoprotein complex   |
| e. g.    | exempli gratia                    |
| EGFR     | Epidermal growth factor receptor  |
| ELC      | Essential light chain             |
| ERM      | Ezrin/Radixin/Moesin              |
| ETM      | Epithelial-mesenchymal transition |
| FC       | Furrow canal                      |
| Figure S | Supplementary figure              |
| FLP      | Flippase                          |
| FRT      | Flippase recognition target       |
| G4       | GAL4                              |
| GBE      | Germ band elongation              |
| GFP      | Green Fluorescent Protein         |
| GO       | Gene Ontology                     |
| GPCR     | G-protein coupled receptor        |
| GST      | Glutathione S-transferase         |
| GTP      | Guanosine triphosphate            |
| HA       | Haemagglutinin                    |
| hs       | Heat shock                        |

---

|        |  |
|--------|--|
| Hu     | Humeral                                    |
| IF     | Immunofluorescence                         |
| IN     | Input                                      |
| IP     | Immunoprecipitation                        |
| m/z    | maternal/zygotic                           |
| mat    | maternal                                   |
| MS     | Mass spectrometry                          |
| NES    | Nuclear export sequence                    |
| NMIIHC | Non-muscle myosin II heavy chain           |
| NPC    | Nuclear pore complex                       |
| nt     | nucleotide                                 |
| N-term | N-terminus                                 |
| PCP    | Planar cell polarity                       |
| RLC    | regulatory light chain                     |
| SAJ    | spot adherens junction                     |
| SAR    | subapical region                           |
| Ser    | Serin                                      |
| sgRNA  | single guide ribonucleic acid              |
| SJ     | Septate junction                           |
| SNP    | single nucleotide polymorphism             |
| Tb     | Tubby                                      |
| Thr    | Threonine                                  |
| TJ     | Tight junction                             |
| tj     | traffic jam                                |
| UAS    | upstream activation sequence               |
| WT     | Wild-type                                  |
| X-EDMD | X-linked Emery–Dreifuss muscular dystrophy |
| ZA     | Zonula adherens                            |
| ♀      | virgin female                              |
| ♂      | male                                       |

## Abstract

The cortical actomyosin cytoskeleton generates the mechanical force driving highly dynamic processes occurring during epithelial morphogenesis, such as cell shape changes during cell division, cell intercalation, and the formation of furrows and tubes. The LIM domain protein Smash (Smash) was shown to modify actomyosin contractility during morphogenesis since *smash*<sup>A35m/z</sup> null mutants show reduced membrane tension, whereas overexpression of Smash leads to apical constriction in the follicle epithelium. Many *smash*<sup>A35m/z</sup> null mutant embryos show strong epithelial morphogenetic defects, likely due to misregulation of the actomyosin cytoskeleton. Although we have several lines of evidence demonstrating that Smash is functioning in a large protein interaction network to control membrane tension via the actomyosin cytoskeleton, the precise mechanism of how Smash functions remains to be elucidated.

This study provides new insight into the molecular working mechanism of Smash. We showed that Smash is required for efficient phosphorylation of the non-muscle myosin II regulatory light chain encoded by *spaghetti squash (sqh)*. The effect of Smash on Sqh phosphorylation appeared to be indirect because Smash did not influence Rok kinase activity *in vitro*. Instead, a novel dominant negative allele of *smash* provides evidence that Smash might be involved in regulating signaling upstream of Rok. In addition, we demonstrated that the myosin binding domain of Smash is crucial to induce actomyosin contractility. We suggest that the myosin binding domain of Smash is necessary to provide scaffolding function for Rok and Myosin II, thereby enabling Sqh phosphorylation, which in turn activates actomyosin contraction driving cell shape changes.

A detailed investigation of the *smash* null and dominant negative allele demonstrated the importance of Smash in regulating the actomyosin cytoskeleton during epithelial morphogenesis, especially during germ band elongation. The generation of CRISPR/Cas9 GFP knock-in lines expands our molecular toolkit to study the spatiotemporal behavior of Smash during morphogenesis, since the sfGFP knock-in line of Smash<sup>PM</sup> faithfully reflected the expression pattern and subcellular localization of Smash as described using an N-terminal  $\alpha$ -Smash antibody. Moreover, the novel sfGFP knock-in lines revealed isoform-specific expression of Smash<sup>PI</sup> in posterior follicle cells during late oogenesis.

Our phenotypic data were supported by the results obtained by a biotin proximity labeling assay, which was used to identify novel Smash-interacting proteins. This assay identified several promising actomyosin-associated proteins as potential Smash interaction partners. Among those were some with a reported function in embryonic morphogenesis and some others uncover a potential involvement of Smash in establishing oocyte polarity, ovulation, muscle development, cytokinesis, or regulating gene expression. A detailed analysis of these proteins and their interaction with Smash during morphogenesis and the other processes is likely to reveal important new insight into the mechanisms of actomyosin regulation.

# 1 Introduction

## 1.1 Establishment of cell polarity in epithelial cells during development

During the embryonic development of multicellular organisms, epithelia are among the first tissues that are formed. Epithelia provide physiological and mechanical barrier functions and are important for tissue and organ formation (Rodriguez-Boulán & Macara, 2014). To enable the proper formation of tissues and organs, epithelial cells possess several unique properties. First, epithelial cells are highly proliferative. They can orientate their mitotic spindle to divide either parallel or perpendicular to the sheet (Ragkousi & Gibson, 2014). Second, epithelial cells can modify their migratory behavior through a process called epithelial-mesenchymal transition (EMT). Thereby, epithelia can adopt a mesenchymal phenotype, allowing them to ingress into a defined region of the embryo. This process is reversible (mesenchymal-epithelial transition, MET). Thus, epithelial cells can constantly switch between an epithelial and a mesenchymal phenotype (Kalluri & Weinberg, 2009; Lim & Thiery, 2012). Third, epithelial cells can change their shape. This is important when cells need to reduce their apical cell perimeter, e. g. during gastrulation or tubulogenesis (Sawyer et al., 2010). A fundamental requirement for all these properties is the establishment of cell polarity, which is defined by the asymmetric distribution of different cellular components, such as organelles, proteins, or lipids, within a cell (Rodriguez-Boulán & Macara, 2014).

Epithelia are highly polarized structures that form apical and basolateral membrane domains, thereby introducing an apicobasal polarity gradient (Rodriguez-Boulán & Macara, 2014). Depending on the type of epithelium, the apical membrane domain, which is facing the environment or the lumen, can fulfill different functions, such as selective absorption, secretion, or sensory transduction. Apical protrusions are often formed to facilitate these functions. The lateral membrane domain faces neighboring cells and is required for intercellular adhesion, communication, and barrier function. These functions are provided by different junctional protein complexes, such as adherens junctions (AJs), desmosomes, gap junctions, or tight junctions (TJs). The basal membrane domain is important for anchoring the epithelium to the underlying tissues (Rehfeld et al., 2017). According to their function, the lipid and protein composition of the respective membrane domains differs (Giepmans & van Ijzendoorn, 2009). The difference in membrane composition is maintained by selective synthesis, targeting, and stabilization. Selective synthesis ensures that membrane components are predominantly synthesized in a defined area of the cell surface. Through targeted vesicle transport along polarized microtubules, newly synthesized membrane components are delivered to their target membrane domain and internalized membrane components are selectively stabilized at defined membrane areas (Giepmans & van Ijzendoorn, 2009; Matter, 2000).

Over the past decades, *Drosophila melanogaster* epithelial morphogenesis has been extensively studied to investigate the mechanisms establishing and regulating cell polarity. In *Drosophila*, the apical membrane domain contains the subapical region (SAR), which functions as a diffusion barrier within the membrane to segregate apical and basolateral membrane domain components. The basolateral domain comprises so-called septate junctions (SJs) that act as a trans-epithelial barrier. In vertebrates, the SAR and SJs are absent. Instead, apically localized TJs fulfill a comparable function. The apical and basolateral domains are separated by the zonula adherens (ZA), a belt-shaped structure consisting of adherens junctions (AJs) which are connected through actin fibers (Knust & Bossinger, 2002). The structure of *Drosophila* and vertebrate epithelial cells is depicted in Figure 1.

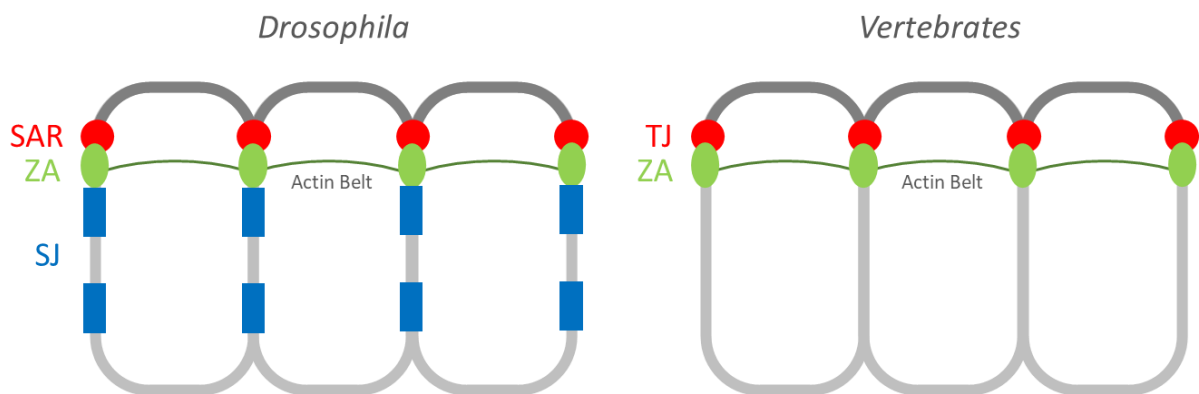


**Figure 1: Comparison of *Drosophila* and vertebrate epithelial cells.** The plasma membrane of *Drosophila* epithelial cells can be divided into an apical domain containing the subapical region (SAR) and a basolateral domain containing septate junctions (SJ). These two domains are separated by the zonula adherens (ZA). In contrast, tight junctions are incorporated into the apical domain of vertebrate epithelial cells. TJs are confined by the ZA (Knust & Bossinger, 2002).

AJs are multiprotein structures consisting of the transmembrane protein E-Cadherin (encoded by *shotgun* [*shg*] in *Drosophila*) that mediates intercellular adhesion by interacting with the extracellular domain of another E-Cadherin, which is anchored in the plasma membrane of neighboring cells. The cytoplasmic domain of E-Cadherin is linked to  $\beta$ -Catenin (encoded by *armadillo* [*arm*] in *Drosophila*) and further proteins such as  $\alpha$ -Catenin,  $\alpha$ -Actinin, Afadin (Canoe [*Cno*] in *Drosophila*), Spectrin, or Vinculin connect the E-Cadherin/ $\beta$ -Catenin complex with the cortical actin cytoskeleton (Figure 2) (Gates & Peifer, 2005). The cortical membrane-anchored actin cytoskeleton provides membrane stability on the one hand and mediates cell shape changes on the other. During shape changing events, AJs provide cell adhesion by connecting neighboring cells, thereby maintaining tissue integrity. Notably, the loss of ZA components leads not only to the loss of cell adhesion but also abolishes cell polarity, highlighting the importance of the ZA in polarity establishment (Bilder et al., 2003; Müller & Wieschaus, 1996).

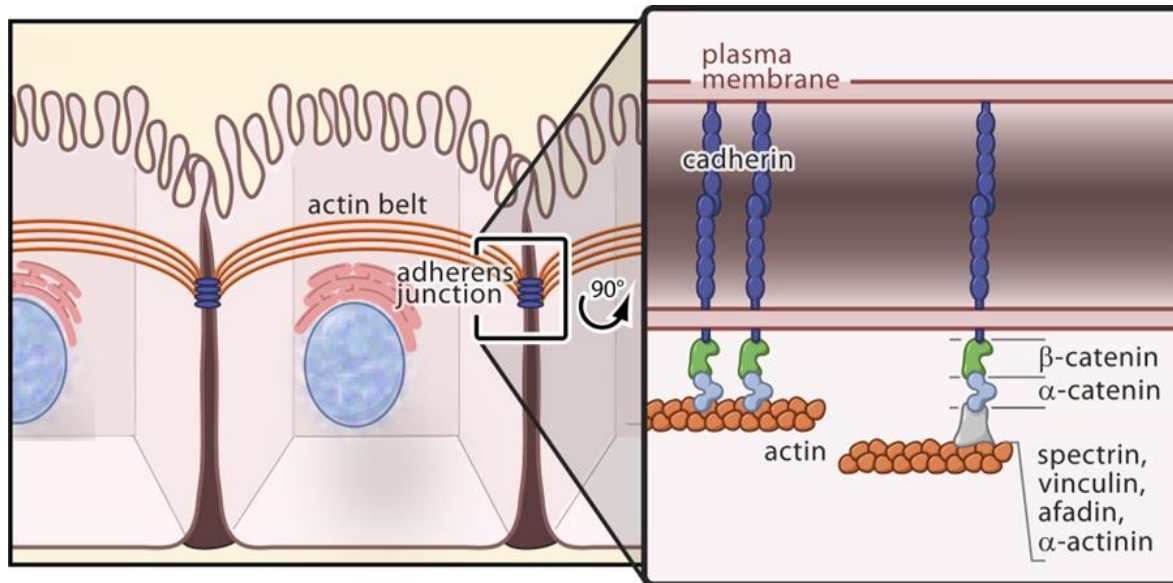


**Figure 2: Organization of the ZA in epithelial cells in vertebrates.** The ZA consists of AJs, which are connected by intracellular actin fibers spanning the whole apical cell cortex. AJs are multiprotein structures composed of the transmembrane protein E-Cadherin, which mediates adhesion between neighboring cells and the cytoplasmic linker protein  $\beta$ -Catenin.  $\beta$ -Catenin binds various scaffolding proteins such as  $\alpha$ -Catenin, Spectrin, Vinculin, Afadin, or  $\alpha$ -Actinin which mediate the interaction with F-actin. Each described vertebrate AJ protein has a homolog in *Drosophila* (Gates & Peifer, 2005).

Epithelial polarity is established very early during embryonic development. After fertilization of the egg, the *Drosophila* embryo undergoes 13 nuclear divisions, forming a syncytial blastoderm that contains around 6000 nuclei. These nuclei assemble as a monolayer beneath the egg membrane before the so-called cellularization process starts. Cellularization describes a process that generates the epithelial blastoderm by enclosing the nuclei with the plasma membrane. Cellularization is initiated by membrane invagination, which leads to the formation of the so-called furrow canal (FC). Along the FC, initial basal adherens junctions (BJs) are formed. As the FC further ingresses, spot adherens junctions (SAJs) are formed along the invaginating membrane. While the BJs resolve as cellularization is completed, the apical SAJs are assembled and will form the ZA later during gastrulation. At the end of cellularization, a contractile actomyosin ring localized at the furrow canal is responsible for completing the enclosure process (Müller & Bossinger, 2003; Schejter & Wieschaus, 1993). The complete process of cellularization is illustrated in Figure 3.

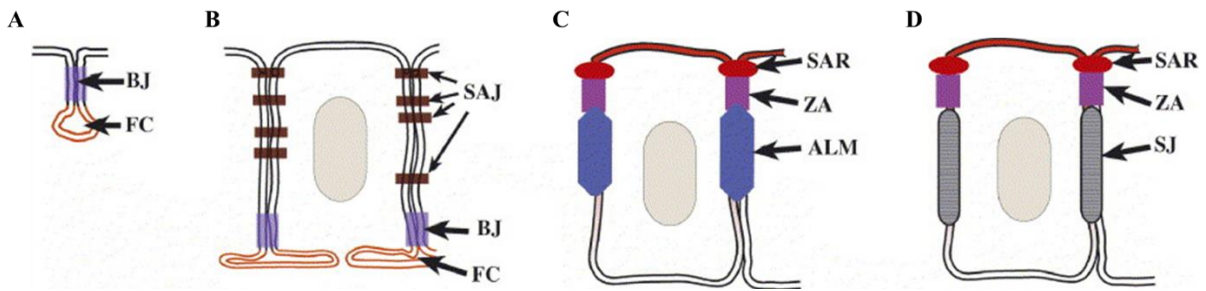


**Figure 3: Cellularization during *Drosophila* embryogenesis.** Cellularization starts in stage 5 embryos and transforms the syncytial blastoderm into a cellular blastoderm. (A) Cellularization is initiated by furrow canal (FC) formation to separate the single blastoderm nuclei. (B) FC formation is accompanied by the formation of basal adherens junctions (BJs). The FC ingresses further basally and eventually starts to widen laterally to enclose the nucleus. During FC ingression, spot adherens junctions (SAJs) are formed along apical and lateral membranes. (C) At the beginning of gastrulation, SAJs accumulate at the apical membrane, where they start the formation of AJs. BJs have dissolved. During gastrulation, the subapical region (SAR) and an apical margin of the lateral membrane (ALM) are established. During ZA maturation, SAR and ALM provide spatial cues for the proper positioning of the ZA. (D) After germ band retraction, ZA maturation is complete. The mature junctional complex consists of SAR, ZA, and SJs (Müller & Bossinger, 2003).

Already during cellularization, epithelial cells exhibit clear apicobasal polarization. The generation and maintenance of cell polarity are mainly dependent on three different key protein complexes: the Bazooka complex, the Crumbs complex, and the Scribble complex (Macara, 2004). The Bazooka complex is composed of the protein Bazooka (Baz, Par3 in vertebrates) that serves as a scaffold for the atypical protein kinase C (aPKC) and its activator partitioning defective 6 (Par6). The core components of the Crumbs complex comprise the transmembrane protein Crumbs (Crb) and the scaffolding protein Stardust (Std) which in turn mediates an interaction with Pals1-associated tight junction protein (PATJ) and Lin7. The Scribble complex contains the proteins Scribble (Scrib), Discs large (Dlg) and Lethal giant larvae (Lgl) (Bulgakova & Knust, 2009; Humbert et al., 2003; Lang & Munro, 2017). The Crumbs complex, aPKC, and Par6 localize to the SAR. In close proximity, Bazooka associates with the ZA. In contrast to that, the components of the Scribble complex are restricted to the basolateral membrane (Bilder et al., 2003; Harris & Peifer, 2005).

Bazooka is the major upstream signaling component in establishing cell polarity since Baz was shown to induce the correct assembly of the ZA (Harris & Peifer, 2004). The phosphorylation of Baz at Ser<sup>980</sup> by aPKC stabilizes the localization of Baz at the ZA (Krahn et al., 2010; Morais-de-Sa et al., 2010). In addition, Par-1 phosphorylates Baz at Ser<sup>151</sup> and Ser<sup>1085</sup> to exclude Baz from the lateral domain, thereby maintaining the accurate subcellular localization of Baz (Benton & St Johnston, 2003). Although Std belongs to the Crumbs complex, Baz interacts with Std via its Postsynaptic density 95/Discs large/Zonula occludens 1 (PDZ) domain, thereby recruiting Std to the apical domain. Baz competes with Crb in binding Std. Upon phosphorylation of Baz by aPKC at Ser<sup>980</sup>, Std is released from Baz and can interact with Crb at the apical domain (Bilder et al., 2003; Krahn et al., 2010).

Although Par-6 and aPKC belong to the Bazooka complex, both can dynamically interact with components of the Crumbs complex to maintain apical membrane identity. Thus, phosphorylation of Crb by aPKC is necessary for proper Crb subcellular localization (Sotillos et al., 2004). Moreover, the C-terminal PDZ binding motif (PBM) of Crb binds not only to Std but also to Par-6 (Kempkens et al., 2006). In addition to the PBM, the cytoplasmic tail of Crb contains a 4.1 protein, Ezrin, Radixin, Moesin (FERM) binding motif (FBM) that enables the interaction with different FERM domain-containing proteins such as Moesin, Yurt, or Expanded (Laprise et al., 2006; Robinson et al., 2010; Wei et al., 2015). These proteins function as linker between Crb and the cytoskeleton.

The Scribble complex controls the formation of a basolateral cell identity. While Scrib and Dlg are restricted to SJs, Lgl localizes along the whole lateral membrane domain (Yamanaka & Ohno, 2008). Although not all members of the Scribble complex share the same subcellular localization, their localization is mutually dependent on each other (Bilder et al., 2000). Moreover, Lgl phosphorylation by aPKC restricts Lgl to the lateral domain (Betschinger et al., 2003; Plant et al., 2003). In turn, Lgl is responsible for removing Crb from the basolateral domain and thereby antagonizes the Crumbs complex (Tanentzapf & Tepass, 2003). It was demonstrated that the Scribble complex is not only important to determine the basolateral but also the apical cell identity since in *scrib* mutants apical proteins such as Arm or Crb are mislocalized, resulting in disorganization of the epithelium (Bilder & Perrimon, 2000).

To sum up, the polarized distribution of the three major polarity complexes is regulated by the competitive behavior of the single components to define the apical and basolateral domains. Moreover, the presence of multiple protein interaction domains enables the recruitment of several additional proteins, making the polarity network highly dynamic (Bulgakova & Knust, 2009; Flores-Benitez & Knust, 2016). The complex interplay of the polarity regulators to determine apicobasal cell polarity in epithelia is illustrated in Figure 4.

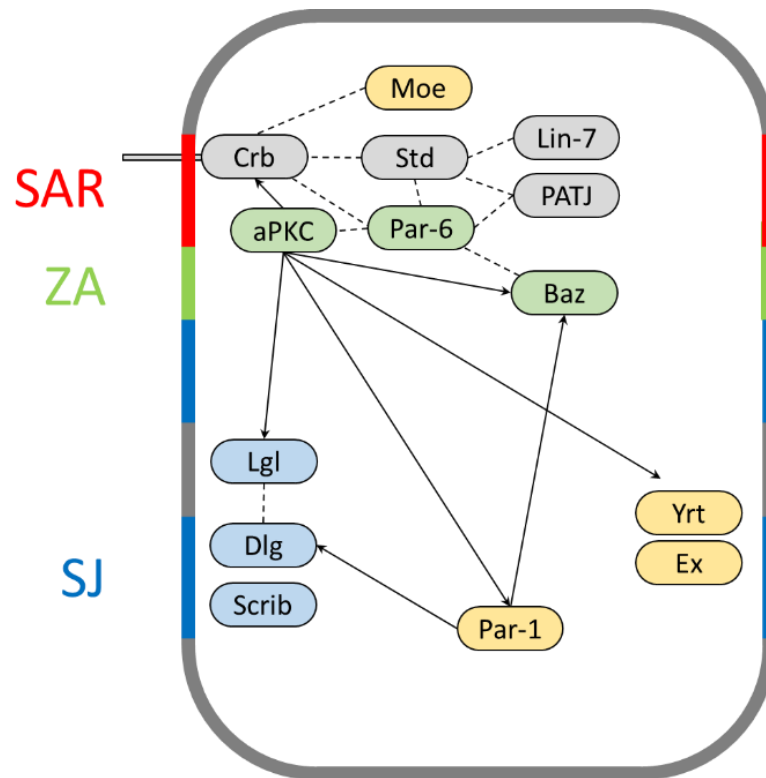


**Figure 4: Establishment of apicobasal polarity in *Drosophila* epithelial cells.** The main polarity regulators belonging to the Bazooka (green), Crumbs (grey), and Scribble (blue) complex are shown. Additional interacting proteins are marked in yellow. Proven interactions are depicted by dotted lines. Phosphorylation is indicated by arrows (modified from Flores-Benitez & Knust, 2016).

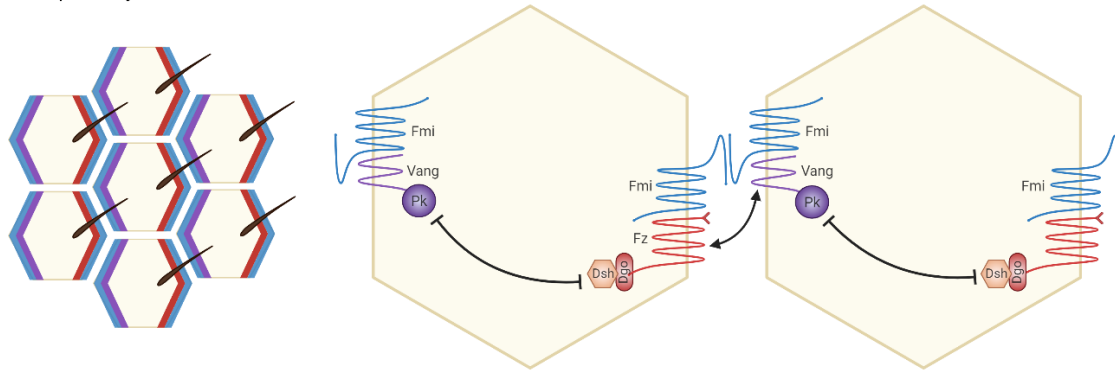
## 1.2 Planar cell polarity is established in multicellular tissues

Unlike apicobasal cell polarity, planar cell polarity (PCP) is established in a perpendicular axis within the plane of an epithelial sheet. PCP is necessary for propagating directional cues along the whole-body plane. In non-motile tissues, PCP is required for the proper formation of external structures in a correct orientation. PCP is also required in motile cell populations, e. g. during convergent extension, where PCP regulates cell rearrangements and cell shape changes via the actomyosin network (Butler & Wallingford, 2018; Torban & Sokol, 2021). In *Drosophila*, PCP was intensively studied, for instance in wings, where trichomes grow in a regular pattern, always pointing from the proximal to the distal end of the wing. In addition, other polarized structures, such as sensory bristles on the thorax or ommatidia in the eyes, were used as models to investigate PCP (Adler, 2002; Gubb & Garcia-Bellido, 1982; Held et al., 1986; Wong & Adler, 1993).

The intense research in *Drosophila* identified two major pathways that are required for the formation of polarized external structures. The first pathway is the Frizzled-dependent PCP pathway, also called the core PCP pathway. As the name suggests, one key component of this pathway is the seven-pass transmembrane receptor protein Frizzled (Fz) which is located at distal surfaces together with the cytoplasmic proteins Dishevelled (Dsh) and Diego (Dgo) (Axelrod, 2001; Feiguin et al., 2001; Strutt, 2001). At the proximal side of the cell, the four-pass transmembrane protein Van Gogh (Vang, also known as Strabismus [Stbm]) and the cytoplasmic protein Prickle (Pk) can be found (Bastock et al., 2003; Tree et al., 2002). Flamingo (Fmi, also known as Starry Night [Stan]), a seven-pass transmembrane cadherin-related protein, is located at proximal as well as distal surfaces, where it mediates homophilic adhesions to recruit Fz and Vang to AJs (Strutt, 2002; Usui et al., 1999). The transmembrane proteins in the core PCP pathway enable the intercellular exchange of polarity information, whereas the cytosolic components are important to amplify intracellular asymmetries and translate the polarity cues into external cell shape changes (Chen et al., 2008; Jenny et al., 2003; Strutt et al., 2011; Tree et al., 2002). Besides the positive feedback amplification through cytoplasmic proteins, negative feedback mechanisms (mutual antagonism of Pk and Dsh) promote the asymmetric enrichment of proteins at opposing cell membranes (Das et al., 2004; Jenny et al., 2005). In addition, the asymmetric protein distribution is maintained by endocytosis and directional protein transport (Butler & Wallingford, 2017). Studies in flies in which components of the core PCP pathway were mutated showed misorientation of the wing trichomes, suggesting that the Fz-dependent PCP pathway is propagating the polarity information from one cell to the other (Wong & Adler, 1993). The components of the core PCP pathway are highly conserved in vertebrates (Goodrich & Strutt, 2011; Jones & Chen, 2007). For example, mutations in the mouse Frizzled 6 homolog lead to similar hair patterning defects as observed in *Drosophila* (Guo et al., 2004).

The second pathway that is involved in the regulation of PCP is the so-called Fat-Dachsous pathway. This pathway comprises the atypical cadherins Fat (Ft) and Dachsous (Ds) as well as the Golgi resident kinase Four-jointed (Fj) (Fulford & McNeill, 2020). At the cellular level, Ft is enriched at proximal sides, where it co-localizes with Vang and Pk. On the opposing distal side, Ds co-localizes with Fz, Dsh, and Dgo. In addition, Ds binds to its downstream effector Dachs. On a tissue-wide level, Ft expression is equally distributed along the wing, while Fj and Ds are expressed in an opposing gradient. Thereby, Ds expression is high in proximal and low in distal parts of the wing, whereas Fj expression is high in distal and low in proximal parts of the wing. Simply reversing this gradient is enough to reverse the wing hair polarity (Matakatsu & Blair, 2004; Simon, 2004). Fj and Ds are proposed to act genetically upstream of the uniformly expressed protein Ft, generating a Ft activity gradient (Yang et al., 2002). Ft and Ds directly interact with each other, thereby forming intercellular adhesions (Matakatsu & Blair, 2004). This interaction is influenced by Fj activity. Phosphorylation of Ft by Fj promotes the Ft-Ds binding ability, while phosphorylation of Ds by Fj leads to a reduced binding ability between Ft and Ds (Brittle et al., 2010; Simon et al., 2010). Whether the core PCP and the Ft/Ds PCP pathway act in parallel or sequentially remains controversial (Casal et al., 2006; Lawrence & Casal, 2018; Lawrence et al., 2007). In general, molecular gradients often provide a global spatial cue that determines the direction of polarity (Torban & Sokol, 2021). There is evidence that the opposing Ds and Ft expression gradients direct the orientation of microtubule-dependent vesicle transport, which is supposed to be essential in establishing initial PCP asymmetries (Matis et al., 2014; Shimada et al., 2006). The core PCP and the Ft/Ds pathway are both depicted in Figure 5.

Core PCP pathway:



Fat-Dachsous pathway:

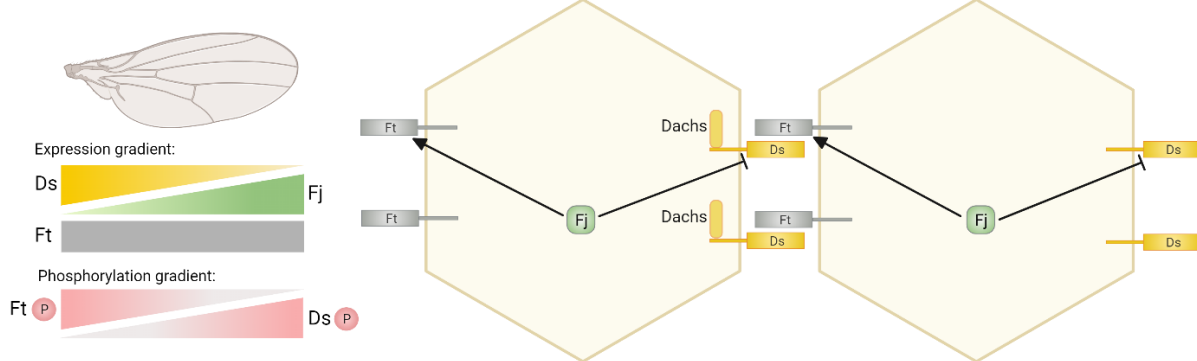


**Figure 5: Core PCP and Fat-Dachsous pathway in *Drosophila*.** The core PCP pathway includes the following protein complexes: the seven-pass transmembrane protein Fz in association with the cytoplasmic proteins Dgo and Dsh enriched at distal sides and the transmembrane protein Vang in association with the cytoplasmic protein Pk enriched at proximal sides. The seven-pass transmembrane protein Fmi is equally distributed at distal and proximal sides and forms homodimers with the extracellular domain of Fmi in adjacent cells. Fmi binds Fz and Vang, thus stabilizing both proteins at opposing membranes. The distal and proximal cytoplasmic components antagonize each other, maintaining the asymmetric distribution of PCP proteins. The cellular asymmetries serve as global cues that are translated into external cell shape changes. The Fat-Dachsous pathway is explained using the wing tissue as an example. The major components of the Fat-Dachsous pathway are Ft, Ds, and Fj. Dachs binds to the cytoplasmic tail of Ds and acts as a downstream effector of Ft/Ds signaling. While Ft is expressed equally along the wing, Ds and Fj are expressed along an opposing gradient. Thereby, Ds is enriched at proximal sides, while Fj is enriched at distal sides of the wing. Ds and Ft form heterodimers between adjacent cells. Heterodimerization is regulated by Fj phosphorylation of both Ds and Ft along a gradient. At proximal sides, a strong Ft phosphorylation enhances Ft-Ds binding, whereas a strong Ds phosphorylation at distal sides weakens Ft-Ds binding (Devenport, 2014; Torban & Sokol, 2021).

Fz is known to be involved in the Wnt signaling pathway (Ackers & Malgor, 2018; Bhanot et al., 1996). Different Wnt proteins act as secreted ligands binding to the Fz receptor and are thought to serve as a global cue for PCP orientation (Sokol, 2015). Two non-redundant Wnt signaling pathways were identified: the canonical Wnt pathway, which is important for primary body axis establishment and the non-canonical Wnt pathway, which contributes to establish PCP thereby controlling various morphogenetic processes via the regulation of actomyosin dynamics (Figure 6) (Petersen & Reddien, 2009; Wodarz & Nusse, 1998). In the canonical pathway, the secreted Wnt ligand is received by the Fz receptor and the co-receptor Lipoprotein receptor-related protein 5/6 (LRP5/6). In the absence of Wnt ligands, the Glycogen synthase kinase 3 beta (GSK3 $\beta$ ) phosphorylates  $\beta$ -Catenin, leading to its

proteasomal degradation. Upon activation of the pathway, Casein kinase-1 (CK1) and GSK3 $\beta$  bind and phosphorylate LRP5/6, resulting in the recruitment of cytoplasmic Dsh and Axin. Dsh stabilizes the Axin-CK1-GSK3 $\beta$  complex at the plasma membrane. Thereby, the phosphorylation  $\beta$ -Catenin is inhibited, resulting in the accumulation of  $\beta$ -Catenin in the cytoplasm.  $\beta$ -Catenin is translocated into the nucleus, where it promotes the expression of Wnt responsive genes, which are relevant for cell proliferation, differentiation, and cell cycle regulation. In the non-canonical pathway, the secreted Wnt ligand is received by the Fz receptor. Cytoplasmic Dsh binds to Fz and transduces the Wnt signal to the downstream effectors Rho1, Rac, and Cdc42. These downstream effectors all belong to the Rho GTPase protein family, whose activation leads to cytoskeleton and junction remodeling (Etienne-Manneville & Hall, 2002; Sit & Manser, 2011).

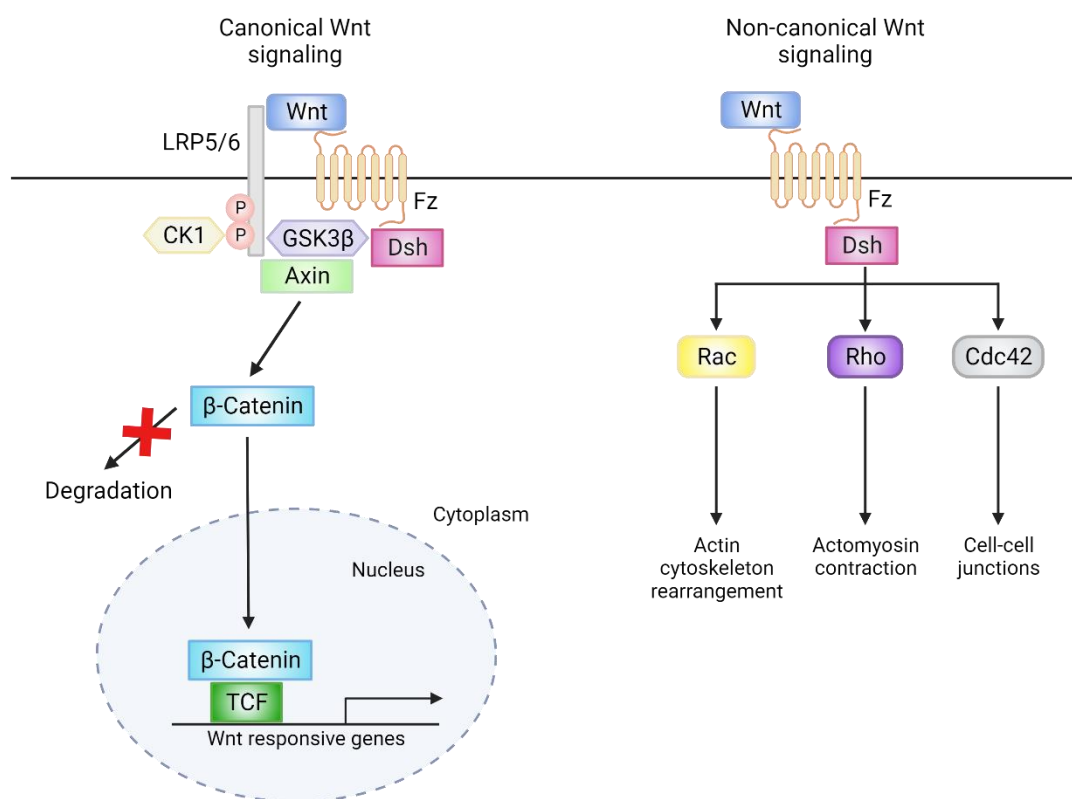


**Figure 6: Canonical and non-canonical Wnt signaling pathway in vertebrates.** When canonical Wnt signaling is inactive, Axin, GSK3 $\beta$  and 1 CK1 form a complex to promote the proteasomal degradation of  $\beta$ -Catenin. Fz and LRP5/6 co-receptor binding to Wnt ligands activate the pathway. Upon activation, CK1 and GSK3 $\beta$  bind and phosphorylate LRP5/6, resulting in the recruitment of cytoplasmic Dsh and Axin. DVL stabilizes the Axin-CK1-GSK3 $\beta$  complex at the plasma membrane, resulting in the accumulation of  $\beta$ -Catenin in the cytoplasm.  $\beta$ -Catenin is translocated into the nucleus, where it promotes the expression of genes relevant for cell proliferation, differentiation, and cell cycle regulation. The non-canonical Wnt/PCP signaling is also activated by Wnt ligands binding to the Fz receptor. In contrast to the canonical pathway, recruited and activated Dsh directly transduces the Wnt signal to downstream effectors, namely Rac, Rho, and Cdc42. The activation of those small RhoGTPases results in actin cytoskeleton and junction remodeling. Each reported protein involved in the vertebrate Wnt signaling pathway has a homolog in *Drosophila* (Sharma et al., 2018).

### 1.3 The actomyosin network is regulated by the Rho-associated protein kinase Rok

Cellular shaping and movements rely on force generation through the contractile actomyosin network spanning the whole apical cell cortex (Guillot & Lecuit, 2013; Heer & Martin, 2017; Perez-Vale & Peifer, 2020; Pilot & Lecuit, 2005). The actomyosin network is composed of actin filaments (F-actin), actin cross linkers, and various myosin proteins functioning as motors. Although all myosin motor proteins provide the same function, namely the force generation by ATP hydrolysis, different classes of myosin participate in various mechanisms. Thus, Myosin V and VI are responsible for cargo transport, Myosin I is involved in intracellular organization, and Myosin VII and X control the dynamics of filopodial assembly. Within this diverse superfamily of proteins, Myosin II drives actomyosin contractility (Hartman & Spudich, 2012). The hexameric Myosin II is composed of two heavy chains, two essential light chains (ELC) and two regulatory light chains (RLC) (Brito & Sousa, 2020; Vicente-Manzanares et al., 2009). In *Drosophila*, myosin II heavy chains are encoded by the gene *zipper*, the RLCs are encoded by the gene *spaghetti squash* (*Sqh*), and the ELCs are encoded by the gene *Mlc* (Edwards et al., 1995; Karess et al., 1991; Young et al., 1993). The N-terminal globular head contains an actin binding site and the catalytic site for ATP hydrolysis. The two different light chains connect the N-terminal head with the C-terminal heavy chains, forming an  $\alpha$ -helical coiled-coil rod domain. Through this rod domain, Myosin II forms bipolar filaments that assemble in between the actin filaments. The energy obtained by ATP hydrolysis is used to mediate the movement of the myosin heads along the adjacent actin filaments, resulting in a sliding motion that leads to the final contraction of the actomyosin network. While the ELCs stabilize the heavy chain structure, the RLC controls Myosin II activity (Brito & Sousa, 2020; Vicente-Manzanares et al., 2009). Myosin II activity is controlled by phosphorylation of Thr20 and Ser21 by the Rho-associated coiled-coil containing protein kinase Rok (Amano et al., 1996; Jordan & Karess, 1997; Tan et al., 1992; Watanabe et al., 2007). In its unphosphorylated form, Myosin II is in its inactive state in which the formation of bipolar filaments is inhibited. Only upon phosphorylation of the RLC by Rok, Myosin II turns into its active state in which it can form bipolar filaments that are incorporated with F-actin (Figure 7).

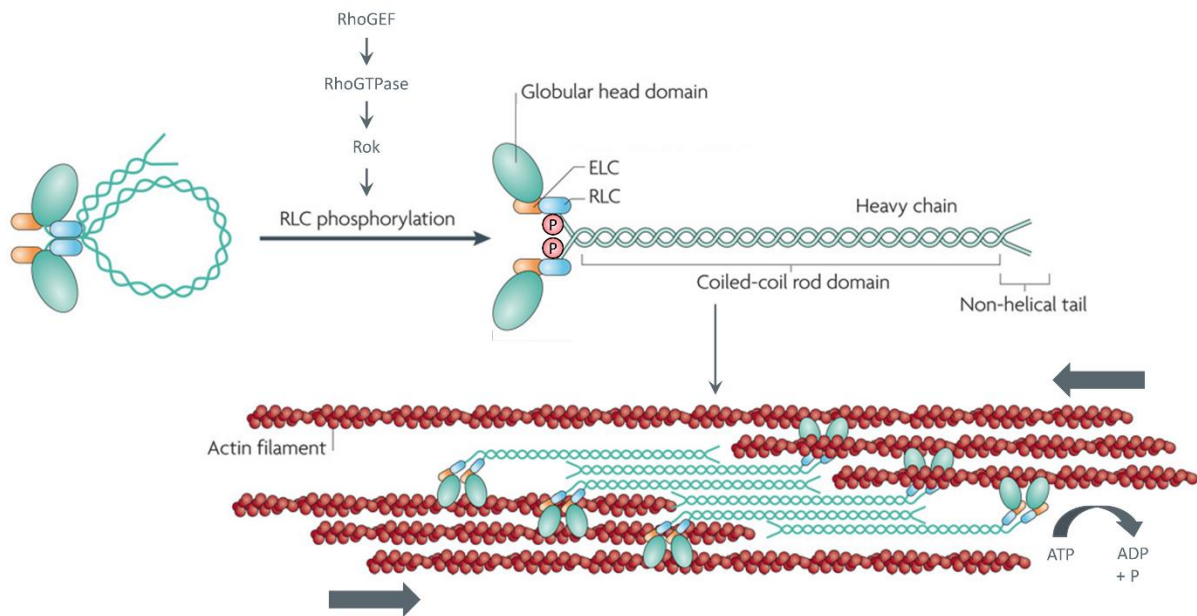


**Figure 7: Rok activates Myosin II and drives actomyosin filament assembly.** Prior to phosphorylation, Myosin II is present in its inactive state. Upon phosphorylation of the RLC by Rok, Myosin II turns into its active state. Thereby, Rok kinase activity is controlled by RhoGTPase upstream signaling. Phosphorylated Myosin II can form bipolar filaments that accumulate in between F-actin. There, the Myosin II head domain catalyzes ATP hydrolysis to obtain energy that is used to conduct the sliding motion of F-actin (modified from Vicente-Manzanares et al., 2009).

Rok is a Ser/Thr-type kinase that is regulated by RhoGTPase upstream signaling. Rok comprises a conserved N-terminal Ser/Thr kinase domain, followed by a coiled coil domain, a Rho binding domain, and a pleckstrin homology (PH) domain at the C-terminus. An autoinhibitory mechanism in which the PH domain binds the kinase domain of Rok leads to Rok inactivation. Upon interaction with GTP-bound RhoGTPase, autoinhibition is suppressed and Rok is activated (Amano et al., 2010). The GTPase-driven activation of Rok is regulated by several upstream signaling pathways, such as Wnt (Figure 6) or Fog signaling (Figure 8). Similar to Wnt proteins, Fog is a secreted ligand that binds to the seven-pass transmembrane G-protein coupled receptor (GPCR) Mist, resulting in the activation of the G-protein Concertina, which in turn leads to the activation of RhoGEF, Rho1, and Rok (Manning & Rogers, 2014).

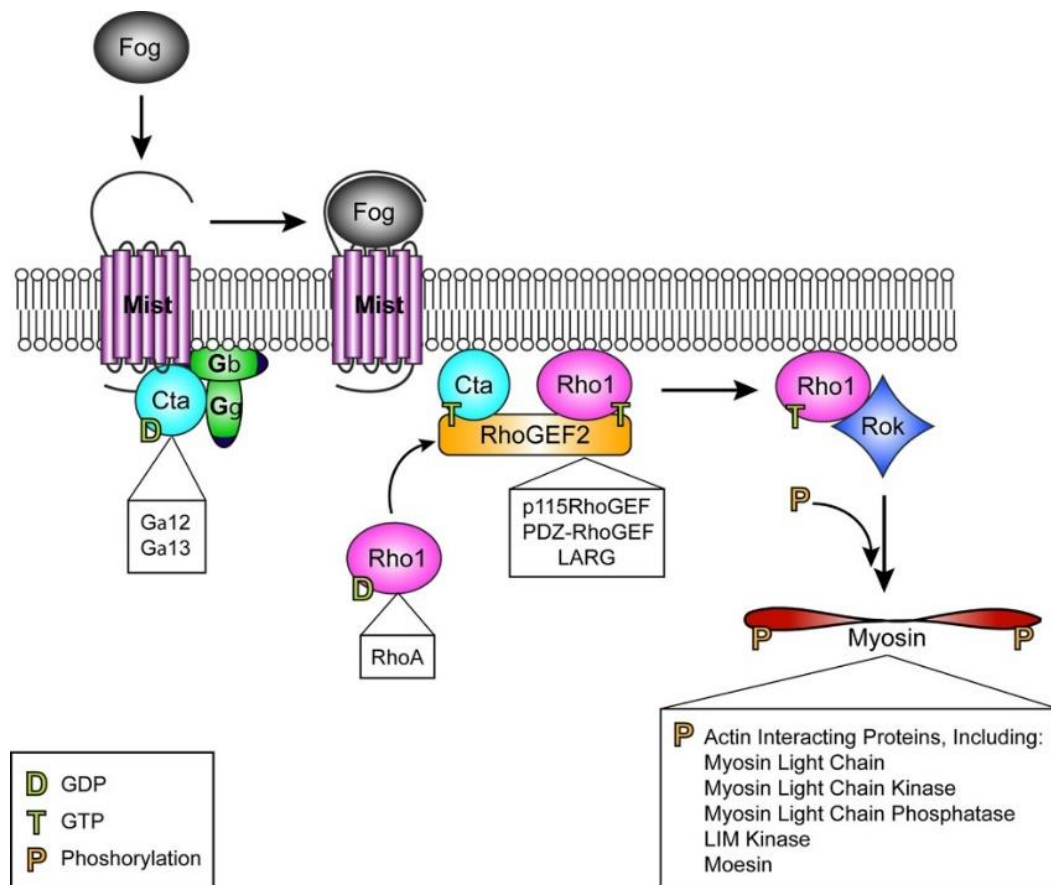


**Figure 8: The Fog signaling pathway regulates Rok kinase activity.** The secreted ligand Fog binds to the GPCR Mist and activates the G-protein Concertina, which in turn leads to the activation of RhoGEF, Rho1, and Rok. Activated Rok phosphorylates its target proteins. Among others, Rok targets for instance the non-muscle myosin II regulatory light chain (Manning & Rogers, 2014).

## 1.4 The tight control of actomyosin and AJs is critical for epithelial morphogenesis

Epithelial tissues are dynamically remodeled during morphogenesis and at the same time they have to provide a robust architecture, making them resilient to mechanical stress. To ensure that tissue remodeling occurs without losing tissue integrity, a tight interplay between the cortical actomyosin network and the AJs is crucial (Perez-Vale & Peifer, 2020). One important mechanism for tissue remodeling is the so-called apical constriction. During apical constriction, the actomyosin network accumulates at the apical cell cortex, where it is connected to AJs. There, pulsatile contractions of the membrane-associated actomyosin network induce the reduction of the apical cell perimeter (Martin et al., 2009; Mason et al., 2013; Sawyer et al., 2010). Apical constriction enables the formation of different invaginations and furrows for instance during gastrulation (Pilot & Lecuit, 2005). In *Drosophila*, gastrulation is initiated after cellularization. First, mesodermal primordia cells start to invaginate to form the ventral furrow. Thereby, cells undergo apical constriction followed by cell shortening. After full internalization, cells start flattening, dividing, and spreading to form the single-layered mesoderm. Second, shortly after the onset of ventral furrow formation, the posterior midgut invagination starts to form. Later in development, the posterior midgut invagination gives rise to the endoderm (Figure 9 A-C) (Leptin, 1999; Sweeton et al., 1991).

In muscle cells, Myosin II and actin filaments are organized antiparallel to each other in a structure called sarcomere. In contrast to this, non-muscle cortical actomyosin networks exhibit a radial, disordered network structure. Thereby, the plus end of F-actin is anchored to AJs at the apical boundaries, while its minus end is oriented towards the apical center. Myosin II and its activator Rok are accumulated at the apical center of a cell, where they induce the pulsatile contraction of the network to reduce the apical cell perimeter (Coravos & Martin, 2016) (Figure 9 D).

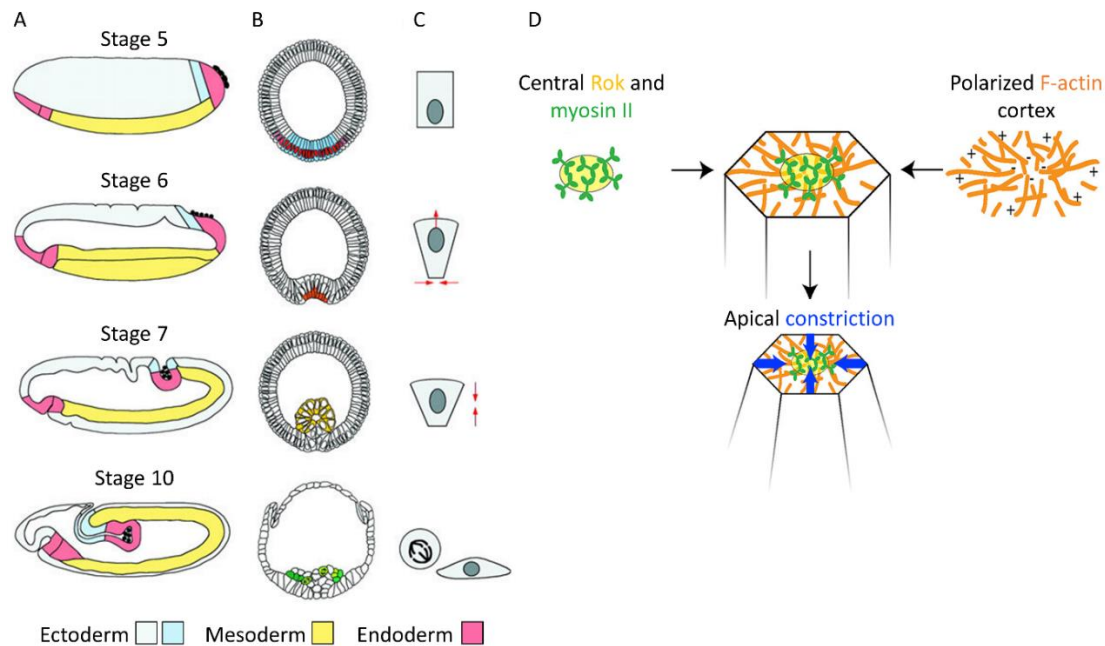


**Figure 9: Apical constriction leads to a reduction of the apical cell perimeter, which is important for gastrulation.** (A) Diagrams of whole embryos indicating the regions of the ectodermal, mesodermal, and endodermal primordia (marked in different colors). Embryonic stages are indicated. In stage 5, the primordia lie at the surface of the embryo. During stage 6, ventral furrow formation occurs. In stage 7, the posterior part of the endoderm starts forming the midgut invagination and the germ band starts extending onto the dorsal side of the embryo. Until stage 10, the midgut invagination is further expanding and the germ band continues to extend. (B) Diagrams of cross sections of embryos at the same stages as those shown in A. In stage 5 embryos, Twist protein (red) localizes in the nucleus and *Snail* RNA (blue) in the cytoplasm. In stage 6 embryos, apical enrichment of Myosin II and Actin (orange) is indicated. In stage 7 embryos, cells undergoing shortening are labeled in yellow. Green labeled cells in stage 10 embryos undergo flattening, division, and spreading. (C) The shape changes of an individual mesodermal cell from the different embryonic stages indicated in A are illustrated. (D) F-actin is distributed in a polarized manner all over the apical cell cortex, while Rok and Myosin II accumulate at the center. Activation of the radially arranged actomyosin network leads to apical constriction (modified from Leptin, 1999; Coravos & Martin, 2016).

Convergent extension is another essential process in tissue remodeling. Here, cells undergo local neighbor exchange events, also known as cell intercalation. Thereby, the cell contacts between anterior/posterior (A/P) interfaces are disassembled, while new junctions are formed along dorsal/ventral (D/V) edges. This rearrangement of cells enables the extension of the epithelial tissue by more than two-fold along the A/P axis, which is accompanied by a reduction in width along the D/V axis (Bertet et al., 2004; Pare & Zallen, 2020). Two types of cell rearrangements occur during convergent extension. The first type is called T1-T2-T3 transition and involves a total of four cells. In the T1 phase, the shrinking of shared interfaces that are oriented along the A/P axis leads to the formation of a transient four-cell vertex state in the T2 phase. Through the establishment of new junctions along the D/V axis in the T3 phase, the four-cell vertex is rapidly disassembled in a perpendicular direction to elongate the tissue. The other type of cell intercalation is rosette formation, which relies on the same principle as the T1-T2-T3 transition with the difference that multiple cells, usually 5-12, are involved (Figure 10) (Guillot & Lecuit, 2013; Pare & Zallen, 2020).

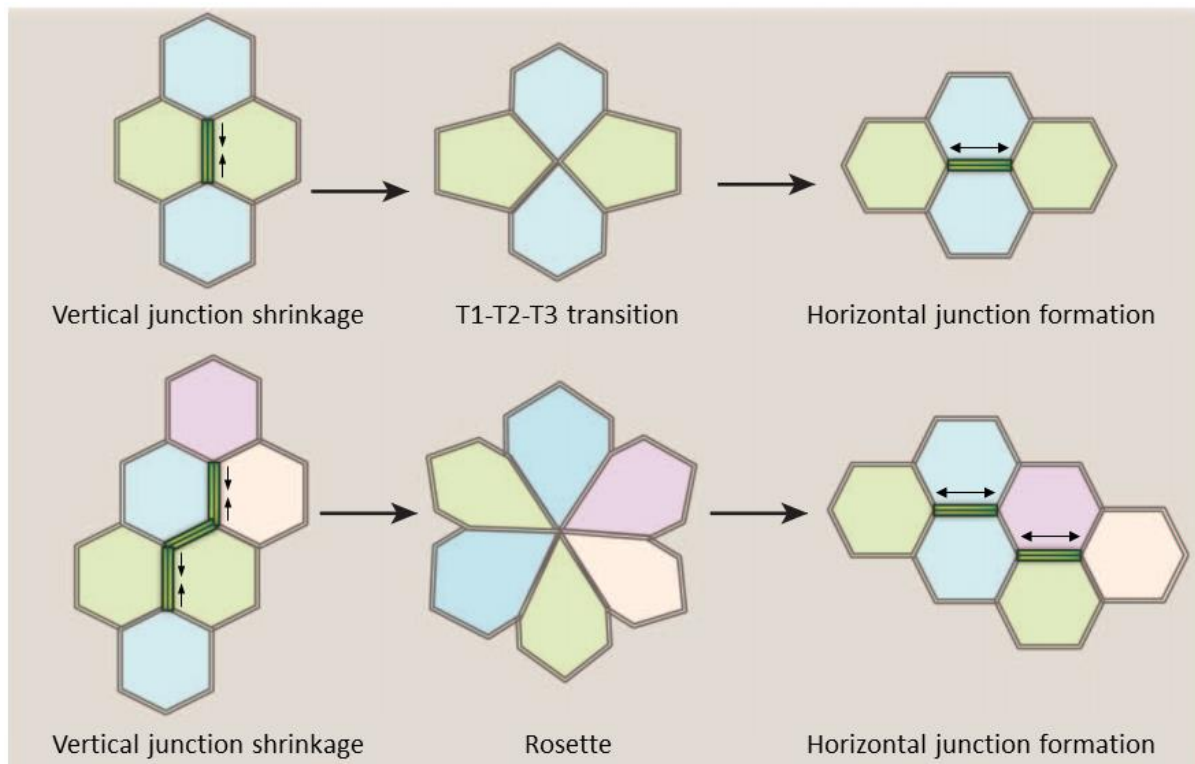


**Figure 10: Cell intercalation causes local cell rearrangements.** Two types of cell intercalation can occur: the so-called T1-T2-T3 transition or rosette formation. During the T1-T2-T3 transition, the shrinking of shared interfaces that are oriented along the A/P axis leads to the formation of a transient four-cell vertex state. This transient state is quickly disassembled in a perpendicular direction to elongate the tissue by establishing new junctions along the D/V axis. Rosette formation relies on the same principle as the T1-T2-T3 transition but involves 5-12 instead of 4 cells (Guillot & Lecuit, 2013).

Cell populations undergoing intercalation are motile and their environment is constantly changing. The regulation of such a complex morphogenetic movement involves the implementation of directional cues from the classical PCP system as well as spatial information that is provided by the polarized localization of certain proteins. Thereby, the activity of these polarized proteins is directly coupled to the cellular behavior. During *Drosophila* germ band elongation, Myosin II, F-actin, and Rok concentrate at edges between anterior and posterior cells, where they destabilize intracellular adhesions and eliminate the junctions by promoting actomyosin contractility (Bertet et al., 2004; Zallen & Wieschaus, 2004; Blankenship et al., 2006). Perpendicular to this, the AJ-associated proteins E-Cadherin and Baz accumulate at D/V interfaces, where they promote the formation and stabilization of new AJs (Zallen & Wieschaus, 2004; Blankenship et al., 2006; Simões et al., 2010). Like the apicobasal polarity system, proteins involved in PCP regulate the localization of each other. For example, Rok is required for the proper distribution of Myosin II at A/P junctions. Moreover, Rok is responsible for the phosphorylation of Baz to exclude it from A/P edges thus promoting Baz accumulation along D/V junctions (Simões et al., 2010).

In addition to Myosin II, F-actin, Rok, Baz, and E-Cadherin, many other proteins modulate actomyosin contractility and junctional stability during cell intercalation (summarized in Figure 11). One of these regulatory proteins is Moesin (Moe). Moe is a member of the ERM (Erzin/Radixin/Moesin) protein family and serves as a linker between AJs and the actin cytoskeleton to maintain cell shape. Moe comprises an N-terminal FERM domain, a central  $\alpha$ -helical domain, and a C-terminal ERM-associated domain that can either bind F-actin or the FERM domain (Fehon et al., 2010). A head-to-tail folding inactivates Moe by masking the F-actin binding site. Moe activity is regulated by Rok phosphorylation, which induces a conformational change into its active form (Matsui et al., 1998). It was found that this phosphorylation is required for proper assembly of the actomyosin network (Speck et al., 2003). Furthermore, Moe was described to be important for cell integrity since junction and polarity markers were lost in cells mutant for the *Moe*<sup>G0323</sup> null allele. These severe effects could be restored by suppressing the Rho1 signaling, suggesting that Moe functions antagonistically to the Rho1 pathway (Speck et al., 2003). This hypothesis was proven by the fact that *Moe* loss of function and Rho1 overexpression led to similar phenotypic defects.

Similar to Moe, Cno functions as linker between the cortical actomyosin cytoskeleton and AJs (Sawyer et al., 2011). During germ band elongation, Cno is enriched at A/P and tricellular junctions together with F-actin and Myosin II. Although the planar polarized localization of F-actin and Myosin II does not alter upon loss of Cno, the loss of Cno drastically impairs germ band elongation since a detachment of the actomyosin cytoskeleton from AJs and reduced adhesion at tricellular junctions occur. It was demonstrated that Cno modulates tricellular adhesion in a tension-sensitive manner, enabling Cno to react quickly to mechanical cues (Yu & Zallen, 2020).

Another actin-associated protein that is involved in the regulation of cell intercalation is Shroom (Shrm). Shrm is enriched at A/P junctions during germ band elongation. The planar polarized enrichment of Shrm at A/P junctions was shown to be dependent on Rho1 signaling (Simões et al., 2014). Shrm was shown to be required for the correct localization and stabilization of Rok, F-actin, and Myosin II at A/P cell interfaces during cell intercalation and at the apical cortex during apical constriction (Bolinger et al., 2010; Haigo et al., 2003; Hildebrand, 2005; Nishimura & Takeichi, 2008; Simões et al., 2014). Shrm directly interacts with Rok, thereby promoting Rok kinase activity to drive cell shape changes (Bolinger et al., 2010; Nishimura & Takeichi, 2008; Zalewski et al., 2016). In agreement with this finding, the loss of Shrm leads to a decrease in junctional tension and defective rosette formation during germ band elongation (Simões et al., 2014), whereas overexpression of Shrm induces apical constriction (Bolinger et al., 2010; Haigo et al., 2003; Hildebrand, 2005).

Actomyosin contractility generates strong mechanical forces. These forces have a strong effect on AJ organization since AJ assembly and disassembly are force sensitive. Ajuba (Jub), a LIM domain-containing protein belonging to the zyxin protein family, is spatiotemporally localized to A/P junctions in response to tension during germ band elongation. Razzell et al., (2018) showed that *jub* mutants display increased rosette formation accompanied by impaired rosette resolution. Although the observed phenotype raises the assumption that Ajuba is involved in regulating actomyosin contractility, it was shown that Ajuba has no effect on actomyosin contractility. Instead, it was demonstrated that Ajuba stabilizes AJs in regions of high tension, thus maintaining cell adhesion during convergent extension. This was proven by the finding that rosettes in *jub* mutant embryos display aberrant gaps between cells, representing defects in cell adhesion most likely caused by the absence of AJ proteins.

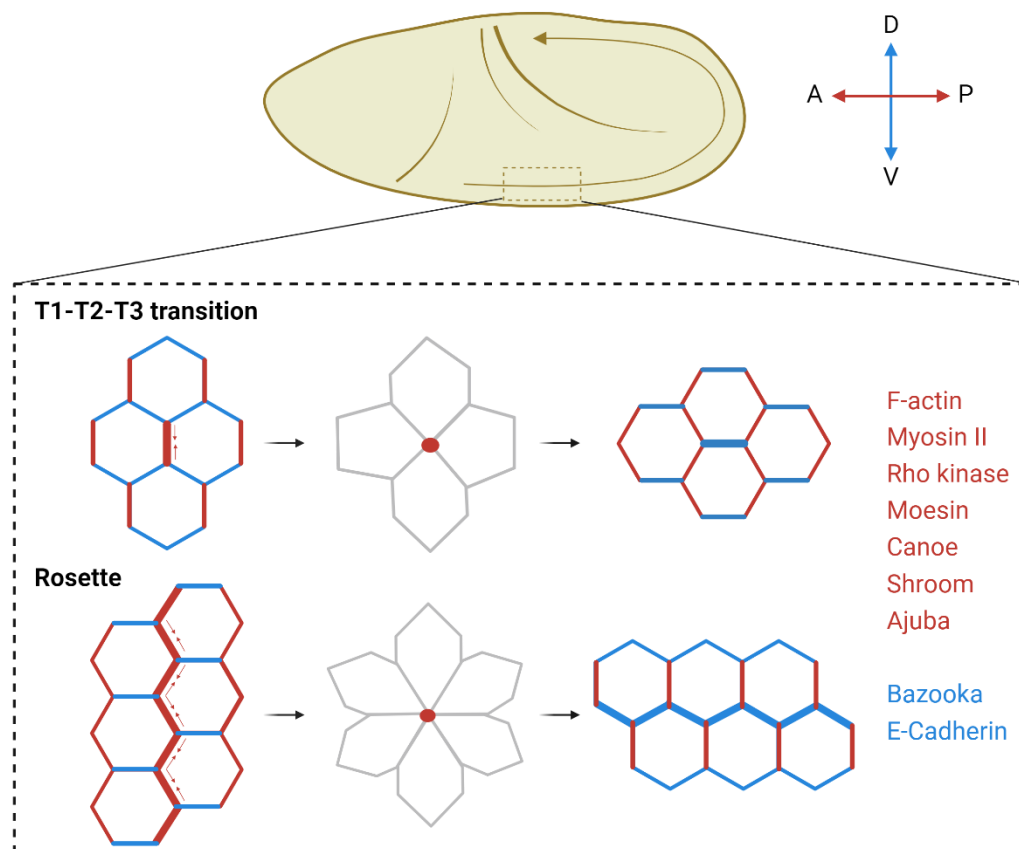


**Figure 11: Proteins are localized in a planar polarized fashion during germ band elongation in *Drosophila* embryos.** Germ band elongation is driven by cell intercalation events. The regulation of cell intercalation events depends on the interplay between the contractile actomyosin network to eliminate junctions along the A/P axis and AJs to establish new cell contacts along D/V junctions. These processes are regulated by the planar polarized enrichment of several proteins. F-actin, Myosin II, Rho kinase, Moesin, Canoe, Shroom, and Ajuba are enriched at A/P junctions, whereas E-Cadherin and Bazooka are enriched at D/V junctions (Pare & Zallen, 2020).

## 1.5 Smallish regulates actomyosin contractility in epithelial cells

The *Drosophila* gene *smallish* (CG43427) encodes a Lin-11, Isl-1, Mec-3 (LIM) domain protein that was originally identified as binding partner of the key polarity regulator Baz in a yeast two-hybrid screen (Beati et al., 2018). In this screen, the three PDZ domains of Baz (aa 291-737) were used as bait. Several isoforms of Smallish (Smash) are expressed in the fly. In total, 10 isoforms of Smash exist. This study mainly focuses on two of these isoforms. With 169 kDa, SmashPM represents the largest isoform containing an N-terminal myosin-binding domain, which is conserved in *Xenopus* Lim domain only 7 (LMO7) and mouse LIMCH1, two  $\alpha$ -helical coiled-coil domains, a LIM domain and a C-terminal PDZ binding motif (PBM). The shorter isoform SmashPI is around 100 kDa large and lacks the myosin binding domain and the two coiled-coil domains, whereas the C-terminal LIM domain and the PBM are present (Figure 12). All predicted domains serve as interfaces for different protein interactions, suggesting that Smash acts as a scaffolding protein.

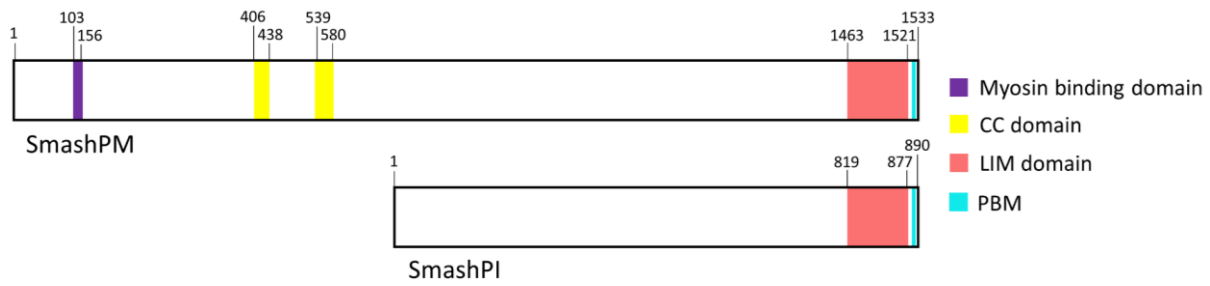


**Figure 12: Protein structure of SmashPM and SmashPI.** SmashPM comprises 1533 aa, forming a myosin binding domain, two coiled-coil domains, and a C-terminal LIM domain terminated by a PBM. SmashPI comprises 889 aa that include the C-terminal LIM domain and the PBM. Numbers indicate the position of a domain within the protein. Different domains are highlighted in different colors. The color code is indicated to the right (modified from Beati et al., 2018).

The characteristic LIM domain is composed of a tandem zinc finger motif that constitutes the sequence  $CX_2CX_{16-23}HX_2CX_2CX_2CX_{16-21}CX_2$  showing a highly conserved arrangement of cysteine and histidine residues functioning as zinc binding sites (Kadmas & Beckerle, 2004). LIM domain-containing proteins are represented in diverse eukaryotic species. Similar to Smash, the vertebrate orthologue of Smash, LMO7, localizes to AJs, where it binds Afadin and  $\alpha$ -Actinin (Ooshio et al., 2004). Moreover, LMO7 was reported to bind non-muscle myosin II heavy chain (NMIIHC) via its myosin-binding domain, facilitating actomyosin filament assembly (Matsuda et al., 2022). Many LIM domain proteins can shuttle between the cytoplasm and the nucleus to regulate gene expression (Kadmas & Beckerle, 2004). LMO7 was shown to be a nucleocytoplasmic shuttling protein regulating gene expression of the nuclear membrane protein Emerin. Moreover, it was reported that LMO7 is enriched at the nuclear envelope, where it directly binds Emerin. The direct interaction between Emerin and LMO7 was suggested to serve as a positive feedback mechanism to regulate *emerin* expression (Holaska et al., 2006). Different studies claimed that LMO7 has an important disease-related function because mutations in *emerin* can be linked to X-linked Emery–Dreifuss muscular dystrophy (X-EDMD) (Holaska et al., 2006; Mull et al.,

2015). Several other studies prove the importance of LMO7 during pathogenesis, as the absence of LMO7 leads to tumor formation (Liu et al., 2021; Nakamura et al., 2011; Tanaka-Okamoto et al., 2009). As a potential tumor suppressor, LMO7 is of enormous importance for clinical research. Investigating the *Drosophila* homolog Smash could help to understand the molecular basis of LMO7 function.

Studies in *smash*<sup>Δ35m/z</sup> null allele mutants revealed that Smash plays a critical role during epithelial morphogenesis since mutant embryos exhibited severe morphogenetic defects. For example, a strongly abnormal and irregular formation of furrows, including the cephalic and segmental furrows, was observed (Beati et al., 2018) (Figure 13).

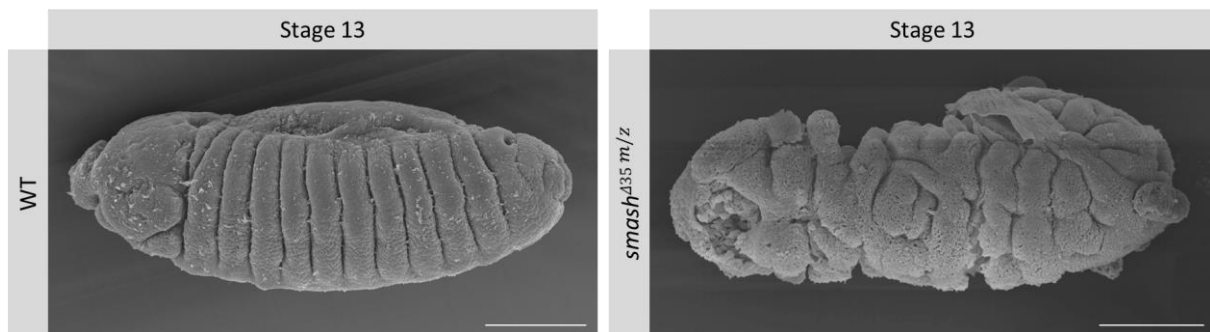


**Figure 13: Scanning electron microscopy of wild-type (WT) and *smash*<sup>Δ35m/z</sup> embryos at stage 13.** In WT, a regularly segmented embryo before dorsal closure is depicted. In *smash*<sup>Δ35m/z</sup> mutant embryos, a strong irregular formation of segmental furrows was observed. Scale bar: 100 μM (Beati et al., 2018).

The following observations were reported in Beati et al. (2018). Smash is detectable from embryonic stage 5 onwards in all ectodermally derived epithelia, including the epidermis, fore- and hindgut, Malpighian tubules, salivary glands, amnioserosa, and tracheal tree. At the subcellular level, Smash is localized at AJs together with its proven interaction partner Baz. Regarding its distribution in the plane of the epithelium, Smash accumulates at A/P junctions, contrary to Baz which is enriched at D/V junctions. In *smash*<sup>Δ35m/z</sup> embryos, apical localization of Baz was not affected, whereas the planar polarized localization of Baz during germ band elongation was reversed as Baz was enriched at A/P junctions. Furthermore, the loss of Smash also affected the planar polarized distribution of other proteins, namely Cno and Sqh. Both are accumulated at A/P junctions during germ band elongation in WT. Upon loss of Smash, both were uniformly distributed, hence losing their planar polarized localization. In contrast, the loss of Smash had no effect on the planar polarized localization of Rok, demonstrating that the subcellular localization of Rok is independent of Smash. The opposite way around, it was found that the loss of Baz, Cno, and F-actin led to an abnormal distribution of Smash, suggesting that these proteins are relevant for proper subcellular localization of Smash. Besides these localization effects, Smash was found to directly interact with Baz, Rok, Cno, and maybe with Sqh. Additional *in vitro* studies showed that Smash directly binds to the actin-associated proteins Shrm and Moe (Peek, 2019). Whether Smash influences the subcellular localization of Shrm or Moe or vice versa has not been investigated yet.

Localization and interaction studies performed so far suggested that Smash acts within a protein network that regulates the proper localization and activation of actomyosin, resulting in directed force generation that finally leads to tissue deformation. The effect of Smash on the actomyosin cytoskeleton was investigated by analyzing Smash overexpressing and knock-out animals. While overexpression of Smash in the follicle epithelium induced apical constriction, laser ablation experiments in the larval epidermis showed that the loss of Smash resulted in reduced junctional tension, proving that Smash is indeed involved in regulating actomyosin architecture, activity, or both. Taken these findings together, the *smash* <sup>$\Delta 35m/z$</sup>  mutant embryonic phenotype probably results from a disrupted PCP system, which in turn affects proper regulation of the actomyosin cytoskeleton. An uncoordinated actomyosin cytoskeleton is thought to cause the formation of aberrant morphological structures in *smash* <sup>$\Delta 35m/z$</sup>  embryos.

In conclusion, the described observations are consistent with a model in which Smash is embedded in a network that is responsible for precise actomyosin contractility during epithelial morphogenesis. The directed actomyosin contractility is dependent on the proper subcellular localization of the single components within this network. Thereby, the single components modulate each other's subcellular localization. Although Smash was shown to be relevant for the proper subcellular localization of several proteins, the exact mechanism by which Smash functions is not fully understood yet.

## 1.6 Scope of this thesis

The aim of this study was to obtain a deeper insight into the molecular mechanism of Smash function. In order to achieve this goal, the following questions were addressed: In which developmental processes is Smash involved? How does Smash regulate the actomyosin cytoskeleton? What is the spatiotemporal behavior of Smash during epithelial morphogenesis, especially during germ band elongation? What are potential Smash-interacting proteins and what is the physiological relevance of these interactions?

To answer these questions, a series of different molecular, biochemical, and histological approaches were combined. To identify developmental processes in which Smash might be involved, a closer investigation of *smash*<sup>Δ35m/z</sup> mutant embryos was performed. As germ band elongation tightly relies on actomyosin contractility, we investigated the involvement of Smash in germ band elongation using bright field live imaging. The contribution of Smash in regulating the actomyosin network was investigated in several experiments. We demonstrated that Smash is required for the phosphorylation of Sqh. To test whether Smash controls actomyosin contractility by directly regulating Rok kinase activity, we performed *in vitro* kinase assays. In addition, overexpression experiments in the follicle epithelium analyzed the involvement of Smash in actomyosin cytoskeleton remodeling and its effect on cell architecture. To study the spatiotemporal behavior of different Smash isoforms during epithelial morphogenesis, CRISPR/Cas9 technology was used to generate SmashPM and SmashPI superfolder GFP (sfGFP) knock-in lines. The novel sfGFP knock-in lines were carefully analyzed with respect to the expression pattern and the subcellular localization of the sfGFP-tagged Smash fusion proteins. Finally, novel Smash-interacting proteins were identified using a biotin proximity labeling assay. We started to closer analyze the interaction between Smash and promising candidates by performing *in vitro* co-IP and *in vivo* localization studies.

## 2 Material & Methods

### 2.1 Material

#### 2.1.1 Fly stocks

**Table 1: List of fly stocks.** The stock name, genotype, respective chromosomes, a short description and the source of the fly stocks are given. Bl. = Bloomington stock number. DGRC = *Drosophila* Genetic Resource Consortium stock number.

| Stock name                  | Genotype   | Chromosome(s) | Description   | Source                   |
|-----------------------------|--|---------------|---|--------------------------|
| Wild-type (WT) stock        |  |               |   |                          |
| w <sup>-</sup>              | w <sup>1118</sup>  | X             | White eyes  | Bl. 5905                 |
| G4 driver stocks            |  |               |   |                          |
| hsflp;;act<CD2<G4           | <i>hsflp;;act&lt;C D2&lt;GAL4</i>  | X, 3          | Ubiquitous driver   | Pignoni & Zipursky, 1997 |
| matatub(15)::G4             | <i>P{matalpha4-GAL-VP16}V37</i>  | 3             | GAL4-VP16 fusion protein expressed under the control of the $\alpha$ -Tub67C promoter. Expressed maternally and loaded into eggs. | Bl. 7063                 |
| matatub(67/15)::G4          | <i>y[1] w[*]; P{matalpha4-GAL-VP16}67; P{matalpha4-GAL-VP16}15</i>                             | 2, 3          | Expresses GAL4-VP16 fusion protein under the control of the alphaTub67C promoter. Expressed maternally and loaded into eggs.      | Bl. 80361                |
| tj:G4                       | <i>y* w*; P{w<sup>+mW.hs</sup> = GawB}NP1624 / CyO, P{w<sup>-</sup> = UAS-lacZ. UW14} UW14</i> | 2             | traffic jam::GAL4 drives expression in somatic cells of the male and female gonad.  | DGRC 104055              |
| <i>smash</i> fly stock      |  |               |   |                          |
| smash <sup>A35</sup>        | <i>smash<sup>A35</sup> / TM6B</i>  | 3             | <i>smash</i> null allele  | Beati et al., 2018       |
| Other stocks                |  |               |   |                          |
| UASp::TurboID:eGFP          | <i>UASp::TurboID: eGFP/CyO</i>   | 2             | Expresses TurboID:eGFP under the control of UASp.   | This work                |
| UASp::eGFP:TurboID :SmashPM | <i>UASp::eGFP: TurboID: SmashPM/CyO</i>  | 2             | Expresses eGFP:TurboID:SmashPM under the control of UASp.   | This work                |
| UASp::eGFP: SmashPM         | <i>UASp::eGFP: SmashPM/CyO</i>   | 2             | Expresses eGFP:SmashPM under the control of UASp.   | Beati et al., 2018       |
| UAST::eGFP: SmashPM         | <i>UAST::eGFP: SmashPM/CyO</i>   | 2             | Expresses eGFP:SmashPM under the control of UAST.   | This work                |
| UAST::eGFP: SmashPM N-term  | <i>UAST::eGFP: SmashPM N-term/CyO</i>  | 2             | Expresses eGFP:SmashPM N-term under the control of UAST.  | This work                |

| Stock name  | Genotype   | Chromosome(s) | Description  | Source                   |
|---|--|---------------|--|--------------------------|
| Other stocks  |  |               |  |                          |
| UAST::eGFP:<br>SmashPM mut                                | <i>UAST::eGFP:<br/>SmashPM<br/>mut/CyO</i>   | 2             | Expresses eGFP:SmashPM mut under the control of UAST.  | This work                |
| UAST::mCD8:eGFP   | <i>y[1] w[*]<br/>P{w[+mC]}=<br/>UAST::mCD8:<br/>eGFP}Ptp4E<br/>[LL4];betaTub6<br/>OD[PinYt]/CyO</i>                | X, 2          | Expresses mCD8:eGFP under the control of UAST.   | Bl. 5136                 |
| UAS::GFP:Lasp   | <i>UAS::GFP:<br/>Lasp/CyO</i>  | 2             | Expresses GFP:Lasp under the control of UAS.   | Suyama et al., 2009      |
| Ajuba <sup>II</sup> ,<br>FRT19A/FM7a, dfd-YFP             | <i>Ajuba<sup>II</sup>,<br/>FRT19A/FM7a,<br/>dfd-YFP</i>  | X             | Contains <i>Ajuba<sup>II</sup></i> allele and a FRT19A site for FLP induced generation of germline clones. Expresses dfd-YFP marker.                       | Das Thakur et al., 2010  |
| Ajuba <sup>54</sup> ,<br>FRT19A/FM7a, dfd-YFP             | <i>Ajuba<sup>54</sup>,<br/>FRT19A/FM7a,<br/>dfd-YFP</i>  | X             | Contains <i>Ajuba<sup>54</sup></i> allele and a FRT19A site for FLP induced generation of germline clones. Expresses dfd-YFP marker.                       | Razzell et al., 2018     |
| ovo <sup>D2</sup> , FRT19A/x <sup>^x</sup> ;<br>hsflp/CyO | <i>ovo<sup>D2</sup>,<br/>FRT19A/x<sup>^x</sup>;<br/>hsflp/CyO</i>  | X, 2          | Contains dominant female sterile <i>ovo<sup>D2</sup></i> mutation, FRT19A site and attached-X chromosomes. Expresses heat-shock flippase.                  | Razzell et al., 2018     |
| sfGFP:SmashPM   | <i>sfGFP:<br/>SmashPM</i>  | 3             | CRISPR line expressing sfGFP:SmashPM   | This work                |
| sfGFP:SmashPI   | <i>lf/CyO;<br/>sfGFP:SmashPI<br/>/TM6B</i>   | 2, 3          | CRISPR line expressing sfGFP:SmashPI   | This work                |
| Injection stock   |  |               |  |                          |
| attP40 ΦC31   | <i>y[1] w[*]<br/>P{y[+t7.7] =<br/>nanos-phiC31<br/>\ int.NLS}X;<br/>P{y[+t7.7] =<br/>CaryP}Msp300<br/>[attP40]</i> | X, 2          | 2nd chromosome attP docking site (25C6) for phiC31 integrase-mediated transformation. Expresses phiC31 integrase under the control of <i>nos</i> promoter. | Bl. 79604                |
| Cas9 stocks   |  |               |  |                          |
| vasa::Cas9  | <i>w[1118]; PBac<br/>{y[+mDint2]=<br/>vas-Cas9}<br/>VK00027</i>  | 3             | Expresses Cas9 protein in the ovary under control of vas regulatory sequences. Construct marked with 3xP3-GFP.   | Bl. 51324                |
| nos::Cas9:mSA   | <i>w,<br/>nos::Cas9:mSA<br/>(attP40)</i>   | 2             | Expression of Cas9 fused to monomeric Streptavidin under control of <i>nos</i> promoter  | Poernbacher et al., 2019 |

### 2.1.2 Primary antibodies

**Table 2: List of primary antibodies.** The antigen, name, host, application, dilution, and source of each primary antibody is listed. IF = Immunofluorescence staining, WB = Western blotting, DAB = Diaminobenzidine tetrahydrochloride staining.

| Antigen                   | Name         | Host       | Application | Dilution          | Source/Reference       |
|---------------------------|--------------|------------|-------------|-------------------|------------------------|
| Smash                     | Smash N-term | guinea pig | IF          | 1:500             | Beati et al., 2018     |
| DE-Cadherin               | DCAD-2       | rat        | IF          | 1:5               | DSHB                   |
| GFP                       | -            | rabbit     | IF, WB      | 1:1000,<br>1:2000 | Invitrogen, A11122     |
| Phosphomyosin light chain | -            | rabbit     | IF, WB      | 1:50,<br>1:1000   | Cell Signaling, #36719 |
| Dlg                       | 4F3          | mouse      | IF          | 1:20              | Hybridoma              |
| Myc                       | 9E10         | mouse      | IF, WB      | 1:200             | Hybridoma              |
| $\beta$ Tub               | -            | mouse      | WB          | 1:20              | DSHB                   |
| Twist                     | -            | rabbit     | DAB         | 1:500             | Roth et al., 1989      |
| Lasp                      | Lasp N-term  | rabbit     | IF          | 1:4000            | Suyama et al, 2009     |
| GST                       | -            | rabbit     | WB          | 1:2000            | Sigma-Aldrich, G7781   |

### 2.1.3 Secondary antibodies

**Table 3: List of secondary antibodies.** The antigen, name, host, application, dilution, and source of each secondary antibody is listed. IF = Immunofluorescence staining, WB = Western blotting, DAB = Diaminobenzidine tetrahydrochloride staining.

| Antigen IgG | Host | Conjugate | Application | Dilution             | Source/Reference                                 |
|-------------|------|-----------|-------------|----------------------|--|
| guinea pig  | goat | AF488     | IF          | 1:200                | Invitrogen, A11073                               |
| guinea pig  | goat | AF647     | IF          | 1:200                | Invitrogen, A21450                               |
| mouse       | goat | AF555     | IF          | 1:200                | Invitrogen, A21424                               |
| mouse       | goat | AF647     | IF          | 1:200                | Invitrogen, A21236                               |
| rabbit      | goat | AF488     | IF          | 1:200                | Invitrogen, A11034                               |
| rabbit      | goat | AF555     | IF          | 1:200                | Invitrogen, A21429                               |
| rabbit      | goat | AF647     | IF          | 1:200                | Invitrogen, A21245                               |
| rat         | goat | AF555     | IF          | 1:200                | Invitrogen, A21434                               |
| rat         | goat | AF647     | IF          | 1:200                | Invitrogen, A21247                               |
| guinea pig  | goat | HRP       | WB          | 1:10000              | Dianova, 106-035-003                             |
| mouse       | goat | HRP       | WB          | 1:10000              | Dianova, 115-035-068                             |
| rabbit      | goat | HRP       | WB          | 1:10000              | Dianova, 111-035-144                             |
| rabbit      | goat | biotin    | DAB         | 1:50,<br>preabsorbed | Jackson ImmunoResearch Laboratories, 111-065-003 |

### 2.1.4 Other conjugates

**Table 4: List of other conjugates.** The protein or peptide, conjugate, application, dilution, and source of each conjugate is listed. IF = Immunofluorescence staining, WB = Western blotting.

| Protein /Peptide | Conjugate | Application | Dilution | Source/Reference                 |
|------------------|-----------|-------------|----------|----------------------------------|
| Phalloidin       | AF555     | IF          | 1:200    | Cell Signaling, 8953             |
| Streptavidin     | AF594     | IF          | 1:500    | Thermo Fisher Scientific, S11227 |
| Streptavidin     | HRP       | WB          | 1:2000   | BioLegend, 405210                |

### 2.1.5 Bacterial strains

For amplification of plasmid DNA, chemical competent MACH1 or DH5 $\alpha$  cells were used.

For expression of proteins, chemical competent BL21 cells were used.

### 2.1.6 Cell Culture

S2 cell line derived from late-stage *Drosophila melanogaster* embryos was used (Schneider, 1972).

### 2.1.7 Plasmids

**Table 5: List of plasmids.** Plasmid name, a short description, the source, and the cloning strategy by which the plasmids were generated are given. “T” = TOPO cloning, “G” = Gateway cloning, “GA” = Gibson assembly, “R” = restriction cloning

| Plasmid name                  | Description  | Source                              | Cloning strategy |
|-------------------------------|--|-------------------------------------|------------------|
| pENTR-D-TOPO                  | Gateway Entry vector for TOPO coning   | Invitrogen                          | -                |
| pENTR-D-TOPO_Rok              | Entry vector containing the CDS of Rok (C $\rightarrow$ T, position 1906)  | This Work                           | T                |
| pENTR-D-TOPO_RokCA            | Entry vector containing the CDS of constitutive active Rok (1-553 aa)  | This Work                           | T                |
| pENTR-D-TOPO_Rok K116         | Entry vector containing the CDS of catalytic inactive Rok (K $\rightarrow$ G, position 116)  | This Work                           | T                |
| pENTR-D-TOPO_ATG:TurboID:Agel | Entry vector containing a start codon, the CDS of TurboID, and an Agel cloning site  | This Work                           | T                |
| pENTR-D-TOPO_TurboID:SmashPM  | Entry vector containing the CDS of TurboID:SmashPM   | Beati, 2013                         | -                |
| pENTR-D-TOPO_Ajuba            | Entry vector containing the CDS of Ajuba   | This Work                           | T                |
| pAMW                          | Destination vector containing an Act5C promoter, a Gateway cassette, and an N-terminal 6x Myc tag                                      | Drosophila Genomics Resource Center | -                |
| pAGW                          | Destination vector containing an Act5C promoter, a Gateway cassette, and an N-terminal GFP tag   | Drosophila Genomics Resource Center | -                |
| pUASp-attB-rfA-eGFP           | Vector for fly injection containing attB site for $\Phi$ C31 mediated integration, UASp element, Gateway cassette, C-terminal eGFP tag | Drosophila Genomics Resource Center | -                |
| pUASp-attB-eGFP-rfA           | Vector for fly injection containing attB site for $\Phi$ C31 mediated integration, UASp element, Gateway cassette, N-terminal eGFP tag | Drosophila Genomics Resource Center | -                |
| pUAST-attB-eGFP-rfA           | Vector for fly injection containing attB site for $\Phi$ C31 mediated integration, UAST element, Gateway cassette, N-terminal eGFP tag | Drosophila Genomics Resource Center | -                |
| pAGW-SmashPM                  | Expresses GFP:SmashPM under the control of Act5c promoter  | Beati, 2013                         | -                |
| pAGW-Rok                      | Expresses GFP:Rok_mut under the control of Act5c promoter  | This Work                           | G                |
| pAGW-RokCA                    | Expresses GFP:RokCA under the control of Act5c promoter  | This Work                           | G                |
| pAGW-Rok K116                 | Expresses GFP:Rok K116 under the control of Act5c promoter   | This Work                           | G                |
| pAMW-Rok                      | Expresses Myc:Rok under the control of Act5c promoter  | Peek, 2019                          | -                |
| pAHW-Rok                      | Expresses HA:Rok under the control of Act5c promoter   | Peek, 2019                          | -                |
| pAGW-RokCA                    | Expresses GFP:RokCA under the control of Act5c promoter  | This Work                           | G                |
| pAGW-Rok K116                 | Expresses GFP:Rok K116 under the control of Act5c promoter   | This Work                           | G                |
| pAMW-Ajuba                    | Expresses GFP:Ajuba under the control of Act5c promoter  | This Work                           | G                |
| pAWM-mCD8                     | Expresses mCD8:Myc under the control of Act5c promoter   | This Work                           | G                |
| pAWG-mCD8                     | Expresses mCD8:GFP under the control of Act5c promoter   | This Work                           | G                |

| Plasmid name                         | Description   | Source                     | Cloning strategy |
|--------------------------------------|---|----------------------------|------------------|
| pGEX-4T-3                            | Cloning vector to express GST-tagged fusion proteins  | Amersham Pharmacia Biotech | -                |
| pGEX-4T-3-Sqh                        | Expresses GST-Sqh   | This Work                  | GA               |
| pWalium-UAS::V5:TurboID:NES          | Expresses TurboID N-terminal tagged with V5 & C-terminal tagged with NES under the control of UAS   | Addgene #116904            | -                |
| pAGW-TurboID:SmashPM                 | Expresses GFP:TurboID:SmashPM fusion protein under the control of Act5c promoter  | This Work                  | R, T, G          |
| pAWG-TurboID                         | Expresses TurboID:GFP under the control of Act5c promoter   | This Work                  | R, T, G          |
| pUASp-attB-rfa-eGFP-TurboID*         | Expresses TurboID:eGFP under the control of UASp  | This Work                  | R, T, G          |
| pUASp-attB-eGFP-rfa-TurboID:SmashPM* | Expresses eGFP:TurboID:SmashPM under the control of UASp  | This Work                  | R, T, G          |
| pUASp-attB-eGFP-rfa-SmashPM*         | Expresses eGFP:SmashPM under the control of UASp  | Beati et al., 2018         | -                |
| pUAST-attB-eGFP-rfa-SmashPM*         | Expresses SmashPM N-terminal tagged with eGFP under the control of UAST   | Beati et al., 2018         | -                |
| pUAST-attB-eGFP-rfa-SmashPM N-term*  | Expresses eGFP:SmashPM N-term under the control of UAST   | This Work                  | G                |
| pUAST-attB-eGFP-rfa-SmashPM mut*     | Expresses eGFP:SmashPM mut under the control of UAST  | This Work                  | G                |
| pBlueScript KS(-)                    | Standard cloning vector containing an MCL.  | Lab stock collection       | -                |
| pScarlessHD-sfGFP-dsRed              | Donor vector for HDR, contains sfGFP CDS and 3xP3::dsRed selection marker flanked by PBac sites   | Addgene #80811             | -                |
| pU6-BbsI-chiRNA                      | U6 promoter drives expression of sgRNA  | Addgene #45946             | -                |
| pU6-BbsI-chiRNA-sgRNA3               | U6 promoter drives expression of sgRNA, targets SmashPM   | This Work                  | R                |
| pBlueScript-sgRNA3_sfGFP*            | Donor repair template containing sfGFP CDS flanked by homolog regions targeting SmashPM   | This Work                  | GA               |
| pU6-BbsI-chiRNA-sgRNA7               | U6 promoter drives expression of sgRNA, targets SmashPI/PJ  | This Work                  | R                |
| pScarlessHD-sfGFP-dsRed-HA-sgRNA7*   | Donor repair template containing the CDS of sfGFP which is flanked by homolog regions targeting SmashPI/PJ & 3xP3::dsRed selection marker flanked by PBac sites | This Work                  | GA               |

\* Plasmid map is shown in the supplementary material

## 2.1.8 Oligonucleotides

**Table 6: List of oligonucleotides.** The list contains names, sequences, and the purpose of the used oligonucleotides.

| Name               | 5'- Sequence -3'                                  | Purpose  |
|--------------------|---|--|
| RokCA_F            | CCAGCTGGACGAGAACTG                                | Amplifies CACC + RokCA + stop codon                      |
| RokCA stop R       | TCAATTGAGGTCGCGTGCCCG                             |  |
| Rok K116G F        | GTACGCCATGGGGCGGCTGTCC                            | Mutagenesis PCR to generate pENTR-D-TOPO_Rok K116        |
| Rok K116G R        | ACCTGGCTGGAGGACTTG                                |  |
| TOPO ATG TurboID F | CACCATGGCTAGCAAAGACAATACTGTG                      | Amplifies ATG:TurboID:Agel                               |
| Turbo:Agel R2      | ACCGGTCTGCAGCTTTTCGGCAGAC                         |  |
| SmashPM:Agel F     | TCCACCGGTGAGGCCACTGATCAGGAGGTC                    | Amplifies Agel:SmashPM:Agel                              |
| Smash:Agel R       | GAAACCGGTTTAGACGCAGCTGAACTTAATG                   |  |
| TOPO Ajuba F       | CACCATGACCACCCAGCGGAC                             | Amplifies CACC + Ajuba + stop codon                      |
| Ajuba R            | TTATCCCATATACTGGTACGAAG                           |  |
| Sqh F2             | TGGTTCCGCGTGGATCCCGATGTCATCCCGTAAGACC             | Amplifies Sqh with overhangs for GA                      |
| Sqh R2             | GCCGCTCGAGTCGACCCGGGTTACTGCTCATCCTTGTC            |  |
| TOPO SmashPM F     | CACCATGGAGGCCACTGATC                              | Amplifies CACC + SmashPM N-term + stop codon             |
| SmashPM N-term R   | TTATGGCTTGGTTGTCGCCTC                             |  |
| SmashPM mut F2     | TGACAATGCGGCATCATCGAGACGAAAACGTG                  | Mutagenesis PCR to generate pENTR-D-TOPO_SmashPM mut     |
| SmashPM mut R2     | AGGTTGTTCCGCCCTCTCTGGCTCCTCCTTC                   |  |
| sgRNA3 F           | CTTCGCAGCATGACCTCTGATCAG                          | Primers to generate pU6-BbsI-chiRNA-sgRNA3               |
| sgRNA3 R           | AAACCTGATCAGGAGGTCATGCTGC                         |  |
| sgRNA3 LHA F       | ACCGCGGTGGCGGCCGCTCTAGAAGTGTGCGAATACCCCTG GCTTAC  | Primers to generate pBlueScript_sgRNA3_sfGFP by GA       |
| sgRNA3 LHA R       | CGCCCTTGGACACAGTGGCCTCCATATGGAGCTC                |  |
| sgRNA3 sfGFP F     | TCCATATGGAGGCCACTGTGTCCAAGGGCGAGGA                |  |
| sgRNA3 sfGFP R     | TGACCTCTGATCAGTCTTGTACAGCTCATCCATGC               |  |
| sgRNA3 RHA F       | ATGAGCTGTACAAGACTGATCAGGAGGTCATGC                 |  |
| sgRNA3 RHA R       | AGGTGACGGTATCGATAAGCTTGATATCGGACGAGCTTAAT GAGGCAC |  |
| sgRNA7 F           | CTTCGATCAACGAAGCTTTGAAT                           | Primers to generate pU6-BbsI-chiRNA-sgRNA7               |
| sgRNA7 R           | AAACATTCAAGAGCTTCGTTGATC                          |  |
| sfGFP sgRNA7 F     | ACAGATCAACGAAGCTCTTGATGGTGTCCAAGGGCGAG            | Primers to generate pScarlessHD-sfGFP-dsRed-sgRNA7 by GA |
| sfGFP sgRNA7 R     | AATAGCTTGACAGCCCAATTTCTGTACAGCTCATCCATGC          |  |
| sgRNA7 LHA R2      | TCCTCGCCCTTGGACACCATCAAGAGCTTCGTTGATCTG           |  |
| sgRNA7 RHA F       | CATGGATGAGCTGTACAAGAAATTGGCGCTGCAAGCTATTG         |  |
| sgRNA7 LHA R       | GGAACCTCCAGATCCACCAAGGGCGCAAGAGCTTCGTTGATC TG     |  |
| sgRNA7 RHA F       | GGTGGTTCAGGAGGTTCCAAGGGCGAATTGGCGCTGCAAGCT ATTG   |  |
| sgRNA7 LHA R       | GGAACCTCCAGATCCACCAAGGGCGCAAGAGCTTCGTTGATC TG     |  |
| sgRNA7 RHA F       | GGTGGTTCAGGAGGTTCCAAGGGCGAATTGGCGCTGCAAGCT ATTG   |  |
| sgRNA LHA OH F     | ATACGACTCACTATAGGGCGAATTGAATTTAGCG                |  |
| sgRNA LHA OH R     | ACCCCTGAGCCGCCGAACCTCCAGATCCACCA                  |  |
| sgRNA RHA OH F     | GGGTGGGAGGTTCTGGTGGTTCAGGAGGTTCCA                 |  |
| sgRNA RHA OH R     | TTAACCTCACTAAAGGGACTAGTCCTGCAGGTT                 |  |

| Name                | 5'- Sequence -3'         | Purpose    |
|---------------------|--------------------------|------------|
| TurboID F1          | GCTAGCAAAGACAATACTGTG    | Sequencing |
| TurboID F1 seq      | CGTGAAGCTGATCATTGGGG     |            |
| SmashPM F1          | GAGGCCACTGATCAGGAGGTC    |            |
| SmashPM F1 seq      | TGATTTGGGGATCGGAACCA     |            |
| SmashPM F2 seq      | CATTGTGTGCACCTAAGCCA     |            |
| SmashPI F1          | GACAAGGCACAACATCCACAGAAG |            |
| SmashPI F2 seq      | ATCTTTTACTCGGGCCTGGA     |            |
| SmashPI F3 seq      | GATAAGATCCGGGAGCAGGG     |            |
| SmashPI F4 seq      | AGCAAAAGCGCAAATCCATG     |            |
| RokCA seq F1        | GGGACGTTAAGCCGATA        |            |
| RokCA seq F2        | GAGTCGAAGGAGGCCAAT       |            |
| Rok seq F3          | GCCGATCAGCATTCTCAG       |            |
| Rok seq F4          | ACAAGTTCAACCAGCTGC       |            |
| GST seq F           | ACCCATCCTGACTTCATGT      |            |
| Sqh Col R           | CGTGCAGATCCTCCTTCTC      |            |
| Ajuba seq F         | GTCTGGATCTCAATGCGCTG     |            |
| Exon9 seq F         | GGCCATCAATTTCCGACA       |            |
| Exon17 seq F        | GCAGGTTCCAGACAATCG       |            |
| SmashPI/PJ genome F | CACCTCATCCCACCCTAC       |            |
| SmashPI/PJ genome R | TCTGTGGATGTTGTGCCT       |            |
| SmashPM genome F    | CGTAGGAGTTCGGTGTC        |            |
| SmashPM genome R    | CTCCTGATCAGTGGCCTC       |            |
| GFP F               | TGAAGTTCATCTGCACCACC     |            |
| GFP R               | GTGTTCTGCTGGTAGTGGTC     |            |
| GFP seq F           | GTGAGCAAGGGCGAGGAGCTGT   |            |
| GFP seq R           | CTTGTACAGCTCGTCCATGCCGA  |            |
| eGFP seq1           | CAAAGACCCCAACGAGAAGC     |            |
| eGFP seq F2         | CATCGACTTCAAGGAGGAC      |            |
| sfGFP seq F         | ATGACGGCACCTACAAGA       |            |
| sfGFP seq R         | ACGTTGTGGCTGTTGAAG       |            |
| M13 F               | TGTAACGACGCGCCAGT        |            |
| M13 R               | GGAAACAGCTATGACCAT       |            |

### 2.1.9 Kits

|  |                          |
|--|--------------------------|
| Pierce™ BCA Protein Assay Kit            | Thermo Fisher Scientific |
| Nucleo Spin® Gel and PCR Clean-up kit    | MACHEREY-NAGEL           |
| pENTR™/D/TOPO™ cloning kit               | Thermo Fisher Scientific |
| Q5 Site-Directed Mutagenesis Kit         | New England Biolabs      |
| GeneArt™ Gibson Assembly Hifi Master Mix | Thermo Fisher Scientific |
| Gateway™ LR Clonase™ II Enzyme-Mix       | Thermo Fisher Scientific |
| NucleoBond XTra Midi Kit                 | MACHEREY-NAGEL           |

### 2.1.10 Imaging systems

|                      |                      |
|----------------------|----------------------|
| LSM 880 Airyscan     | Carl Zeiss Jena GmbH |
| LSM 980 Airyscan 2   | Carl Zeiss Jena GmbH |
| Binocular Stemi 2000 | Carl Zeiss Jena GmbH |
| Axio Imager Z1       | Carl Zeiss Jena GmbH |

### 2.1.11 Technical devices

|                         |                       |
|-------------------------|-----------------------|
| ChemoCam Imager         | Intas Science Imaging |
| Mastercycler            | Eppendorf             |
| Turbo Cycler            | Blue-Ray Biotech      |
| Incubator Function Line | Heraeus               |
| Incubator HT Minitron   | Infors                |
| Centrifuge Z 216 M      | Hermle                |
| Centrifuge Z 446 K      | Hermle                |
| Nanophotometer P330     | Implen                |
| Thermomix Comfort       | Eppendorf             |
| Biophotometer           | Eppendorf             |

### 2.1.12 Software

Geneious Prime® 2023.0.4  
Fiji ImageJ 2.9.0  
Zen Black 2.3 SP1 FP3  
RStudio 2023.03.1  
IBM SPSS Statistics 29.0.1.0  
BioRender  
Perseus 1.6.15.0

## 2.2 Methods

### 2.2.1 Fly work

#### 2.2.1.1 Fly breeding

Flies were kept in vials containing standard fly food at 25 °C. Embryos were obtained by keeping flies in a cage at 25 °C, where they laid their eggs on an apple juice plate.

#### 2.2.1.2 Fly Food Standard medium (Ashburner 1989)

Add following ingredients in 8 L heated water and mix until foam forms:

|                |       |
|----------------|-------|
| Agar Agar      | 50 g  |
| Brewer's yeast | 168 g |
| Soy flour      | 95 g  |

The following ingredients were added one by one. Mix in between:

|              |       |
|--------------|-------|
| Malt extract | 450 g |
| Treacle      | 400 g |
| Polenta      | 712 g |

Cook the food for 45 minutes. Let it cool down to 60 °C and add 45 ml of propionic acid and 150 ml of 10 % Nipagin. Distribute food into vials.

#### 2.2.1.3 Apple agar plates

|                  |        |
|------------------|--------|
| Agar Agar        | 20 g   |
| Sugar            | 8.5 g  |
| Apple juice      | 170 ml |
| H <sub>2</sub> O | 500 ml |

The mixture was heated until the agar had dissolved completely. The solution was cooled down to 60 °C. Then, 10 ml of 10 % Nipagin was added, and the solution was poured into petri dishes. Store plates at 4 °C.

#### 2.2.1.4 Gal4-UAS System

The Gal4-UAS system is a two-component system that was originally derived from yeast. It was adapted to *Drosophila* to drive ectopic, tissue-specific gene expression (Brand & Perrimon, 1993). This system consists of the Gal4 transcriptional activator and its binding site, the so-called upstream activation sequence (UAS). A specific promoter drives the expression of Gal4. The Gal4 protein binds to the UAS and thereby it can control the transcriptional activation of its downstream target (Brand & Perrimon, 1993). Depending on the used promoter and the UAS element (UAS<sub>T</sub> or UAS<sub>Sp</sub>) (Rørth, 1998), the expression of the target gene can vary in strength, period, and localization. In *Drosophila*, flies from a driver and a reporter line need to be crossed, resulting in progeny expressing Gal4 and the target gene under the control of UAS.

### 2.2.1.5 Fly crossing

For the TurboID proximity labeling assay, the following fly crosses were set up:

1. ♀; P{matalpha4-GAL-VP16}V37 x ♂ w; UASp::TurboID:eGFP
2. ♀; P{matalpha4-GAL-VP16}V37 x ♂ w; UASp::eGFP:TurboID:SmashPM
3. ♀; P{matalpha4-GAL-VP16}V37 x ♂ w; UASp::eGFP:SmashPM

F<sub>2</sub> embryos were used for the assay.

For overexpression experiments in the follicle epithelium, the following crosses were set up:

1. ♀ tj:G4 x ♂ UAST::mCD8:eGFP ;
2. ♀ tj:G4 x ♂ ; UAST::eGFP:SmashPM
3. ♀ tj:G4 x ♂ ; UAST::eGFP:SmashPM N-term
4. ♀ tj:G4 x ♂ ; UAST::eGFP:SmashPM mut

The offspring of these crosses was used for the experiment.

To induce stochastic overexpression in the follicle epithelium, the following crosses were set up:

1. ♀ hsflp;;act<CD2<G4 x ♂ UAST::mCD8:eGFP ;
2. ♀ hsflp;;act<CD2<G4 x ♂ ; UAST::eGFP:SmashPM
3. ♀ hsflp;;act<CD2<G4 x ♂ ; UAST::eGFP:SmashPM N-term
4. ♀ hsflp;;act<CD2<G4 x ♂ ; UAST::eGFP:SmashPM mut

The adult female offspring of these crosses were heat-shocked at 37°C for 10 minutes in a water bath. One day after heat-shock treatment, ovaries were dissected.

For the generation of germline clones, the FLP/FRT *ovo*<sup>D</sup> system (Chou & Perrimon, 1992) was used. This system is based on a recombinant flippase (FLP) that originates from *Saccharomyces cerevisiae*. It targets specific DNA regions, so-called flippase recognition target (FRT) sites, mediating site-directed recombination during mitosis. This system often uses a heat-shock (hs) promoter, enabling the controlled induction of mitotic recombination. In combination with the germline-dependent female sterile *ovo*<sup>D</sup> mutation, it is possible to create homozygous mutant germline clones. In this study, females carrying the *ovo*<sup>D2</sup> mutation were used (Busson et al., 1983). The expression of the flippase was induced by heat-shock treatment of F<sub>1</sub> L2 larvae at 37 °C for 2 h in a water bath on two consecutive days. To generate germline clones of the respective mutant allele, the following crosses were set up:

$$F_0: \text{♀} \frac{\text{mutant allele, FRT19A}}{\text{FM7}} \times \text{♂} \frac{\text{ovoD2, FRT19A}}{\text{xx}^{\wedge}}; \text{hsflp}$$

$$F_1: \text{♀} \frac{\text{mutant allele, FRT19A}}{\text{ovoD2, FRT19A}}; \text{hsflp} \times \text{♂} \frac{\text{FM7a, dfd-YFP}}{y}$$

F<sub>2</sub> generation was used for analysis.

#### **2.2.1.6 Injection**

Early blastula stage embryos were used for injection. Embryos were dechorionated with 6.5 % sodium hypochlorite for 45 seconds. Embryos were washed thoroughly with water and arranged in a line on a piece of agar. Embryos were attached to a cover slip using heptane glue. Embryos were dried for 10 minutes. After drying, embryos were covered with VOLTALEF Oil 3S (Samaro). Using fine glass capillaries, DNA was injected into the posterior pole of the embryos. For attP site recombination, 400 ng/ $\mu$ l plasmid was injected. For the CRISPR/Cas9 approach, 100 ng/ $\mu$ l sgRNA vector and 500 ng/ $\mu$ l donor vector were injected.

#### **2.2.1.7 Live imaging of embryos**

For live imaging, embryos were dechorionated with 6.5 % sodium hypochlorite for 45 seconds. Embryos were left in water until they were arranged for imaging to prevent them from drying out. Embryos were arranged on an apple juice agar plate. Using heptane glue, they were carefully attached to a cover slip. Embryos were covered with VOLTALEF Oil 3S (Samaro) and placed on a slide. To avoid squeezing the embryos, a small spacer was placed between the cover slip and the slide. Embryos were imaged at 21 °C. Time-lapse live imaging was performed using a ZEISS Axio Imager Z1 microscope.

### 2.2.2 Molecular biology

Molecular methods were performed according to standard protocol.

To clone the TurboID constructs for the biotin proximity labeling assay, the sequence of TurboID was amplified from pUAS-V5-TurboID-NES (Addgene plasmid #116904) with the addition of an N-terminal CACC tag for TOPO cloning and a C-terminal AgeI restriction site. The obtained sequence for TurboID with additional tags was introduced into the pENTR-D-TOPO cloning vector using the pENTR™/D/TOPO™ cloning kit. The sequence of SmashPM was amplified by using primers that flank SmashPM with AgeI restriction sites. pENTR-D-TOPO-TurboID:AgeI and AgeI:SmashPM:AgeI were digested with AgeI. The desired fragments were gel purified and used for ligation. The vector pENTR-D-TOPO-TurboID:AgeI and pENTR-D-TOPO\_TurboID:SmashPM were used for LR reaction to insert TurboID:AgeI and TurboID:SmashPM into the desired destination vectors.

For overexpression experiments in follicle epithelium, the CDS of SmashPM N-term and SmashPM mut were cloned into the pENTR-D-TOPO cloning vector. pENTR-D-TOPO\_SmashPM and pENTR-D-TOPO\_mCD8 were available in the lab stock collection. pENTR-D-TOPO\_SmashPM was used as a template for mutagenesis PCR to generate pENTR-D-TOPO\_SmashPM mut. The origin sequence encodes EEWQNNLDNWKSS. Codons encoding amino acids highlighted in red were mutated in such a way that the respective amino acid residues were replaced by alanine (A). The corresponding primers can be found in Table 6. To generate pENTR-D-TOPO\_SmashPM N-term, pENTR-D-TOPO\_SmashPM was used as a template to amplify SmashPM N-term with corresponding primers (see Table 6). SmashPM N-term comprises the first 1929 bp of SmashPM. An additional stop codon was added at the end of the sequence. pENTR-D-TOPO\_SmashPM, pENTR-D-TOPO\_SmashPM N-term, pENTR-D-TOPO\_SmashPM mut, and pENTR-D-TOPO\_mCD8 were inserted into the desired destination vectors by using LR reaction.

To generate an in-frame sfGFP knock-in insertion line, a homology-directed repair (HDR) CRISPR/Cas9 approach was used. For this purpose, three components were needed: the Cas9 enzyme, a target-specific sgRNA, and a donor repair template mediating the site-directed insertion. To supply the Cas9 enzyme, nos::Cas9:mSA expressing embryos were used for injection of the sgRNA and the donor repair template. For the selection of a suitable sgRNA, the Optimal Target Finder Tool (Gratz et al., 2014) was used. The vasa-Cas9 line (BL# 551324) genome was used as a reference. Natural occurring single nucleotide polymorphisms (SNPs) can lower the target efficiency of the sgRNA. Thus, the target region in the nos::Cas9:mSA fly strain was checked for SNPs. No SNPs were detected compared to the reference genome. As a sfGFP knock-in for both isoforms, SmashPM and SmashPI, was desired, two different sgRNAs were generated. Since sfGFP should be introduced close to the start of the coding region, the respective sequence information about both isoforms was pasted separately into the program. The genomic target sequence should fulfill the following requirements:

- 20-nt long
- followed by a 3-nt PAM sequence: NGG
- begin with a G to optimize U6-driven transcription

The parameters of the tool were set as follows:

- Selected guide length (nt): 20
- Find: All CRISPR targets
- Stringency: High
- PAM: NGG only

As depicted in Figure 14, the sgRNAs were inserted into the pU6-BbsI-chiRNA vector via the BbsI restriction sites according to the protocol described in (Gratz et al., 2015).

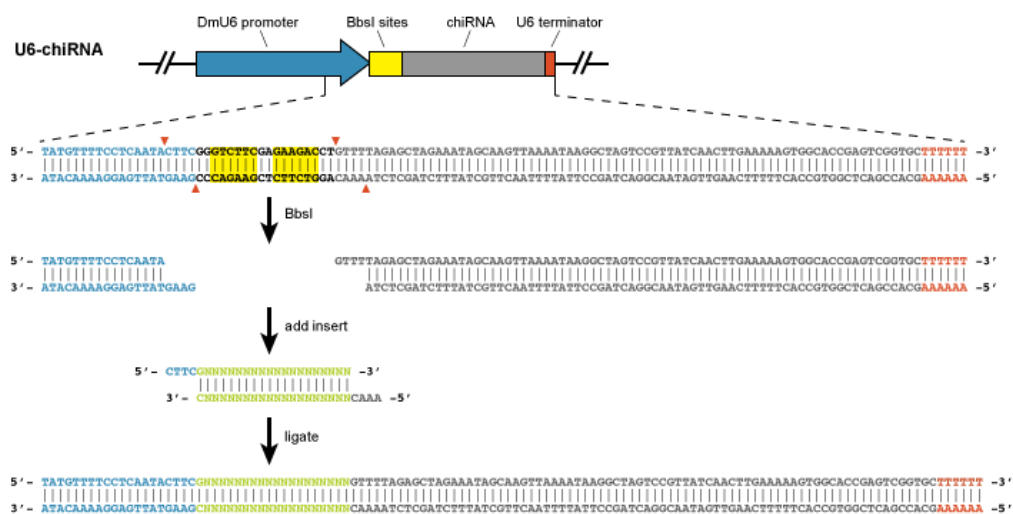


**Figure 14: Cloning procedure for the pU6-chiRNA vector.** pU6-chiRNA contains a DmU6 promoter, a BbsI restriction site, a chiRNA sequence, and an U6 terminator. The BbsI restriction sites are used to insert the sgRNA sequence into the vector backbone (source: flycrispr.org).

For this purpose, primers need to be ordered 5' phosphorylated. They were designed as described in the following template:

sense oligo: 5'- **CTTCG** (19 nt) -3'

antisense oligo: 3'- C (19 nt) **CAAA** -5'

Example:

genomic sequence: 5'- GATTACCGCTATCAGGTACCTGG -3'

sense oligo: 5'- **CTTCG**ATTACCGCTATCAGGTACC -3'

antisense oligo: 3'- CTAATGGCGATAGTCCGTGG**CAAA** -5'

For reasons of simplicity, only the sgRNAs leading to a successful in-frame sfGFP knock-in will be further mentioned.

For sfGFP tagging of SmashPM, following sgRNA was chosen:

Location: chr3R:4698577..4698599, - strand, 0 off targets (high stringency)

Selected target: sgRNA3

CAGCATGACCTCCTGATCAGTGG

Sense oligo: 5'- **CTTC**G\_CAGCATGACCTCCTGATCAG -3'

Antisense oligo: 3'- **C**GTCGTA**CTGGAGGACTAGTCCAAA** -5'

For sfGFP tagging of SmashPI, following sgRNA was chosen:

Location: chr3R:4708163..4708185, + strand, 0 off Targets (high stringency)

Selected target: sgRNA7

GATCAACGAAGCTCTGAATTGG

Sense oligo: 5'- **CTTC**GATCAACGAAGCTCTGAAT -3'

Antisense oligo: 3'- **CTAGTTGCTTCGAGAACTTACAAA** -5'

The donor repair vectors were generated by Gibson assembly using the GeneArt Gibson Assembly<sup>®</sup> Cloning kit. Therefore, the corresponding homology arms (app. 1 kb long sequences flanking the insertion site) for each sgRNA were synthesized from genomic DNA extracted from *vasa*:Cas9 flies (BL #51324). The pScarlessHD-sfGFP-dsRed vector was used in combination with sgRNA7 and its respective homology arms, while pBlueScriptKS(-) vector was used in combination with sgRNA3 and its respective homology arms. The pScarlessHD-sfGFP-dsRed vector contains a sfGFP cassette and an additional dsRed marker cassette for the identification of positive flies. After identification of positive flies, the dsRed cassette was removed and a sfGFP in-frame insertion remains. Here, only the homology arms were inserted into the already existent vector backbone. In contrast to this, the multiple cloning site (MCS) of pBlueScriptKS(-) was used to insert a sfGFP cassette flanked by the homology arms. Positive flies were identified as described in (Kina et al., 2019) via genotyping.

Both vectors, pScarlessHD-sfGFP-dsRed and pBlueScriptKS(-), were digested with EcoRI. The homology arms were amplified with appropriate primers, creating overhangs necessary for Gibson assembly. In addition, the sequence of sfGFP was amplified with appropriate primers, creating overhangs to insert it into the pBlueScriptKS(-) flanked by the homology arms. pScarlessHD-sfGFP-dsRed was assembled with the two homology arms, while the pBlueScriptKS(-) was assembled with sfGFP flanked by the homology arms. Primer information can be found in Table 6.

In a final step, nos::Cas9:mSA (Poernbacher et al., 2019) expressing embryos were injected with following vector combinations:

1. pU6-BbsI-chiRNA\_sgRNA3 + pBlueScriptKS(-)\_sfGFP\_sgRNA3
2. pU6-BbsI-chiRNA\_sgRNA7 + pScarlessHD-sfGFP-dsRed\_sgRNA7

Plasmid maps can be found in the supplementary material.

### **2.2.3 Biochemical methods**

#### **2.2.3.1 Sample preparation for mass spectrometry (MS)**

Embryos of the desired genotype were snap-frozen in liquid nitrogen. Embryos were homogenized in 1 ml of ice-cold RIPA lysis buffer (50 mM Tris-HCl pH 8.0, 150 mM NaCl, 0.5 % sodium deoxycholate, 1 % NP-40, 0.1 % SDS) freshly supplied with protease inhibitors (Pepstatin, Pefablock, Leupeptin and Aprotinin, dilute 1:500) using a motorized pistil. The protein lysate was incubated for 1 h at 4 °C under rotation. Afterwards, the lysate was centrifuged for 10 minutes at maximum speed at 4 °C. The supernatant was transferred into a fresh tube. The protein concentration was determined by using the Pierce™ BCA Protein Assay Kit. 2 mg of protein in 1 ml of buffer was used for the assay. Protein lysate was incubated for 1 h at 4 °C with 50 µl equilibrated Pierce™ Streptavidin Agarose (Thermo Fisher Scientific) beads. After incubation, beads were washed as follows: 1x with RIPA lysis buffer, 3x with wash buffer 1 (50 mM Tris-HCl pH 8.0, 150 mM NaCl, 0.1 % NP-40), 2x with wash buffer 2 (50 mM Tris-HCl pH 8.0, 150 mM NaCl, 0.5 mM EDTA). After the last wash, the buffer was completely removed and the beads were resuspended in 50 µl elution buffer (2 M Urea, 50 mM Tris-HCl pH 8.0, 5 mM DTT). 50 ng of trypsin (provided by CECAD Proteomics Facility) were added to each sample. Samples were incubated for 30 minutes at RT while shaking gently. Next, 50 µl digestion buffer (2 M Urea, 50 mM Tris-HCl pH 8.0, 50 mM CAA) was added to each sample. Samples were incubated for 30 minutes in the dark at RT while shaking gently. After incubation, samples were centrifuged for 2 minutes at 2500 x g and the supernatant was transferred into a new tube. Additional 50 µl elution buffer was added to the beads, centrifugation was repeated and both supernatants were combined. 50 ng LysC and 100 ng trypsin (provided by CECAD Proteomics Facility) were added to the supernatant and the samples were incubated overnight at 37 °C in the dark while shaking at 1000 rpm. On the following day, samples were acidified by the addition of 1 % formic acid (FA) and purified by Stage Tip purification according to the protocol provided by the CECAD proteomics facility. Purified samples were subjected to the CECAD Proteomics Facility to perform mass spectrometry analysis.

#### **2.2.3.2 Protein extraction from embryos**

Embryos were collected from agar apple juice plates, dechorionated, and snap-frozen in liquid nitrogen. Embryos were homogenized with a pistil in 500 µl ice-cold TNT lysis buffer (50 mM Tris HCl pH 8.0, 150 NaCl, 1 % Triton X-100, add proteinase inhibitors freshly before use). The samples were centrifuged for 10 minutes at maximum speed at 4 °C. The supernatant was transferred into a fresh vial. The samples were directly processed or they were stored at -80 °C until proceeding.

### 2.2.3.3 Protein extraction from S2 cells

Cells were transferred from the 6-well plate into a tube. Samples were centrifuged for 5 minutes at 1000 x g and the supernatant was discarded. Cells were washed three times in 1x PBS. Cells were centrifuged at 1000 x g for 2 minutes and resuspended in 500 µl - 1 ml TNT lysis buffer (50 mM Tris HCl pH 8.0, 150 NaCl, 1 % Triton X-100, proteinase inhibitors were added freshly before use). The samples were kept on ice for 30 minutes and gently mixed. Next, the cells were centrifuged for 10 minutes at 13000 rpm at 4 °C to remove the cell debris. The supernatant was transferred into a fresh 1.5 ml tube. The samples were directly processed or they were stored at -80 °C until proceeding.

### 2.2.3.4 Determination of protein concentration

The protein concentration of a lysate was determined with the Pierce™ BCA Protein Assay Kit (Thermo Fisher Scientific) according to the manufacturer's protocol.

### 2.2.3.5 Immunoprecipitation

Immunoprecipitation (IP) was performed either on embryonic or S2 cell lysates. Protein lysates were adjusted to 0.5 -1 mg protein in 500 µl lysis buffer supplemented with proteinase inhibitors. Before IP, 15 µl input sample was taken from the lysate. For IP, 15 µl GFP-Trap® beads (Chromotek) were used according to the manufacturer's protocol. Samples were incubated for 1 - 1 ½ h at 4 °C under rotation. Samples were centrifuged at 2500 x g for 2 minutes at 4 °C and the supernatant was discarded. Samples were washed three times with lysis buffer. Afterwards, 15 µl 2x SDS loading dye were added to the input samples and the beads. Samples were boiled for 10 minutes at 98 °C. Samples were stored at -20 °C until use. Shortly before use, they were again boiled for 5 minutes at 98 °C.

2X SDS loading dye:    125 mM Tris-HCl pH 6.8  
                              3 mM EDTA  
                              0.05 % Bromophenol blue  
                              10 % β-Mercaptoethanol  
                              5 % SDS  
                              20 % Glycerol

### 2.2.3.6 SDS-PAGE

Sodium dodecyl sulfate polyacrylamide gel electrophoresis (SDS-PAGE) is used to separate proteins based on their molecular weight. Thereby, proteins are denatured and supplemented with SDS. SDS attaches to the unfolded proteins to prevent refolding. Moreover, it decorates the protein with negative charges, which are required for protein separation. Upon creating an electrical field, negatively charged proteins migrate towards the positively charged anode. Their migration speed depends on their molecular weight. Thus, smaller proteins move faster than larger proteins through the polymerized gel. The migration speed can also be modified by the gel density (Gallagher & Wiley, 2012; Walker, 2002).

Gels were loaded with protein ruler and samples supplied with 2x SDS loading dye. They were run in a BioRad Protein III electrophoresis chamber containing 1x SDS running buffer at 170 V for 1 h.

1x SDS running buffer: 192 mM Glycine  
25 mM Tris  
0.1 % SDS

### 2.2.3.7 Western blot

After SDS-PAGE, separated proteins were transferred onto a nitrocellulose membrane by Western blotting. Therefore, a wet blotting system was used. The protein transfer was performed in a BioRad system containing 1x Western transfer buffer at 100 V at 4 °C for 1 h. Again, negatively charged proteins migrate towards the positively charged anode, thus being transferred onto the nitrocellulose membrane. A successful transfer was confirmed by Ponceau S staining. Next, the membrane was blocked for 30-60 min in Western blot blocking buffer under slight agitation. Afterwards, the membrane was incubated overnight at 4°C with the primary antibody in Western blot blocking buffer. Western blot blocking buffer containing 3 % BSA without skim milk powder was used when a phosphospecific antibody or a streptavidin-based conjugate was used for detection.

On the next day, the membrane was washed three times for 10-15 minutes with TBST while shaking. Then, it was incubated with the secondary HRP-conjugated antibody for 2 h at RT under soft agitation. The membrane was washed again and the proteins were detected by applying a chemiluminescent reagent (BM Chemiluminescence Blotting Substrate (POD), Boehringer/Roche Diagnostics). The signal was detected with the ChemoCamImager by Intas Science Imaging.

Transfer buffer: 25 mM Tris  
192 mM Glycine  
20 % MeOH  
TBST: 20 mM Tris pH 8.0  
150 mM NaCl  
0.2 % Tween-20  
Blocking buffer: 3 % Skim Milk Powder  
1 % BSA in TBST

### 2.2.3.8 Purification of GST-tagged proteins

BL21 *E. coli* bacteria were transformed with a vector expressing the protein of interest tagged with a GST tag. A 5 ml preculture was grown overnight at 37 °C under 200 rpm shaking. The next day, 100 ml of culture was inoculated with the preculture and was grown at 37 °C under 200 rpm shaking until OD = 0.6 was reached. Protein expression was induced by adding 0.5 mM Isopropyl- $\beta$ -D-thiogalactopyranosid (IPTG) and 2% EtOH. Growth was continued overnight at 16 °C under 200 rpm shaking. The next day, bacteria were harvested by centrifugation for 10 minutes at 4500 x g and the pellet was frozen in liquid nitrogen. The frozen pellet was resuspended in 5 mL lysis-buffer (50 mM Tris-HCl, pH 8.0; 100 mM NaCl; 1 mM EDTA; 1 mM EGTA, 5 mM DTT, Pefa Block, Leupeptin, Pepstatin, Apotinin, lysozyme [1 mg/mL]). Samples were incubated for 1 h on ice. Samples were sonicated on ice. A Bandelin Sonoplus HD 2070 sonicator was used with the following settings: 80 % intensity, cycle 7, 6 x 10 sec pulse and a 20 sec cooling period in between.

Triton X-100 was added to a final concentration of 1 %. Samples were gently rotated for 30 minutes at 4 °C. Samples were centrifuged at maximum speed for 30 min at 4 °C. The supernatant was transferred into a fresh tube and incubated with 50  $\mu$ L equilibrated Pierce™ Glutathione-Agarose (Thermo Fisher Scientific) for 1 h at 4 °C under rotation. Afterwards, samples were centrifuged for 5 minutes at 2500 x g and the supernatant was again transferred into a fresh tube. The supernatant can be stored at -80 °C and reused again. The beads were washed 4x in 1 mL wash buffer (50 mM Tris-HCl, pH 8.0; 300 mM NaCl, 1 mM EDTA, Leupeptin, Pepstatin, Apotinin, 5 mM DTT). Samples were centrifuged each time at 500 x g for 5 min. Proteins were eluted from beads 4x with 50  $\mu$ L elution buffer (50 mM Tris, 300 mM NaCl, 1 mM EDTA, 1 mM EGTA, 20 mM glutathione pH 7.5, Leupeptin, Pepstatin, Apotinin, 5 mM DTT). After each elution step, the eluate was transferred into a fresh tube. Eluate was frozen at -80 °C. Pooled eluate was concentrated to 1 mg/mL with Vivaspin® 20 1000 MWCO PES (SARTORIUS) according to the manufacturer's protocol.

### 2.2.3.9 Kinase assay

For the kinase assay, GFP-tagged proteins were expressed in S2 cells as described in section 2.2.4.2. Protein lysates were prepared as described in section 2.2.3.3. In addition to proteinase inhibitors, phosphatase inhibitors (Pierce™ Phosphatase Inhibitor Mini Tablets, Thermo Fisher Scientific) were added to the lysis buffer. IP was performed as described in section 2.2.3.5. After the last washing step, one additional washing step with kinase buffer (50 mM Tris-HCl pH 7.5, 5 mM MgCl<sub>2</sub>, 1 mM DTT, protease inhibitors) was performed. Kinase buffer was completely removed from GFP-trap beads. For the kinase assay, all samples were covered with 17 µl kinase buffer and 1 µl of GST:Sqh (1 µg/µl) was added to each sample. When all tubes were prepared, the reaction was started by adding 2 µl ATP mix (0.3 µl 10 mM ATP and 1.7 µl kinase buffer per sample). Samples were incubated at 30 °C for 30 minutes. Samples were centrifuged at 2500 x g for 2 minutes at 4 °C. The supernatant was transferred into a new tube. 20 µl of 2x SDS loading dye was added to the beads and the supernatant. Samples were boiled for 10 minutes at 98 °C and subjected to SDS-PAGE and Western blot analysis.

## 2.2.4 Cell culture

### 2.2.4.1 Cultivation of S2 cells

S2 cells are immortalized cells derived from *Drosophila melanogaster* late-stage embryos (Schneider, 1972). They were grown at 26 °C in *Drosophila* Schneider's medium (Life technologies) supplemented with fetal bovine serum (FBS, 10%) and antibiotics (50 U Penicillin, 50 µg/ml Streptomycin). Cells were passaged once a week.

### 2.2.4.2 Cell transfection

Cells were passaged 3 days before transfection. After 3 days, the cells were counted with a Neubauer counting chamber. The transfection was performed on a 6-well plate. Each well contains 1x10<sup>6</sup> cells / 1 ml of medium. A total of 3 ml was used. FuGENE® HD transfection reagent (Promega) was used. The transfection mix contains 2 µg of each plasmid supplemented with 8 µl FuGENE® (1:4 DNA:FuGENE® ratio) in a total volume of 150 µl. Cells were incubated for 72 h at 26 °C post-transfection.

For the TurboID proximity labeling assay, cells were supplemented with a final concentration of 50 µM biotin.

## 2.2.5 Histology

### 2.2.5.1 Formaldehyde (FA) fixation of embryos

Embryos of the desired genotype were dechorionated with 6.5 % sodium hypochlorite for 3 minutes. The embryos were washed thoroughly with water and transferred into a vial. They were fixed for 20 minutes in a solution containing an equal amount of heptane and 4 % formaldehyde. Afterwards, the lower phase of fixation solution was removed and an equal volume of methanol was added. Embryos were vortexed vigorously to remove the vitelline membrane. The whole solution was discarded and the embryos were washed three times in methanol. Samples can be stored in methanol at -20 °C until proceeding with immunofluorescence staining. Critical IF stainings were directly processed without storage in methanol. This includes the use of  $\alpha$ -phosphomyosin light chain antibody and the IF staining of *Ajuba* germline clones.

### 2.2.5.2 Paraformaldehyde (PFA) fixation of embryos

Because some antibodies are sensitive to methanol, paraformaldehyde fixation was used instead of FA fixation. The procedure is the same. Methanol is replaced by 80 % ethanol and formaldehyde is replaced by paraformaldehyde. PFA fixation was used in combination with phalloidin.

### 2.2.5.3 Immunofluorescence (IF) staining of embryos

After fixation, embryos were washed three times for 10 minutes in PBSTx 0.1 % (PBS + 0.1 % Triton X-100). Next, they were blocked for 30 minutes in blocking buffer (PBSTx 0.1 % + 5 % Normal Horse Serum [NHS]). Embryos were incubated overnight at 4 °C with the primary antibody in blocking buffer. The next day, primary antibodies were discarded. The embryos were washed again three times for 10 minutes with PBSTx 0.1 %. Then they were incubated for 2 h at room temperature with secondary antibodies conjugated to a fluorophore in blocking solution. Subsequently, the embryos were incubated for 20 minutes in PBSTx 0.1 % containing Hoechst dye (1:1000) followed by two washing steps for 10 minutes in PBSTx 0.1 %. Embryos were mounted in Vectashield® Antifade Mounting Media (Vector Laboratories).

#### **2.2.5.4 Diaminobenzidine tetrahydrochloride (DAB) staining of embryos**

Embryos were fixed according to the protocol for FA fixation of embryos. After fixation, embryos were washed three times for 20 minutes with 0.1 % PBSTx. Embryos were blocked in blocking buffer (0.1 % PBSTx + 5 % NHS) for 1 h. Embryos were incubated with  $\alpha$ -Twist AB in blocking buffer (1:50) overnight at 4 °C under slight agitation. The next day, embryos were washed three times for 20 minutes with 0.1 % PBSTx. Embryos were incubated with  $\alpha$ -rabbit-biotin secondary antibody in 0.1 % PBSTx for 2 h at RT under slight agitation. Embryos were again washed three times for 20 minutes with 0.1 % PBSTx. VECTASTAIN® ABC-HRP Kit was used to detect the biotinylated secondary antibody. ABC mix was prepared (Solution A and B were diluted 1:50 in PBS) and incubated for 30 minutes at RT. Embryos were incubated with ABC mix for 30 minutes at RT. Embryos were washed three times for 15 minutes with 0.1 % PBSTx. Embryos were transferred into a multi-well plate and the remaining solution was discarded. 160  $\mu$ l of PBS, 40  $\mu$ l of DAB and 4  $\mu$ l of H<sub>2</sub>O<sub>2</sub> (0.1 %) were added to the embryos to start the reaction. To stop the reaction, the solution was discarded and the embryos were washed several times with 0.1 % PBSTx.

#### **2.2.5.5 Fixation and immunofluorescence staining of ovaries and imaginal discs**

Ovaries and imaginal discs from L3 larvae were dissected on ice in 1x PBS. They were transferred into a 1.5 ml tube and fixed for 10 minutes in 4 % FA at RT under slight agitation. Afterwards, the tissue was washed three times for 10 minutes in PBSTx 0.3 %. Next, samples were blocked for 30 minutes in blocking buffer (PBSTx 0.3 % + 5 % NHS). The tissue was incubated overnight at 4 °C with the primary antibody in blocking buffer. The next day, primary antibodies were discarded. The samples were washed again three times for 10 minutes with PBSTx 0.3 %. Then they were incubated for 1 h at RT with secondary antibodies conjugated to a fluorophore in blocking solution. Subsequently, the samples were incubated for 10 minutes in PBSTx 0.3 % containing Hoechst dye (1:1000) followed by two washing steps for 10 minutes in PBSTx 0.3 %. Ovaries and imaginal discs were mounted in Vectashield® Antifade Mounting Media (Vector Laboratories).

### **2.2.6 Mass spectrometry data analysis**

Data obtained by mass spectrometry was analyzed using Perseus (1.6.15.0). For the analysis, raw data was uploaded in Perseus. Categorical variables were removed, Label-Free Quantification (LFQ) intensity values were  $\log_2$  transformed, intensity Based Absolute Quantification (iBAQ) intensity values were  $-\log_{10}$  transformed. Technical replicates were annotated as groups. Data was filtered based on values appearing in at least three out of four replicates in at least one group. Missing values were imputed from the normal distribution. ANOVA and Student's T-test were performed using standard parameters (FDR = 0.05 and S0 = 0.2) for statistical analysis. Cut-off lines were modulated by FDR and S0. Data was exported and used to build figures in RStudio.

### 3 Results

#### 3.1 *smash*<sup>Δ35m/z</sup> null allele mutant embryos show early morphogenetic defects

Multiple aspects of morphogenesis rely on actomyosin contractility, which is regulated by a complex protein interaction network (Agarwal & Zaidel-Bar, 2019; Miao & Blankenship, 2020). Previous work identified the LIM domain-containing protein Smash as a novel player within this network regulating actomyosin contractility (Beati et al., 2018). The importance of Smash during morphogenesis becomes clear in *smash*<sup>Δ35m/z</sup> null allele mutant embryos, which show severe, in most cases lethal, morphogenetic defects. Despite of these severe morphogenetic defects, some embryos survive and develop until adulthood, revealing a highly variable phenotype that is not fully penetrant. A detailed phenotypic analysis of *smash*<sup>Δ35m/z</sup> mutants is required to improve our understanding of Smash function. To investigate the variability and penetrance of the mutant phenotype, the embryonic morphology of *smash*<sup>Δ35m/z</sup> mutants was observed throughout all developmental stages. To better visualize the structure of the embryos, α-Twist staining labeling the mesoderm was performed. Figure 15 gives an overview of the variability of the *smash*<sup>Δ35m/z</sup> mutant phenotype in different embryonic stages.

A fraction of embryos showed a WT-like appearance. The other fraction consisted of abnormal embryos showing defects already very early during morphogenesis. During early embryonic development stages 5-6, Twist staining was frequently irregular and appeared in a speckled pattern on the ventral side of the embryos compared to WT-like embryos. A fraction of these early embryos appeared to have problems in ventral furrow formation with the invagination process being only partially completed (9/18 embryos showed the described morphogenetic defects). During stages 7-8, the rapid phase of germ band elongation takes place. Although *smash*<sup>Δ35m/z</sup> embryos looked abnormal because of the irregular Twist staining (12/23 stage embryos), germ band elongation appeared to be initiated. In stages 9-10, germ band elongation was almost complete, revealing that abnormal embryos were able to stretch their germ band. Nevertheless, the mesoderm was often not fully invaginated (20/37 embryos). In stages 11-12, most of the analyzed embryos superficially showed a WT-like phenotype (14/17 embryos). Later embryonic stages (13-16) usually showed a strongly defective morphology, for example, irregular segmentation or the formation of abnormal, additional furrows (23/47 embryos showed morphogenetic defects). A lethality assay revealed that only 9 % (n = 277) of *smash*<sup>Δ35m/z</sup> null mutants reached the larval stage, whereas no increased lethality was observed in zygotic *smash*<sup>Δ35</sup> mutants (see supplementary material for further details).

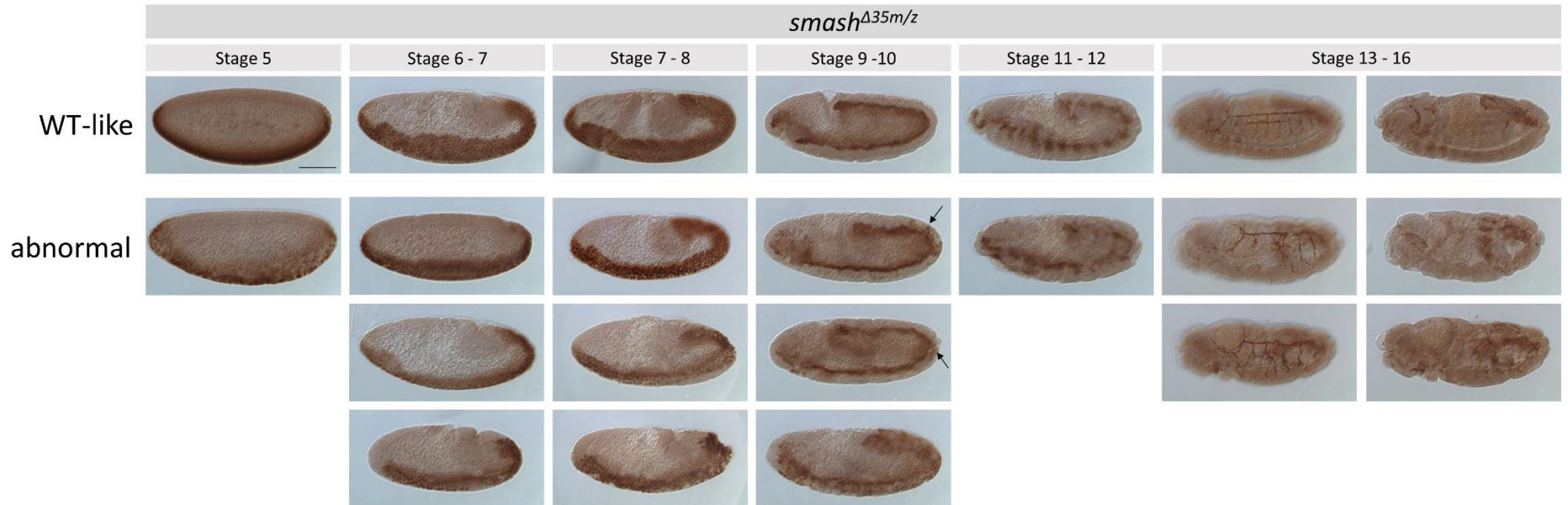


**Figure 15: Phenotypic analysis of *smash*<sup>Δ35m/z</sup> mutant embryos.** Using single embryos as an example, the phenotypic variability of *smash*<sup>Δ35m/z</sup> mutant embryos is shown in different embryonic stages. Arrows point to mesoderm, which was not completely invaginated. Stages are indicated above the panels. Staging was performed according to Campos-Ortega & Hartenstein (1997). Embryos were stained with  $\alpha$ -Twist antibody. Scale bar: 100  $\mu$ m.

### 3.2 The phosphorylation of Sqh is strongly reduced upon loss of Smash

Morphogenetic defects occurring in *smash*<sup>A35m/z</sup> mutant embryos raise the question: What is the reason for these defects? Previous studies showed that actomyosin contractility is reduced in *smash*<sup>A35m/z</sup> null mutant embryos (Beati et al., 2018). Since actomyosin contractility is regulated by the amount of phosphorylated Sqh (Vasquez et al., 2016; Vasquez et al., 2014), we tested whether Sqh phosphorylation is affected in *smash*<sup>A35m/z</sup> mutant embryos. The first evidence for this was already shown in Peek (2019). In *w*<sup>1118</sup> embryos, which we used as WT reference, membrane-associated Smash was detected using an antibody against the N-terminus of Smash. The membrane-associated Smash signal co-localized with phosphomyosin and E-Cadherin signals (Figure 16). In contrast, the membrane-associated signal of Smash was abolished in *smash*<sup>A35m/z</sup> mutant embryos. Instead, a speckled pattern appeared that was later found to be caused most likely by cross-reactivity of the  $\alpha$ -Smash N-terminal antibody with *Wolbachia* bacteria present in the *smash*<sup>A35</sup> mutant fly stock. Moreover, the amount of phosphorylated Sqh was drastically reduced in *smash*<sup>A35m/z</sup> embryos compared to WT (Figure 16).

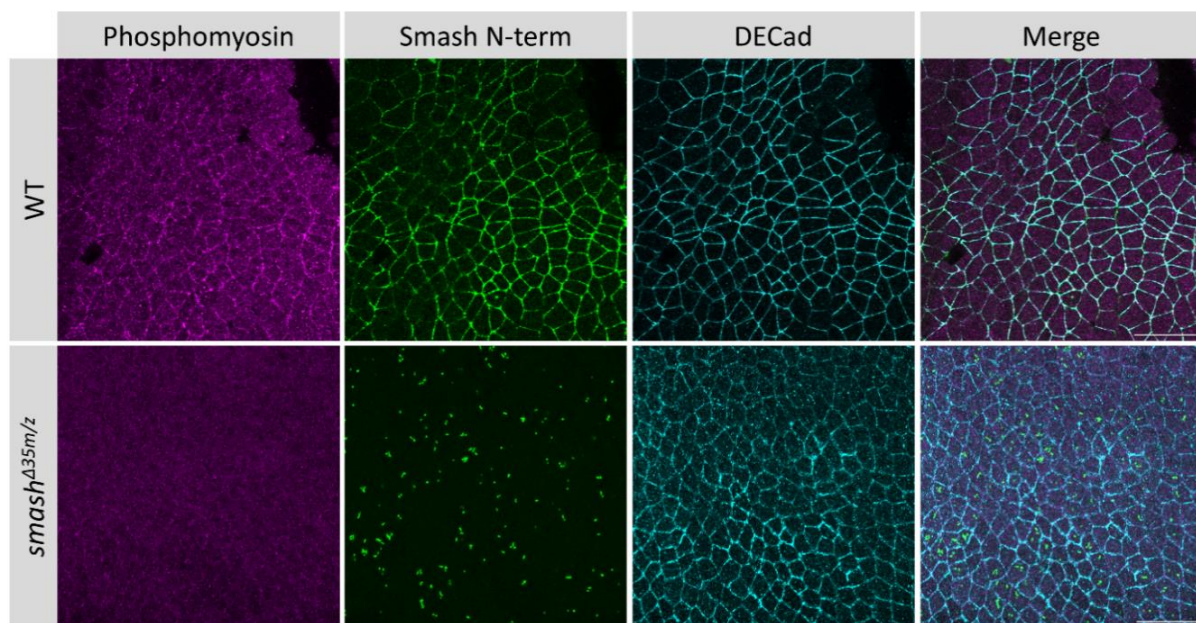


**Figure 16: Phosphomyosin signal is reduced in *smash*<sup>A35m/z</sup> mutant embryos compared to WT.** Optical sections above the ventral midline of stage 8 embryos are depicted. Antibodies used for IF staining are indicated above each panel. Scale bar: 20  $\mu$ m.

Although the *smash*<sup>A35</sup> embryonic phenotype could only be observed when maternal and zygotic Smash was fully depleted, there is evidence that Smash is not a classical maternal gene since paternal genotype seems to influence the phenotype of the offspring. In embryos from homozygous mutant mothers that were mated with males heterozygous for the *smash*<sup>A35</sup> mutation, residual Sqh phosphorylation was detected. This was correlated with a weak expression of Smash, most likely of zygotic origin (Figure S 1). A strong reduction of Sqh phosphorylation only occurs in the complete absence of Smash (Figure 16). In conclusion, the loss of Smash leads to a strong decrease in Sqh phosphorylation.

### 3.3 Smash does not affect the phosphorylation of Sqh *in vitro*

The strong reduction of Sqh phosphorylation in *smash*<sup>Δ35m/z</sup> mutant embryos is a plausible reason for the observed morphogenetic defects. Nevertheless, the question remains: Why is there such a strong decrease in Sqh phosphorylation level? It was shown that Smash directly interacts with Rok (Peek, 2019). Rok is responsible for Sqh phosphorylation, thereby activating actomyosin contractility (Amano et al., 1996; Amano et al., 2010; Verdier, Guang Chao, et al., 2006). Moreover, it has been shown that Shroom, another Smash and Rok binding partner, directly affects Rok activity (Nishimura & Takeichi, 2008; Peek, 2019; Zalewski et al., 2016). Thus, a potential mechanism by which Smash might modify Sqh phosphorylation level is to act on Rok kinase activity, maybe together with Shroom. To test whether Smash has a direct effect on Rok kinase activity, an *in vitro* kinase assay was established in which the kinase activity of different Rok variants was investigated in the presence and absence of Smash. For this purpose, full-length GFP:Rok, constitutively active GFP:RokCA, and catalytically inactive GFP:Rok K116 were co-expressed in S2 cells either with GFP:SmashPM or GFP as a control. Rok kinase activity was measured by the amount of phosphorylated Sqh. The contribution of Shroom was neglected in this experiment. Respective input samples are depicted in Figure S 2. Distinct bands in the presence of constitutively active GFP:RokCA and full-length GFP:Rok were detected (Figure 17). As expected, the band intensity in GFP:RokCA samples was slightly higher compared to GFP:Rok samples. In contrast, no or only very weak bands appeared when catalytically inactive GFP:Rok K116 or no Rok was supplied. The latter two samples served as negative controls. Comparing the band intensity between samples containing GFP or GFP:SmashPM either in the presence of GFP:RokCA or GFP:Rok, no significant difference was observed. In conclusion, this assay revealed that Rok kinase activity is independent of Smash *in vitro*.

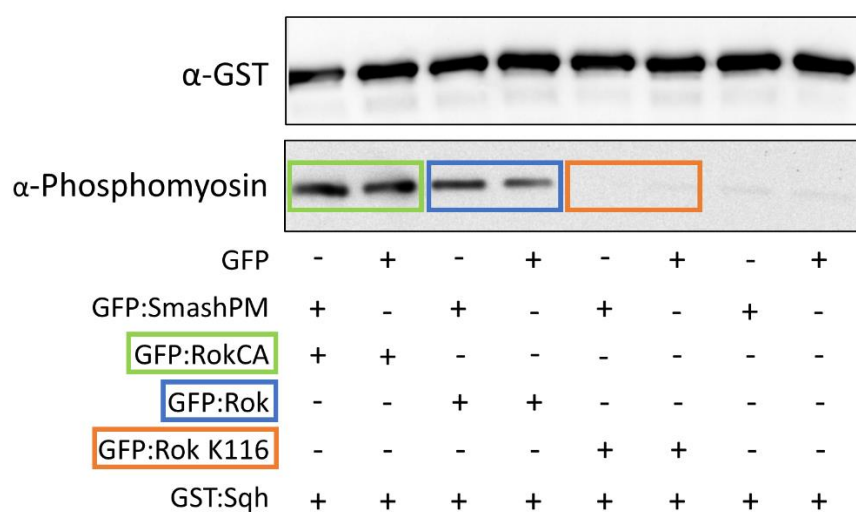


**Figure 17: Smash does not affect the phosphorylation of Sqh *in vitro*.** An *in vitro* kinase assay was performed to test whether Smash affects Rok kinase activity. Sqh phosphorylation was used to estimate Rok kinase activity. GFP:RokCA, GFP:Rok, and GFP:Rok K116 were co-expressed either with GFP:SmashPM or GFP in S2 cell culture. The kinase assay was performed after enrichment of GFP-tagged proteins from cell lysates.

### 3.4 The subcellular localization of Smash is dependent on Rok

The correct subcellular localization of proteins is important for morphogenesis because impaired subcellular protein localization often leads to morphogenetic defects (Bilder et al., 2003; Simões et al., 2010; Wodarz et al., 2000). Beati et al. (2018) and Peek (2019) demonstrated that the subcellular localization of Baz, Cno, and Sqh was altered during germ band elongation in *smash*<sup>*Δ35m/z*</sup> mutant embryos, whereas Rok subcellular localization was unaffected. The opposite way around, the loss of Baz, Cno, and F-actin led to an abnormal distribution of Smash. The effect upon loss of Sqh or Rok on the subcellular localization of Smash has not been investigated yet. Since the interaction between Smash and Rok appears to fulfill an important function in regulating actomyosin contractility during morphogenesis, this study focused on analyzing the subcellular localization of Smash upon loss of Rok during germ band elongation. For this purpose, *Rok*<sup>2</sup> germline clones were generated to determine the subcellular localization of Smash. It was reported that the subcellular localization of AJ-associated proteins such as Baz and  $\beta$ -Catenin was disturbed in *Rok*<sup>2</sup> germline clones (Simões et al., 2010). Therefore, we also investigated the subcellular localization of E-Cadherin, another AJ-associated protein. WT embryos were used as control.

The epithelial architecture in *Rok*<sup>2</sup> embryos was strongly defective in comparison to WT embryos. The typical, very regular honeycomb pattern of epithelial cells observed in WT became irregular in size and shape in *Rok*<sup>2</sup> embryos (Figure 18 A). In WT embryos, Smash was significantly enriched at A/P junctions (Figure 18 A & B) whereas E-Cadherin was significantly enriched at D/V junctions (Figure 18 A & D). In contrast, Smash and E-Cadherin were equally distributed at A/P and D/V junctions in *Rok*<sup>2</sup> embryos (Figure 18 A, B & D). To compare the distribution of Smash and E-Cadherin between WT and *Rok*<sup>2</sup> embryos, we calculated the mean AP/DV ratio. An AP/DV ratio of 1 means that the protein was equally distributed at A/P and D/V junctions. An AP/DV ratio > 1 means that the protein was enriched at A/P junctions and an AP/DV ratio < 1 means that the protein was enriched at D/V junctions. Observed differences between WT and *Rok*<sup>2</sup> embryos in Smash localization were statistically significant (Figure 18 C), whereas the differences in E-Cadherin localization were not statistically significant (Figure 18 E). From these results, we conclude that Rok regulates the subcellular localization of Smash during germ band elongation. E-Cadherin localization was also altered in *Rok*<sup>2</sup> embryos albeit the observed differences between WT and *Rok*<sup>2</sup> embryos were not statistically significant.

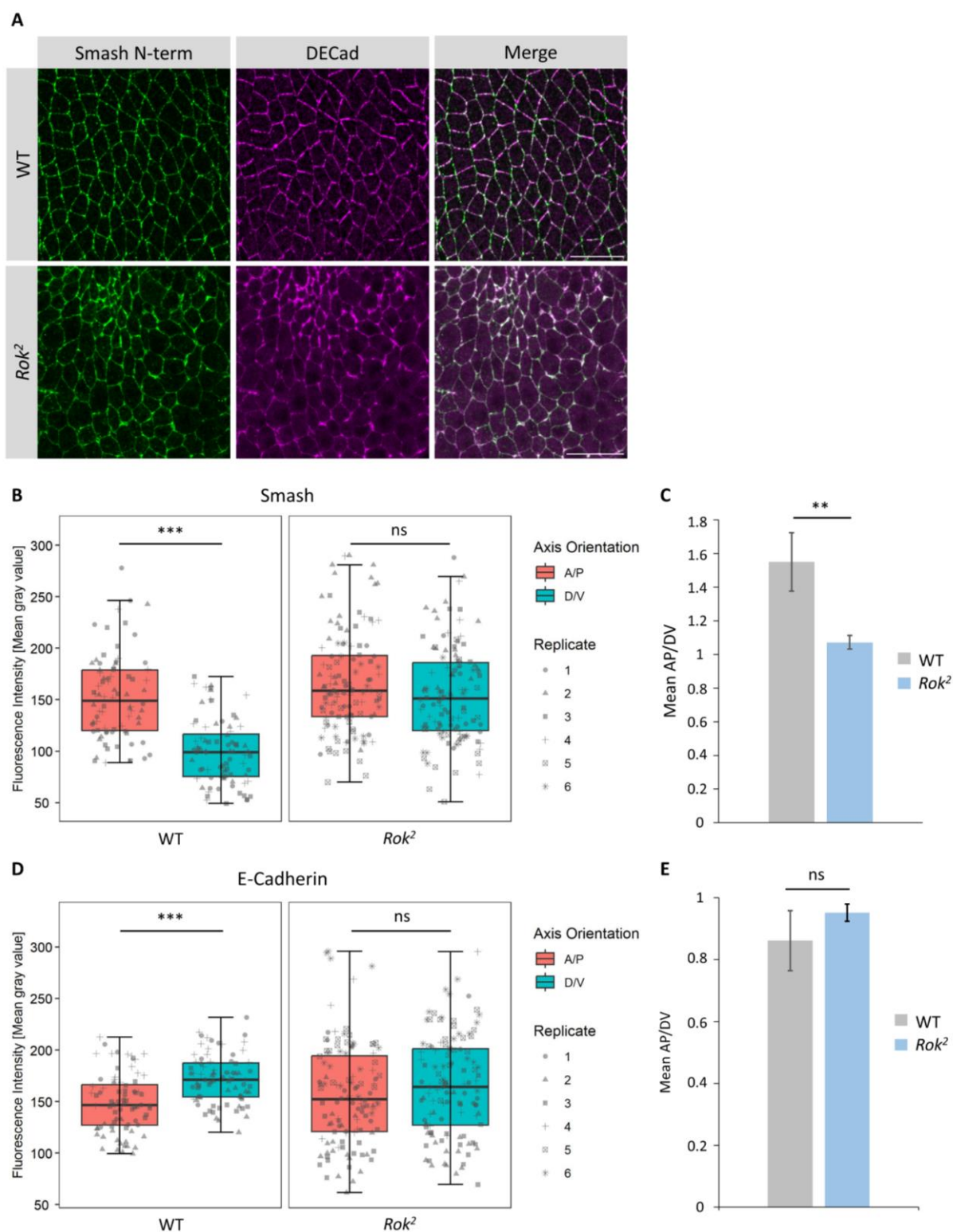


**Figure 18: Smash planar polarized localization is affected in *Rok<sup>2</sup>* embryos.** (A) An optical section of WT and *Rok<sup>2</sup>* embryos (Stage 8) is depicted. Antibodies used for IF staining are indicated above each panel. Scale bar: 20  $\mu$ m. (B & D) Smash and E-Cadherin signals were measured at A/P (60 - 90  $^{\circ}$ ) and D/V (0 -25  $^{\circ}$ ) junctions in WT and *Rok<sup>2</sup>* embryos (Stage 7 & 8). The measured signal is given as mean gray value. A Mann-Whitney U test were performed to determine the statistical significance of the difference between two samples. The significance level is indicated with asterisks. '\*\*\*':  $p < 0.0001$ ; '\*\*':  $p < 0.001$ ; ns: not significant. WT  $n = 80$ , *Rok<sup>2</sup>*  $n = 120$ . (C & E) The mean AP/DV ratio was calculated. A Mann-Whitney U test was performed to identify the statistically significant difference between two samples. The significance level is indicated. '\*\*\*':  $p < 0.001$ ; ns: not significant. WT  $n = 4$ , *Rok<sup>2</sup>*  $n = 6$ .

### 3.5 Investigation of Smash sfGFP knock-in lines

As the processes driving morphogenesis are highly dynamic, it is important that the involved components can continuously sense their environment and quickly react to changes. Therefore, a dynamic redistribution of proteins is required (summarized in Butler & Wallingford, 2018 and Zallen, 2007). Because Smash apparently functions as an actomyosin regulator, it is expected that Smash is also behaving in a highly dynamic manner. To gain a deeper insight into the spatiotemporal behavior of Smash, CRISPR/Cas9 sfGFP knock-in lines were generated to trace Smash during morphogenesis using live imaging. sfGFP is a derivative of GFP, but compared to GFP, sfGFP has a faster maturation time and a more robust folding behavior, thus maintaining fluorescent properties of the protein (Pedelacq et al., 2006). The aim was to generate two fly lines in which sfGFP was inserted to tag the N-terminal end of either SmashPM or SmashPI. A schematic overview of the CRISPR/Cas9 strategy is depicted in Figure 19. The detailed experimental design is described in the material & methods section.

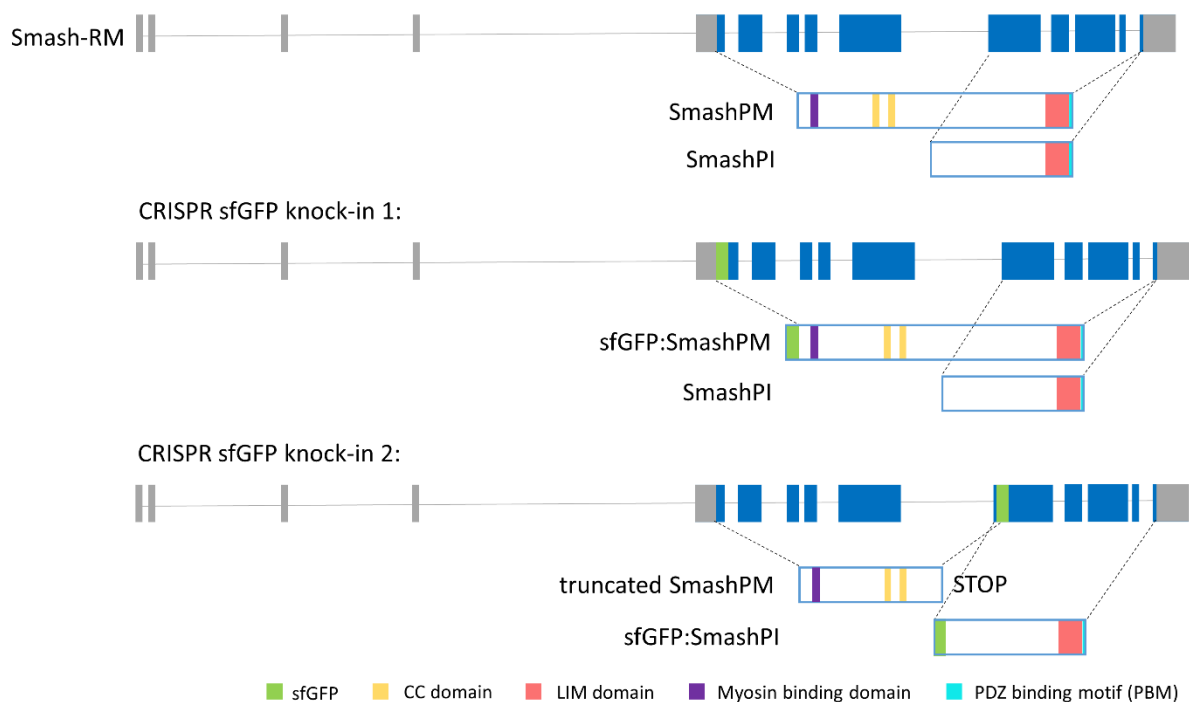
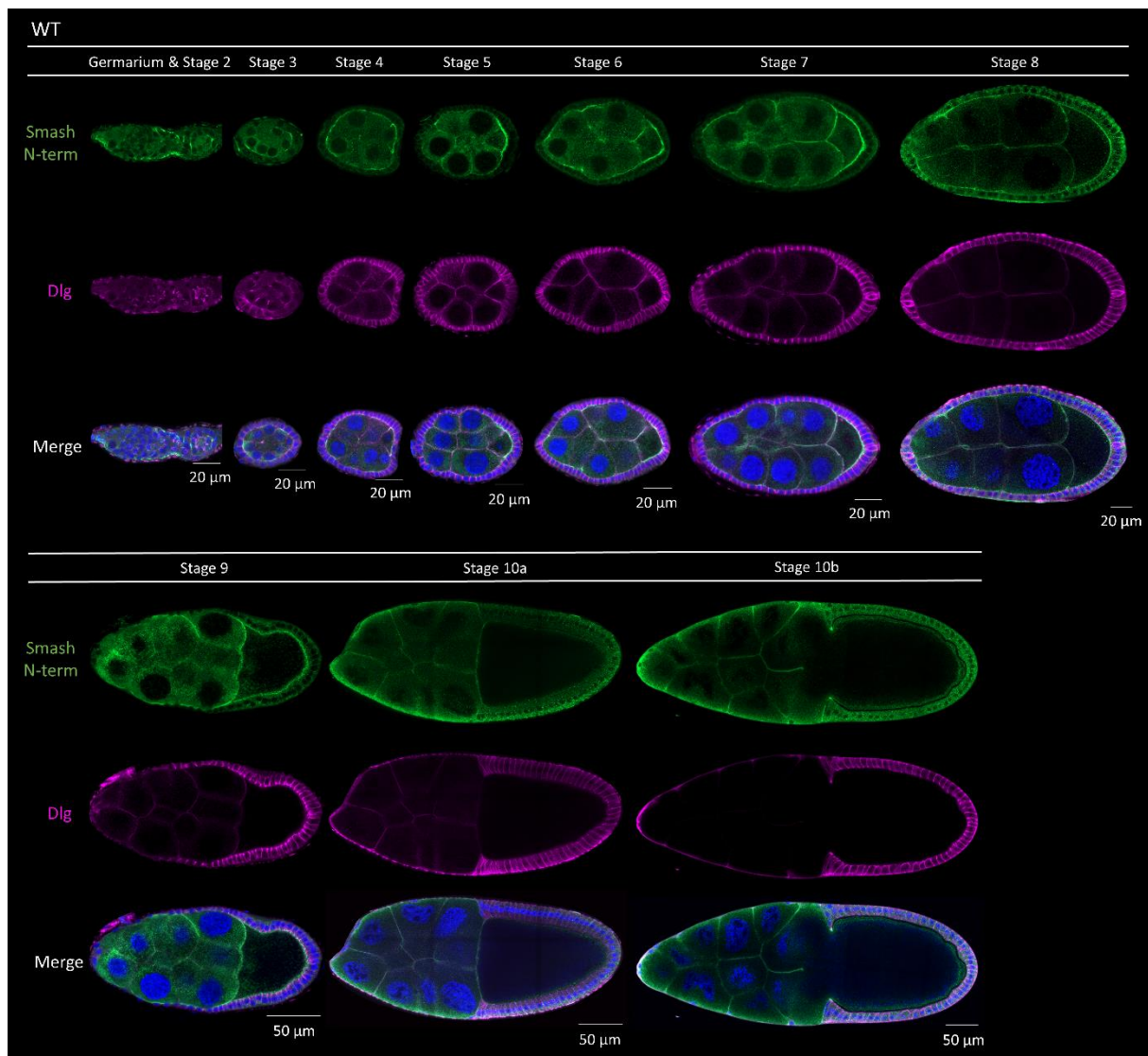


**Figure 19: CRISPR/Cas9 strategy to generate sfGFP knock-in lines targeting the *Smash* locus.** Two independent sfGFP knock-in approaches were designed. The first approach uses a sgRNA targeting the N-terminus of SmashPM. The second approach uses a sgRNA targeting the N-terminus of SmashPI, thereby interfering with the reading frame of SmashPM. In addition to functional sfGFP:SmashPI, it is predicted that a truncated version of SmashPM is translated due to an early stop codon. As a derivative of GFP, sfGFP was used for tagging. The functional domains of Smash and sfGFP are highlighted in different colors. The color code is indicated.

### **3.6 sfGFP:SmashPM resembles the localization pattern of endogenous SmashPM**

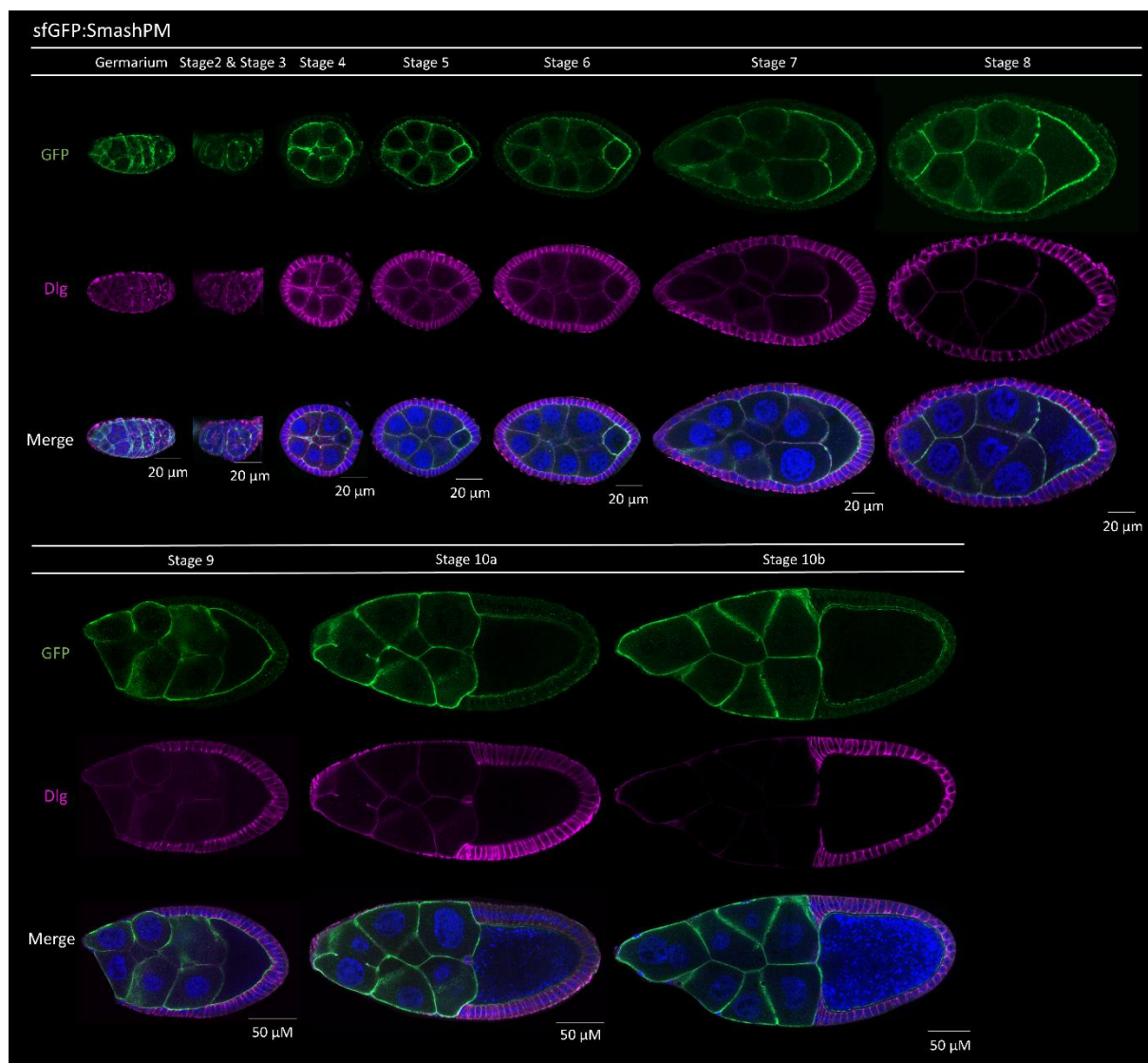
Following the strategy summarized in Figure 19, multiple independent fly lines were obtained. These fly lines were verified by PCR and fully sequenced to check that the sfGFP was inserted in the correct reading frame. For further details, see material & methods section. Promising fly lines were subjected to closer analysis by checking the expression pattern of the sfGFP fusion proteins. It is known that Smash is not only expressed in embryos but also in ovaries, thus making ovaries an additional interesting organ to study the expression pattern of the sfGFP fusion proteins.

Figure 20 depicts the endogenous expression pattern of SmashPM in WT ovaries. Here, SmashPM was already expressed in the germarium. From stage 2-4, SmashPM is localized at the apical cortex of follicle cells. This signal was equally distributed throughout the whole egg chamber. From stage 5-9, SmashPM signal became polarized as it increased specifically at the interface between follicle cells and the maturing oocyte at the posterior pole, but SmashPM signal was still detectable at the interface between follicle and nurse cells. Moreover, SmashPM was also detected at membranes in-between nurse cells. In stages 10a and 10b, a clear SmashPM signal at the nurse cell membranes was visible. A faint SmashPM signal was detected in the apical cortex of follicle cells and at the oocyte membrane.



**Figure 20: Endogenous SmashPM expression in WT ovaries.** Smash is expressed in all egg chamber stages in WT ovaries. Stages are indicated above the panels. Antibodies used for IF staining are indicated on the left side of the panels. Sizes of scale bars are indicated below the scale bars.

The localization pattern of sfGFP:SmashPM (Figure 21) was indistinguishable from the localization pattern of endogenous SmashPM, which was detected with the  $\alpha$ -Smash N-terminal antibody in WT ovaries. Compared to the signal using the antibody against the N-terminus of Smash, the GFP signal of sfGFP:SmashPM appeared much stronger, in particular in stage 10a and 10b ovaries (Figure 22 B). This may be due to penetration problems of the antibody in late-stage egg chambers. Compared to the endogenous SmashPM signal in WT ovaries, sfGFP:SmashPM signal allowed imaging at higher resolution. In stage 6 ovaries, sfGFP:SmashPM was detected at the apical cortex of follicle cells and at the oocyte membrane, creating a signal that appeared as a double line. In contrast, endogenous SmashPM appeared as a thick, single line in stage 6 WT egg chambers (Figure 22 A). During maturation of the egg chambers, the follicle cells and the oocyte became more separated from each other by the development of the vitelline membrane. With progressive maturation of the egg chamber, the endogenous SmashPM signal appeared more obviously as a double line (Figure 22 B).



**Figure 21: sfGFP:SmashPM expression in ovaries.** sfGFP:SmashPM is expressed in all egg chamber stages. Stages are indicated above the panels. Antibodies used for IF staining are indicated on the left side of the panels. Sizes of scale bars are indicated below the scale bars.

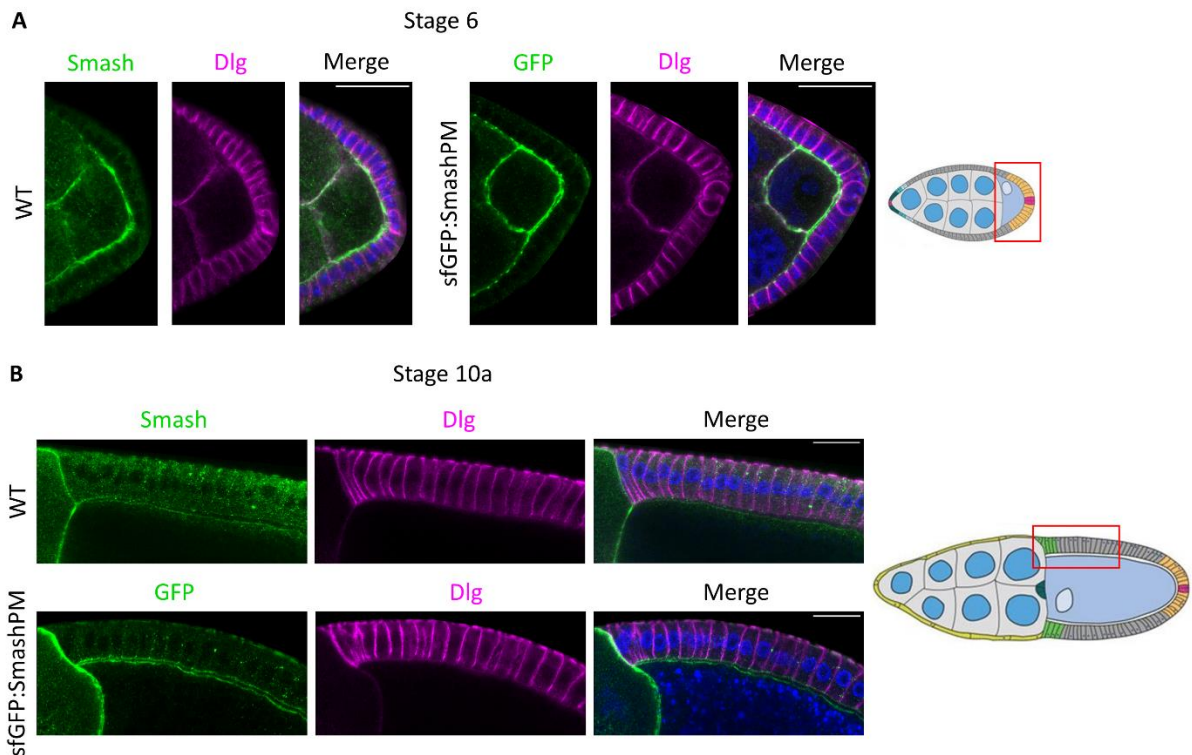


**Figure 22: Close-up of egg chambers showing endogenous SmashPM and sfGFP:SmashPM localization pattern.** (A) Sagittal sections of stage 6 WT and sfGFP:SmashPM egg chambers are shown. (B) Sagittal sections of stage 10a WT and sfGFP:SmashPM egg chambers are shown. (A & B) Antibodies used for IF staining are indicated above each panel. In the right panel, schematic drawings of egg chambers are shown. The red boxes frame the region that is depicted in the close-up. Schematic drawings of egg chambers were copied from Duhart et al. (2017). Scale bar: 20  $\mu$ m.

The detailed expression pattern of SmashPM in embryos has been described earlier in Beati et al. (2018). SmashPM expression can be detected from stage 5 onwards in all ectodermally derived tissues, including the epidermis, fore- and hindgut, Malpighian tubules, salivary glands, amnioserosa, and tracheal tree. Moreover, SmashPM expression was found in the somatic body wall muscles, the pharynx muscles, and the visceral muscles surrounding the midgut. SmashPM is associated with adherens junctions and during germ band elongation it is specifically enriched at A/P cell borders. The expression pattern of SmashPM was first investigated using an antibody against the N-terminus of Smash. Analyzing the expression pattern of sfGFP:SmashPM revealed that sfGFP:SmashPM precisely resembles the previously described expression pattern. An example of the sfGFP:SmashPM expression pattern in embryos (Stage 7 & 8) is depicted in Figure 23.

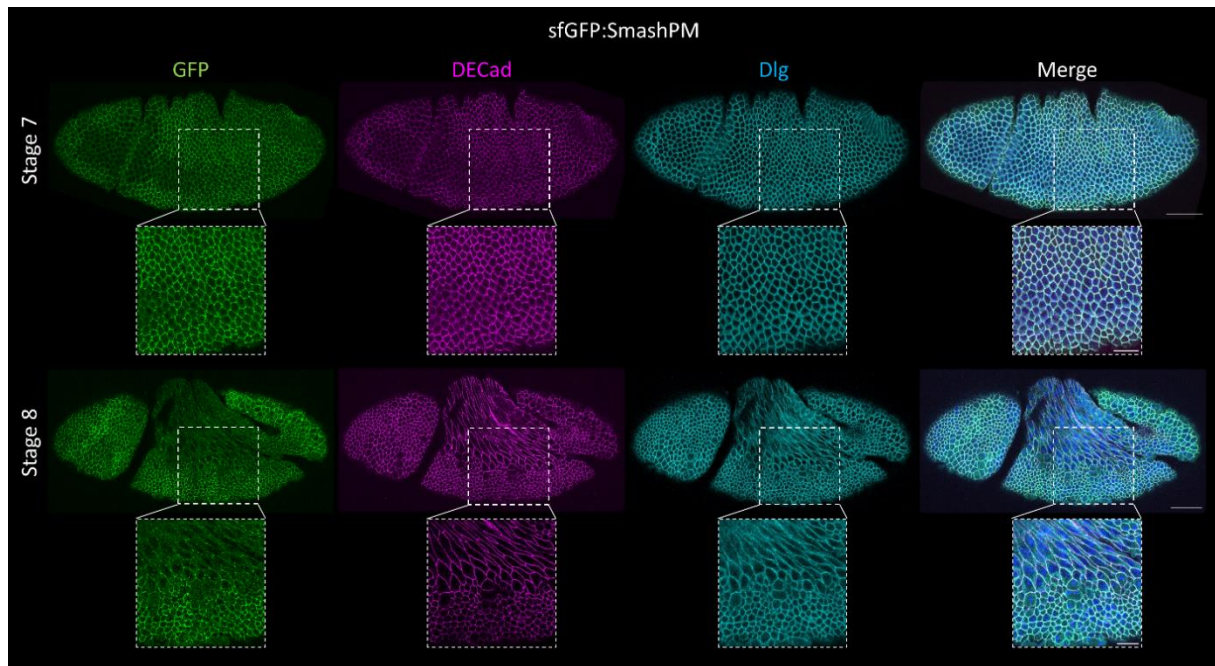


**Figure 23: sfGFP:SmashPM expression in embryos.** In stage 7 & 8 embryos, sfGFP:SmashPM is expressed and localizes at the ZA, resembling the endogenous localization pattern of Smash. Antibodies used for IF staining are indicated above each panel. Scale bar: 50  $\mu$ m. Scale bar close-up: 20  $\mu$ m.

In addition to ovaries and embryos, sfGFP:SmashPM was also expressed in imaginal discs. The expression pattern of sfGFP:SmashPM in wing discs is shown as an example (Figure S 3). Similar as in ovaries and embryos, sfGFP:SmashPM resembled the localization pattern of endogenous SmashPM in wing discs.

### **3.7 sfGFP:SmashPI is specifically expressed in posterior follicle cells in ovaries**

Similar to the new CRISPR line expressing sfGFP:SmashPM, the expression pattern of sfGFP:SmashPI was analyzed in detail. In ovaries, the expression pattern of sfGFP:SmashPI was completely different from endogenous Smash detected with the  $\alpha$ -Smash N-terminal antibody and sfGFP:SmashPM. Until stage 8, sfGFP:SmashPI was not expressed at all. From stage 9 onwards, sfGFP:SmashPI was expressed in posterior follicle cells only. Here, sfGFP:SmashPI was enriched at the apical side of the posterior follicle cells. To some extent it was also localized in the cytosol (Figure 24). This strictly limited expression pattern suggests that SmashPI may have a specific function exclusively in posterior follicle cells. To verify this hypothesis, the expression pattern of sfGFP:SmashPI was analyzed in embryos and in wing discs. sfGFP:SmashPI was expressed neither in embryos nor in the wing disc (Figure S 3 & S 4). During the preparation of sfGFP:SmashPI expressing ovaries, an increased appearance of mature egg chambers was observed. A representative example of this is depicted in Figure S 5. Elaborate statistical analysis has not been performed yet. Closer observation of sfGFP:SmashPI expressing ovaries revealed some remaining but aberrant Smash signal throughout all stages when the antibody against the N-terminus of SmashPM was used. Similar observations were made in embryos. Although no sfGFP:SmashPI signal was detected (Figure S 4), an aberrant signal appeared when using the antibody against the N-terminus of SmashPM (Figure 25).

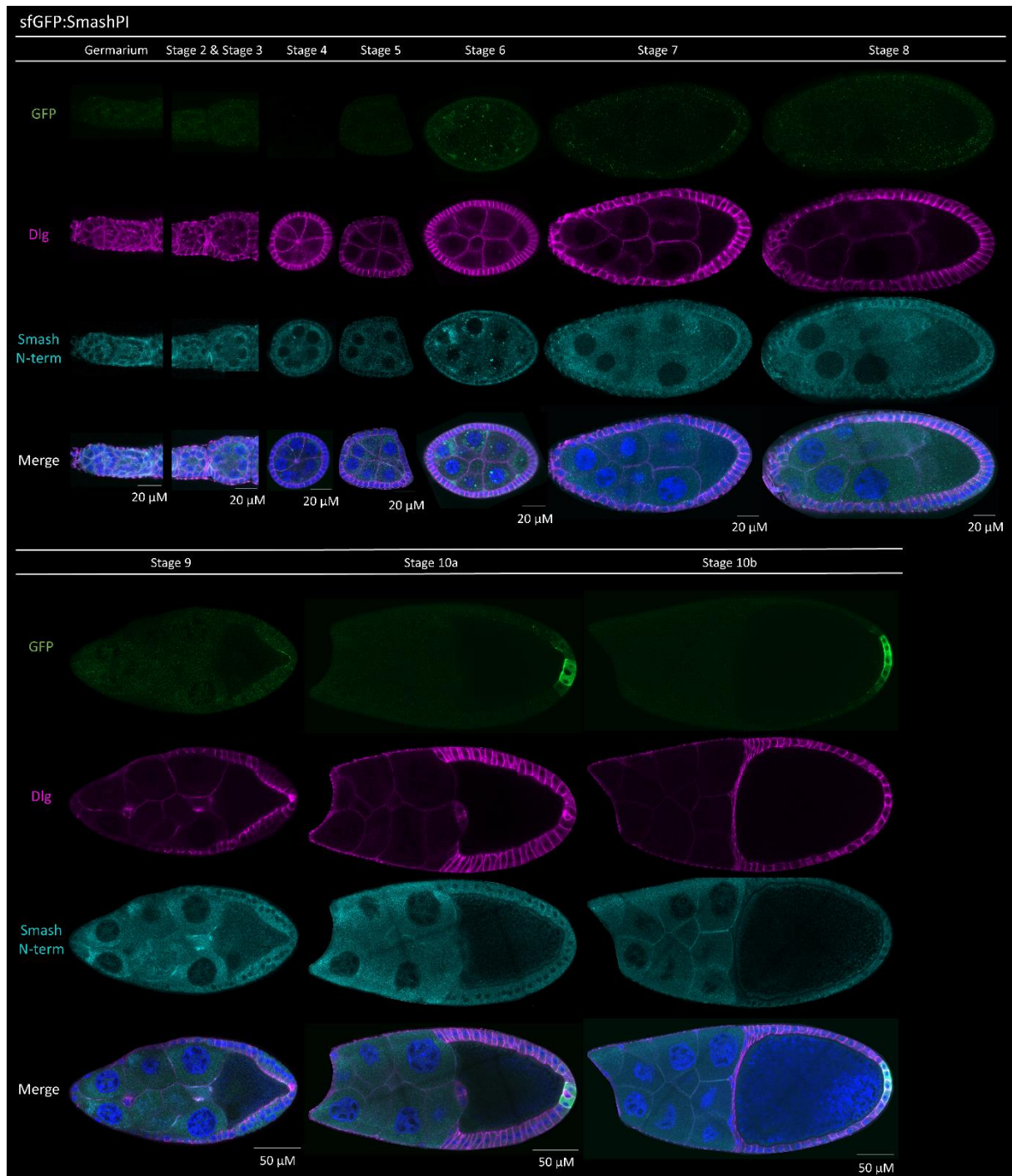


**Figure 24: sfGFP:SmashPI expression in ovaries.** The expression pattern of sfGFP:SmashPI is shown in all egg chamber stages. Using the antibody against the N-terminus of Smash, an aberrant signal for Smash was detected throughout all stages. Stages are indicated above the panels. Antibodies used for IF staining are indicated on the left side of the panels. Sizes of scale bars are indicated below the scale bars.

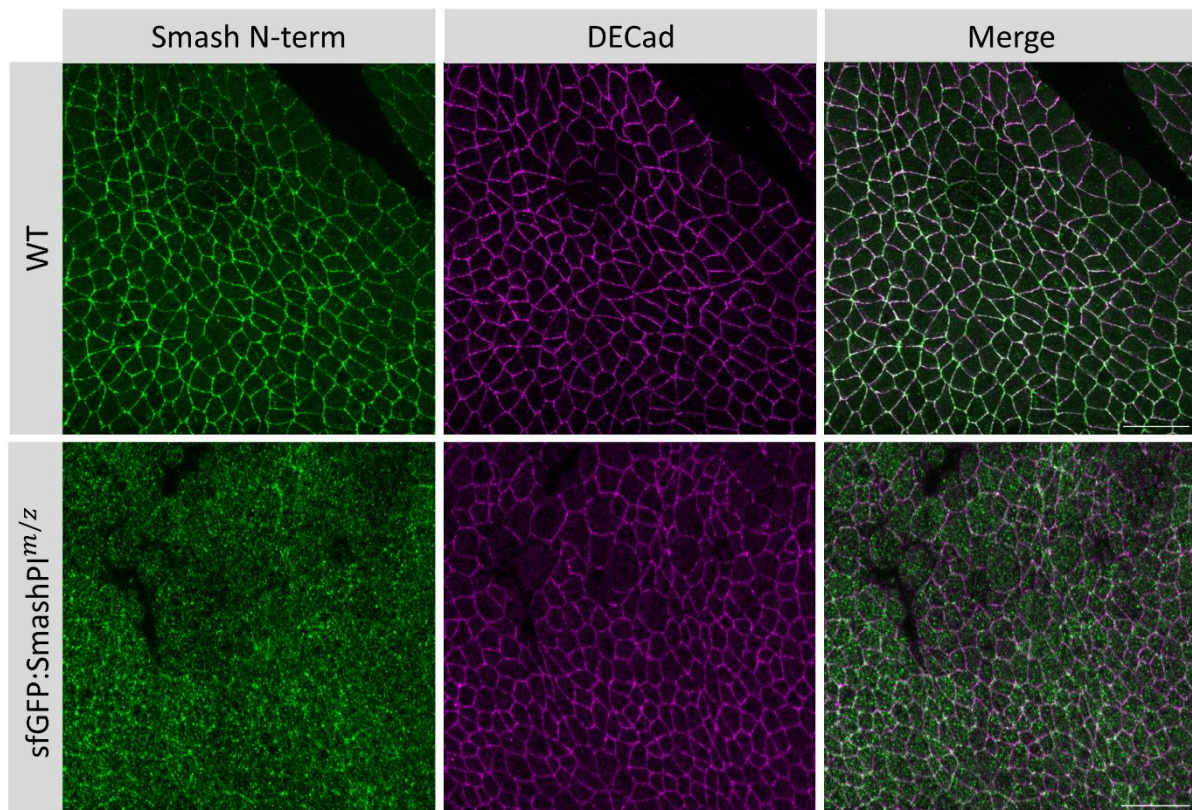


**Figure 25: An aberrant signal was detected in sfGFP:SmashPI<sup>m/z</sup> embryos when the antibody against the N-terminus of SmashPM was used.** Optical sections of stage 8 embryos above the ventral midline are depicted. Antibodies used for IF staining are indicated above each panel. Scale bar: 20  $\mu$ m.

As a second independent approach, Western blot analysis was used to determine the expression status of sfGFP:SmashPM and sfGFP:SmashPI in different tissues (Figure 26). In agreement with the IF staining, concise bands can be detected in sfGFP:SmashPM embryos and in ovaries. A weak band of lower molecular weight appeared in sfGFP:SmashPI ovaries. Again, this finding was in agreement with the results of IF staining, where sfGFP:SmashPI was detected only in a few cells in late-stage ovaries. A similar band was also detected in sfGFP:SmashPI embryos. This observation was in contrast to the results of the IF staining, where no sfGFP:SmashPI was detected in embryos.

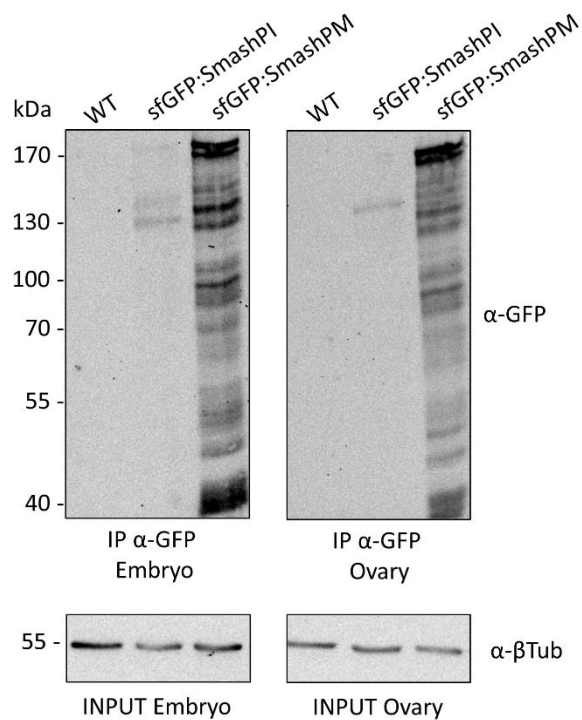


**Figure 26: Detection of sfGFP fusion proteins in embryos and ovaries.** The presence of sfGFP:SmashPM and sfGFP:SmashPI in embryos and ovaries was detected by Western blotting using  $\alpha$ -GFP antibody. Proteins were enriched by IP against GFP. WT tissue was used as reference. Protein detection with  $\alpha$ - $\beta$ Tub antibody was used as loading control. Predicted molecular weight of proteins: sfGFP:SmashPI = 128.5 kDa, sfGFP:SmashPM = 195.7 kDa,  $\beta$ -Tubulin = 50.8 kDa.

Closer observation of embryos homozygous for sfGFP:SmashPI revealed that these embryos had strong morphogenetic defects. This phenotype appeared to be even more severe than the one described in *smash* <sup>$\Delta$ 35m/z</sup> mutant embryos, suggesting that the new allele has a dominant negative effect. Figure 27 provides an overview of the sfGFP:SmashPI<sup>m/z</sup> phenotype. For better visualization of structures, embryos were stained with  $\alpha$ -Twist and arranged by stage. In some stage 5 embryos, an abnormal Twist signal could be detected in the anterior part of the embryo. During stage 6, ventral furrow formation was defective. Stage 7-8 embryos showed defects during germ band elongation that went along with the formation of aberrant, additional furrows on the ventral side of the embryo. In stage 9-10 embryos, germ band elongation continued to some extent, but the embryos looked abnormal since the mesoderm was not fully invaginated and they looked somehow twisted. Many embryos had deep, additional furrows, which made a clear identification of the stage impossible. Putative stage 13-16 embryos looked twisted. Moreover, the usually well-structured tracheal tree was completely disordered.

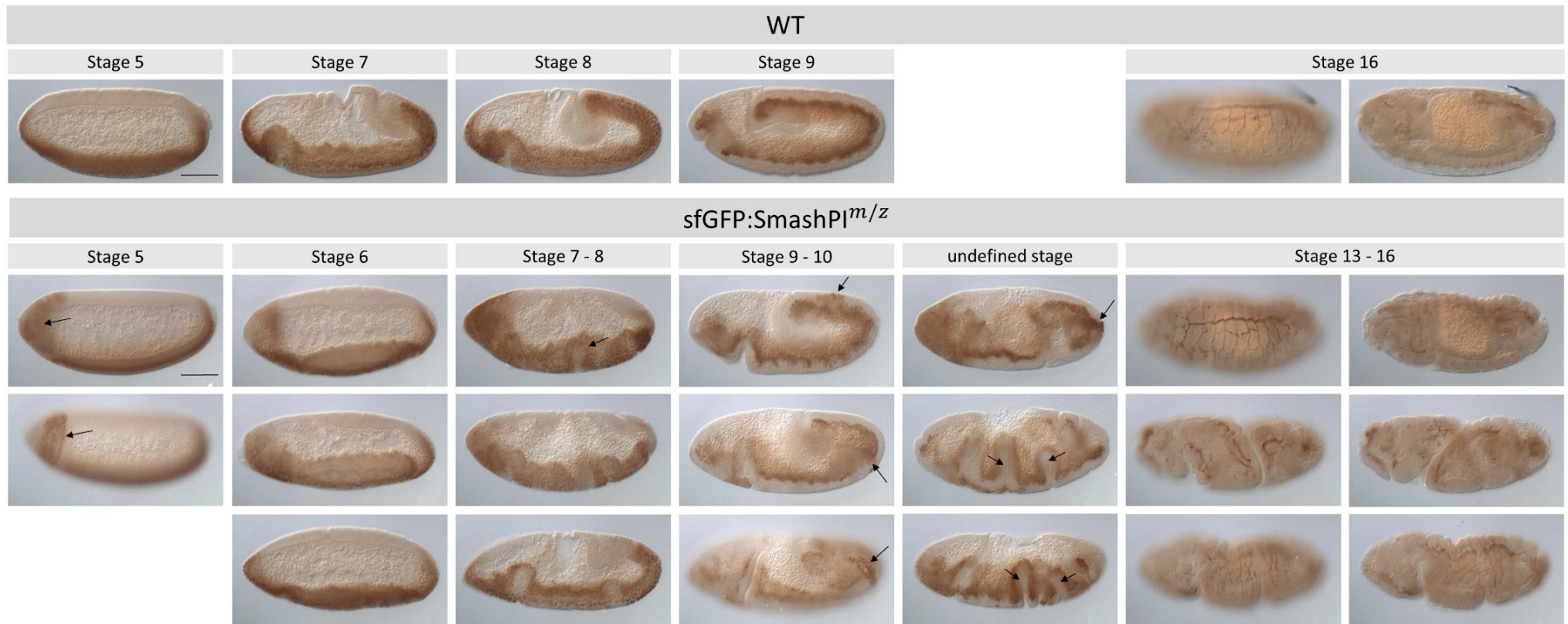
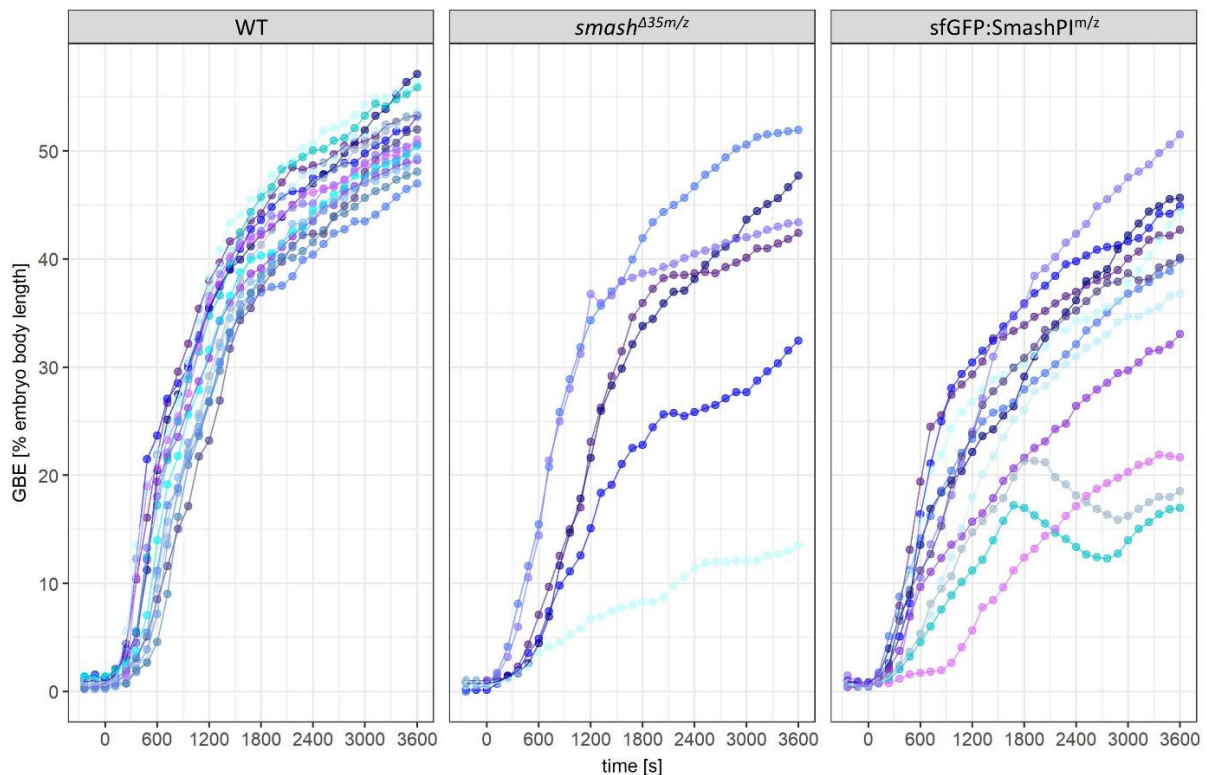


**Figure 27: Phenotypic analysis of sfGFP:SmashPI<sup>m/z</sup> embryos.** Using single embryos as an example, the phenotypic variability of sfGFP:SmashPI<sup>m/z</sup> embryos is shown in different embryonic stages. Stages are indicated above the panels. Staging was performed according to Campos-Ortega & Hartenstein (1997). Embryos were stained with  $\alpha$ -Twist antibody. Arrows point to regions where abnormalities occur (e. g. mesoderm mislocalization or aberrant furrow formation). Scale bar: 100  $\mu$ m.

### 3.8 *smash*<sup>Δ35m/z</sup> and sfGFP:SmashPI<sup>m/z</sup> embryos show impaired germ band elongation

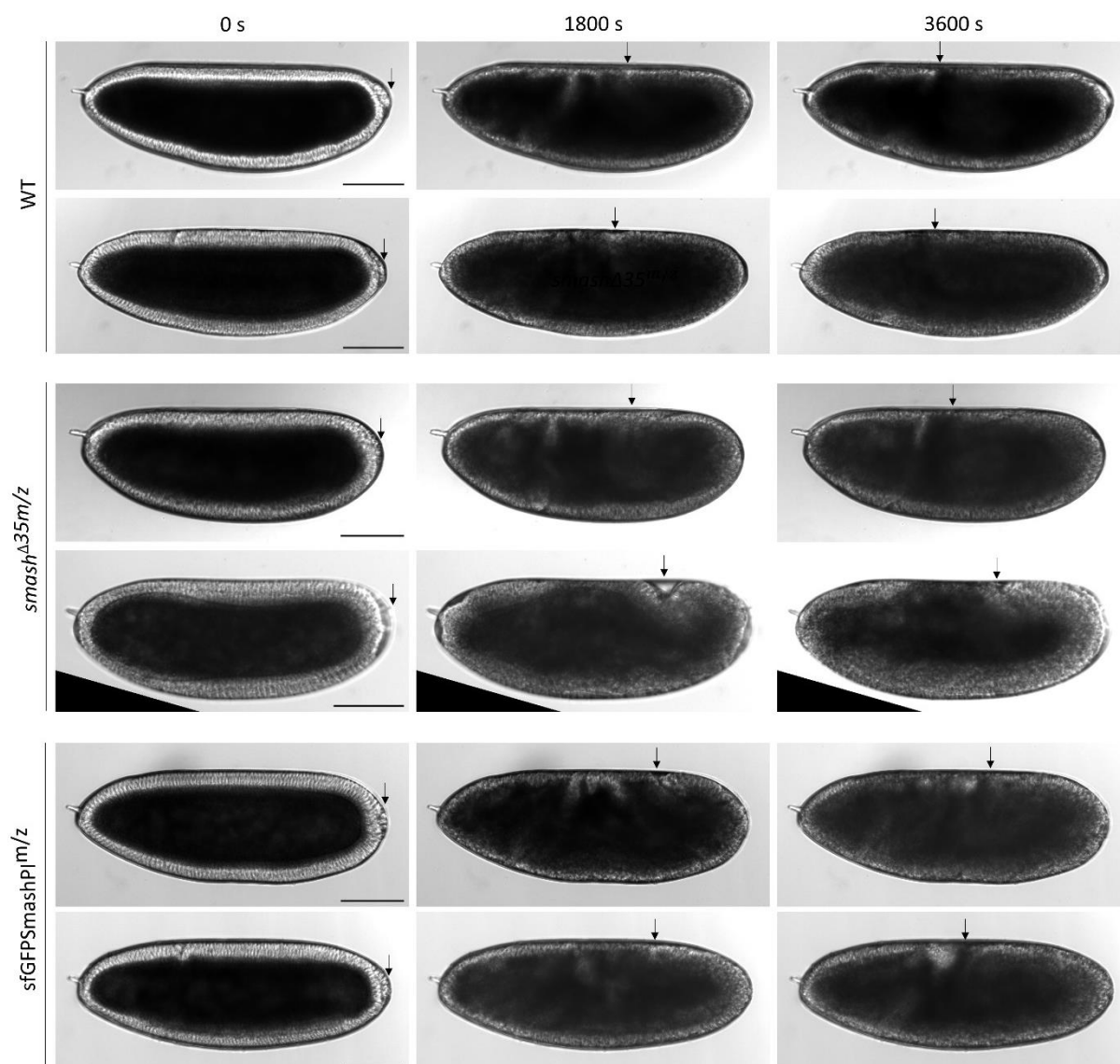
Both *smash*<sup>Δ35m/z</sup> and sfGFP:SmashPI<sup>m/z</sup> embryos showed very severe morphogenetic defects throughout all developmental stages. It was reported that *smash*<sup>Δ35m/z</sup> mutant embryos have PCP defects during germ band elongation (Beati et al., 2018). Whether PCP is also affected in sfGFP:SmashPI<sup>m/z</sup> has not been analyzed yet. Defective PCP often results in impaired germ band elongation (Blankenship et al., 2006; Sawyer et al., 2011; Simões et al., 2010; Simões et al., 2014). To investigate how the complete loss of Smash or the dominant negative effect of the new allele affects germ band elongation, live imaging was performed using *smash*<sup>Δ35m/z</sup> and sfGFP:SmashPI<sup>m/z</sup> embryos. WT embryos were used as reference. Embryos were recorded by brightfield microscopy for 1 hour after the onset of germ band elongation.

Figure 28 illustrates the germ band elongation (GBE) behavior of single embryos in each genotype relative to their body length. Already on the first view, it became apparent that there was a greater variation between single embryos in *smash*<sup>Δ35m/z</sup> and sfGFP:SmashPI<sup>m/z</sup> compared to WT control embryos. In both genotypes, some embryos performed almost as good as WT, while others had strong difficulties to elongate their germ band.



**Figure 28: Relative germ band elongation in WT, *smash*<sup>Δ35m/z</sup>, and sfGFP:SmashPI<sup>m/z</sup> embryos.** GBE was recorded for 1 h after onset. Single embryo recordings are represented in different colors. GBE was normalized against embryo body length. WT n = 16, *smash*<sup>Δ35m/z</sup> n = 6, sfGFP:SmashPI<sup>m/z</sup> n = 12.

In Figure 29, exemplary embryos of each genotype during different time points of live imaging are illustrated.



**Figure 29: Live imaging of WT,  $smash^{\Delta 35m/z}$ , and sfGFP:SmashPI $^{m/z}$  embryos.** Screen shots of time-lapse live imaging recordings of WT,  $smash^{\Delta 35m/z}$  and sfGFP:SmashPI $^{m/z}$  embryos are shown at 0 s, 1800 s and 3600 s after germ band elongation onset. Pole cells were used as a reference point to measure germ band elongation. The arrows point to the tip of the elongating germ band. Scale bar: 100  $\mu$ m.

For better comparison of genotypes, the mean GBE [%] was calculated (Figure S 6 & S 7). Table 7 compares the mean GBE of the three genotypes after 1800 s and 3600 s. After 1800 s, GBE relative to embryo body length in WT has reached 41.1 % ending with 51.9 % after 3600 s. After both measured timepoints, neither  $smash^{\Delta 35m/z}$  nor sfGFP:SmashPI $^{m/z}$  embryos reached a comparable length as WT embryos. Statistical analysis revealed that those differences in length were significant (Table S 1).

**Table 7: Summary mean GBE in WT,  $smash^{\Delta 35m/z}$ , and sfGFP:SmashPI $^{m/z}$  embryos.** Mean GBE was measured after 1800 s and 3600 s. SD: standard deviation. WT n = 16,  $smash^{\Delta 35m/z}$  n = 6, sfGFP:SmashPI $^{m/z}$  n = 12

| Mean GBE [%] | WT                    | $smash^{\Delta 35m/z}$ | sfGFP:SmashPI $^{m/z}$ |
|--------------|-----------------------|------------------------|------------------------|
| after 1800 s | 41.4 (SD $\pm$ 3.12)  | 30.3 (SD $\pm$ 12.6)   | 26.8 (SD $\pm$ 7.45)   |
| after 3600 s | 51.9 (SD $\pm$ (2.93) | 38.6 (SD $\pm$ 13.9)   | 36.4 (SD $\pm$ 11.4)   |

In addition, the measured data was used to calculate the speed of GBE in all three genotypes (Figure 30). Again, there was a high variability between single *smash*<sup>Δ35m/z</sup> and sfGFP:SmashPI<sup>m/z</sup> embryos during the whole recording. This was also true for WT embryos during the first 1800 s of recording. After this timepoint, variability decreased. Using the calculated mean speed, a statistical test to determine the significance of the differences between genotypes was performed (Figure S 8 & S 9, Table S 2). At the beginning of the measurements, no significant difference was observed. From 360 s onwards, the mean GBE speed of *smash*<sup>Δ35m/z</sup> embryos was significantly lower compared to WT. This was also true for sfGFP:SmashPI<sup>m/z</sup> embryos but from 840 s onwards. No statistically significant difference between *smash*<sup>Δ35m/z</sup> and sfGFP:SmashPI<sup>m/z</sup> embryos was observed.

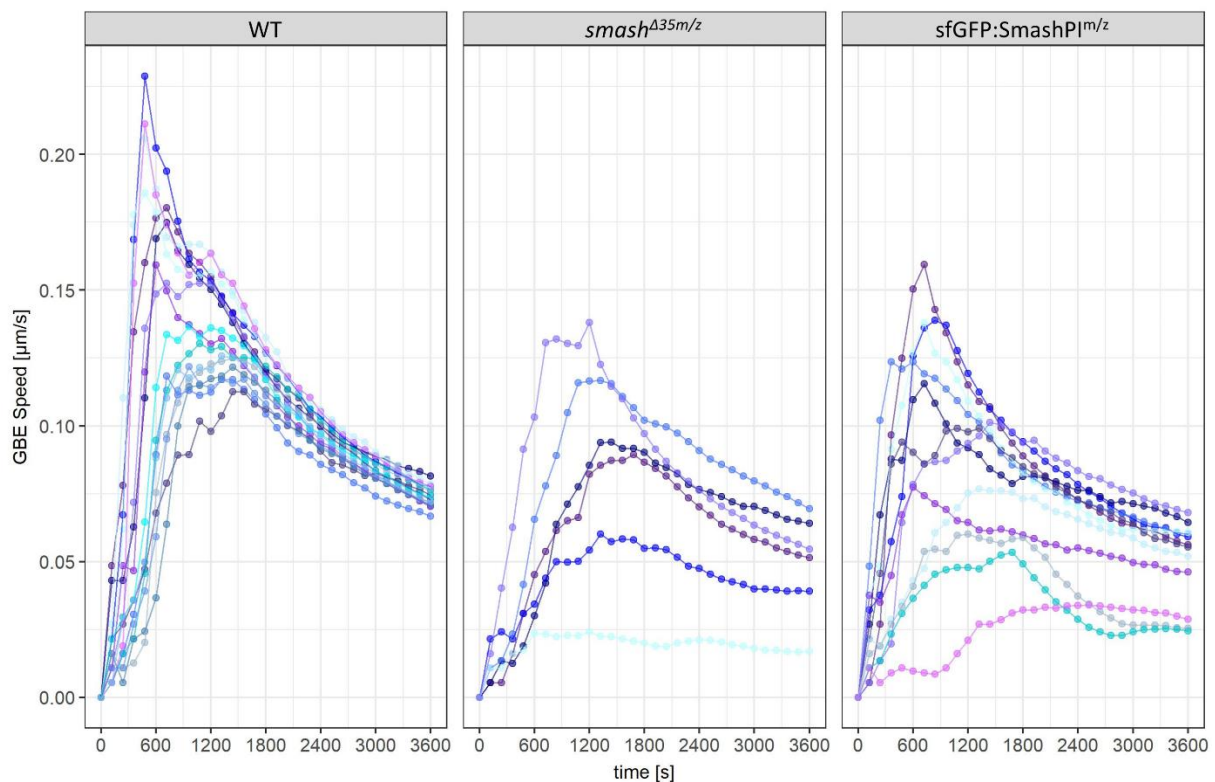


**Figure 30: Relative germ band elongation speed in WT, *smash*<sup>Δ35m/z</sup>, and sfGFP:SmashPI<sup>m/z</sup> embryos.** GBE speed of single embryos is represented in different colors. WT n = 16, *smash*<sup>Δ35m/z</sup> n = 6, sfGFP:SmashPI<sup>m/z</sup> n = 12.

The low number of recorded *smash*<sup>Δ35m/z</sup> embryos resulted from a remarkably high number of embryos that did not undergo cellularization. Out of all recorded embryos, 10 % of WT did not undergo cellularization. This amount drastically increased up to 78 % in *smash*<sup>Δ35m/z</sup> mutants. 65 % of sfGFP:SmashPI<sup>m/z</sup> embryos did not undergo cellularization. To sum up, live imaging revealed that germ band elongation and probably also cellularization were impaired in *smash*<sup>Δ35m/z</sup> and sfGFP:SmashPI<sup>m/z</sup> embryos.

### 3.9 SmashPM N-term has a reduced ability to promote F-actin enrichment

Although *smash*<sup>A35m/z</sup> and sfGFP:SmashPI<sup>m/z</sup> embryos both showed morphogenetic defects, their phenotypic appearance was not the same since the defects in sfGFP:SmashPI<sup>m/z</sup> embryos appeared to be more severe and more penetrant than the ones occurring in *smash*<sup>A35m/z</sup> mutant embryos. The major difference between these two genotypes was that *smash*<sup>A35m/z</sup> is a null allele. Hence, no Smash protein was expressed at all. In contrast, a signal with abnormal subcellular localization was detected in sfGFP:SmashPI<sup>m/z</sup> embryos using the antibody against the N-terminus of Smash (Figure 25). Due to an out-of-frame insertion of sfGFP into the SmashPM reading frame, a premature stop codon is predicted, creating a truncated version of SmashPM that is likely to produce this abnormal fluorescence signal. In the following, this truncated version of SmashPM will be called SmashPM N-term. As depicted in Figure 19, SmashPM N-term carries the myosin binding domain and two coiled coil domains. It is possible that these domains are still functional. This leads to a scenario in which SmashPM N-term can still engage in some protein-protein interactions but probably in an unregulated manner because functionally important domains of SmashPM located at the C-terminus are missing due to the early stop codon. Another possible scenario is that SmashPM N-term is non-functional because of misfolding. Based on the severity and penetrance of morphogenetic defects occurring in sfGFP:SmashPI<sup>m/z</sup> embryos, we hypothesize that SmashPM N-term is still functional but in an unregulated manner.

In order to clarify whether SmashPM N-term has maintained residual function, an overexpression experiment in the follicle epithelium was performed. In addition to SmashPM N-term, full-length SmashPM and SmashPM mut, which carries mutations in the predicted myosin binding domain, were used for overexpression. As a non-functional membrane-bound protein, mCD8 was included as negative control. To visualize the proteins, they were tagged with eGFP. For tissue-specific overexpression in the follicle epithelium, the *tj::Gal4* driver line was used. In this experiment, full-length SmashPM functioned as positive control. A previous experiment in the follicle epithelium showed that SmashPM overexpression resulted in strong apical constriction, demonstrating that Smash is involved in the regulation of actomyosin contractility in the apical cell cortex (Beati et al, 2018; Peek, 2019). SmashPM overexpression was accompanied by the enrichment of F-actin in the apical cell cortex, suggesting that Smash induces actomyosin-driven apical constriction by promoting F-actin enrichment. Similar findings were reported in Matsuda et al. (2022). They reported that *Xenopus* LMO7 facilitates actomyosin filament assembly to drive apical constriction. This was demonstrated by mutating the myosin binding domain of *Xenopus* LMO7 in such a way that it could no longer bind to the NMIIHC. As a result, mutated *Xenopus* LMO7 was no longer able to promote actomyosin filament assembly (Matsuda et al., 2022). Based on the sequence information of *Xenopus* LMO7, the homologous site for myosin binding was identified and mutated in Smash. In our experiment, SmashPM mut was used to investigate more closely the contribution of the myosin binding domain of Smash regarding its function to promote actomyosin contractility. If SmashPM N-

term retained some residual function, we hypothesize that it should be able to promote apical F-actin enrichment, resulting in apical constriction. The main results of the overexpression experiment in the follicle epithelium are summarized in Figure 31.

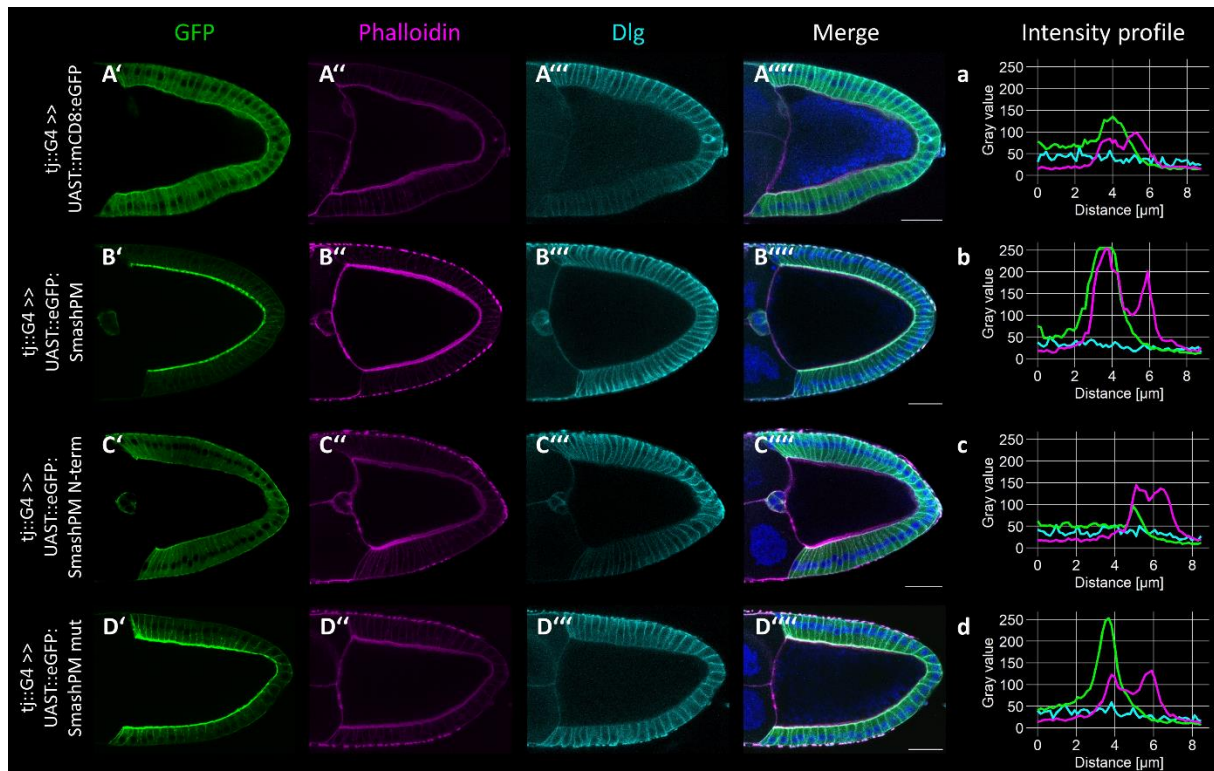


**Figure 31: Overexpression of mCD8:eGFP, eGFP:SmashPM, eGFP:SmashPM N-term, and eGFP:SmashPM mut in the follicle epithelium.** Sagittal sections of stage 10a ovaries are shown. mCD8:eGFP (A'-A'''), eGFP:SmashPM (B'-B'''), eGFP:SmashPM N-term (C'-C'''), and eGFP:SmashPM mut (D'-D''') were overexpressed under the control of the traffic jam (tj) Gal4. For intensity profiles (a-d), the fluorescence intensity of a representative cell of each genotype was measured perpendicular to the apical follicle cell membrane from the cytosol to the oocyte using ImageJ. The intensities of GFP (A', B', C' & D', green line in intensity profile), phalloidin (A'', B'', C'' & D'', magenta line in intensity profile) and Dlg (A''', B''', C''' & D''', cyan line in intensity profile) signals were measured. Scale bar: 30  $\mu\text{m}$ .

All four eGFP fusion proteins were successfully overexpressed in the follicle epithelium (Figure 31 A', B', C' & D'). These proteins showed different subcellular localizations. The mCD8:eGFP control was associated with the apical and basolateral plasma membrane and was also present in the cytosol (Figure 31 A'). A very similar pattern was observed for eGFP:SmashPM N-term (Figure 31 C'). In sharp contrast, eGFP:SmashPM and eGFP:SmashPM mut were enriched at the ZA of the follicular epithelium, close to the apical membrane. Almost no cytosolic signal was detected (Figure 31 B' & D'). Since *Xenopus* LMO7 was described to promote actomyosin filament assembly (Matsuda et al., 2022), the amount and the distribution of F-actin were examined by phalloidin staining in ovaries overexpressing the eGFP fusion proteins in the follicle epithelium (Figure 31 A'', B'', C'' & D''). Myosin II was not analyzed. mCD8:eGFP control ovaries showed a weak phalloidin signal in the apical cortex of follicle cells. Moreover, a weak phalloidin signal was detected at the oocyte membrane (Figure 31 A'' & Figure S 10). A similar distribution and intensity of phalloidin signal was observed in eGFP:SmashPM N-term and eGFP:SmashPM mut overexpressing ovaries (Figure 31 C'' & D'' & Figure S 10). In contrast, the

phalloidin signal in eGFP:SmashPM overexpressing ovaries appeared much stronger compared to the other genotypes (Figure 31 B'' & Figure S 10).

Intensity profiles visualize the intensity of fluorescence signals measured in a representative follicle cell of each investigated genotype (Figure 31 a-d). In general, only one prominent peak occurred for eGFP-tagged fusion proteins that were enriched at the apical cell cortex, but two prominent peaks occurred for the phalloidin signal because F-actin was enriched at the apical cortex of follicle cells and at the oocyte membrane (Figure 31 A''-D'' & Figure S 10). The intensity of the Dlg signal was constantly low throughout all measurements, missing any obvious peaks. In the following, the focus will be on overlapping peaks representing GFP and phalloidin signals measured at the apical cortex in follicle cells. In mCD8:eGFP overexpressing control ovaries, peaks for GFP and phalloidin signals were both rather low (Figure 31 a). In contrast to control ovaries, the peaks for GFP and phalloidin signal in eGFP:SmashPM overexpressing ovaries were both quite high (Figure 31 b). In eGFP:SmashPM N-term overexpressing ovaries, the phalloidin peak was slightly higher than the GFP peak (Figure 21 c). An opposite effect was seen in eGFP:SmashPM mut overexpressing ovaries. In this case, the GFP peak was much higher compared to the phalloidin peak (Figure 31 d). These initial trends were verified by a detailed analysis, in which the fluorescence signals of GFP and phalloidin were measured in multiple follicle cells in different ovaries of each genotype. The fluorescence signals were measured at the apical cell cortex and in the cytosol. The results are illustrated in Figure 32-34 and Figure S 11-S 15.

First, the subcellular localization of the different eGFP-tagged fusion proteins was analyzed more closely. The distribution of the eGFP-tagged fusion proteins was quantified by a membrane/cytosol ratio (Figure 32) which was calculated from measured fluorescence intensities at the apical cell cortex and in the cytosol (Figure S 11 & S 12). A membrane/cytosol ratio of 1 would indicate an equal protein distribution of the proteins at the apical membrane and in the cytosol. The membrane/cytosol ratio for each investigated genotype is greater than 1, indicating that all proteins are enriched at the apical cell cortex. Nevertheless, there are striking differences between the genotypes. While mCD8:eGFP and eGFP:SmashPM N-term overexpressing ovaries had a comparably low GFP membrane/cytosol ratio indicating a weak apical membrane enrichment, eGFP:SmashPM and eGFP:SmashPM mut overexpressing ovaries showed a comparably high GFP membrane/cytosol ratio indicating a strong apical membrane enrichment. The differences between these two groups were statistically significant.

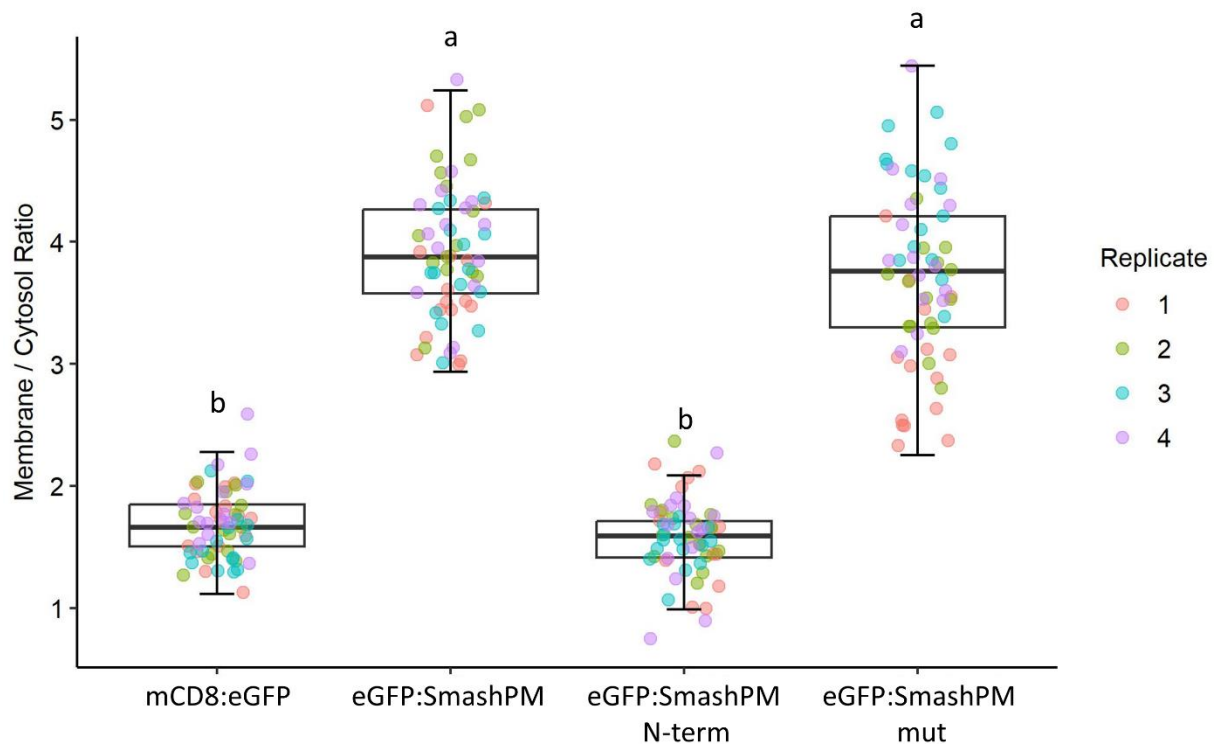


**Figure 32: GFP membrane/cytosol ratio in follicle cells.** mCD8:eGFP, eGFP:SmashPM, eGFP:SmashPM N-term, and eGFP:SmashPM mut overexpressing ovaries were examined. The straight-line tool in ImageJ was used for analysis. The mean gray value was used for calculations. A value of 1 would mean an equal GFP intensity at the apical membrane and in the cytosol. The color code represents the replicate to which a data point belongs to.  $n = 60$  (4 replicates, 15 cells per replicate). Kruskal-Wallis test and a post hoc Dunn test were performed to identify the statistically significant difference between two samples. Compact letter display (CLD) is used to visualize a statistically significant difference. Same letters mean that samples do not differ in a statistically significant manner from each other. For more details on the significance level, see Table S 5.

Next, the phalloidin signal was investigated in detail. Figure 33 shows the intensity of the phalloidin signal at the apical cortex in follicle cells of each genotype. Phalloidin intensity in eGFP:SmashPM overexpressing ovaries was the highest among all tested genotypes, followed by eGFP:SmashPM N-term overexpressing ovaries. The lowest phalloidin intensity was found in eGFP:SmashPM mut and mCD8:eGFP overexpressing ovaries. The latter two were not significantly different from each other.

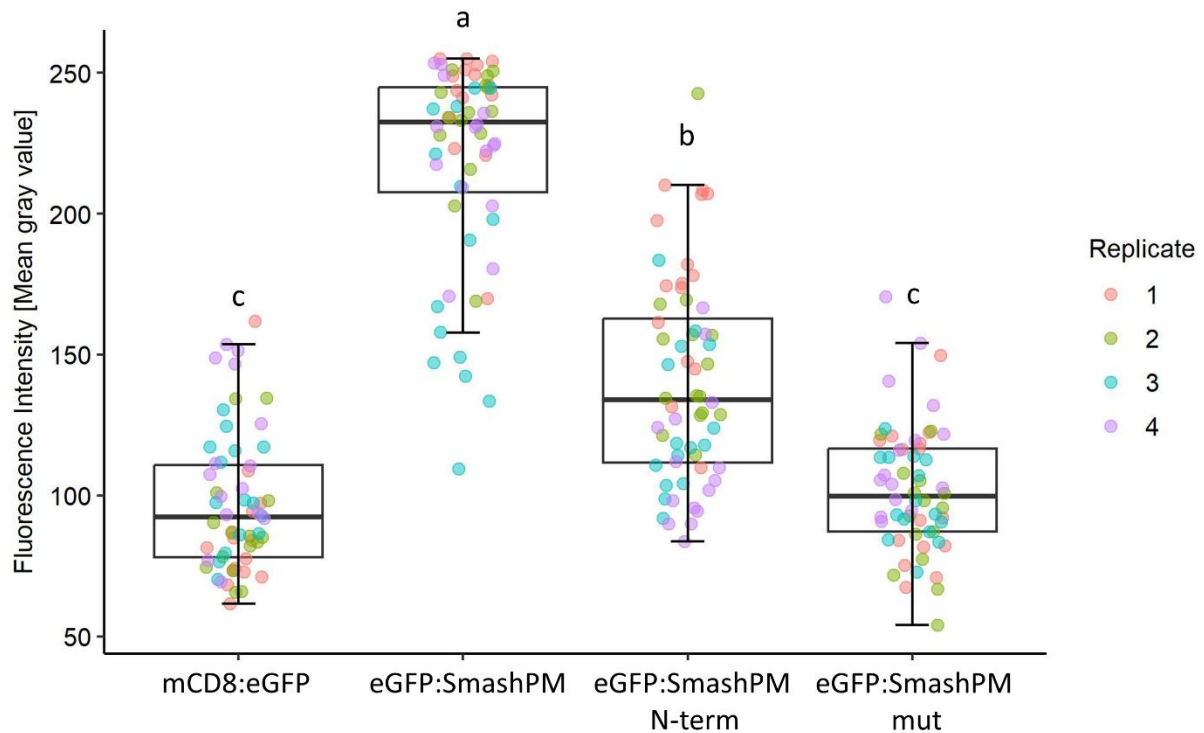


**Figure 33: Phalloidin intensity at the apical cell cortex of follicle cells.** mCD8:eGFP, eGFP:SmashPM, eGFP:SmashPM N-term, and eGFP:SmashPM mut overexpressing ovaries were examined. The straight-line tool in ImageJ was used for analysis. The mean gray value was used for calculations. The color code represents the replicate to which a data point belongs to.  $n = 60$  (4 replicates, 15 cells per replicate). Kruskal-Wallis test and a post hoc Dunn test were performed to identify the statistically significant difference between two samples. Compact letter display (CLD) is used to visualize a statistically significant difference. Same letters mean that samples do not differ in a statistically significant manner from each other. For more details on the significance level, see Table S 6.

In general, cytosolic phalloidin intensity was significantly lower compared to apical phalloidin intensity in each genotype (Figure S 15). Although the cytosolic phalloidin signal is generally low, slight differences were observed between genotypes (Figure S 14). The cytosolic phalloidin signal in eGFP:SmashPM overexpressing ovaries was significantly increased compared to mCD8:eGFP control ovaries whereas cytosolic phalloidin signal in eGFP:SmashPM mut overexpressing ovaries was significantly decreased compared to control. No statistically significant difference in cytosolic phalloidin intensity was observed between eGFP:SmashPM N-term and mCD8:eGFP control ovaries.

Since we aimed to investigate the ability of the different Smash fusion proteins to induce F-actin enrichment at the apical cell cortex, we finally summarized our results to draw a correlation between GFP and phalloidin fluorescence intensities at the apical membrane (Figure 34). A moderate GFP and phalloidin signal was detected at the apical cortex of follicle cells in mCD8:eGFP overexpressing ovaries. In contrast, apical GFP and phalloidin signals in eGFP:SmashPM overexpressing ovaries occurred both at a comparable level and were much higher than the signals in mCD8:eGFP control. In eGFP:SmashPM N-term overexpressing ovaries, GFP signal at the apical cortex in follicle cells was as low as in mCD8:eGFP control. Even though the localization pattern of eGFP:SmashPM N-term did not resemble the localization pattern of eGFP:SmashPM, the phalloidin signal in eGFP:SmashPM N-term overexpressing ovaries was slightly increased compared to the mCD8:eGFP control. In contrast, phalloidin signal in eGFP:SmashPM mut overexpressing ovaries was not increased compared to the mCD8:eGFP control, although eGFP:SmashPM mut mimicked the eGFP:SmashPM localization pattern as the GFP intensity for eGFP:SmashPM mut and eGFP:SmashPM were at a comparably high level.

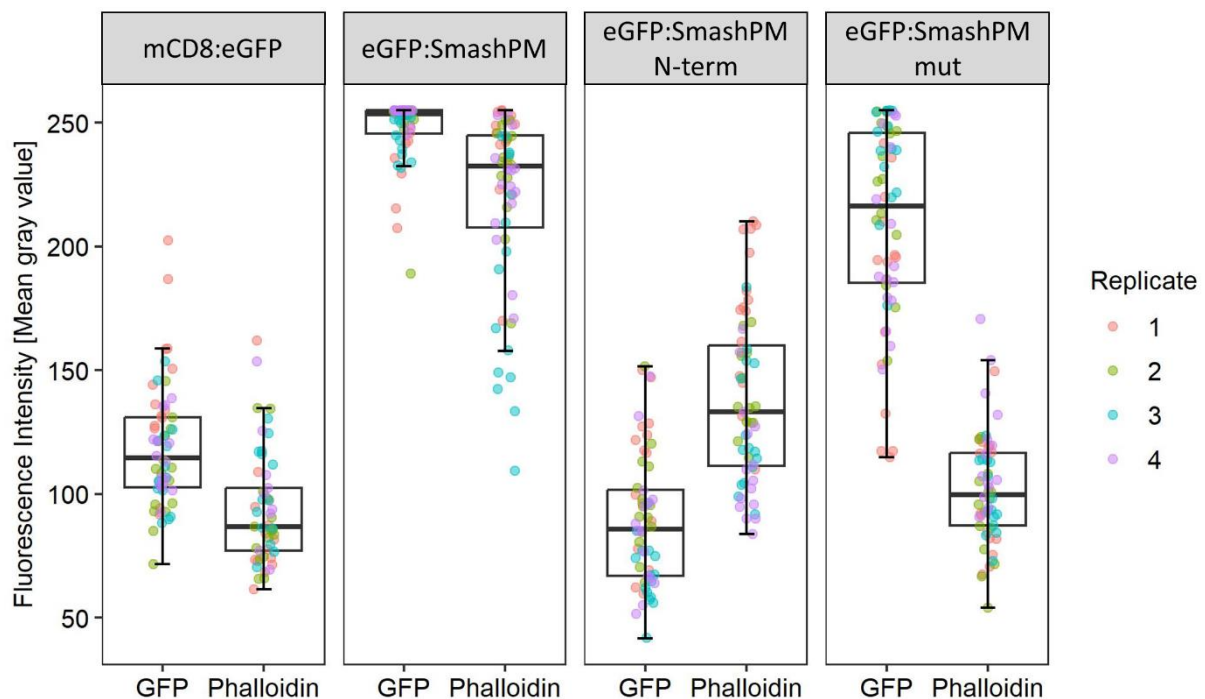


**Figure 34: Correlation between apical GFP and phalloidin signal in follicle cells.** mCD8:eGFP, eGFP:SmashPM, eGFP:SmashPM N-term, and eGFP:SmashPM mut overexpressing ovaries were examined. The straight-line tool in ImageJ software was used for analysis. The mean gray value was used for calculations. The color code represents the replicate to which a data point belongs to. n = 60 (4 replicates, 15 cells per replicate). No further statistics were performed since this figure is just summarizing Figure 33 & S 11. For statistical analysis, refer to Table S 3 & Table S 6.

In summary, full-length Smash was enriched at the apical cortex. There, it promoted F-actin enrichment in a manner dependent on the myosin binding domain. SmashPM mut, which lacked the myosin binding domain, was no longer able to promote F-actin enrichment. SmashPM N-term failed to localize properly within the cell. Nevertheless, it retained some ability to promote F-actin enrichment at the apical cortex, albeit to a lower extent than full-length SmashPM.

During preparation of the ovaries, morphological abnormalities were observed in ovaries overexpressing full-length eGFP:SmashPM (Figure 35). In single ovarioles, young egg chamber stages were present and did not show any abnormalities, whereas later egg chamber stages and embryos formed tubular-like structures. In general, eGFP:SmashPM overexpressing ovarioles appeared to be more flexible and resilient against mechanically applied stretching compared to control. We wondered whether these drastic changes in the tissue might influence the egg-laying efficiency of female flies. We tested our hypothesis by measuring the egg-laying rate of the different genotypes. Indeed, the egg-laying rate of eGFP:SmashPM overexpressing flies was only 12.7 % of the egg-laying rate of mCD8:eGFP overexpressing control flies. eGFP:SmashPM overexpressing embryos often looked abnormal since the formation of dorsal appendages was defective. No larvae hatched. eGFP:SmashPM N-term and eGFP:SmashPM mut overexpressing ovaries did not show obvious defects. The egg-laying rate in these two genotypes was slightly reduced compared to control but not as strong as in eGFP:SmashPM overexpressing flies. Relative to mCD8 control, the egg-laying rate was 84.5 % in eGFP:SmashPM N-term and 78.0 % in eGFP:SmashPM mut overexpressing flies.

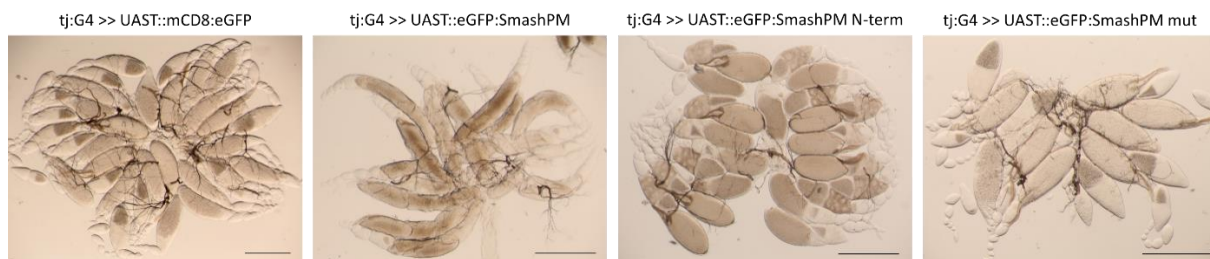


**Figure 35: Abnormal morphology in eGFP:SmashPM overexpressing ovaries.** Ovaries overexpressing mCD8:eGFP, eGFP:SmashPM, eGFP:SmashPM N-term, and eGFP:SmashPM mut under the control of tj:G4 are shown. Scale bar: 500  $\mu$ m.

Another striking observation was that embryos developing from ovaries overexpressing eGFP:SmashPM N-term appeared shorter in length but larger in width compared to control embryos (Figure 36 C). To quantify this observation, length and width of respective embryos were measured. Embryos developing from eGFP:SmashPM overexpressing ovaries were not investigated since no properly shaped embryos were formed. Indeed, embryos developing from eGFP:SmashPM N-term overexpressing ovaries were shorter in length (average length: 398  $\mu$ m  $\pm$  15  $\mu$ m) and larger in width (average width: 188  $\mu$ m  $\pm$  20  $\mu$ m) compared to mCD8 control embryos (average length: 419  $\mu$ m  $\pm$  35  $\mu$ m, average width: 149  $\mu$ m  $\pm$  20  $\mu$ m) (Figure 36). Interestingly, embryos developing from ovaries overexpressing eGFP:SmashPM mut were larger in length (average length: 445  $\mu$ m  $\pm$  27  $\mu$ m) and in width (average width: 171  $\mu$ m  $\pm$  20  $\mu$ m) compared to mCD8 control embryos.

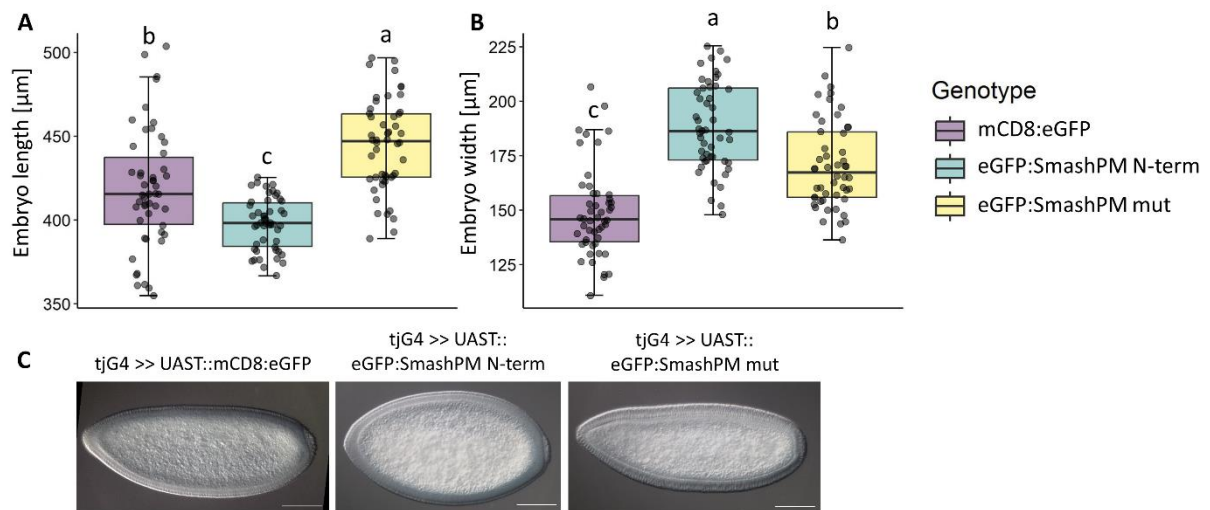


**Figure 36: Determination of embryo length and width.** (A & B) Embryos developing from mCD8:eGFP, eGFP:SmashPM N-term, and eGFP:SmashPM mut overexpressing ovaries were investigated. The straight-line tool in ImageJ was used for analysis. Genotypes were labeled in different colors (color code is indicated on the right in panel B). ANOVA analysis and a post hoc Tukey HSD test were performed to identify the statistically significant difference between two samples. Compact letter display (CLD) is used to visualize a statistically significant difference. Same letters mean that samples do not differ in a statistically significant manner from each other.  $n = 50$ ,  $p < 0.0001$ . (A) The embryo length of the different genotypes is shown. (B) The embryo width of the different genotypes is shown. (C) An exemplary embryo of each genotype is shown. Scale bar: 100  $\mu\text{m}$ .

### 3.10 Overexpression of SmashPM and SmashPM N-term induces cell shape changes

Overexpression experiments in the follicle epithelium revealed that Smash promoted F-actin enrichment in the apical cortex of follicle cells, presumably through its myosin binding domain. SmashPM N-term also promoted F-actin enrichment in the apical cortex of follicle cells but to a much lower extent. Apical enrichment of actomyosin filaments is a requirement for apical constriction (Coravos & Martin, 2016; Martin et al., 2009; Young et al., 1991). Previous overexpression studies had already demonstrated the ability of SmashPM to induce apical constriction (Beati et al., 2018; Peek, 2019). To figure out whether SmashPM N-term retains some residual function, we focused on the question whether overexpression of Smash N-term affects cell morphology. Since SmashPM N-term promotes apical F-actin enrichment in follicle cells, we hypothesized that SmashPM N-term might also be able to induce apical constriction. Based on the data by Matsuda et al. (2022), we assumed that SmashPM mut is no longer able to induce apical constriction. To study the effect of the different Smash variants on cell morphology, a heat-shock inducible FLP/FRT system to induce stochastic overexpression of proteins in the follicle epithelium was used. eGFP-tagged mCD8, SmashPM, SmashPM N-term and SmashPM mut were overexpressed under the control of *hsflp*; *act<CD2<G4* as driver line.

Stochastic overexpression of the different eGFP fusion proteins was observed in single follicle cells (Figure 37 A-D). mCD8:eGFP was localized at the plasma membrane but also in the cytosol (Figure 37 A). A very similar pattern was observed for eGFP:SmashPM N-term (Figure 37 C). In contrast, eGFP:SmashPM and eGFP:SmashPM mut were enriched at the apical cortex (Figure 37 B & D). Almost no cytosolic signal was detected. In eGFP:SmashPM overexpressing cells, strong shrinkage of the apical cell diameter was observed (Figure 37 B). These cell shape changes also affected the positioning of the nuclei. In cells overexpressing eGFP:SmashPM, the nucleus was localized more basally compared to cells that did not overexpress eGFP:SmashPM. On the first view, no obvious cell shape changes were detected in mCD8:eGFP, eGFP:SmashPM N-term, and eGFP:SmashPM mut overexpressing cells (Figure 37 A, C & D).

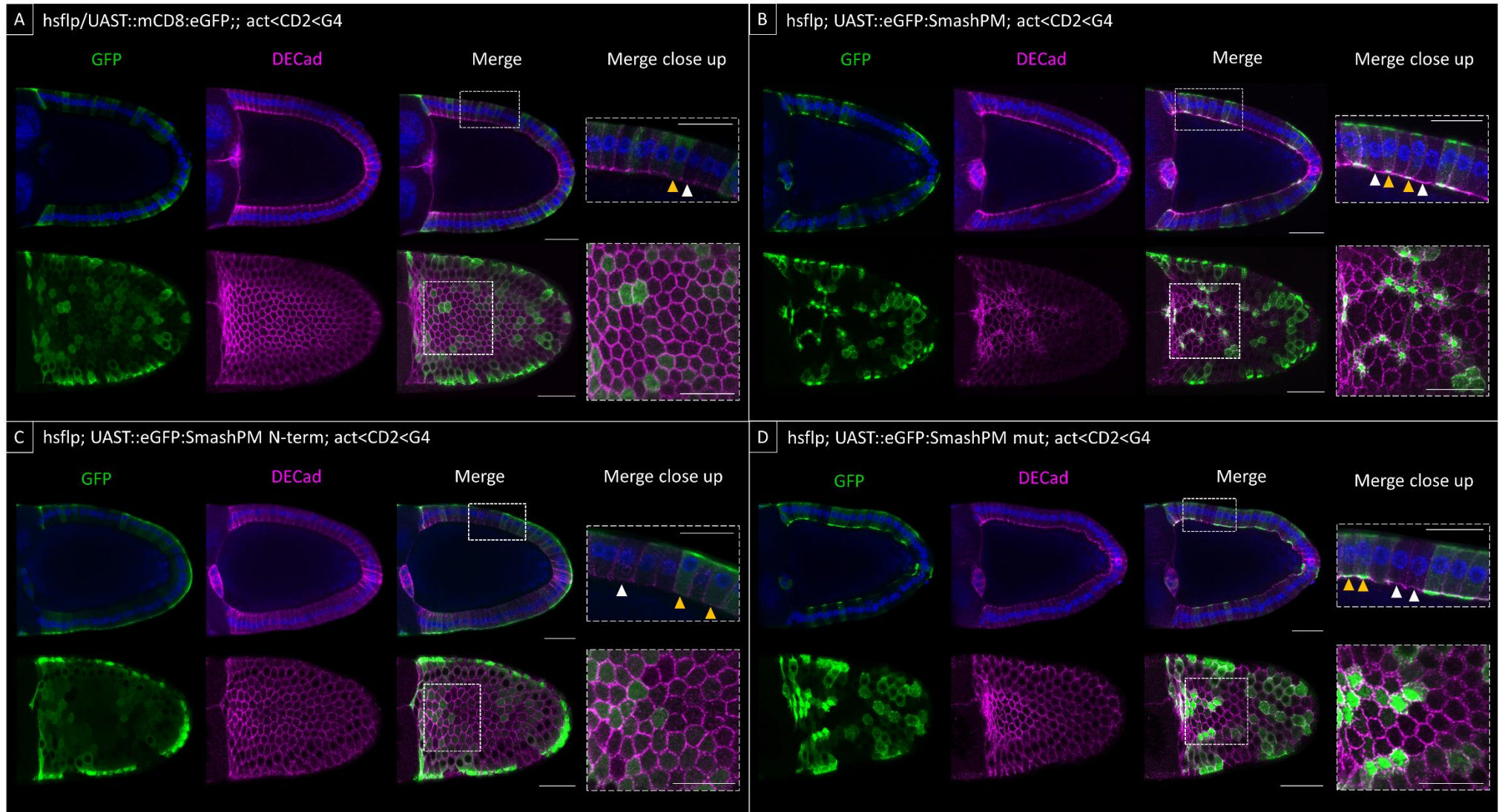


**Figure 37: Stochastic overexpression of SmashPM variants in the follicle epithelium.** (A) mCD8:eGFP, (B) eGFP:SmashPM, (C) eGFP:SmashPM N-term, and (D) eGFP:SmashPM mut overexpression in single follicle cells was induced by 10 min heat-shock treatment at 37°C. Ovaries were dissected and stained the following day. Genotypes of the respective female flies are indicated on the top left of each panel. Sagittal and superficial sections of stage 10a ovaries are shown. White arrow heads point to GFP-negative cells. Yellow arrow heads point to GFP-positive cells. For further details on the experiment, see material & methods section. Scale bar: 30  $\mu\text{m}$ , scale bar close-up: 20  $\mu\text{m}$ .

To quantify the effect of SmashPM variants on cell morphology, the apical cell area of GFP-negative and GFP-positive cells was measured (Figure 38).

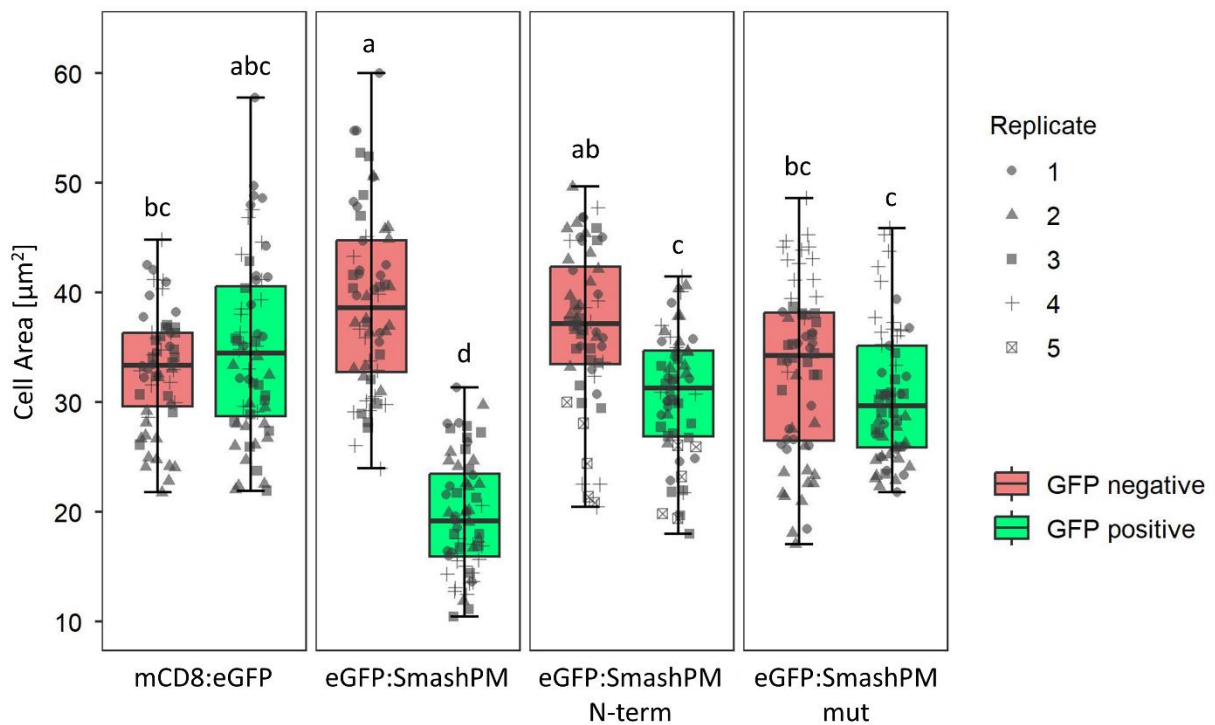


**Figure 38: Apical cell area in follicle epithelium upon stochastic overexpression of mCD8:eGFP, eGFP:SmashPM, eGFP:SmashPM N-term, and eGFP:SmashPM mut.** The apical cell area of GFP-positive and GFP-negative follicle cells in immediate vicinity to GFP-positive cells was measured in mCD8:eGFP, eGFP:SmashPM, eGFP:SmashPM N-term, and eGFP:SmashPM mut overexpressing ovaries using ImageJ. Only GFP-negative cells adjacent to at least one GFP-positive cell were scored. Kruskal-Wallis test and a post hoc Dunn test were performed to determine the statistical significance of the difference between two samples. Compact letter display (CLD) is used to visualize a statistically significant difference. Same letters mean that samples do not differ in a statistically significant manner from each other. For more details on the significance level, see Table S 8. The different symbols of data points correspond to a single replicate.  $n = 60$ .

As Figure 37 already suggested, overexpression of eGFP:SmashPM had a strong effect on the apical cell area. Compared to eGFP:mCD8 overexpressing cells, the apical cell area in eGFP:SmashPM overexpressing cells was drastically reduced. The apical cell area of GFP-negative cells adjacent to eGFP:SmashPM overexpressing cells was significantly larger compared to GFP-negative mCD8 control cells. A similar trend was observed in eGFP:SmashPM N-term overexpressing ovaries. In this case, GFP-positive cells had a significantly smaller cell area compared to GFP-negative cells. In contrast to eGFP:SmashPM overexpressing ovaries, the difference in cell area between eGFP:SmashPM N-term ovaries and eGFP:mCD8 control ovaries was not statistically significant. The cell area in eGFP:SmashPM mut overexpressing ovaries was comparable to eGFP:mCD8 overexpressing ovaries in both GFP-positive and GFP negative cells. In summary, I conclude that overexpression of full-length SmashPM had a clear effect on cell morphology as strong apical constriction was induced. SmashPM N-term was also capable to induce this response but to a lesser extent, whereas overexpression of SmashPM mut did not affect the apical cell area.

### 3.11 Identification of novel Smash interaction partners by biotin proximity labeling

According to our current state of knowledge, we can state that Smash is an actomyosin-associated protein important for planar cell polarity and for epithelial morphogenesis. Nevertheless, the knowledge about how Smash provides its function is quite limited. To improve our understanding of Smash function, unbiased identification of potential Smash interaction partners would help to complete the picture of the Smash interaction network. To discover new Smash-interacting proteins, a biotin proximity labeling assay was used. Here, a more efficient and faster version of the biotin ligase BirA, namely TurboID (Branon et al., 2018), was fused to the N-terminal end of SmashPM. SmashPM and TurboID served as controls. For visualization of the proteins, they were tagged with eGFP. Using a maternal  $\alpha$ -Tubulin67C Gal4 driver line, these fusion proteins were expressed in embryos under the control of an UASp promoter. Details on cloning are provided in the material & methods section.

In short, this approach works as follows: upon supply of biotin, proteins in close proximity to the TurboID fusion protein become biotinylated. After cell lysis, biotinylated proteins are efficiently enriched by affinity purification using streptavidin agarose beads. Enriched proteins are processed for mass spectrometry analysis. Compared to a classical co-IP approach, harsh lysis conditions without the need to preserve intact protein complexes can be used. The advantage of this system is that even weak and transient interactions can be detected. The disadvantage is that not all potential interacting proteins might be labeled because of the steric properties of the fusion protein. Moreover, there is the possibility of obtaining false-positive candidates. However, false-positive candidates can be identified and eliminated by including appropriate controls. In Figure 39, the workflow is schematically summarized.

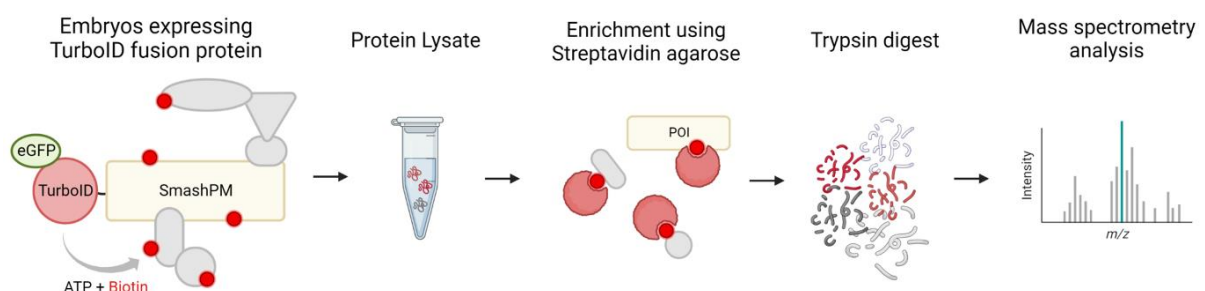


**Figure 39: Workflow of the biotin proximity labeling assay.** The TurboID fusion protein was expressed in embryos under the control of UASp promoter using a maternal  $\alpha$ -Tubulin67C Gal4 driver. Upon supply of biotin, TurboID starts labeling all proteins in close proximity. Protein lysates were prepared from embryos. The biotinylated proteins were enriched by using streptavidin agarose beads. Enriched proteins were trypsin digested, purified, and subjected to MS analysis.

To test the functionality of the TurboID fusion proteins, they were transfected into S2 cells (Figure 40). GFP:TurboID:SmashPM and GFP:SmashPM were both enriched at the membrane, thus showing the same localization. In contrast, GFP:TurboID and GFP were both distributed in the whole cell. Cells expressing TurboID:GFP and GFP:TurboID:SmashPM underwent strong biotinylation (biotin signal was visualized with streptavidin, which specifically binds biotin), whereas in cells expressing GFP:SmashPM or GFP a weak biotin signal was detected, most likely due to biotinylation processes occurring under normal physiological conditions. The signal of TurboID fusion proteins co-localized with the biotin signal.

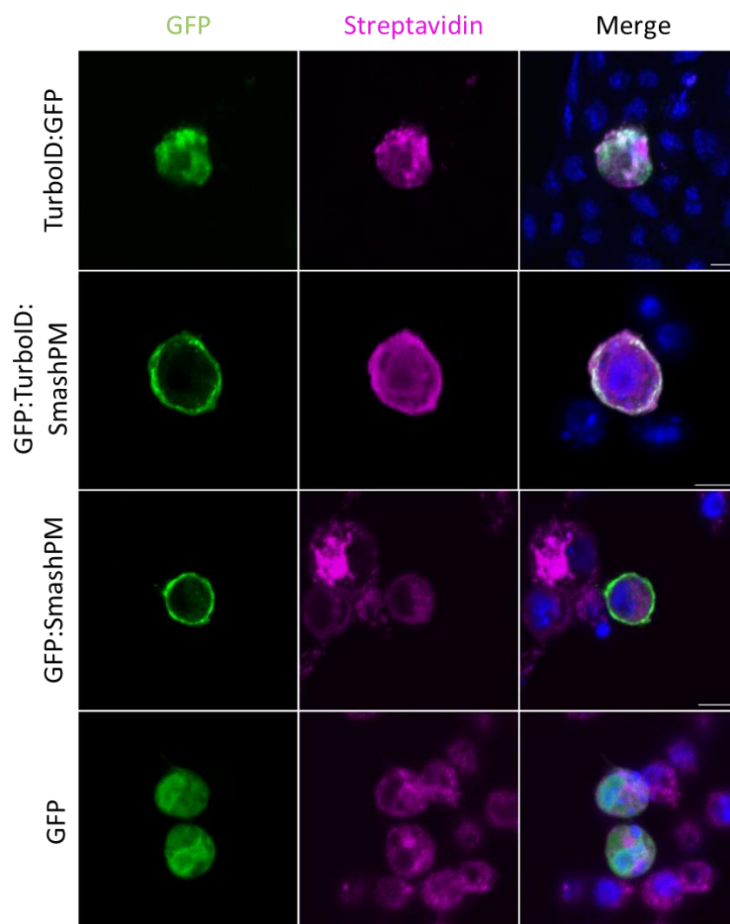


**Figure 40: Expression of TurboID fusion proteins in S2 cells.** TurboID:GFP, GFP:TurboID:SmashPM, GFP:SmashPM, and GFP were expressed in S2 cell culture under the control of the Act5c promoter. Cells were supplied with 50 mM biotin directly after transfection. Antibodies and conjugated affinity proteins used for IF staining are indicated above each panel. Scale bar: 5  $\mu$ M.

TurboID:GFP, GFP:TurboID:SmashPM, GFP:SmashPM, and GFP expressing cells were further analyzed by Western blotting to determine the biotinylation efficiency of TurboID. In Figure 41, multiple bands of various sizes were detected in the presence of TurboID, indicating efficient biotinylation. In contrast, only two clear bands appear in the absence of TurboID. Because these two bands appeared in all samples, it is likely that this is just unspecific background signal probably originating from proteins that always undergo strong biotinylation.

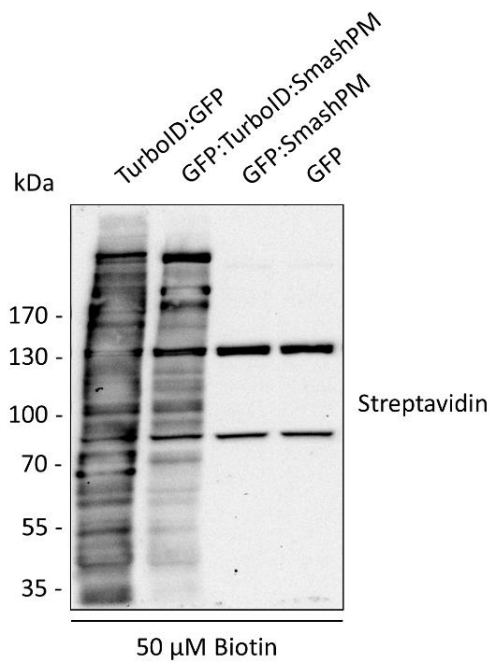


**Figure 41: Efficient biotinylation occurs in S2 cells expressing TurboID fusion proteins.** TurboID:GFP, GFP:TurboID:SmashPM, GFP:SmashPM, and GFP were expressed in S2 cell culture under the control of the Act5c promoter. Cells were supplied with 50 mM biotin directly after transfection. Cells were used to prepare whole cell lysate for Western blotting. To detect biotinylation, streptavidin coupled to horse reddish peroxidase (HRP) was used.

After verifying the functionality of TurboID fusion proteins in cell culture, we generated transgenic flies expressing the respective eGFP-tagged fusion proteins. A prerequisite for a functional proximity labeling assay is that eGFP:TurboID:SmashPM is active in the correct place. Thus, the subcellular localization of the fusion proteins was investigated in the embryonic epithelium. Figure 42 shows that eGFP:TurboID:SmashPM was localized at the membrane perfectly reflecting the localization of eGFP:SmashPM without the TurboID fusion. In contrast, TurboID:eGFP was distributed throughout the whole cell.

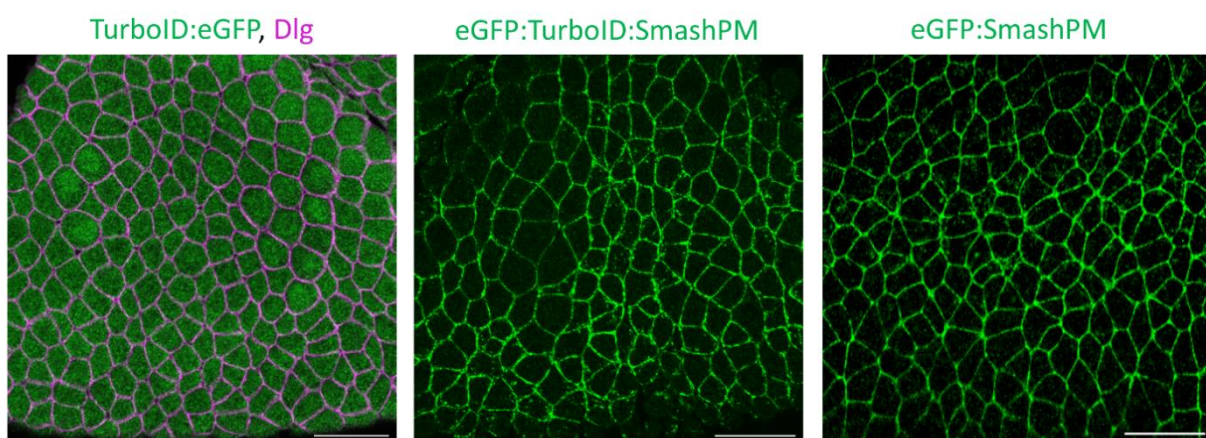


**Figure 42: Subcellular localization of fusion proteins in the embryonic epithelium.** Expression of UASp::TurboID:eGFP, UASp:eGFP:TurboID:SmashPM, and UASp:eGFP:SmashPM was induced by using a maternal  $\alpha$ -Tubulin67C Gal4 driver. Optical sections of stage 8 embryos above the ventral midline are depicted.  $\alpha$ -GFP antibody was used for IF staining to visualize the eGFP fusion proteins.  $\alpha$ -Dlg antibody was used for IF staining to mark the cell borders. Scale bar: 20  $\mu$ M.

Although the subcellular localization of eGFP:TurboID:SmashPM looked promising, it was not clear whether this fusion protein was functional with respect to the biotinylation of proteins in its vicinity. To test the functionality of the TurboID fusion proteins, the biotinylation efficiency was again investigated by Western blotting. Before this could be done, however, it had to be clarified how the biotin could efficiently be supplied to the embryo. Unfortunately, only few data have been published on biotin proximity labeling experiments in flies. Branon et al. (2018) reported about the use of TurboID in *D. melanogaster* and *C. elegans* but without specifically targeting a protein of interest. Mannix et al. (2019) successfully uncovered new ring canal-associated proteins by using APEX. Zhang et al. (2021) were interested in cytoophidia-associated proteins. In the latter paper, experiments were done on larvae, pupae, and adult flies but not on embryos. Thus, it has not been reported yet how biotin can be efficiently delivered to the embryo. Since embryos are covered with the chorion and the vitelline membrane to protect them from the environment, it was not clear whether and how an easy and sufficient external biotin supply could be provided.

First test experiments to establish the final protocol were performed on ovaries because they are easier to access than embryos. Therefore, flies expressing TurboID fusion proteins were fed overnight with yeast paste, a biotin-rich food, and ovaries were dissected the next day. One set of ovaries was not further treated. Two other sets of ovaries were incubated in Schneider's Medium containing 1 mM biotin for either 10' or 30' minutes. Surprisingly, no striking difference was observed between the samples. These observations led to the following hypothesis: TurboID is so fast and efficient that the smallest amounts of biotin are sufficient to induce efficient biotinylation in a very short period of time. If the smallest amounts of biotin are already sufficient for efficient biotinylation in ovaries, could it be enough to feed the parental generation with biotin-supplemented food to ensure adequate biotin delivery to the embryo? Indeed, this was the case. Because standard fly food already contains a high concentration of biotin, it was not even necessary to prepare a special biotin-supplemented food. Figure 43 displays the efficient biotinylation of proteins in the presence of TurboID in embryos. In comparison, the amount of biotinylated proteins is much lower in eGFP:SmashPM expressing control embryos. Furthermore, it can be seen that eGFP:TurboID:SmashPM and TurboID:eGFP underwent self-biotinylation (Figure 43). We conclude that, with respect to proper subcellular localization and efficient biotinylation of target proteins, the eGFP:TurboID:SmashPM fusion protein is apparently functional.

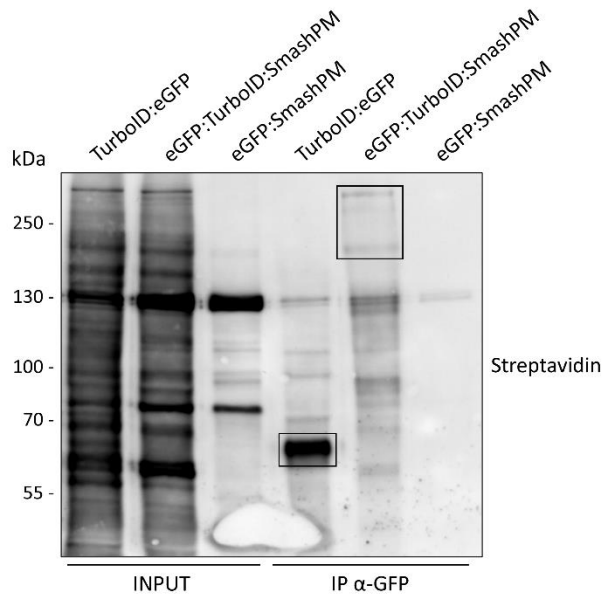


**Figure 43: TurboID efficiently biotinylates proteins in embryos.** Expression of UASp::TurboID:eGFP, UASp:eGFP:TurboID:SmashPM, and UASp:eGFP:SmashPM was induced in embryos by using a maternal  $\alpha$ -Tubulin67C Gal4 driver. Embryos were used to prepare protein lysates. Whole embryo lysates were used for immunoprecipitation against GFP. Input and immunoprecipitated samples were analyzed by Western blotting. The respective bands for TurboID:eGFP and eGFP:TurboID:SmashPM were outlined with boxes. To detect biotinylation, streptavidin coupled to HRP was used. Predicted molecular weight of proteins: TurboID:eGFP = 64.3 kDa, eGFP:SmashPM:TurboID = 233.0 kDa.

After verifying the functionality of the TurboID fusion proteins, embryos expressing either eGFP:TurboID:SmashPM, eGFP:SmashPM, or TurboID:eGFP were processed for mass spectrometry analysis. Further details on the procedure can be found in material & methods section. The results of the mass spectrometry analysis are depicted in Figure 44.

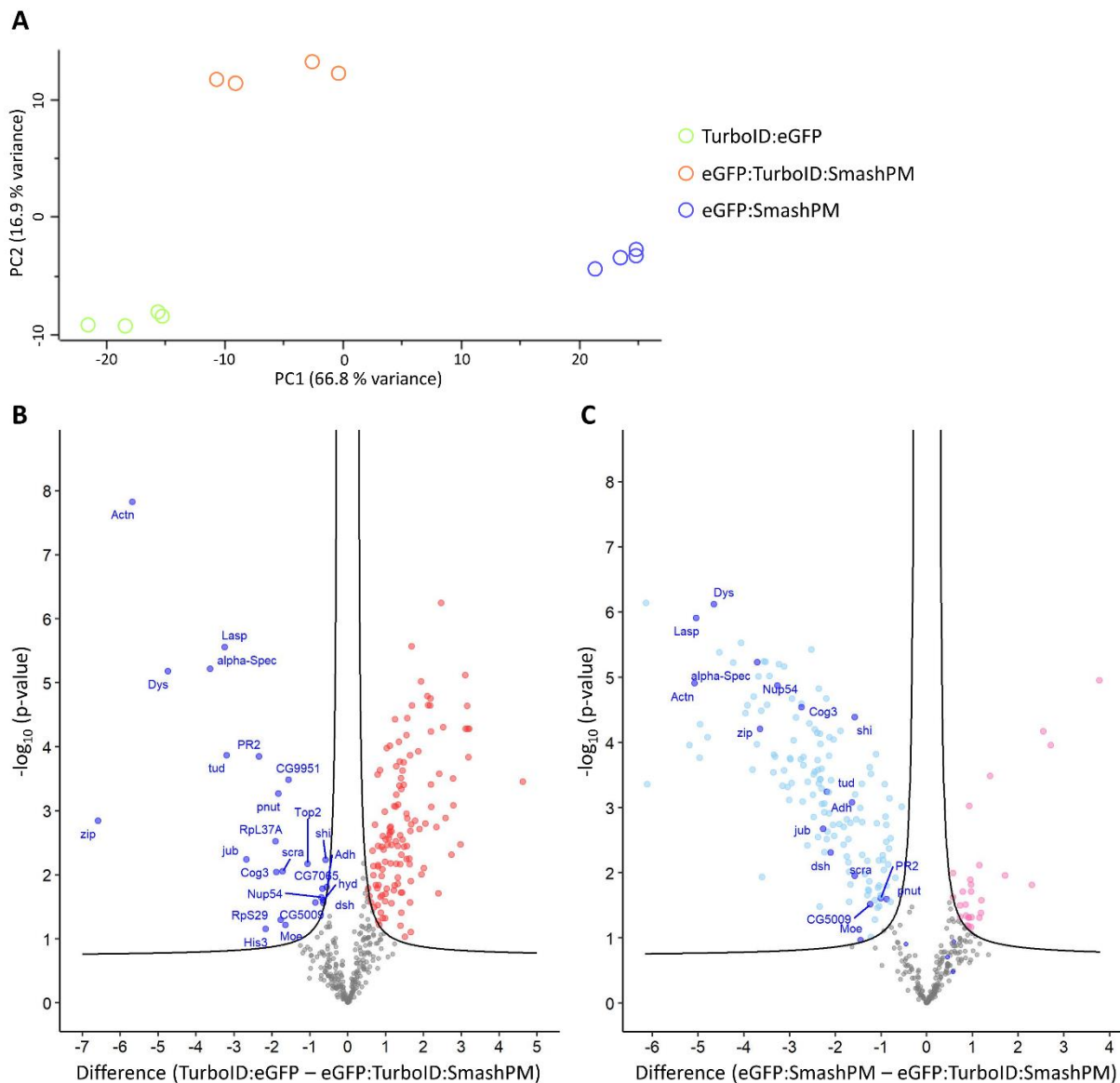


**Figure 44: Proteomic analysis identifies novel, potential Smash-interacting proteins.** (A) Principal component analysis (PCA) of protein profiles detected in TurboID:eGFP, eGFP:TurboID:SmashPM, and eGFP:SmashPM. PC1 captures 66.8 % variance and PC2 captures 16.9 % variance across the different genotypes. (B) Volcano plot showing significant differences in protein abundance between TurboID:eGFP and eGFP:TurboID:SmashPM. (C) Volcano plot showing significant differences in protein abundance between eGFP:SmashPM and eGFP:TurboID:SmashPM. (B & C) The X-axis depicts the difference in protein abundance, which is given in  $\log_2$  fold change, and Y-axis shows the significance level (p-value) in  $-\log_{10}$  scale. The black cut-off lines represent the threshold that indicates whether the protein abundance is significantly different. Significantly decreased protein abundance is highlighted in dark or light blue, and significantly increased protein abundance is highlighted in red or pink. Grey dots represent non-significant scores. The names of the genes encoding the proteins that show a significantly decreased protein abundance in both comparisons were indicated in dark blue. These proteins were considered as high-confidence interaction partner of Smash. For more details on data analysis, see material & methods section.

The MS results revealed that the expressed TurboID fusion proteins were enriched in all respective samples, consistent with the observed self-biotinylation of the TurboID fusion proteins expressed in embryos (Figure 43). The technical replicates of each genotype clustered together in the PCA, revealing similarities within and differences across the genotypes (Figure 44 A). The volcano plots compare the protein abundance in the different genotypes. Thereby, TurboID:eGFP and eGFP:SmashPM overexpressing embryos were separately compared to eGFP:TurboID:SmashPM overexpressing embryos (Figure 44 B & C). In both cases, proteins that were statistically significantly enriched against eGFP:TurboID:SmashPM (red and pink dots) were not further investigated because these are likely to be unspecific background. Interesting candidates are the ones that were statistically significantly decreased compared to eGFP:TurboID:SmashPM (dark and light blue dots). For those candidates, GO term analysis was performed to get an idea about the characteristics of the identified proteins (Chen et al., 2013; Kuleshov et al., 2016) (Figure S 16 & S 17). In both cases, actin binding, tubulin binding, and microtubule binding proteins make up the top three categories when sorted by molecular function. Upon sorting by biological processes, cytoskeleton organization, morphogenesis of an epithelium, and actomyosin contractile ring assembly built the top three categories when TurboID:eGFP was compared to eGFP:TurboID:SmashPM. The top three categories sorted by biological processes when comparing eGFP:SmashPM to eGFP:TurboID:SmashPM were nuclear export, RNA export from nucleus, and protein localization to nucleus. Additional information on the GO term analysis can be found in Table S 9-9. For further analysis, only the proteins whose abundance was significantly decreased in both cases (TurboID:eGFP – eGFP:TurboID:SmashPM and eGFP:SmashPM – eGFP:TurboID:SmashPM) were considered as potential, high-confidence interaction partner of Smash. These candidates were labeled with their respective gene names and marked as dark blue dots. Table 8 gives an overview of the identified, potential interaction partners of Smash and a brief functional description of each (source: <https://flybase.org/>).

**Table 8: New Smash-interacting proteins identified by biotin proximity labeling.** Potential Smash-interacting proteins are listed with their gene name and a brief functional description (source: <https://flybase.org/>).

| N° | Interacting protein                          | Genes                           | Function  |
|----|--|---------------------------------|---|
| 1  | $\alpha$ -Actinin                            | <i>Actn</i>                     | $\alpha$ -Actinin encodes an actin cross-linking protein with muscle and non-muscle specific isoforms, which are produced by alternative splicing. The muscle isoform has a role in muscle development while the non-muscle isoform localizes to ovarian ring canals and has a role in cytoskeletal remodeling of follicle cells. |
| 2  | Alcohol dehydrogenase                        | <i>Adh</i>                      | Alcohol dehydrogenase encodes an alcohol and acetaldehyde dehydrogenase involved in alcohol and acetaldehyde metabolism.  |
| 3  | $\alpha$ -Spectrin                           | <i><math>\alpha</math>-Spec</i> | $\alpha$ -Spectrin encodes an essential protein that interacts with the products of $\beta$ -Spectrin to form a heterotetramer. It is believed to function in asymmetric division of germ line stem cells via cytoplasmic structures called spectrosomes and fusomes.   |
| 4  | Conserved oligomeric Golgi complex subunit 3 | <i>Cog3</i>                     | Involved in ER-Golgi transport.   |

| N° | Interacting protein                     | Genes         | Function  |
|----|---|---------------|---|
| 5  | Peroxisomal acyl-coenzyme A oxidase 1   | <i>CG5009</i> | Catalyzes the desaturation of acyl-CoAs to 2-trans-enoyl-CoAs. First enzyme of the fatty acid beta-oxidation pathway.   |
| 6  | Polarity protein Dishevelled            | <i>dsh</i>    | Required to establish coherent arrays of polarized cells and segments in embryos. Plays a role in wingless ( <i>wg</i> ) signaling, possibly through the reception of the <i>wg</i> signal by target cells and subsequent redistribution of Arm protein in response to that signal in embryos. This signal seems to be required to establish planar cell polarity and identity.                                       |
| 7  | Dystrophin, isoforms A/C/F/G/H          | <i>Dys</i>    | Dystrophin encodes a cytoplasmic protein that connects the actin cytoskeleton to the extracellular matrix via the receptor encoded by Dg. In addition, the product of <i>Dys</i> serves as a cytoplasmic scaffold for the membrane localization of different signaling factors, including <i>nos</i> , which regulates expression of miRNAs to adapt cellular homeostasis to changes induced by stress and dystrophy. |
| 8  | LIM domain-containing protein Ajuba     | <i>jub</i>    | Ajuba LIM protein encodes a LIM domain-containing protein that binds to and inhibits activation of the Hippo pathway kinase encoded by <i>wts</i> . It localizes to adherens junctions in a tension-dependent manner.   |
| 9  | LIM and SH3 domain protein Lasp         | <i>Lasp</i>   | Lasp encodes a member of the nebulin family. It plays subtle roles in modulating the actin cytoskeleton in ovaries, testes, and muscles, by serving as a scaffold protein binding multiple partners, especially actin and myosin.   |
| 10 | Moesin                                  | <i>Moe</i>    | Moesin encodes an Ezrin, Radixin, Moesin (ERM) protein involved in cortical cytoskeleton stability. It regulates Crb and Rho1. <i>Moe</i> contributes to apical-basal polarity, mitotic spindle organization and epithelial integrity.  |
| 11 | Nucleoporin Nup54                       | <i>Nup54</i>  | Component of the nuclear pore complex (NPC), a complex required for the trafficking across the nuclear envelope.  |
| 12 | Peanut                                  | <i>pnut</i>   | peanut encodes a protein that belongs to the septin family of polymerizing GTPases. Together with the products of <i>Septin1</i> and <i>Septin2</i> , it forms the septin complex. It participates in cytokinesis and other processes that involve organization of the cell cortex.   |
| 13 | Tyrosine protein kinase PR2             | <i>PR2</i>    | Likely to act as a downstream effector of <i>Cdc42</i> during dorsal closure, acting in a kinase independent manner with the other ACK family member <i>Ack</i> to positively regulate expression of <i>zip</i> by promoting the endocytosis of EGFR in the <i>amnioserosa</i> .  |
| 14 | Actin-binding protein Anilin            | <i>scra</i>   | <i>scra</i> encodes a homolog of Anilin, a conserved pleckstrin homology domain (PLEKH) containing protein that binds actin, non-muscle myosin II and microtubules. It stabilizes the contractile ring and is required for completion of cytokinesis.   |
| 15 | Dynamin                                 | <i>shi</i>    | Microtubule-associated force-producing protein which is involved in the production of microtubule bundles, and which can bind and hydrolyze GTP. Implicated in endocytic protein sorting.   |
| 16 | Maternal protein Tudor                  | <i>tud</i>    | Required during oogenesis for the formation of primordial germ cells and for normal abdominal segmentation.   |
| 17 | Non-muscle myosin II heavy chain Zipper | <i>zip</i>    | Non-muscle myosin appears to be responsible for cellularization. Required for morphogenesis and cytokinesis.  |

### 3.12 Smash interacts with Ajuba

The proximity labeling assay uncovered 17 new, potential Smash-binding proteins. Among these, a promising candidate is Ajuba (Jub), an adherens junction-associated, tension-sensitive, LIM domain-containing protein (Razzell et al., 2018; Schimizzi & Longmore, 2015). To confirm the interaction between Smash and Jub, an *in vitro* co-IP experiment was performed. For this purpose, GFP:SmashPM and Myc:Ajuba fusion proteins were co-expressed in S2 cells with corresponding controls. Figure S 18 shows that GFP:SmashPM and Myc:Ajuba co-localize in S2 cells. The results of the co-IP are illustrated in Figure 45. After co-IP against GFP, proteins were detected with  $\alpha$ -GFP and  $\alpha$ -Myc antibodies. Protein detection using the  $\alpha$ -GFP antibody shows distinct bands in each sample, indicating that GFP:SmashPM and GFP were enriched. Protein detection with the  $\alpha$ -Myc antibody revealed a single band in the sample in which GFP:SmashPM and Myc:Ajuba were co-expressed in S2 cells but not in controls. Thus, Myc:Ajuba co-immunoprecipitated with GFP:SmashPM, suggesting an interaction of both proteins with each other.

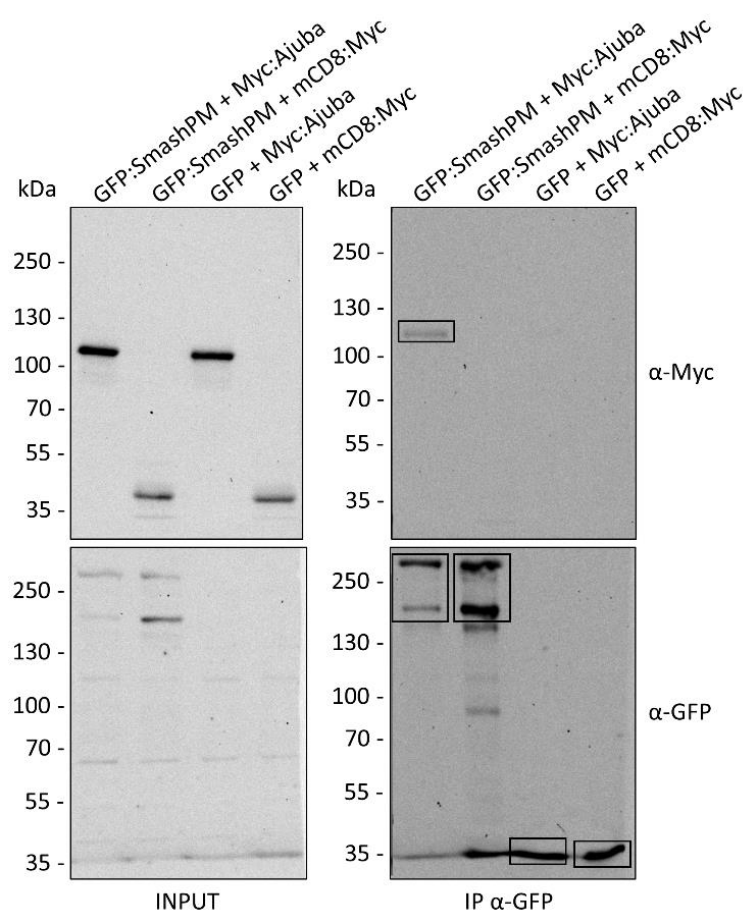


**Figure 45: Myc:Ajuba co-immunoprecipitated with GFP:SmashPM.** Indicated fusion proteins were co-expressed in S2 cells. Protein lysates from S2 cells were used for IP against GFP. The respective bands for Myc:Ajuba, GFP:SmashPM, and GFP were outlined with boxes. Antibodies used for protein detection are indicated on the right of the panels. Predicted molecular weight of proteins: GFP:SmashPM = 197.8 kDa, GFP = 26.9 kDa, Ajuba:Myc = 88.9 kDa, mCD8:Myc = 36.4 kDa.

While our TurboID and co-IP data revealed a physical interaction between Smash and Jub, it was not clear whether this interaction was functionally relevant. Since Smash was demonstrated to be involved in the regulation of PCP, we wanted to know whether Jub PCP was dependent on Smash and vice versa. First, Smash PCP was analyzed upon loss of Jub in *Jub<sup>54</sup>* and *Jub<sup>II</sup>* germline clones (Das Thakur et al., 2010; Razzell et al., 2018). Here, we encountered the technical problem that IF staining of these embryos using the antibody against the N-terminus of Smash created an unspecific dotted pattern superimposed with the specific junctional signal of Smash. This phenomenon was only observed in some fly strains and resembled the pattern described in embryos infected with *Wolbachia* bacteria (Veneti et al., 2004). About 30% of all Bloomington fly strains carry these bacteria (Clark et al., 2005). In fact, antibiotic treatment as described in (Fry & Rand, 2002) abolished the occurrence of dots, strongly indicating that these dots are caused by cross-reactivity of our  $\alpha$ -Smash N-term antibody serum with *Wolbachia* bacteria. Despite the presence of the dotted *Wolbachia* pattern, the membrane-associated Smash signal was strong enough to be measured. Figure 46 depicts the Smash fluorescence signal detected in *Jub<sup>54</sup>* germline clones. A similar pattern was observed in *Jub<sup>II</sup>* germline clones.

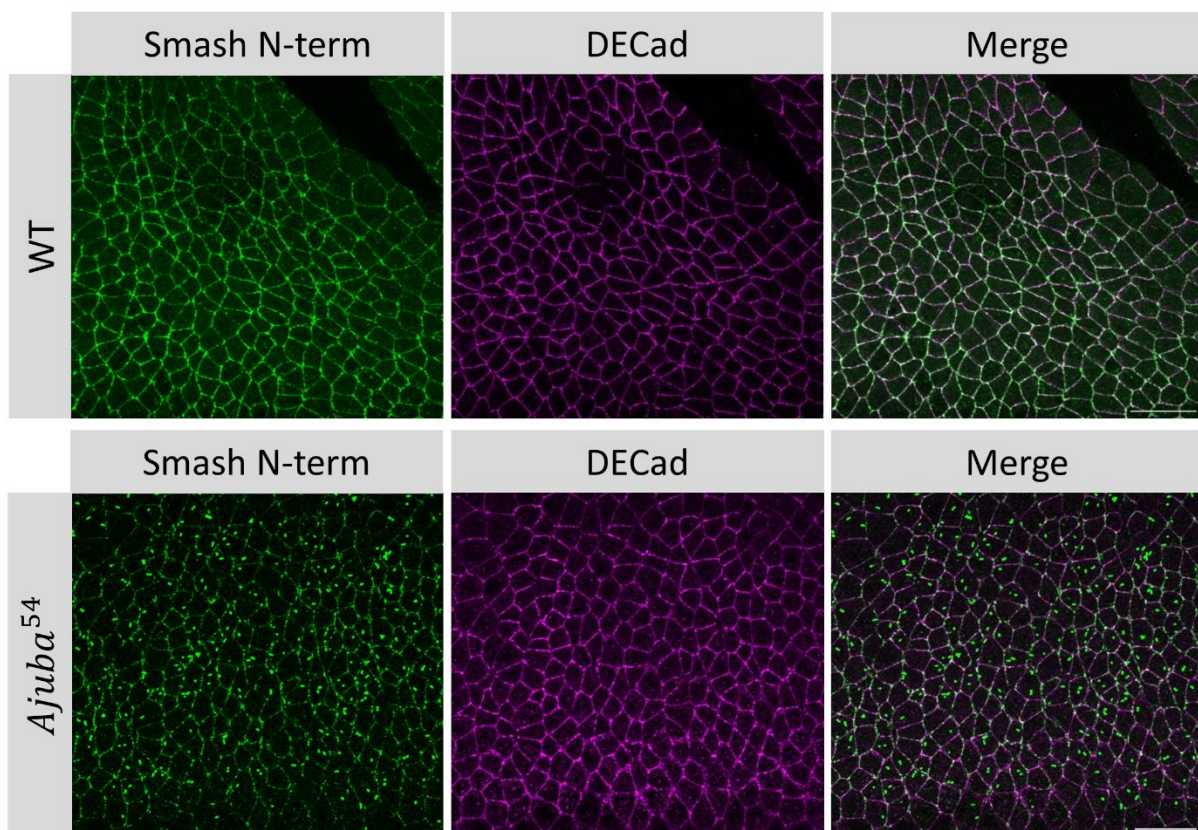


**Figure 46: Nonspecific dots appeared in *Jub<sup>54</sup>* germline clones when the antibody against the N-terminus of Smash was used.** Optical sections of stage 8 embryos above the ventral midline are depicted. Antibodies used for IF staining are indicated above each panel. Scale bar: 20  $\mu$ m.

Smash PCP was quantified in *Jub<sup>54</sup>* and *Jub<sup>II</sup>* germline clones. WT was used as reference. We found that Smash was significantly enriched at A/P junctions in WT, *Jub<sup>54</sup>*, and *Jub<sup>II</sup>* stage 7-8 embryos (Figure 47 A). To compare protein localization between genotypes, the mean AP/DV ratio was calculated for each genotype. An AP/DV ratio of 1 means that the protein was equally distributed at A/P and D/V junctions. The AP/DV ratio of Smash in *Jub<sup>54</sup>* and *Jub<sup>II</sup>* germline clones was not statistically significantly different compared to WT (Figure 47 B), suggesting that the loss of Jub did not affect Smash PCP. Whether Jub PCP is dependent on Smash is still unclear since this experiment has not been completed yet.

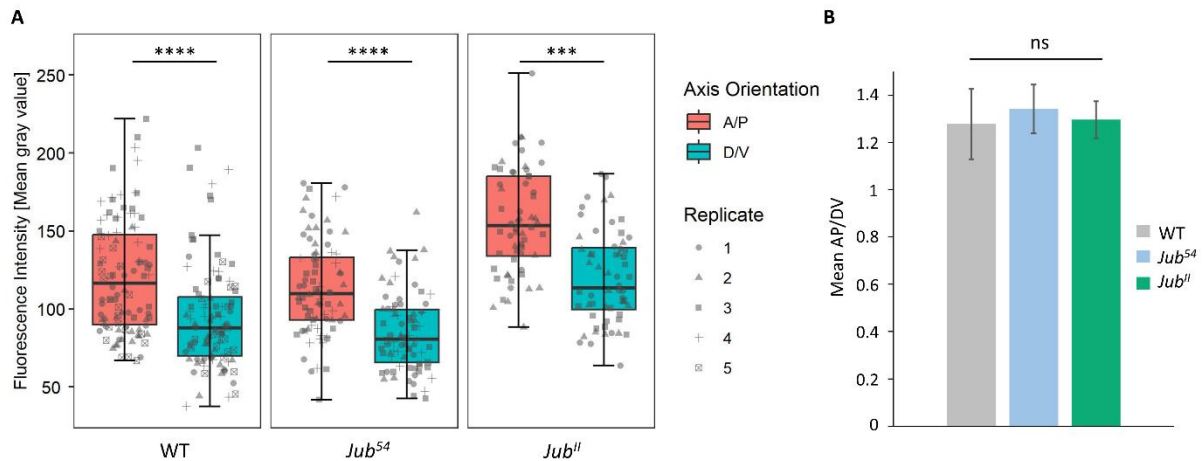


**Figure 47: The planar polarity of Smash is unaffected in *Jub* germline clones compared to WT.** (A) The mean gray value of the Smash signal at A/P (60 - 90 °) and D/V (0 -25 °) oriented axes measured in WT, *Jub<sup>54</sup>*, and *Jub<sup>II</sup>* stage 7-8 embryos is shown. Kruskal-Wallis test and a post hoc Dunn test were performed to determine the statistical significance of the difference between two samples. The significance level is indicated with asterisks. ‘\*\*\*\*’:  $p < 0.0001$ ; ‘\*\*\*’:  $p < 0.001$ . WT  $n = 100$ , *Jub<sup>54</sup>*  $n = 80$ , *Jub<sup>II</sup>*  $n = 60$ . (B) The mean AP/DV ratio was calculated. A Kruskal-Wallis test was performed to identify the statistically significant difference between two samples. The significance level is indicated. ns: not significant. WT  $n = 5$ , *Jub<sup>54</sup>*  $n = 4$ , *Jub<sup>II</sup>*  $n = 3$ .

### 3.13 Smash co-localizes with Lasp in ovaries and embryonic epithelium

A second promising potential interacting protein of Smash, which was identified in the proximity labeling assay, is Lasp. Lasp was described to function as actomyosin scaffolding protein in ovaries, testis, and muscles (Fernandes & Schock, 2014; Lee et al., 2008; Suyama et al., 2009). Moreover, it was reported that Lasp is required to tether *oskar* mRNA at the posterior pole of the oocyte (Suyama et al., 2009). The posterior localization of Lasp and *oskar* mRNA in the oocyte is reminiscent of the highly specific expression pattern of SmashPI in the posterior follicle cells, thus raising the question whether Smash might participate in this important step of early polarity establishment. To better understand the relationship between Lasp and Smash, their expression patterns were studied in ovaries as well as in embryos (Figure 48 & 49). In ovaries, Smash and Lasp co-localize at the nurse cell and the oocyte membrane. In addition, Smash was localized at the apical cortex in follicle cells, while Lasp was not. In embryonic epithelium, both proteins were associated with membranes and co-localized at AJs.

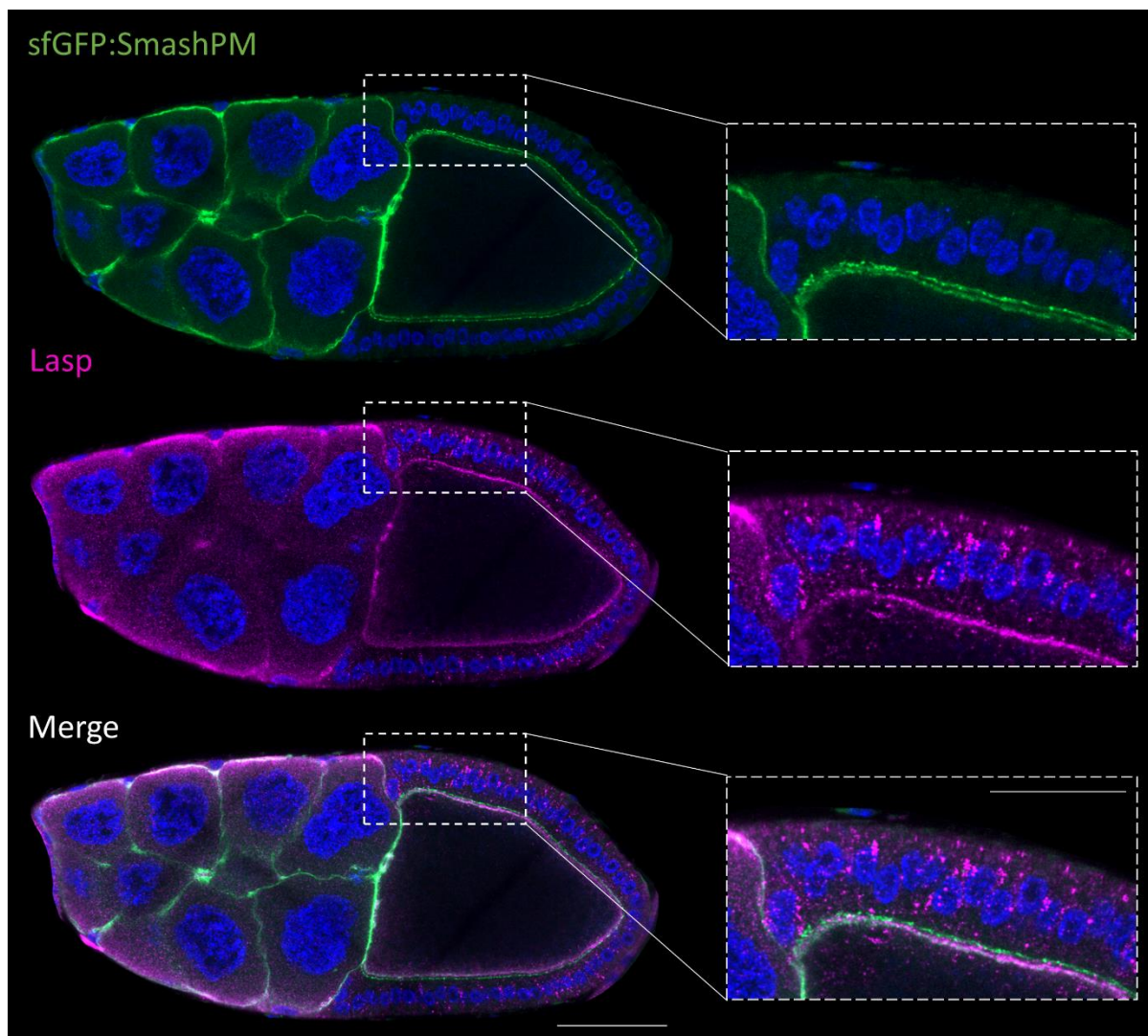


**Figure 48: sfGFP:SmashPM partially co-localizes with Lasp in ovaries.** A sagittal section of a stage 10a ovary is depicted. sfGFP:SmashPM was detected with an  $\alpha$ -GFP antibody. Lasp was detected with an antibody against the N-terminus of Lasp. Scale bar: 50  $\mu$ m, scale bar close-up: 20  $\mu$ m.

matG4 >> UAS::GFP:Lasp

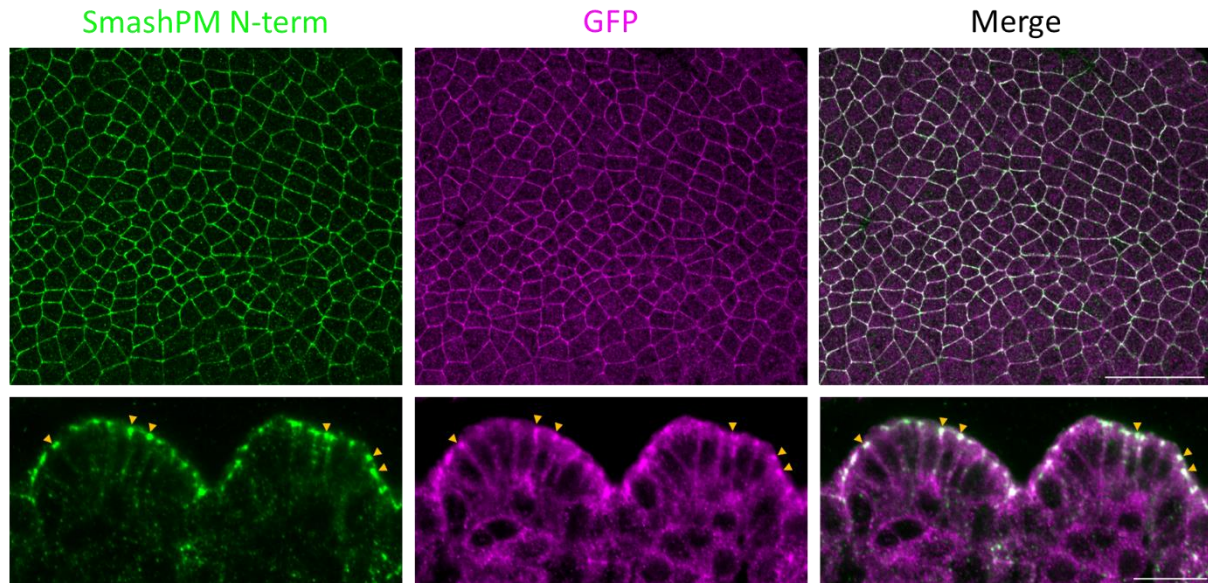


**Figure 49: SmashPM co-localizes with GFP:Lasp in embryonic epithelium.** UAS:GFP:Lasp was overexpressed in embryonic epithelium using the maternal  $\alpha$ -Tubulin67C Gal4 driver line. In the upper panel, an optical section of a stage 8 embryo above the ventral midline is depicted. In the lower panel, a cross-section of a stage 13 embryo is shown. Yellow arrow heads point to AJs where Smash and Lasp co-localized. Antibodies used for IF staining are indicated above the panels. Scale bar upper panel: 30  $\mu$ m, scale bar lower panel: 10  $\mu$ m.

In summary, Lasp and Smash showed partial co-localization in ovaries and overexpressed GFP:Lasp co-localized with Smash in the embryonic neuroectodermal epithelium.

## 4 Discussion

### 4.1 Course and objective of the discussion

In the following sections, I will discuss the results of this study and highlight new insights. First, I will discuss the detailed analysis of the *smash*<sup>Δ35m/z</sup> embryonic phenotype, stressing the possibly responsible molecular mechanism. Next, I will point out the insight we could gain from the newly generated sfGFP knock-in fly strains. Afterwards, I will discuss the role of the potential new Smash-interacting proteins identified by the biotin proximity labeling assay. Finally, I will summarize my key findings and propose future research questions.

### 4.2 Description of the *smash*<sup>Δ35m/z</sup> embryonic phenotype

A prerequisite for morphogenesis is the accurate regulation of actomyosin contractility to enable cell shape changes (Guillot & Lecuit, 2013; Heer & Martin, 2017; Perez-Vale & Peifer, 2020; Pilot & Lecuit, 2005). Thereby, the subcellular localization of the actomyosin network is important. Smash was described to modify actomyosin contractility directly and to regulate the correct subcellular localization of different actomyosin-associated proteins, thus being an important player during morphogenesis (Beati et al., 2018; Peek, 2019).

The importance of Smash during morphogenesis becomes clear in *smash*<sup>Δ35m/z</sup> mutant embryos since these embryos show strong morphogenetic defects. This study shows that the morphogenetic defects occurring in *smash*<sup>Δ35m/z</sup> mutant embryos appear already during early development. Live imaging of *smash*<sup>Δ35m/z</sup> embryos revealed that there might be defects occurring already during cellularization, an early actomyosin driven process during epithelial morphogenesis (Sokac & Wieschaus, 2008a, 2008b), since there was a remarkably high number of *smash*<sup>Δ35m/z</sup> embryos that did not undergo cellularization. Out of all recorded embryos, 10 % of WT did not undergo cellularization, most likely due to inappropriate handling prior to recording. This amount drastically increased up to 78 % in *smash*<sup>Δ35m/z</sup> mutants. All embryos were treated the same, thus ruling out the possibility of bias during preparation. Defects continued during development as labeling of the mesoderm in fixed *smash*<sup>Δ35m/z</sup> embryos revealed abnormal ventral furrow formation (Figure 15). Moreover, live imaging analysis showed that germ band elongation was impaired in *smash*<sup>Δ35m/z</sup> mutant embryos. We demonstrated that GBE was reduced in length and speed (Figure 28, 30, S 6-S 9). As live imaging was only performed over a limited time period, it is not clear how these embryos would have developed further. By combining live imaging data of early embryonic stages and the phenotypes observed in fixed *smash*<sup>Δ35m/z</sup> embryos throughout all developmental stages, a broad variety of phenotypic defects was observed. As Smash was reported to regulate actomyosin contractility (Beati et al., 2018; Peek, 2019), these findings are not unexpected, considering that major aspects of epithelial morphogenesis are actomyosin-driven processes. The high lethality rate observed in *smash*<sup>Δ35m/z</sup> embryos (91 %) is most likely caused by a combination of morphogenetic defects. For more clarity, live imaging of several, single embryos would

be necessary to identify whether there is a certain timepoint at which development arrests or whether embryos could complete embryogenesis but finally die from the severity of accumulated defects. In conclusion, our results suggest that Smash function is required during several stages of embryogenesis.

The defects in *smash*<sup>Δ35m/z</sup> embryos, which are described in this study, are most likely caused by the strong reduction in Sqh phosphorylation level (Figure 16). The phosphorylation of Sqh is necessary to enable actomyosin filament assembly and contraction (Tan et al., 1992; Watanabe et al., 2007). Because Sqh phosphorylation was decreased in *smash*<sup>Δ35m/z</sup> embryos, actomyosin filament assembly was impaired, resulting in reduced junctional tension (Beati et al., 2018). We assume that coordinated cell shape changes were strongly impaired in *smash*<sup>Δ35m/z</sup> embryos, resulting in the described morphogenetic defects. To verify this hypothesis, future experiments should study the cellular defects occurring during morphogenesis through live imaging. The analysis of cell intercalation events during GBE would be worthwhile since these are likely to be abnormal in *smash*<sup>Δ35m/z</sup> mutant embryos.

Reduced phosphorylation of Sqh is most likely one of the major causes of the *smash*<sup>Δ35m/z</sup> embryonic phenotype. However, it is not clear what causes this strong reduction. Since Sqh is phosphorylated by Rok, a simple explanation could be a change in Rok kinase activity (Amano et al., 1996; Amano et al., 2010). Shroom, another Smash-binding protein (Peek, 2019), was reported to promote Rok kinase activity (Zalewski et al., 2016). Therefore, we asked whether Smash might have a similar function as Shroom and could directly affect Rok kinase activity. To test this hypothesis, an *in vitro* kinase assay was performed. No direct effect of Smash on Rok kinase activity was observed (Figure 17), leaving the possibility of an alternative mechanism to modulate Rok kinase activity.

Another possible mechanism by which Smash could affect Rok kinase activity is that Smash provides scaffolding functions for Rok and its substrates. It is not trivial to directly prove a scaffolding function, but we have several lines of evidence supporting this hypothesis. The different functional domains of Smash serve as interface for various protein-protein interactions. Due to its structural properties, Smash fulfills important requirements to be able to function as a scaffold. Moreover, it was shown that Smash directly binds to Rok, Shrm, Baz, and maybe Sqh (Peek, 2019). While Shrm interacts with Rok to promote its kinase activity (Bolinger et al., 2010; Nishimura & Takeichi, 2008; Zalewski et al., 2016), Baz and Sqh are phosphorylation targets of Rok (Amano et al., 1996; Amano et al., 2010; Simões et al., 2010) meaning that Rok must come in close vicinity to these proteins to catalyze the phosphorylation reaction. We have evidence suggesting that Smash is required for the efficient phosphorylation of Sqh and Baz. We have already discussed that the phosphorylation of Sqh is abolished upon loss of Smash (Figure 16). From this finding, we conclude that Smash is necessary to bring Rok and Sqh closely together to enable Sqh phosphorylation. In the case of Baz, it was reported that Baz is mislocalized in *smash*<sup>Δ35m/z</sup> embryos (Beati et al., 2018; Peek, 2019). The phosphorylation of Baz by Rok is necessary for proper Baz planar polarized localization at D/V junctions during GBE (Simões et al., 2010). In *smash*<sup>Δ35m/z</sup> embryos, Baz is enriched at A/P junctions, suggesting that Baz is no longer phosphorylated

by Rok (Beati et al., 2018; Peek, 2019). Further experiments need to be conducted to prove this assumption, but in general, the mislocalization of Baz in *smash*<sup>Δ35m/z</sup> embryos is another, indirect proof that Smash might provide scaffolding function for Rok and its phosphorylation targets. In future experiments, mass spectrometry can be used to investigate the phosphorylation status of several Rok target proteins in *smash*<sup>Δ35m/z</sup> embryos. If our hypothesis turns out to be true and Smash provides scaffolding function for Rok and its phosphorylation targets, we hypothesize that protein phosphorylation by Rok is reduced or even completely abolished in *smash*<sup>Δ35m/z</sup> embryos. Moreover, it could be interesting to investigate whether Smash is also phosphorylated by Rok since the phosphorylation of Smash by Rok could serve as another possible mechanism to regulate Smash function, localization, or both.

As it has been shown for Baz subcellular localization (Simões et al., 2010), this study demonstrated that the subcellular localization of Smash is dependent on Rok (Figure 18). The mechanism by which Rok regulates the subcellular localization of Smash has not been investigated yet. As already discussed, it is a reasonable hypothesis that Smash localization might be dependent on phosphorylation by Rok. Considering that Smash might act as a scaffold for Rok to provide substrate specificity, it is also possible that Rok recruits Smash through direct interaction at A/P junctions, where both proteins co-localize during GBE (Beati et al., 2018; Peek, 2019). Furthermore, we analyzed the subcellular localization of the AJ protein E-Cadherin in *Rok*<sup>2</sup> embryos. We found that the distribution of E-Cadherin was slightly altered in *Rok*<sup>2</sup> compared to WT embryos, although the differences were not statistically significant. These results are in contrast with Simões et al., (2010) who showed that the subcellular localization of the AJ protein β-Catenin is strongly impaired upon loss of Rok. A possible explanation for these different results could lie in the properties of these two adherens junction-associated proteins. While β-Catenin is a cytosolic protein that can be easily redistributed in the cell, E-Cadherin is an integral plasma membrane protein, limiting its ability to move.

In summary, we provided evidence that Smash regulates morphogenesis by modifying actomyosin contractility, which is determined by the Sqh phosphorylation level. We suggest that Smash regulates the phosphorylation level of Sqh by modulating Rok kinase activity, possibly by providing scaffolding function for Rok and its substrates, including Sqh. However, the exact mechanism by which Smash modulates Rok kinase activity remains to be elucidated. Figure 50 visualizes our preliminary model for the molecular working mechanism of Smash. In the course of the discussion, we will refer to this model and develop it further.

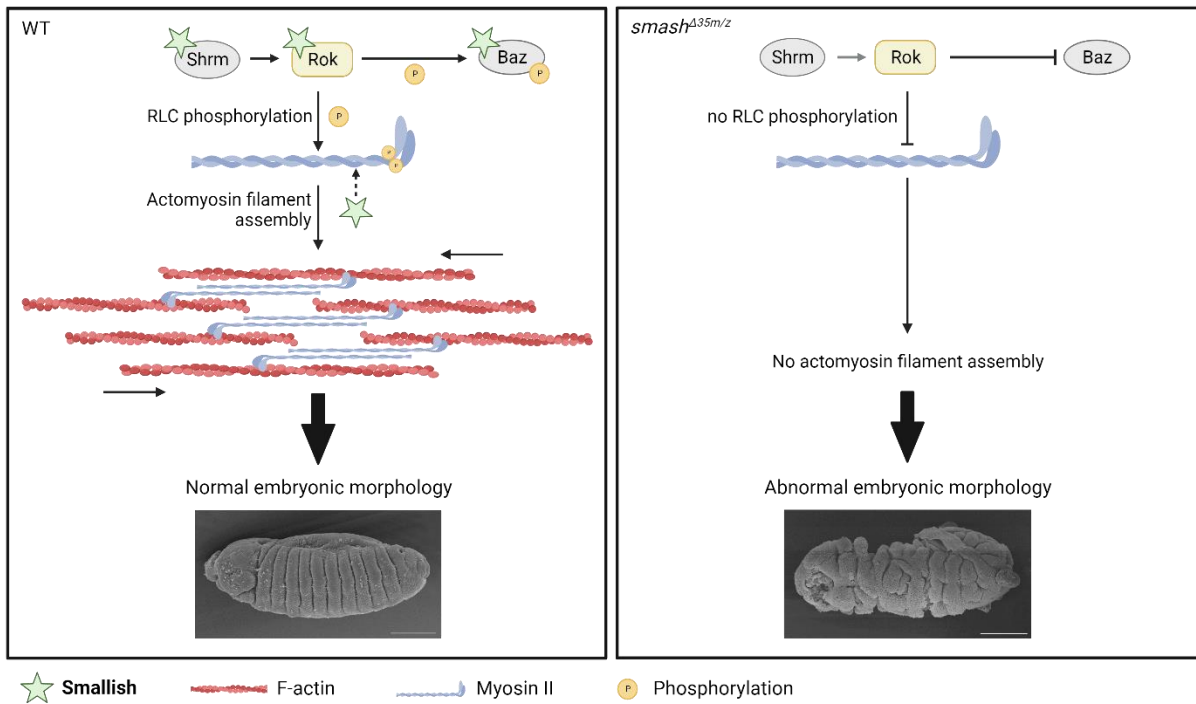


**Figure 50: The molecular working mechanism of Smash – Model No. 1.** In WT embryos, Smash interacts with Baz, Shrm, Rok, and Myosin II. Shrm promotes Rok kinase activity. Rok in turn binds and phosphorylates Baz and Sqh. Upon Sqh phosphorylation, actomyosin filament assembly is induced. The actomyosin network drives changes in cell architecture. Therefore, the tight regulation of actomyosin filament assembly is crucial for proper morphogenesis. In *smash<sup>Δ35m/z</sup>* embryos, Sqh phosphorylation is drastically reduced, resulting in impaired actomyosin filament assembly. Consequently, membrane tension is decreased in *smash<sup>Δ35m/z</sup>* embryos, which finally causes the abnormal embryonic morphology. Unless otherwise stated, arrows between proteins indicate a direct interaction between these proteins. The dashed arrow indicates a possible protein-protein interaction. Scale bar: 100  $\mu\text{m}$ .

### 4.3 A CRISPR/Cas9 approach reveals new insight into Smash function

Studying the spatiotemporal behavior of Smash during embryogenesis would improve our understanding of Smash function. For this purpose, we generated Smash sfGFP knock-in flies using CRISPR/Cas9 technology. A novel fly strain expressing sfGFP:SmashPM resembles the endogenous Smash expression pattern based on what is known from IF staining using an antibody against the N-terminus of Smash (compare Figure 20, 21, and 22 for expression pattern in ovaries, compare Figure 23 and Beati et al. (2018) for expression in embryos, see Figure S 3 for expression pattern in wing discs). This novel fly strain is a great addition to our molecular toolkit to study the spatiotemporal behavior of Smash during morphogenesis in future experiments. In addition, this fly strain enables us to overcome typical problems occurring during IF staining, such as non-specific antibody binding or insufficient penetration of the antibody into the tissue.

The generation of a sfGFP knock-in fly line to tag the shorter isoform SmashPI has led to insightful new findings. We demonstrated that sfGFP:SmashPI was expressed in a highly specific pattern in posterior follicle cells in egg chambers from stage 9 onwards (Figure 24). sfGFP:SmashPI was neither expressed in embryos nor in imaginal discs, raising the possibility that sfGFP:SmashPI is exclusively expressed in posterior follicle cells (Figure S 3 & S 4). For a definitive statement, the expression pattern of sfGFP:SmashPI must be analyzed in all remaining tissues that have not been investigated yet, e. g. the brain or the gut in larvae and adult flies.

During stages 7-10 of oogenesis, the last steps to establish an anterior-posterior polarity axis in the oocyte take place (Milas & Telley, 2022). During this process, the posterior follicle cell fate is determined by the ligand Gurken. Posterior follicle cells receive the Gurken signal from the oocyte, which leads to the activation of epidermal growth factor receptor (EGFR) signaling, which in turn is necessary for cell fate determination (González-Reyes et al., 1995; Neuman-Silberberg & Schupbach, 1993; Roth et al., 1995). Moreover, EGFR signaling is required for the asymmetric distribution of polarity determinants within the oocyte. Accordingly, *bicoid* mRNA is delivered to the anterior pole, while *oskar* mRNA is delivered to the posterior pole via microtubule-dependent transport (Frohnhofer & Nüsslein-Volhard, 1986; González-Reyes et al., 1995; Lehmann & Nüsslein-Volhard, 1986). The latter process takes place during stage 10a, exactly the stage in which sfGFP:SmashPI expression is detected, raising the possibility that SmashPI might be involved in oocyte polarization. Further experiments are required to test this hypothesis. In general, one could investigate the posterior enrichment of *oskar* mRNA in the oocyte in *smash*<sup>435</sup> mutants. However, this experiment would not unravel the isoform-specific contribution within this process. To identify the isoform-specific contribution in tethering *oskar* mRNA to the posterior pole of the oocyte, the respective isoforms need to be expressed separately in *smash*<sup>435</sup> mutant background. Another way to study the effect of SmashPI on tethering *oskar* mRNA to the posterior pole of the oocyte would be to specifically knock out SmashPI in an otherwise wild-type background expressing SmashPM.

Another prominent characteristic of the sfGFP:SmashPI knock-in fly strain is the occurrence of severe morphogenetic defects during embryogenesis in embryos from homozygous mothers (Figure 27) which appear to be even stronger and more penetrant than the defects occurring in *smash*<sup>Δ35m/z</sup> embryos. Live imaging analysis revealed that sfGFP:SmashPI<sup>m/z</sup> embryos show similar defects comparable to *smash*<sup>Δ35m/z</sup> embryos during early development. 65 % of sfGFP:SmashPI<sup>m/z</sup> and 78 % of *smash*<sup>Δ35m/z</sup> embryos did not undergo cellularization. Furthermore, GBE length and speed in both sfGFP:SmashPI<sup>m/z</sup> and *smash*<sup>Δ35m/z</sup> embryos were reduced compared to WT. Compared to WT, a generally higher variability of phenotypic defects occurred within sfGFP:SmashPI<sup>m/z</sup> and *smash*<sup>Δ35m/z</sup> embryos. This variability is reflected in the size of the error bars (Figure S 6 & S 8). The higher variability between embryos within the same genotype can be interpreted as an indication for a less robust system. Due to the high number of embryos that died before cellularization, the sample size that makes up our data set is quite low (*smash*<sup>Δ35m/z</sup> embryos n = 6, sfGFP:SmashPI<sup>m/z</sup> embryos n = 12). Since the variability between the embryos within the same genotype is very high, this small sample size might not be sufficient to fully cover the whole variety of defects that occur. To obtain a more representative data set, the present data set should be expanded in the future.

A closer look at the sfGFP:SmashPI<sup>m/z</sup> embryonic phenotype reveals a strong similarity to *folded gastrulation (fog)* mutants (Sweeton et al., 1991). *fog* mutants have defects in ventral furrow formation (irregular and delayed but occurs) and posterior gut fold formation (Costa et al., 1994). Moreover, and as the name already suggests, a concomitant phenomenon during gastrulation in *fog* mutants is the formation of additional, aberrant furrows. Interestingly, a very similar phenomenon was described in lung tumor formation in LMO7 knock-out mice, where the bronchiolar epithelium forms apical protrusions and invaginates at the basement membrane (Tanaka-Okamoto et al., 2009). More recently, it was found that Fog also affects cell intercalation during GBE (Kerridge et al., 2016). The similarity of sfGFP:SmashPI<sup>m/z</sup> and *fog* mutant embryonic phenotype suggests that Smash may act on Rok kinase activity by interfering with the Fog signaling pathway, e. g. by regulating the subcellular localization of Rok upstream activators. Because the activation of Fog signaling is locally restricted, mislocalization of single components within the pathway might already be sufficient to disrupt the signaling cascade.

To further investigate whether Smash interferes with Fog signaling and thereby indirectly regulates Rok kinase activity, future experiments could analyze the embryonic phenotype of double mutants (*fog, smash<sup>A35</sup>* and *fog, sfGFP:SmashPI*). If both proteins are active in the same pathway, the phenotype would not be stronger in the double mutant compared to the single mutants. If both proteins would act in two parallel pathways, we would expect enhanced morphogenetic defects in doubly mutant embryos. In addition, the subcellular localization of Fog signaling components could be studied in *smash<sup>A35m/z</sup>* mutant embryos. If Smash interferes with the Fog signaling pathway, we expect that some Fog signaling components will mislocalize and therefore Fog signaling will be disturbed. The potential involvement of Smash in Rok upstream signaling is implemented in our model, as visualized in Figure 51.

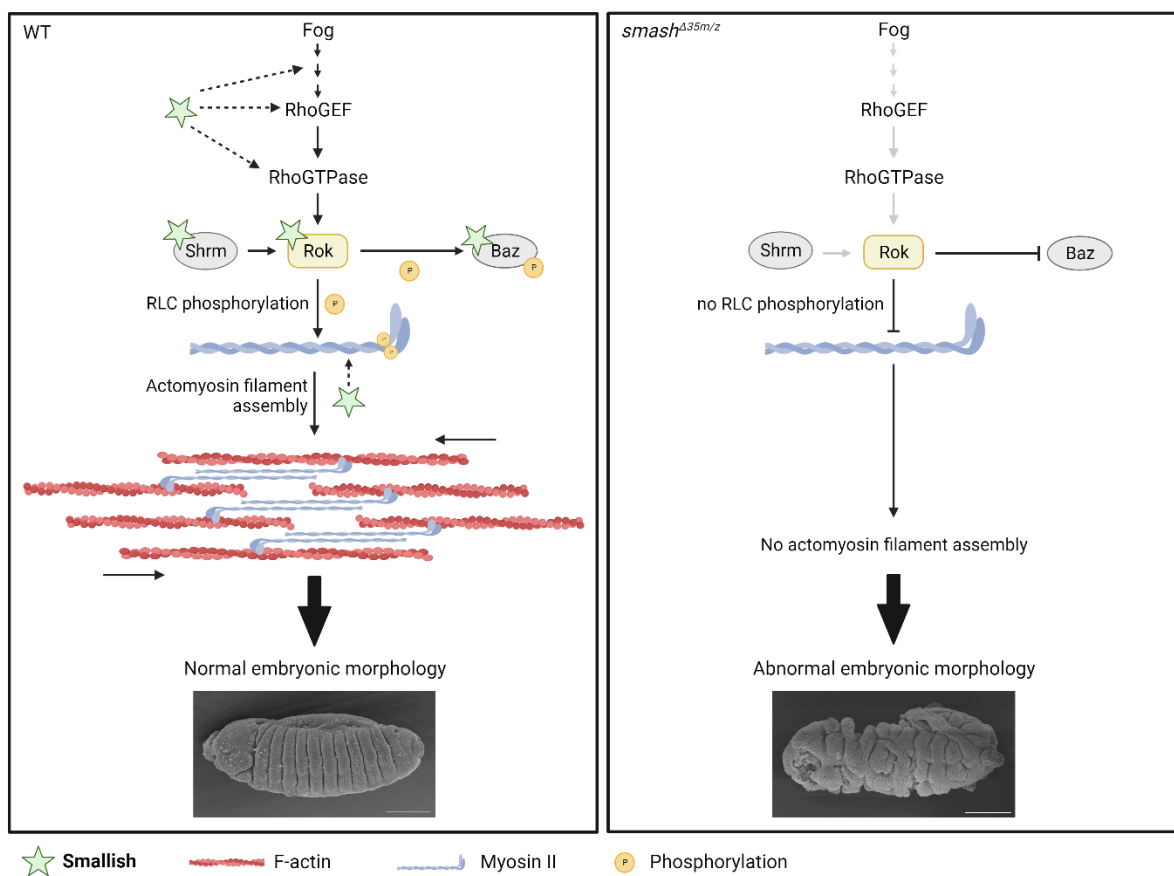


**Figure 51: The molecular working mechanism of Smash – Model No. 2.** In WT embryos, Smash interacts with Baz, Shrm, Rok, and Myosin II. Rok is activated by Fog signaling. Smash could interfere with Fog signaling to regulate Rok kinase activity. Moreover, Shrm promotes Rok kinase activity. Rok in turn binds and phosphorylates Baz and Sqh. Upon Sqh phosphorylation, actomyosin filament assembly is induced. The actomyosin network drives changes in cell architecture. Therefore, the tight regulation of actomyosin filament assembly is crucial for proper morphogenesis. In *smash<sup>A35m/z</sup>* embryos, Sqh phosphorylation is drastically reduced, most likely because of impaired Rok kinase activity. Defective actomyosin filament assembly results in reduced membrane tension, which finally causes the abnormal embryonic morphology. Unless otherwise indicated, arrows between two proteins indicate a proven interaction. The dashed arrows indicate a potential interaction between two proteins. Scale bar: 100  $\mu$ m.

After comparing the *smash*<sup>Δ35m/z</sup> with sfGFP:SmashPI<sup>m/z</sup> embryonic phenotype, we wondered why the sfGFP:SmashPI<sup>m/z</sup> embryonic phenotype is more severe and more penetrant compared to the *smash*<sup>Δ35m/z</sup> embryonic phenotype. In this study, we demonstrated that sfGFP:SmashPI<sup>m/z</sup> embryos do neither express sfGFP:SmashPI (Figure S 4) nor full-length SmashPM but showed some abnormal signal when the antibody against the N-terminus of Smash was used (Figure 25), indicating that a truncated version of SmashPM (SmashPM N-term) is still expressed in embryos. We propose that this truncated, mislocalized SmashPM protein is not fully functional as it lacks conserved domains, including the LIM domain and PDZ binding motif at the C-terminus, but it may have a dominant negative effect because it could still engage in protein-protein interactions, for instance via the myosin binding domain or the two coiled coil domains. Consequently, we suggest that the stronger and more penetrant phenotype of sfGFP:SmashPI<sup>m/z</sup> embryos compared to *smash*<sup>Δ35m/z</sup> null mutant embryos where no Smash protein is expressed is caused by a dominant-negative effect of the mislocalized N-terminal fragment of SmashPM. In Beati et al. (2018) stochastic overexpression in the follicle epithelium revealed that full-length SmashPM modifies cell architecture by promoting F-actin enrichment at the apical cell cortex, which induces apical constriction.

In our study, we combined stochastic overexpression and overexpression in the whole follicle epithelium to investigate the effect of SmashPM N-term on the actomyosin network and on cell architecture. We showed that SmashPM N-term was strongly mislocalized compared to SmashPM, probably due to the missing C-terminus (Figure 31 & 32). Compared to SmashPM, SmashPM N-term was significantly less enriched at the apical cell cortex (Figure 32). Nevertheless, the subtle localization of SmashPM N-term at the apical cell cortex was correlated with a slight enrichment of F-actin compared to the mCD8 control (Figure 33 & 34). Despite the fact that SmashPM N-term was strongly mislocalized, F-actin was not enriched in the cytosol (Figure S 14) suggesting that SmashPM N-term is able to recruit or stabilize F-actin in a junction-dependent manner. In agreement with these findings, SmashPM N-term overexpressing cells induce a weak apical constriction response, albeit to a lower extent compared to cells overexpressing full-length SmashPM, suggesting that not only F-actin but also myosin filaments are likely to be involved.

Matsuda et al. (2022) reported that the myosin binding domain and the α-Actinin binding domain in *Xenopus* LMO7 are sufficient to promote actomyosin filament assembly to induce apical constriction, whereas the myosin binding domain alone could not induce apical constriction. Interestingly, truncated *Xenopus* LMO7 variants did not show obvious localization defects since they were still enriched at the apical membrane. Thus, the contribution of protein localization to induce apical constriction was not investigated in Matsuda et al. (2022), whereas we assume that mislocalization of SmashPM N-term is an important factor explaining the reduced ability of SmashPM N-term to promote apical constriction. We speculate that the scaffolding function of SmashPM N-term might be impaired because of mislocalization or because of missing protein interaction domains. Both possible causes are

mutually dependent on each other since missing protein interaction domains might cause mislocalization and mislocalization might prevent protein interactions because SmashPM N-term is not acting in the right place.

Matsuda et al. (2022) stated that apical constriction is inhibited upon mutating the myosin binding domain in full-length *Xenopus* LMO7. Consistent with this finding, we demonstrated that mutating the myosin binding site of Smash was sufficient to completely abolish its ability to induce apical constriction (Figure 37 & 38). We did not observe F-actin enrichment at the apical cell cortex in follicle cells expressing SmashPM mut, indicating that F-actin enrichment is dependent on the myosin binding domain (Figure 33). We did not investigate the localization of myosin filaments, but based on the findings in Matsuda et al. (2022), we suggest that the myosin binding domain is necessary to recruit both F-actin and myosin, thus promoting the formation of actomyosin filaments at the apical cell cortex. Since actomyosin filament assembly is dependent on the phosphorylation of Sqh by Rok, we propose that Smash binds to Myosin II via its myosin binding domain and there it provides scaffolding function for Rok. Since vertebrate LMO7 binds  $\alpha$ -Actinin (Ooshio et al., 2004), it is likely that Smash also binds  $\alpha$ -Actinin. Assuming that Smash interacts with  $\alpha$ -Actinin, Smash may support the crosslinking function of  $\alpha$ -Actinin to stabilize the actomyosin network. As the whole process appears to take place in a junction-dependent manner, we assume that Smash serves as linker between the actomyosin cytoskeleton and AJs, presumably also together with  $\alpha$ -Actinin.

Comparable to the observations described in Beati et al. (2018), we demonstrated that apically enriched full-length SmashPM can reinforce apical F-actin localization, thus inducing a strong apical constriction response in follicle cells (Figure 33 & 38). Interestingly, F-actin was not only enriched in follicle cells but also at the oocyte membrane (Figure 31). Other studies found that actomyosin subcellular localization can be regulated by mechanical cues (Fernandez-Gonzalez et al., 2009; Pouille et al., 2009). We assume that overexpression of SmashPM produces additional tension at the apical cell cortex of follicle cells, which is then transferred to the oocyte. This mechanical cue might promote the enrichment of F-actin at the oocyte membrane to provide more stiffness and prevent squeezing of the oocyte. In contrast to the results reported in Beati et al. (2018), we observed that eGFP-negative cells adjacent to eGFP-positive cells in ovaries stochastically overexpressing eGFP:SmashPM are significantly larger compared to mCD8:eGFP control ovaries. These differences probably arose from different ways of evaluating and presenting the data. We argue that our obtained data appear logical since adjacent eGFP-negative cells need to expand their surface to compensate for the drastic shrinkage of eGFP-positive cells overexpressing eGFP:SmashPM to prevent premature tissue rupture of the follicle epithelium.

---

In summary, this experimental series demonstrated that SmashPM is able to promote actomyosin filament assembly at the apical cell cortex in a junction-dependent manner via the myosin binding domain. We propose a mechanism in which Smash provides scaffolding function for Myosin II and Rok to promote Sqh phosphorylation, thereby inducing actomyosin filament assembly, which finally results in tissue deformation. A scaffolding function of Smash to bring Rok and Sqh together is very likely since Smash was shown to interact with both proteins (Peek, 2019). In addition, future experiments must explore whether the enhanced actomyosin filament assembly observed upon eGFP:SmashPM overexpression is indeed dependent on Rok. eGFP:SmashPM overexpression in combination with Rok knock-out using RNAi against Rok will either verify or reject this hypothesis. The subcellular localization of SmashPM is considered to be important for apical constriction, since mislocalized SmashPM N-term showed a reduced ability to promote apical constriction. Based on these results, we can conclude that SmashPM N-term retains some functionality, which might promote the severity of occurring morphogenetic defects in sfGFP:SmashPM<sup>m/z</sup> embryos compared to *smash*<sup>Δ35m/z</sup> embryos. We suggest that properly regulated actomyosin filament assembly is impaired in sfGFP:SmashPM<sup>m/z</sup> embryos due to mislocalization of SmashPM N-term, resulting in uncoordinated cell shape changes. In addition, further factors that were not investigated yet cannot be excluded. For example, there is the possibility that SmashPM N-term influences the subcellular localization of other actomyosin-associated proteins. Resulting defects in PCP might have an additional, negative impact on morphogenesis. The main results of this experiment are summarized in Figure 52.

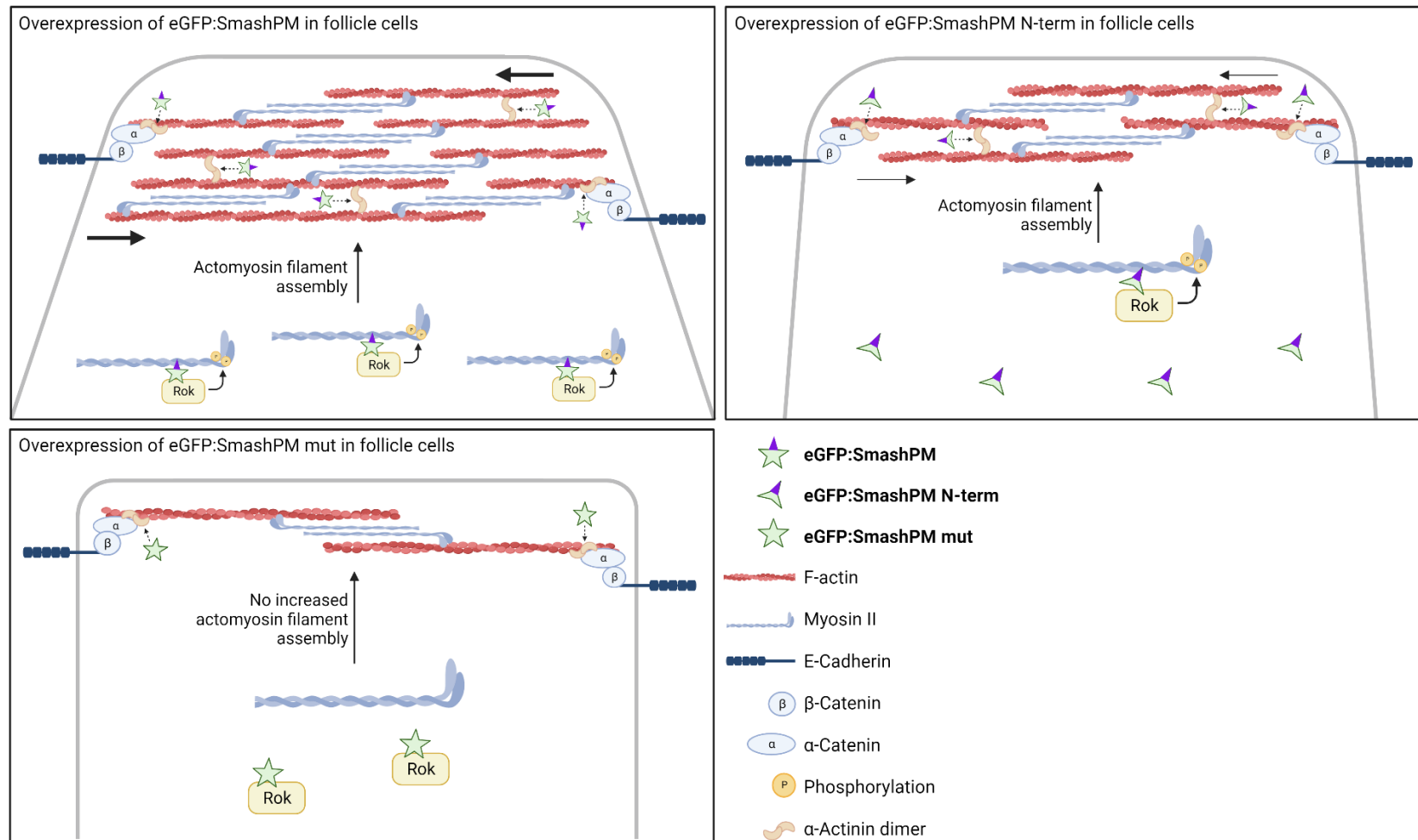


**Figure 52: Graphical summary of overexpression experiments in the follicle epithelium.** In eGFP:SmashPM overexpressing cells (upper panel, left) eGFP:SmashPM interacts with Myosin II via its myosin binding domain (purple). Smash provides scaffolding function for Rok and Myosin II, thereby facilitating Sqh phosphorylation, resulting in increased actomyosin filament assembly. If Smash interacts with  $\alpha$ -Actinin, it is conceivable that Smash also functions as a scaffold between Actin filaments and between the actomyosin network and AJs. In eGFP:SmashPM N-term overexpressing cells (upper panel, right), eGFP:SmashPM N-term is not enriched at the apical cell cortex, thereby preventing eGFP:SmashPM N-term from acting as a scaffold for Rok and Myosin II, which led to a reduced actomyosin filament assembly. In eGFP:SmashPM mut overexpressing cells (lower panel, left) eGFP:SmashPM mut cannot interact with Myosin II because of its mutated myosin II binding domain. Smash does not provide scaffolding function for Rok and Myosin II. Consequently, Rok cannot catalyze the phosphorylation of Myosin II and no increased actomyosin filament assembly occurs. In each scenario, actomyosin filaments are assembled in a junction-dependent manner. The dashed arrows indicate a potential interaction between Smash and  $\alpha$ -Actinin.

Towards the end of oogenesis, rupture of the follicle epithelium is required for ovulation, a process in which the mature oocyte is released into the oviduct (Deady et al., 2015). Follicle epithelium rupture is dependent on Rok-activated actomyosin contractility (not published, personal communication Stella Eun Cho, Jianjun Sun Lab, University of Connecticut). Since Smash is expressed in the follicle epithelium, it is highly likely that Smash contributes to the actomyosin-driven rupture of the follicle epithelium. We have several lines of evidence supporting this hypothesis. The first evidence can be found in the ovarian morphology of sfGFP:SmashPI flies. Although an elaborate statistical analysis is still outstanding, sfGFP:SmashPI ovaries appeared to accumulate mature egg chambers (Figure S 5). The accumulation of more than two mature egg chambers in an ovariole, which is often observed in sfGFP:SmashPI ovarioles, is described as egg-retention phenotype. An egg-retention phenotype could point to ovulation defects (Beard et al., 2023). However, it must be considered that this is not necessarily the case, as the egg-retention phenotype can also result from a general blockage in the egg-laying process itself. Beard et al. (2023) proposes a robust assay that is composed of a series of different experimental approaches to reliably identify ovulation defects. To investigate whether sfGFP:SmashPI flies have ovulation defects, future experiments based on the guidelines in Beard et al. (2023) will be conducted.

The second evidence that Smash might be involved in follicle epithelium rupture at the end of oogenesis is the phenotype observed in eGFP:SmashPM overexpressing ovaries. Overexpression of eGFP:SmashPM in the follicle epithelium led to abnormal morphology in late egg chamber stages (Figure 35) and the egg-laying rate in these flies was drastically reduced compared to control flies. A milder but nonetheless striking phenotype was observed in ovaries overexpressing eGFP:SmashPM N-term in the follicle epithelium. Embryos developing from these ovaries were significantly shorter in length and larger in width compared to control embryos (Figure 36). A preliminary experiment revealed that the egg-laying rate in flies overexpressing eGFP:SmashPM N-term was slightly reduced compared to mCD8:eGFP control flies, but a more elaborate statistical analysis needs to be performed to determine statistically significant differences in the egg-laying rates between genotypes. In conclusion, these experiments provide evidence that Smash might be involved in ovulation and in the regulation of the oocyte architecture. Future experiments using *smash*<sup>Δ35</sup> ovaries could provide a deeper insight into the involvement of Smash within this process.

#### 4.4 Turboid proximity labeling assay identifies novel Smash interaction partners

The regulation of actomyosin dynamics is dependent on a complex protein interaction network. Together with proven binding partners such as Rok, Baz, Cno, Shrm, and Moe, Smash represents a component of this network. To obtain a better understanding of how Smash provides its function, investigating the Smash interaction network could help to determine the hierarchical order of Smash within the network. To identify new Smash-interacting proteins, a biotin proximity labeling assay was performed. Using this unbiased assay, 17 novel, potential Smash interaction partners were identified (Figure 44, Table 8). In the following section, I will briefly describe the characteristics of these potential Smash-interacting proteins. I will discuss which role these proteins might play in morphogenetic and cell polarity-related processes. Moreover, I will highlight additional processes Smash might be involved in. Finally, I will outline open questions and what future experiments could be performed to verify and qualify the novel protein interactions with Smash.

##### **Ajuba:**

Among potential Smash-interacting proteins, the tension-sensitive, LIM domain-containing protein Ajuba is a promising candidate (Razzell et al., 2018; Schimizzi & Longmore, 2015). Similar to Smash, Ajuba contains a LIM domain, which serves as protein-protein interaction domain often providing scaffolding function (Kadmas & Beckerle, 2004). Smash-Jub interaction was verified by *in vitro* co-IP experiments. It is not unlikely that Smash and Jub might interact with each other via their LIM domains. Experimental proof for this still has to be provided. Both proteins are enriched at A/P junctions during germ band elongation (Beati et al., 2018; Razzell et al., 2018). Due to Jub's tension-sensitive properties (Razzell et al., 2018), it is highly likely that its subcellular localization is dependent on Smash since Smash regulates junctional tension. To investigate whether Jub's localization is dependent on Smash, the PCP of Jub in *smash*<sup>Δ35m/z</sup> embryos will be investigated. Results are still outstanding. We do know though that Smash PCP was not affected in *Jub* germline clones (Figure 47). Beati et al. (2018) performed similar experiments in which Smash PCP was investigated. The determined AP/DV ratio for Smash in WT embryos was much higher in Beati et al. (2018) compared to this study. This deviation was most likely caused by differences during sample preparation or data evaluation.

##### **Lasp:**

Another potential interaction partner for Smash is Lasp. Lasp encodes a member of the nebulin family in *Drosophila* and is the homolog of human *Lasp-1*. Lasp contains two nebulin repeat domains comprising a conserved actin-binding motif, a LIM and a Src homology 3 (SH3)-protein binding domain. Lasp was described to play a role in cytoskeleton remodeling by providing scaffolding function for F-actin and Myosin II (Fernandes & Schock, 2014). Interestingly, Lasp is important for efficient anchoring of *oskar* mRNA via F-actin at the posterior pole of the oocyte in *Drosophila* (Suyama et al., 2009). We demonstrated that Lasp co-localizes with Smash in embryonic epithelium and partially in ovaries,

pointing to a biologically relevant interaction between these two proteins. In stage 10a ovaries, both proteins are localized at the nurse cell and oocyte membrane. Additionally, Smash localizes at the apical cell cortex in follicle cells but Lasp does not (Figure 48). The ability of Smash to promote F-Actin enrichment at the oocyte membrane was demonstrated by overexpressing SmashPM in follicle cells (Figure 31 & S 10). These findings raise the possibility that Smash might be involved in tethering *oskar* mRNA via F-actin at the posterior pole of the oocyte. The highly specific localization pattern of sfGFP:SmashPI in posterior follicle cells further strengthens this assumption. At this point, it must be mentioned that it is not yet clear what role SmashPI could play in this process. Unlike SmashPM, SmashPI does not have a myosin binding domain. Therefore, SmashPI is not able to promote actomyosin filament assembly. Because of its C-terminal LIM domain, we suggest that SmashPI might fulfill either a regulatory or a scaffolding function. Whether any of the Smash isoforms is really involved in polarization of the mature oocyte by tethering *oskar* mRNA at the posterior oocyte pole remains to be further elucidated.

#### **$\alpha$ -Actinin:**

Another potential interacting protein identified by the TurboID assay is  $\alpha$ -Actinin.  $\alpha$ -Actinin is required for crosslinking of F-actin filaments and for linking actin filaments to adherens junctions (Sjoblom et al., 2008). The vertebrate homologue of Smash, LMO7, was reported to interact with  $\alpha$ -Actinin via its  $\alpha$ -Actinin binding domain (Ooshio et al., 2004). An *in vitro* co-IP experiment will verify whether Smash can also bind  $\alpha$ -Actinin. An  $\alpha$ -Actinin binding domain in Smash has not been identified yet. Using the sequence information of vertebrate LMO7 could help to identify such a domain. It is conceivable that Smash incorporates its function together with  $\alpha$ -Actinin in two different ways: either by promoting F-actin filament crosslinking or by coupling F-actin to adherens junctions. To examine the biological relevance of the interaction between Smash and  $\alpha$ -Actinin in *Drosophila* embryos, further experiments, such as co-localization studies, need to be conducted. Beati et al. (2028) already demonstrated that Smash and  $\alpha$ -Actinin co-localize at myotendinous junctions of somatic muscles suggesting a physiological relevant interaction these two proteins for muscle development.

$\alpha$ -Actinin belongs to the spectrin protein superfamily. Proteins within this family are characterized by the presence of spectrin repeats (SRs). Thereby, the number of SRs within the different proteins can vary considerably. Moreover, several proteins have been described that carry both an actin-binding calponin homology domain (ABD) and a calcium-binding EF-hand motif. In this respect, known vertebrate variants of  $\alpha$ -Actinin carry a total of four SRs, an N-terminal ABD, and a C-terminal EF hand motif. There is evidence showing that an  $\alpha$ -Actinin like precursor gave rise to the other proteins nowadays belonging to the spectrin superfamily (Broderick & Winder, 2005; Pascual et al., 1997; Thomas et al., 1997).

**$\alpha$ -Spectrin:**

As the name already suggests, Spectrin is another member of the spectrin superfamily. Spectrin forms large heterotetramers comprising two  $\alpha$  and two  $\beta$  subunits.  $\alpha$ -Spectrin contains 20 SRs, while  $\beta$ -Spectrin contains 17 SRs. SRs are involved in the formation of tetramers and they serve as a binding interface for multiple protein interactions to build a membrane-bound cytoskeleton that maintains cell shape (Bennett & Baines, 2001; Machnicka et al., 2012). Unlike  $\alpha$ -Actinin or  $\beta$ -Spectrin,  $\alpha$ -Spectrin does not have an ABD. Instead, it contains a SH3 domain. SH3 domains mediate protein-protein interactions and contribute to actin cytoskeleton remodeling or cell proliferation, respectively (Kurochkina & Guha, 2013). In agreement,  $\alpha$ -Spectrin was described to be important for regulating the cell cycle and actin dynamics (Metral et al., 2009). One way how  $\alpha$ -Spectrin can modify actin dynamics was reported in Bialkowska et al. (2005). They showed that the SH3 domain of  $\alpha$ -Spectrin is crucial for the activation of RhoGTPase Rac, a well-known cytoskeleton regulator. Taking these findings into account, it is not very surprising that  $\alpha$ -Spectrin was identified as a further potential Smash-interacting protein (Figure 44). It remains to be investigated whether and how Smash and  $\alpha$ -Spectrin interact with each other to modify actin dynamics. *In vitro* co-IP experiments and *in vivo* localization studies can provide initial evidence whether Smash interacts with  $\alpha$ -Spectrin and whether this interaction has biological relevance.

**Dystrophin:**

Another putative interacting protein of Smash, which also belongs to the spectrin superfamily, is Dystrophin. In *Drosophila*, different isoforms of Dystrophin are encoded. They comprise a highly conserved N-terminal ABD followed by SRs and a cysteine-rich C-terminus (Neuman et al., 2001). During embryogenesis, the isoform DLP2 is expressed in the visceral mesoderm, in muscle attachment sites, in muscle fibers, and in the gut (van der Plas et al., 2006), thus sharing a partially overlapping expression pattern with Smash (Beati et al., 2018). Dystrophin does not act on its own, but it is incorporated into the so-called dystrophin glycoprotein complex (DGC). DGC is a membrane-spanning complex with extra- and intracellular domains. The extracellular domains link the muscle cell membrane to the extracellular matrix, while the intracellular domains are connected with the cytoskeleton, thus providing muscle membrane stability. Thereby, Dystrophin serves as intracellular binding interface for several cytoskeletal components, such as F-actin, intermediate filaments, and microtubules (Gao & McNally, 2015). As Smash modulates the actomyosin dynamics in epithelial cells and was shown to be expressed in myotendinous junctions of somatic muscles (Beati et al., 2018), it is conceivable that Smash is involved in the organization of F-actin filaments during somatic muscle development. Furthermore, the scaffolding properties of Smash could be involved in mediating the binding between Dystrophin and F-actin. Future research will address these open questions to better understand the potential involvement of Smash in somatic muscle development. This is of special interest since mutations in dystrophin were found to cause Duchenne and Becker muscular dystrophy,

a muscle-degenerating disease (Hoffman et al., 1987). A similar effect can be seen in *Drosophila* larvae and adults when DLP17 is mutated (van der Plas et al., 2007) making *Drosophila* an appropriate model to study. Thus, understanding the interaction between Smash and Dystrophin is important because it might have clinical relevance.

### **Moesin:**

Peek (2019) demonstrated a direct binding between Smash and Moe *in vitro*. Finding Moe as an already verified Smash-interacting protein in our biotin proximity labeling assay reinforces the functionality of our assay. Moe and Smash are both enriched at the apical cortex in epithelial cells, where they control the apical cell perimeter (Beati et al., 2018; McCartney & Fehon, 1996; Polesello et al., 2002; Salis et al., 2017). Moe inhibits Rho1, thereby acting as negative regulator of Rok (Speck et al., 2003). A possible involvement of Smash in regulating Rok upstream signaling has already been discussed. In contrast to Moe, we hypothesize that Smash functions as Rok activator because the loss of Smash led to a strong reduction in Sqh phosphorylation (Figure 16). Consequently, we assume that Rok kinase activity was impaired in *smash*<sup>A35m/z</sup> embryos. Since Moe is also a phosphorylation target of Rok (Matsui et al., 1998), we hypothesize that the loss of Smash might impair Moe function. To what extent Moe function will be impaired by the loss of Smash must be investigated in future experiments.

As the TurboID screen reveals  $\alpha$ -Spectrin as potential Smash-interacting protein, we hypothesize that Smash might modulate actin dynamics together with  $\alpha$ -Spectrin. Similarly, Moe was suggested to function as linker between Crumbs and  $\beta$ -Spectrin (Medina et al., 2002). Moreover, Moe is important to establish the anterior-posterior polarity axis in the oocyte as failure of proper *oskar* mRNA localization upon loss of Moe occurs (Polesello et al., 2002). Similar defects can be seen in *DRok*<sup>2</sup> mutant oocytes (Verdier, Johndrow, et al., 2006). Milder but comparable defects can be seen upon loss of Lasp (Suyama et al., 2009). A contribution of Smash in establishing oocyte polarity by regulating the localization of *oskar* mRNA was already discussed in this work. Considering that several Smash-interacting proteins are involved in regulating *oskar* mRNA localization in the oocyte, it becomes even more likely that Smash contributes to this process.

More recently, Moe was reported to have nuclear activity as it was shown to be involved in mRNA export (Kristo et al., 2017). Today, it is known that many cytoskeleton-associated proteins can play an important role in the nucleus (Kristo et al., 2016; Percipalle & Vartiainen, 2019). Studying their role in the nucleus is challenging, because gene knock-out would not only affect the nuclear protein population but also the cytosolic one. Therefore, the effect of nuclear Moe was studied in flies only expressing Moe which was tagged to a nuclear export sequence (NES), constantly removing Moe from the nucleus. These flies show various abnormalities such as delayed development, decreased lifespan, egg production, and climbing ability, as well as male genitalia rotation (Bajusz et al., 2021). Closer analysis revealed that the nuclear export of Moe led to a drastic change in gene expression, most likely causing the observed defects. Similar to *Drosophila* Moe, the vertebrate homolog of Smash, LMO7,

can shuttle between the cytoplasm and the nucleus, where it was shown to regulate gene expression of *emerin*, which encodes a nuclear membrane protein (Holaska et al., 2006).

**Nup54:**

So far, there has been no evidence that Smash has a nuclear function. Thus, it was very exciting to find Nup54 in the TurboID assay. Nup54 is a component of the nuclear pore complex (NPC) which is required for trafficking across the nuclear envelope. Moe was also found to interact with components of the NPC, namely Nup98 (Kristo et al., 2017). In accordance with these findings, GO term analysis revealed that TurboID:SmashPM targeted several proteins that can be associated with nuclear export, RNA export from the nucleus or protein localization to the nucleus, for example Nup98 and its binding partner Moe (Figure S 17 & Table S 13). Taken together, these findings raise the question whether Smash might have some nuclear activity like vertebrate LMO7 and its binding partner Moe. First, the interaction between Smash and Nup54 or Nup98 should be verified. Second, a careful re-analysis of the Smash localization pattern should be performed. It should be investigated whether a nuclear-associated localization of Smash can be detected. Under normal conditions, the  $\alpha$ -Smash N-terminal antibody does not detect nuclear Smash signal, maybe because the signal is below the detection level. Perhaps there are some external cues that can promote Smash localization into the nucleus. Third, by tagging Smash with an NES, a similar approach as described in Bajusz et al. (2021) can be performed to study Smash nuclear activity.

**Dishevelled:**

Dishevelled (Dsh) is a highly conserved, cytosolic protein that is part of both the canonical,  $\beta$ -catenin-dependent and non-canonical Wnt signal transduction pathway. In the non-canonical branch of the pathway, a member of the Frizzled receptor family receives Wnt signals, which are transduced via Dsh to the downstream effectors Rho1, Rac, and Cdc42. These downstream effectors all belong to the Rho GTPase protein family, whose activation results in cytoskeleton remodeling (Etienne-Manneville & Hall, 2002; Sit & Manser, 2011). Dsh was identified as another potential Smash-interacting protein (Figure 44), raising the possibility that Smash controls actomyosin filament assembly by interfering with Rho GTPase signaling pathways. A similar hypothesis was already discussed when Smash was suggested to regulate components of the Fog signaling pathway in which Rho1 is involved. The interaction with Dsh provides further evidence supporting this hypothesis. To investigate the physiological relevance of Smash-Dsh binding, a detailed characterization of this interaction should be conducted in the future. Moreover, it should be tested whether Smash affects Rho1, Rac, or Cdc42 activity, e. g. by regulating their subcellular localization. A special focus should be on Rho1 since Rho1 is an effector of both the Fog and non-canonical the Wnt signaling pathway. In addition, the fact that Rho1 signaling is supposed to act antagonistically to Moe makes it interesting to study. Maybe Smash acts as a mediator between those two opposing pathways.

**Scraps & Peanut:**

*scraps* (*scra*) encodes a homolog of Anilin. It was described to be involved in cellularization and cytokinesis, both processes requiring ingression of the plasma membrane (Field & Alberts, 1995; Field et al., 2005; Oegema et al., 2000). Anilin is supposed to act as a scaffolding protein for cleavage furrow components as it is enriched at furrow ingression sites where it interacts with F-actin, myosin, Peanut (Pnut) and other septins (Field & Alberts, 1995; Kinoshita et al., 2002; Straight et al., 2005). Pnut belongs to the septin protein family and together with Anilin it promotes furrow ingression (Adam et al., 2000; Field et al., 2005; Maddox et al., 2007; Neufeld & Rubin, 1994). Anilin and Pnut were identified as potential Smash-interacting proteins. At first glance, an interaction between Smash and Anilin or Pnut seems a bit counterintuitive because Smash is excluded from the contractile ring during cytokinesis (Beati et al., 2018). However, it is not unusual that interacting proteins are not co-localizing. Sometimes, mutual regulation by excluding each other from a certain domain is necessary for proper cellular function. Many examples of this can be found in the regulation of cell polarity (Flores-Benitez & Knust, 2016). To name just one concrete example: the interaction between Baz and Rok. Although Baz and Rok are interacting proteins, regarding their planar polarized distribution they are enriched at opposing surfaces. Rok is enriched at A/P junctions where it actively excludes Baz by phosphorylation, resulting in Baz enrichment at D/V junctions (Simões et al., 2010). In addition, Rok enrichment at A/P junctions is maintained by the Crumbs complex which exclude Rok from D/V junctions (Sidor et al., 2020). In conclusion, just because Smash is not localized at the contractile ring, this does not necessarily mean that Smash is not important for this process. To investigate whether Smash is involved in furrow ingression, cytokinesis events and cellularization should be carefully studied in *smash<sup>A35m/z</sup>* null mutant embryos. Live imaging already revealed that a significant high fraction of *smash<sup>A35m/z</sup>* null mutant embryos did not undergo cellularization. Whether this was just a secondary effect caused by e. g. inappropriate handling of the embryos or whether Smash is indeed important for cellularization needs to be investigated in future experiments.

**Shibire:**

Among all novel identified potential Smash interaction partners, there is one very interesting candidate, namely *shibire* (shi), encoding *Drosophila* Dynamin, a large GTPase required for endocytic vesicle fission (Chappie et al., 2011; Chen et al., 1991; Ferguson & De Camilli, 2012). During vesicle fission, F-actin filaments are enriched at the sites of vesicle budding (Collins et al., 2011). Dynamin itself was reported to modify the actin cytoskeleton during vesicle fission to promote its own recruitment (Taylor et al., 2012). Although many morphogenetic processes depend on endocytosis-driven membrane remodeling (Fabrowski et al., 2013; Lee & Harland, 2010; Lepage & Bruce, 2014), the capability of Dynamin to modify the actin cytoskeleton was found to be not restricted to vesicle fission. Instead, Dynamin was shown to have a global role in regulating the actin cytoskeleton in epithelial cells, as the loss of Dynamin leads to drastic defects in cell polarity (Chua et al., 2009). It was suggested that Dynamin can modulate the actin cytoskeleton by interacting with different actin-regulating effector proteins (Gu et al., 2010). These findings raise the question whether Smash is one of the proteins that interact with Dynamin to modulate the actin cytoskeleton. To gain more insight about a potential Smash-Dynamin interaction, Dynamin subcellular localization could be investigated in *smash*<sup>Δ35m/z</sup> null mutant embryos.

**Tudor:**

Tudor (Tud) is a maternal gene that is required for germ cell determination and abdominal segment formation during oogenesis (Ephrussi & Lehmann, 1992). Together with *oskar* mRNA, Tud is localized at the posterior pole plasm of the oocyte but functions downstream of *oskar* (Anne, 2010; Bardsley et al., 1993; Ephrussi & Lehmann, 1992). A role of Smash in tethering *oskar* mRNA to the posterior pole of the oocyte was already discussed in this study. Since Tud is co-localizing with *oskar* mRNA, a participation of Smash in tethering Tud to the posterior pole of the oocyte is conceivable.

**Zipper:**

Another newly identified candidate to interact with Smash is Zipper (Zip). *zip* encodes the non-muscle myosin II heavy chain in *Drosophila*. Recently, *Xenopus* LMO7 was described to interact with NMIIHC, thereby promoting actomyosin filament assembly (Matsuda et al., 2022). Overexpression experiments in the follicle epithelium performed in this study (Figure 31-38 and Figure S 11-S 15) prove the importance of the myosin binding domain of Smash in regulating actomyosin contractility. Taking these new findings into account, one must reconsider previous findings in which Smash is supposed to interact with non-muscle myosin II regulatory light chain Sqh (Beati et al., 2018; Peek, 2019). Peek (2019) claimed that the co-IP of Sqh was not very well reproducible, thus making these results debatable. As possible explanation, it was suggested that the Smash-Sqh interaction is indirect. Having these new findings, Smash-Sqh interaction indeed might be indirect since Smash could bind Zip via its myosin binding domain. Experimental proof for this is still outstanding. However, it was shown that Smash modifies Sqh PCP during germ band elongation (Beati et al., 2018; Peek, 2019). A possible

explanation is that Sqh and Zip assemble to form one functional myosin unit (Brito & Sousa, 2020). Therefore, it can be assumed that Sqh and Zip are always co-localizing. Even though Smash most likely regulates the subcellular localization of Zip, this will indirectly affect the localization of Sqh.

**PR2:**

Finally, PR2 was identified as another potential Smash-interacting protein. PR2 belongs to the activated Cdc42 kinase (Ack) gene family, comprising an N-terminal SAM (sterile  $\alpha$ -motif), a tyrosine kinase, a SH3 domain, a CRIB (Cdc42/Rac interactive binding) domain, a proline-rich region, and C-terminal ubiquitin-associating domains (Abdallah et al., 2013). Interestingly, PR2 was described to be involved in promoting the expression of *zip* during dorsal closure (Zahedi et al., 2008). The mechanism by which PR2 activates *zip* expression is not known yet. Now that there is some evidence that Smash might have nuclear activity, is it possible that Smash itself can regulate *zip* expression, e. g. by promoting PR2 import into the nucleus? How Smash interacts with PR2 and whether Smash can promote *zip* expression will be further elucidated.

**Adh, Cog3 & ACOX1:**

Alcohol dehydrogenase, conserved oligomeric Golgi complex subunit 3 (Cog3) and peroxisomal acyl-coenzyme A oxidase 1 (ACOX1) were not further discussed as potential Smash-interacting proteins because there is no obvious link to Smash function.

**General evaluation of the TurboID assay:**

Already known interacting partners of Smash, such as Rok, Baz, Cno, or Shrm could not be identified within this screen. A possible explanation for this can be found in the artificial properties of the technique. Due to the steric properties of the TurboID fusion protein, not all Smash-interacting proteins will be labeled with biotin, thus missing a portion of potential candidates. It should be noted again that all identified proteins within this screen are only potential Smash-interacting proteins. Whether Smash indeed interacts with these proteins and whether this binding has physiological relevance needs to be investigated in future experiments. For this purpose, the AI system AlphaFold, an extremely powerful tool to predict protein's 3D structure based on its amino acid sequence, can be used to investigate the potential interaction between Smash and the candidates, which were identified by the TurboID screen (Jumper et al., 2021; Varadi et al., 2022).

In contrast to a classical co-IP experiment to identify interacting proteins, the proximity labeling technique carries a higher risk of identifying false-positive proteins because all proteins in close proximity will be labeled, but just because proteins are in close proximity, this does not necessarily mean that these proteins bind each other. To distinguish false-positive from real candidates, appropriate controls have to be included. In this study, we decided to include two controls: eGFP:SmashPM and TurboID:eGFP expressing embryos. The first control, eGFP:SmashPM expressing embryos, was used to determine the biotinylation background. Proteins whose abundance was significantly enriched in eGFP:TurboID:SmashPM expressing embryos compared to eGFP:SmashPM

expressing embryos were considered to be high-confidence Smash interaction candidates. The second control, TurboID:eGFP expressing embryos, was used to determine unspecific biotinylation of TurboID. In contrast to eGFP:TurboID:SmashPM, TurboID:eGFP was distributed throughout the whole cell. Therefore, we assume that proteins in the whole cell were potential biotinylation targets. This data set alone is not very meaningful, but in comparison with the data obtained from eGFP:TurboID:SmashPM expressing embryos, specific targets of eGFP:TurboID:SmashPM were identified. Proteins whose abundance was significantly enriched in eGFP:TurboID:SmashPM expressing embryos compared to TurboID:eGFP expressing embryos were considered to be high-confidence interactors of Smash. Combining both controls provides a stringent screening method to identify potential new Smash-interacting proteins. Thus, only those proteins that came up as high-confidence interactors in both assays (eGFP:TurboID:SmashPM vs. eGFP:SmashPM and eGFP:TurboID:SmashPM vs. TurboID:eGFP) were discussed here and considered for further analysis. For a lower screening stringency, one can consider to include only one of the mentioned controls. Altogether, we conclude that the biotin proximity labeling assay was an effective and reliable technique to successfully identify novel Smash-interacting proteins. The insight we gained from this assay were implemented in our final model that visualizes our current understanding of the molecular working mechanism of Smash (Figure 53).

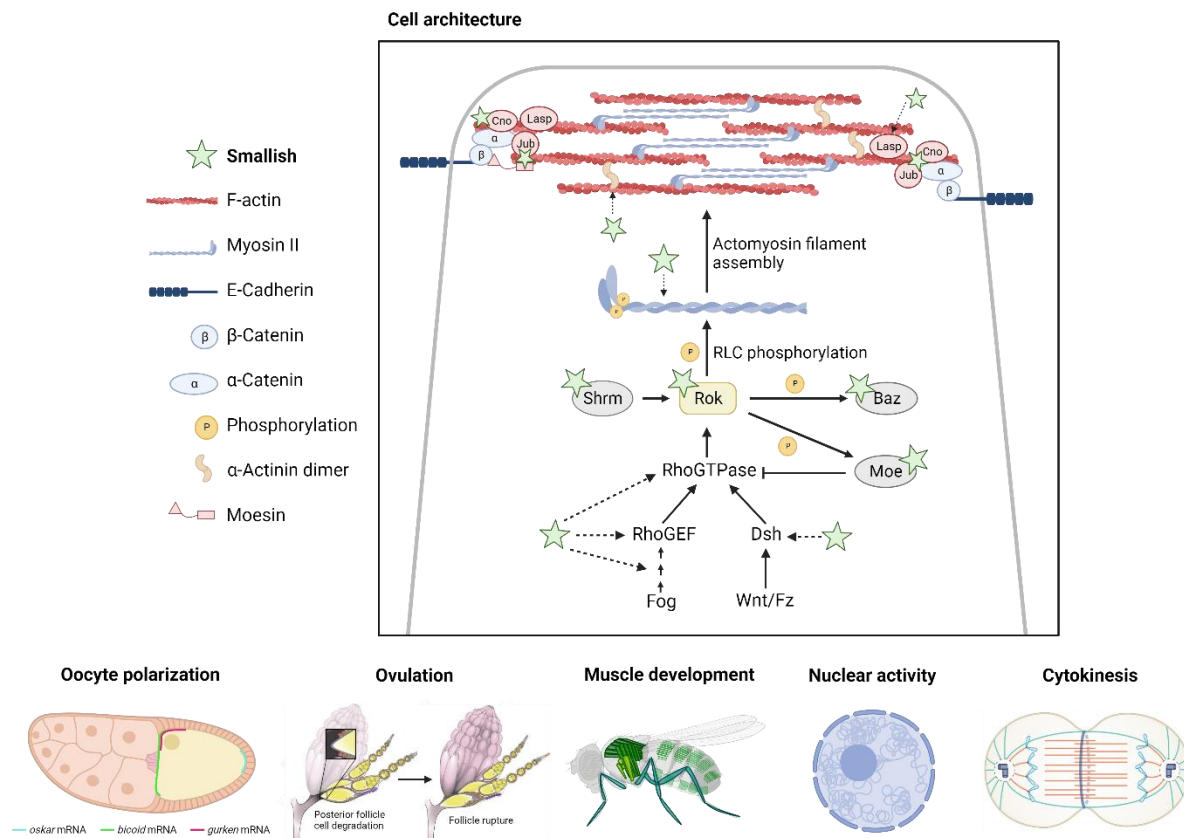


**Figure 53: The molecular working mechanism of Smash – Final Model.** The TurboID proximity labeling assay identified many potential Smash-interacting proteins that need to be verified in future experiments. In combination with already known Smash-interacting proteins, such as Baz, Cno, Jub, Moe, Shrm, and Rok, we suggest a model in which Smash interacts with many actomyosin-associated proteins to modulate cell architecture by regulating actomyosin contractility. Actomyosin contractility is determined by Rok kinase activity and in turn Rok kinase activity is controlled by Fog and Wnt upstream signaling pathways. It is possible that Smash interferes with both upstream signaling pathways to regulate Rok kinase activity, most likely by providing scaffolding function for proteins, e. g. for Dsh and RhoGTPase or for RhoGTPase and Rok. Moreover, we suggest that Smash provides scaffolding function for Rok and its phosphorylation targets, including Baz, Moe, and Myosin II. Although not directly proven yet, we have evidence that Smash binds to Myosin II via its heavy chain encoded by *zipper*. Upon actomyosin filament assembly, Smash might fulfill further scaffolding functions. Together with Cno, Jub, Moe, and possibly also Lasp, Smash might connect the actomyosin network to AJs. Moreover, Smash may facilitate actomyosin network stability together with  $\alpha$ -Actinin by interlinking actin filaments. Many more potential Smash-interacting proteins were identified by the TurboID proximity labeling assay. From these novel, potential Smash-interacting proteins, new implications about the involvement of Smash in regulating oocyte polarity, ovulation, muscle development, gene expression, and cytokinesis can be drawn. Arrows between two proteins indicate a proven interaction. Dashed arrows indicate a potential interaction between two proteins. Ovulation scheme was copied from Deady et al. (2017). Cytokinesis scheme was copied from Lens & Medema (2019).

## 4.5 Conclusion

Smash was reported to have an important function during epithelial morphogenesis since Smash actively promotes actomyosin contractility (Beati et al., 2018; Peek, 2019). There are several lines of evidence indicating that Smash acts within a large protein interaction network to regulate actomyosin contractility. However, how Smash functions at the molecular level is not fully understood yet.

This work provides new insight into the molecular working mechanism of Smash. Detailed analysis of *smash*<sup>Δ35m/z</sup> null allele mutant embryos revealed that Smash is probably involved in several actomyosin-driven processes occurring early during development, such as cellularization, ventral furrow formation, and germ band elongation. Future live imaging experiments of *smash*<sup>Δ35m/z</sup> null allele mutants at the cellular level will help to further investigate the contribution of Smash within these processes.

The spatiotemporal behavior of Smash during epithelial morphogenesis has not been investigated yet. Instead, however, the basis for this was created. Two novel, isoform-specific fly lines expressing either sfGFP:SmashPM or sfGFP:SmashPI were generated using CRISPR/Cas9 technology. In this work, the expression pattern of both sfGFP fusion proteins was documented in detail. From this study, we conclude that sfGFP:SmashPM precisely resembles the previously reported expression pattern and subcellular localization of endogenous Smash, thus being a great gain for our molecular toolkit. sfGFP:SmashPM expressing flies can be used in future experiments to analyze the spatiotemporal behavior of SmashPM in living embryos. Using the sfGFP:SmashPI expressing flies, it was possible for the first time to show an isoform-specific localization pattern.

Furthermore, this work provides several lines of evidence on how Smash functions to regulate actomyosin contractility. Actomyosin contractility is dependent on the phosphorylation level of Sqh. We demonstrated that Smash affects Sqh phosphorylation since Sqh phosphorylation is strongly reduced, almost completely abolished, in *smash*<sup>Δ35m/z</sup> mutants. The mechanism by which Smash regulates Sqh phosphorylation is probably indirect since Smash did not affect Rok kinase activity *in vitro*. Overexpression experiments in the follicle epithelium revealed a distinct physiological relevance of the myosin binding domain of Smash in regulating actomyosin contractility since this domain was necessary to promote F-actin enrichment in an AJ-dependent manner, thereby enabling tissue deformation. As Smash binds Rok and most likely Myosin II via its myosin binding domain, we suggest that Smash mediates an interaction between Rok and Myosin II to catalyze the phosphorylation of Sqh. In addition, we suggest that Smash regulates Rok kinase activity by interfering with Rok's upstream activators, as the dominant negative characteristics of the sfGFP:SmashPI<sup>m/z</sup> fly strain cause an embryonic phenotype that was reminiscent of *fog* mutant embryos.

The newly found, potential Smash-interacting proteins support a model in which Smash regulates the actomyosin cytoskeleton to drive tissue remodeling, presumably by providing various scaffolding functions. Moreover, these candidates improve our understanding of Smash since there are new implications about the involvement of Smash in regulating oocyte polarity, ovulation, muscle development, cytokinesis, and possibly gene expression (Figure 53). This data provides important, game-changing insights that will guide future experiments. For example, the subcellular localization of these proteins can be studied in *smash*<sup>Δ35m/z</sup> mutants and vice versa, Smash localization can be investigated upon loss of the respective protein to check whether the protein localization is dependent on each other.

In summary, this work supports and expands our current knowledge on Smash function. Several lines of evidence demonstrate the importance of Smash in regulating morphogenesis by actively modifying actomyosin contractility. Finally, this work proposes exciting questions that should be explored in future research.

## References

- Abdallah, A. M., Zhou, X., Kim, C., Shah, K. K., Hogden, C., Schoenherr, J. A., Clemens, J. C., & Chang, H. C. (2013). Activated Cdc42 kinase regulates Dock localization in male germ cells during *Drosophila* spermatogenesis. *Dev Biol*, *378*(2), 141-153. <https://doi.org/10.1016/j.ydbio.2013.02.025>
- Ackers, I., & Malgor, R. (2018). Interrelationship of canonical and non-canonical Wnt signalling pathways in chronic metabolic diseases. *Diab Vasc Dis Res*, *15*(1), 3-13. <https://doi.org/10.1177/1479164117738442>
- Adam, J. C., Pringle, J. R., & Peifer, M. (2000). Evidence for Functional Differentiation among *Drosophila* Septins in Cytokinesis and Cellularization. *Molecular Biology of the Cell*, *11*(9), 3123-3135. <https://doi.org/10.1091/mbc.11.9.3123>
- Adler, P. N. (2002). Planar signaling and morphogenesis in *Drosophila*. *Dev Cell*, *2*(5), 525-535. [https://doi.org/10.1016/s1534-5807\(02\)00176-4](https://doi.org/10.1016/s1534-5807(02)00176-4)
- Agarwal, P., & Zaidel-Bar, R. (2019). Principles of Actomyosin Regulation In Vivo. *Trends Cell Biol*, *29*(2), 150-163. <https://doi.org/10.1016/j.tcb.2018.09.006>
- Amano, M., Ito, M., Kimura, K., Fukata, Y., Chihara, K., Nakano, T., Matsuura, Y., & Kaibuchi, K. (1996). Phosphorylation and activation of myosin by Rho-associated kinase (Rho-kinase). *J Biol Chem*, *271*(34), 20246-20249. <https://doi.org/10.1074/jbc.271.34.20246>
- Amano, M., Nakayama, M., & Kaibuchi, K. (2010). Rho-Kinase/ROCK: A Key Regulator of the Cytoskeleton and Cell Polarity. *Cytoskeleton (Hoboken)*, *67*(9), 545-554. <https://doi.org/10.1002/cm.20472>
- Anne, J. (2010). Targeting and anchoring Tudor in the pole plasm of the *Drosophila* oocyte. *PLoS One*, *5*(12), e14362. <https://doi.org/10.1371/journal.pone.0014362>
- Axelrod, J. D. (2001). Unipolar membrane association of Dishevelled mediates Frizzled planar cell polarity signaling. *Genes & Development*, *15*(10), 1182-1187. <https://doi.org/10.1101/gad.890501>
- Bajusz, C., Kristo, I., Abonyi, C., Venit, T., Vedelek, V., Lukacsovich, T., Farkas, A., Borkuti, P., Kovacs, Z., Bajusz, I., Marton, A., Vizler, C., Lipinszki, Z., Sinka, R., Percipalle, P., & Vilmos, P. (2021). The nuclear activity of the actin-binding Moesin protein is necessary for gene expression in *Drosophila*. *FEBS J*, *288*(16), 4812-4832. <https://doi.org/10.1111/febs.15779>
- Bardsley, A., McDonald, K., & Boswell, R. E. (1993). Distribution of tudor protein in the *Drosophila* embryo suggests separation of functions based on site of localization. *Development*, *119*(1), 207-219. <https://doi.org/10.1242/dev.119.1.207>
- Bastock, R., Strutt, H., & Strutt, D. (2003). Strabismus is asymmetrically localised and binds to Prickle and Dishevelled during *Drosophila* planar polarity patterning. *Development*, *130*(13), 3007-3014. <https://doi.org/10.1242/dev.00526>
- Beard, A., Oramas, R., & Sun, J. (2023). Assessing Oviposition in *Drosophila melanogaster*. In M. S. Giedt & T. L. Tootle (Eds.), *Drosophila Oogenesis. Methods in Molecular Biology* (Vol. 2626, pp. 253-276). Humana. [https://doi.org/10.1007/978-1-0716-2970-3\\_13](https://doi.org/10.1007/978-1-0716-2970-3_13)
- Beati, H., Peek, I., Hordowska, P., Honemann-Capito, M., Glashauser, J., Renschler, F. A., Kakanj, P., Ramrath, A., Leptin, M., Luschnig, S., Wiesner, S., & Wodarz, A. (2018). The adherens junction-associated LIM domain protein Smallish regulates epithelial morphogenesis. *J Cell Biol*, *217*(3), 1079-1095. <https://doi.org/10.1083/jcb.201610098>
- Beati, S. A. H. (2013). Functional analysis of the *Drosophila* gene smallish (CG43427). *Doctoral thesis, Georg-August-Universität Göttingen*. <http://dx.doi.org/10.53846/goediss-4055>

- Bennett, V., & Baines, A. (2001). Spectrin and Ankyrin-Based Pathways: Metazoan Inventions for Integrating Cells Into Tissues. *Physiological Reviews*, *81*(3).  
<https://doi.org/10.1152/physrev.2001.81.3.1353>
- Benton, R., & St Johnston, D. (2003). Drosophila PAR-1 and 14-3-3 inhibit Bazooka/PAR-3 to establish complementary cortical domains in polarized cells. *Cell*, *115*(6), 691-704.  
[https://doi.org/10.1016/s0092-8674\(03\)00938-3](https://doi.org/10.1016/s0092-8674(03)00938-3)
- Bertet, C., Sulak, L., & Lecuit, T. (2004). Myosin-dependent junction remodelling controls planar cell intercalation and axis elongation. *Nature*, *429*(6992), 667-671.  
<https://doi.org/doi:10.1038/nature02590>
- Betschinger, J., Mechtler, K., & Knoblich, J. A. (2003). The Par complex directs asymmetric cell division by phosphorylating the cytoskeletal protein Lgl. *Nature*, *422*(6929), 326-330.  
<https://doi.org/10.1038/nature01486>
- Bhanot, P., Brink, M., Samos, C. H., Hsieh, J. C., Wang, Y., Macke, J. P., Andrew, D., Nathans, J., & Nusse, R. (1996). A new member of the frizzled family from Drosophila functions as a Wingless receptor. *Nature*, *382*(6588), 225-230. <https://doi.org/10.1038/382225a0>
- Bialkowska, K., Saido, T. C., & Fox, J. E. (2005). SH3 domain of spectrin participates in the activation of Rac in specialized calpain-induced integrin signaling complexes. *J Cell Sci*, *118*(Pt 2), 381-395.  
<https://doi.org/10.1242/jcs.01625>
- Bilder, D., Li, M., & Perrimon, N. (2000). Cooperative regulation of cell polarity and growth by Drosophila tumor suppressors. *Science*, *289*(5476), 113-116.  
<https://doi.org/10.1126/science.289.5476.113>
- Bilder, D., & Perrimon, N. (2000). Localization of apical epithelial determinants by the basolateral PDZ protein Scribble. *Nature*, *403*(6770), 676-680. <https://doi.org/10.1038/35001108>
- Bilder, D., Schober, M., & Perrimon, N. (2003). Integrated activity of PDZ protein complexes regulates epithelial polarity. *Nat Cell Biol*, *5*(1), 53-58. <https://doi.org/10.1038/ncb897>
- Blankenship, J. T., Backovic, S. T., Sanny, J. S., Weitz, O., & Zallen, J. A. (2006). Multicellular rosette formation links planar cell polarity to tissue morphogenesis. *Dev Cell*, *11*(4), 459-470.  
<https://doi.org/10.1016/j.devcel.2006.09.007>
- Bolinger, C., Zasadil, L., Rizaldy, R., & Hildebrand, J. D. (2010). Specific isoforms of drosophila shroom define spatial requirements for the induction of apical constriction. *Dev Dyn*, *239*(7), 2078-2093. <https://doi.org/10.1002/dvdy.22326>
- Brand, A. H., & Perrimon, N. (1993). Targeted gene expression as a means of altering cell fates and generating dominant phenotypes. *Development*, *118*, 401-415.  
<https://doi.org/10.1242/dev.118.2.401>
- Branon, T. C., Bosch, J. A., Sanchez, A. D., Udeshi, N. D., Svinkina, T., Carr, S. A., Feldman, J. L., Perrimon, N., & Ting, A. Y. (2018). Efficient proximity labeling in living cells and organisms with TurboID. *Nat Biotechnol*, *36*(9), 880-887. <https://doi.org/10.1038/nbt.4201>
- Brito, C., & Sousa, S. (2020). Non-Muscle Myosin 2A (NM2A): Structure, Regulation and Function. *Cells*, *9*(7). <https://doi.org/10.3390/cells9071590>
- Brittle, A. L., Repiso, A., Casal, J., Lawrence, P. A., & Strutt, D. (2010). Four-jointed modulates growth and planar polarity by reducing the affinity of dachsous for fat. *Curr Biol*, *20*(9), 803-810.  
<https://doi.org/10.1016/j.cub.2010.03.056>
- Broderick, M. J., & Winder, S. J. (2005). Spectrin, alpha-actinin, and dystrophin. *Adv Protein Chem*, *70*, 203-246. [https://doi.org/10.1016/S0065-3233\(05\)70007-3](https://doi.org/10.1016/S0065-3233(05)70007-3)
- Bulgakova, N. A., & Knust, E. (2009). The Crumbs complex: from epithelial-cell polarity to retinal degeneration. *J Cell Sci*, *122*(Pt 15), 2587-2596. <https://doi.org/10.1242/jcs.023648>

- Busson, D., Gans, M., Komitopoulou, K., & Masson, M. (1983). Genetic analysis of three dominant female sterile mutations located on X chromosome. *Genetics*, *105*, 309-325. <https://doi.org/10.1093/genetics/105.2.309>
- Butler, M. T., & Wallingford, J. B. (2017). Planar cell polarity in development and disease. *Nat Rev Mol Cell Biol*, *18*(6), 375-388. <https://doi.org/10.1038/nrm.2017.11>
- Butler, M. T., & Wallingford, J. B. (2018). Spatial and temporal analysis of PCP protein dynamics during neural tube closure. *Elife*, *7*. <https://doi.org/10.7554/eLife.36456>
- Campos-Ortega, J. A., & Hartenstein, V. (1997). *The Embryonic Development of Drosophila melanogaster* (2 ed.). Springer-Verlag Berlin, Heidelberg. <https://doi.org/10.1007/978-3-662-22489-2>
- Casal, J., Lawrence, P. A., & Struhl, G. (2006). Two separate molecular systems, Dachous/Fat and Starry night/Frizzled, act independently to confer planar cell polarity. *Development*, *133*(22), 4561-4572. <https://doi.org/10.1242/dev.02641>
- Chappie, J. S., Mears, J. A., Fang, S., Leonard, M., Schmid, S. L., Milligan, R. A., Hinshaw, J. E., & Dyda, F. (2011). A pseudoatomic model of the dynamin polymer identifies a hydrolysis-dependent powerstroke. *Cell*, *147*(1), 209-222. <https://doi.org/10.1016/j.cell.2011.09.003>
- Chen, E. Y., Tan, C. M., Kou, Y., Duan, Q., Wang, Z., Meirelles, G. V., Clark, N. R., & Ma'ayan, A. (2013). Enrichr: interactive and collaborative HTML5 gene list enrichment analysis tool. *BMC Bioinformatics*, *14*, 128. <https://doi.org/10.1186/1471-2105-14-128>
- Chen, M. S., Obar, R. A., Schroeder, C. C., Austin, T. W., Poodry, C. A., Wadsworth, S. C., & Vallee, R. B. (1991). Multiple forms of dynamin are encoded by shibire, a Drosophila gene involved in endocytosis. *Nature*, *351*(6327), 583-586. <https://doi.org/10.1038/351583a0>
- Chen, W. S., Antic, D., Matis, M., Logan, C. Y., Povelones, M., Anderson, G. A., Nusse, R., & Axelrod, J. D. (2008). Asymmetric homotypic interactions of the atypical cadherin flamingo mediate intercellular polarity signaling. *Cell*, *133*(6), 1093-1105. <https://doi.org/10.1016/j.cell.2008.04.048>
- Chou, T., & Perrimon, N. (1992). Use of a Yeast Sitespecific Recombinase to Produce Female Germline. *Genetics*, *131*(3), 643-653. <https://doi.org/10.1093/genetics/131.3.643>
- Chua, J., Rikhy, R., & Lippincott-Schwartz, J. (2009). Dynamin 2 orchestrates the global actomyosin cytoskeleton for epithelial maintenance and apical constriction. *Proc Natl Acad Sci U S A*, *106*(49), 20770-20775. <https://doi.org/10.1073/pnas.0909812106>
- Clark, M. E., Anderson, C. L., Cande, J., & Karr, T. L. (2005). Widespread prevalence of wolbachia in laboratory stocks and the implications for Drosophila research. *Genetics*, *170*(4), 1667-1675. <https://doi.org/10.1534/genetics.104.038901>
- Collins, A., Warrington, A., Taylor, K. A., & Svitkina, T. (2011). Structural organization of the actin cytoskeleton at sites of clathrin-mediated endocytosis. *Curr Biol*, *21*(14), 1167-1175. <https://doi.org/10.1016/j.cub.2011.05.048>
- Coravos, J. S., & Martin, A. C. (2016). Apical Sarcomere-like Actomyosin Contracts Nonmuscle Drosophila Epithelial Cells. *Dev Cell*, *39*(3), 346-358. <https://doi.org/10.1016/j.devcel.2016.09.023>
- Costa, M., Wilson, E. T., & Wieschaus, E. (1994). A putative cell signal encoded by the folded gastrulation gene coordinates cell shape changes during Drosophila gastrulation. *Cell*, *76*(6), 1075-1089. [https://doi.org/10.1016/0092-8674\(94\)90384-0](https://doi.org/10.1016/0092-8674(94)90384-0)
- Das, G., Jenny, A., Klein, T. J., Eaton, S., & Mlodzik, M. (2004). Diego interacts with Prickle and Strabismus/Van Gogh to localize planar cell polarity complexes. *Development*, *131*(18), 4467-4476. <https://doi.org/10.1242/dev.01317>

- Das Thakur, M., Feng, Y., Jagannathan, R., Seppa, M. J., Skeath, J. B., & Longmore, G. D. (2010). Ajuba LIM proteins are negative regulators of the Hippo signaling pathway. *Curr Biol*, *20*(7), 657-662. <https://doi.org/10.1016/j.cub.2010.02.035>
- Deady, L. D., Li, W., & Sun, J. (2017). The zinc-finger transcription factor Hindsight regulates ovulation competency of *Drosophila* follicles. *Elife*, *6*. <https://doi.org/10.7554/eLife.29887>
- Deady, L. D., Shen, W., Mosure, S. A., Spradling, A. C., & Sun, J. (2015). Matrix metalloproteinase 2 is required for ovulation and corpus luteum formation in *Drosophila*. *PLoS Genet*, *11*(2), e1004989. <https://doi.org/10.1371/journal.pgen.1004989>
- Devenport, D. (2014). The cell biology of planar cell polarity. *J Cell Biol*, *207*(2), 171-179. <https://doi.org/10.1083/jcb.201408039>
- Duhart, J. C., Parsons, T. T., & Raftery, L. A. (2017). The repertoire of epithelial morphogenesis on display: Progressive elaboration of *Drosophila* egg structure. *Mech Dev*, *148*, 18-39. <https://doi.org/10.1016/j.mod.2017.04.002>
- Edwards, K. A., Chang, X. J., & Kiehart, D. P. (1995). Essential light chain of *Drosophila* nonmuscle myosin II. *J Muscle Res Cell Motil*, *16*(5), 491-498. <https://doi.org/10.1007/BF00126433>
- Ephrussi, A., & Lehmann, R. (1992). Induction of germ cell formation by oskar. *Nature*, *358*(6385), 387-392. <https://doi.org/10.1038/358387a0>
- Etienne-Manneville, S., & Hall, A. (2002). Rho GTPases in cell biology. *Nature*, *420*(6916), 629-635. <https://doi.org/10.1038/nature01148>
- Fabrowski, P., Necakov, A. S., Mumbauer, S., Loeser, E., Reversi, A., Streichan, S., Briggs, J. A., & De Renzis, S. (2013). Tubular endocytosis drives remodelling of the apical surface during epithelial morphogenesis in *Drosophila*. *Nat Commun*, *4*, 2244. <https://doi.org/10.1038/ncomms3244>
- Fehon, R. G., McClatchey, A. I., & Bretscher, A. (2010). Organizing the cell cortex: the role of ERM proteins. *Nat Rev Mol Cell Biol*, *11*(4), 276-287. <https://doi.org/10.1038/nrm2866>
- Feiguin, F., Hannus, M., Mlodzik, M., & Eaton, S. (2001). The ankyrin repeat protein Diego mediates Frizzled-dependent planar polarization. *Dev Cell*, *1*(1), 93-101. [https://doi.org/10.1016/s1534-5807\(01\)00010-7](https://doi.org/10.1016/s1534-5807(01)00010-7)
- Ferguson, S. M., & De Camilli, P. (2012). Dynamin, a membrane-remodelling GTPase. *Nat Rev Mol Cell Biol*, *13*(2), 75-88. <https://doi.org/10.1038/nrm3266>
- Fernandes, I., & Schock, F. (2014). The nebulin repeat protein Lasp regulates I-band architecture and filament spacing in myofibrils. *J Cell Biol*, *206*(4), 559-572. <https://doi.org/10.1083/jcb.201401094>
- Fernandez-Gonzalez, R., Simoes Sde, M., Roper, J. C., Eaton, S., & Zallen, J. A. (2009). Myosin II dynamics are regulated by tension in intercalating cells. *Dev Cell*, *17*(5), 736-743. <https://doi.org/10.1016/j.devcel.2009.09.003>
- Field, C. M., & Alberts, B. M. (1995). Anillin, a Contractile Ring Protein That Cycles from Nucleus to the Cell Cortex. *The Journal of Cell Biology*, *131*(1), 165-178. <https://doi.org/10.1083/jcb.131.1.165>
- Field, C. M., Coughlin, M., Doberstein, S., Marty, T., & Sullivan, W. (2005). Characterization of anillin mutants reveals essential roles in septin localization and plasma membrane integrity. *Development*, *132*(12), 2849-2860. <https://doi.org/10.1242/dev.01843>
- Flores-Benitez, D., & Knust, E. (2016). Dynamics of epithelial cell polarity in *Drosophila*: how to regulate the regulators? *Curr Opin Cell Biol*, *42*, 13-21. <https://doi.org/10.1016/j.ceb.2016.03.018>

- Frohnhofer, H. G., & Nüsslein-Volhard, C. (1986). Organization of anterior pattern in the *Drosophila* embryo by the maternal gene bicoid. *Nature*, *324*, 120-125. <https://doi.org/10.1038/324120a0>
- Fry, A. J., & Rand, D. M. (2002). Wolbachia interactions that determine *drosophila melanogaster* survival. *Evolution*, *50*(10), 1976-1981. <https://doi.org/10.1111/j.0014-3820.2002.tb00123.x>
- Fulford, A. D., & McNeill, H. (2020). Fat/Dachsous family cadherins in cell and tissue organisation. *Curr Opin Cell Biol*, *62*, 96-103. <https://doi.org/10.1016/j.ceb.2019.10.006>
- Gallagher, S. R., & Wiley, E. A. (2012). *Current Protocols Essential Laboratory Techniques*. John Wiley & Sons.
- Gao, Q. Q., & McNally, E. M. (2015). The Dystrophin Complex: Structure, Function, and Implications for Therapy. *Compr Physiol*, *5*(3), 1223-1239. <https://doi.org/10.1002/cphy.c140048>
- Gates, J., & Peifer, M. (2005). Can 1000 reviews be wrong? Actin, alpha-Catenin, and adherens junctions. *Cell*, *123*(5), 769-772. <https://doi.org/10.1016/j.cell.2005.11.009>
- Giepmans, B. N., & van Ijzendoorn, S. C. (2009). Epithelial cell-cell junctions and plasma membrane domains. *Biochim Biophys Acta*, *1788*(4), 820-831. <https://doi.org/10.1016/j.bbamem.2008.07.015>
- González-Reyes, A., Elliott, H., & St Johnston, D. (1995). Polarization of both major body axes in *Drosophila* by gurken torpedo signalling. *Nature*, *375*, 654-658. <https://doi.org/10.1038/375654a0>
- Goodrich, L. V., & Strutt, D. (2011). Principles of planar polarity in animal development. *Development*, *138*(10), 1877-1892. <https://doi.org/10.1242/dev.054080>
- Gratz, S. J., Rubinstein, C. D., Harrison, M. M., Wildonger, J., & O'Connor-Giles, K. M. (2015). CRISPR-Cas9 Genome Editing in *Drosophila*. *Curr Protoc Mol Biol*, *111*, 31.32. <https://doi.org/10.1002/0471142727.mb3102s111>
- Gratz, S. J., Ukken, F. P., Rubinstein, C. D., Thiede, G., Donohue, L. K., Cummings, A. M., & O'Connor-Giles, K. M. (2014). Highly specific and efficient CRISPR/Cas9-catalyzed homology-directed repair in *Drosophila*. *Genetics*, *196*(4), 961-971. <https://doi.org/10.1534/genetics.113.160713>
- Gu, C., Yaddanapudi, S., Weins, A., Osborn, T., Reiser, J., Pollak, M., Hartwig, J., & Sever, S. (2010). Direct dynamin-actin interactions regulate the actin cytoskeleton. *EMBO J*, *29*(21), 3593-3606. <https://doi.org/10.1038/emboj.2010.249>
- Gubb, D., & Garcia-Bellido, A. (1982). A genetic analysis of the determination of cuticular polarity during development in *Drosophila melanogaster*. *J Embryol Exp Morphol*, *68*(1), 37-57. <https://doi.org/10.1242/dev.68.1.37>
- Guillot, C., & Lecuit, T. (2013). Mechanics of epithelial tissue homeostasis and morphogenesis. *Science*, *340*(6137), 1185-1189. <https://doi.org/10.1126/science.1235249>
- Guo, N., Hawkins, C., & Nathans, J. (2004). Frizzled6 controls hair patterning in mice. *Proc Natl Acad Sci U S A*, *101*(25), 9277-9281. <https://doi.org/10.1073/pnas.0402802101>
- Haigo, S. L., Hildebrand, J. D., Harland, R. M., & Wallingford, J. B. (2003). Shroom induces apical constriction and is required for hinge point formation during neural tube closure. *Curr Biol*, *13*(24), 2125-2137. <https://doi.org/10.1016/j.cub.2003.11.054>
- Harris, T. J., & Peifer, M. (2004). Adherens junction-dependent and -independent steps in the establishment of epithelial cell polarity in *Drosophila*. *J Cell Biol*, *167*(1), 135-147. <https://doi.org/10.1083/jcb.200406024>
- Harris, T. J., & Peifer, M. (2005). The positioning and segregation of apical cues during epithelial polarity establishment in *Drosophila*. *J Cell Biol*, *170*(5), 813-823. <https://doi.org/10.1083/jcb.200505127>

- Hartman, M. A., & Spudich, J. A. (2012). The myosin superfamily at a glance. *J Cell Sci*, *125*(Pt 7), 1627-1632. <https://doi.org/10.1242/jcs.094300>
- Heer, N. C., & Martin, A. C. (2017). Tension, contraction and tissue morphogenesis. *Development*, *144*(23), 4249-4260. <https://doi.org/10.1242/dev.151282>
- Held, L. I., Jr., Duarte, C. M., & Derakhshanian, K. (1986). Extra joints and misoriented bristles on *Drosophila* legs. *Prog Clin Biol Res*, *217A*, 293-296. <https://www.ncbi.nlm.nih.gov/pubmed/3092245>
- Hildebrand, J. D. (2005). Shroom regulates epithelial cell shape via the apical positioning of an actomyosin network. *J Cell Sci*, *118*(Pt 22), 5191-5203. <https://doi.org/10.1242/jcs.02626>
- Hoffman, E. P., Brown, R. H., Jr., & Kunkel, L. M. (1987). Dystrophin: the protein product of the Duchenne muscular dystrophy locus. *Cell*, *51*(6), 919-928. [https://doi.org/10.1016/0092-8674\(87\)90579-4](https://doi.org/10.1016/0092-8674(87)90579-4)
- Holaska, J. M., Rais-Bahrami, S., & Wilson, K. L. (2006). Lmo7 is an emerin-binding protein that regulates the transcription of emerin and many other muscle-relevant genes. *Hum Mol Genet*, *15*(23), 3459-3472. <https://doi.org/10.1093/hmg/ddl423>
- Humbert, P., Russell, S., & Richardson, H. (2003). Dlg, Scribble and Lgl in cell polarity, cell proliferation and cancer. *BioEssays*, *25*(6), 542-553. <https://doi.org/10.1002/bies.10286>
- Jenny, A., Darken, R. S., Wilson, P. A., & Mlodzik, M. (2003). Prickle and Strabismus form a functional complex to generate a correct axis during planar cell polarity signaling. *EMBO J*, *22*(17), 4409-4420. <https://doi.org/10.1093/emboj/cdg424>
- Jenny, A., Reynolds-Kenneally, J., Das, G., Burnett, M., & Mlodzik, M. (2005). Diego and Prickle regulate Frizzled planar cell polarity signalling by competing for Dishevelled binding. *Nat Cell Biol*, *7*(7), 691-697. <https://doi.org/10.1038/ncb1271>
- Jones, C., & Chen, P. (2007). Planar cell polarity signaling in vertebrates. *BioEssays*, *29*(2), 120-132. <https://doi.org/10.1002/bies.20526>
- Jordan, P., & Karess, R. (1997). Myosin light chain-activating phosphorylation sites are required for oogenesis in *Drosophila*. *J Cell Biol*, *139*(7), 1805-1819. <https://doi.org/10.1083/jcb.139.7.1805>
- Jumper, J., Evans, R., Pritzel, A., Green, T., Figurnov, M., Ronneberger, O., Tunyasuvunakool, K., Bates, R., Zidek, A., Potapenko, A., Bridgland, A., Meyer, C., Kohl, S. A. A., Ballard, A. J., Cowie, A., Romera-Paredes, B., Nikolov, S., Jain, R., Adler, J., . . . Hassabis, D. (2021). Highly accurate protein structure prediction with AlphaFold. *Nature*, *596*(7873), 583-589. <https://doi.org/10.1038/s41586-021-03819-2>
- Kadmas, J. L., & Beckerle, M. C. (2004). The LIM domain: from the cytoskeleton to the nucleus. *Nat Rev Mol Cell Biol*, *5*(11), 920-931. <https://doi.org/10.1038/nrm1499>
- Kalluri, R., & Weinberg, R. A. (2009). The basics of epithelial-mesenchymal transition. *J Clin Invest*, *119*(6), 1420-1428. <https://doi.org/10.1172/JCI39104>
- Karess, R. E., Chang, X. J., Edwards, K. A., Kulkarni, S., Aguilera, I., & Kiehart, D. P. (1991). The regulatory light chain of nonmuscle myosin is encoded by spaghetti-squash, a gene required for cytokinesis in *Drosophila*. *Cell*, *65*(7), 1177-1189. [https://doi.org/10.1016/0092-8674\(91\)90013-o](https://doi.org/10.1016/0092-8674(91)90013-o)
- Kempkens, O., Medina, E., Fernandez-Ballester, G., Ozuyaman, S., Le Bivic, A., Serrano, L., & Knust, E. (2006). Computer modelling in combination with in vitro studies reveals similar binding affinities of *Drosophila* Crumbs for the PDZ domains of Stardust and DmPar-6. *Eur J Cell Biol*, *85*(8), 753-767. <https://doi.org/10.1016/j.ejcb.2006.03.003>
- Kerridge, S., Munjal, A., Philippe, J. M., Jha, A., de las Bayonas, A. G., Saurin, A. J., & Lecuit, T. (2016). Modular activation of Rho1 by GPCR signalling imparts polarized myosin II activation during morphogenesis. *Nat Cell Biol*, *18*(3), 261-270. <https://doi.org/10.1038/ncb3302>

- Kina, H., Yoshitani, T., Hanyu-Nakamura, K., & Nakamura, A. (2019). Rapid and efficient generation of GFP-knocked-in *Drosophila* by the CRISPR-Cas9-mediated genome editing. *Dev Growth Differ*, *61*(4), 265-275. <https://doi.org/10.1111/dgd.12607>
- Kinoshita, M., Field, C. M., Coughlin, M. L., Straight, A. F., & T.J., M. (2002). Self- and Actin-Templated Assembly of Mammalian Septins. *Developmental Cell*, *3*(6), 791-802. [https://doi.org/10.1016/S1534-5807\(02\)00366-0](https://doi.org/10.1016/S1534-5807(02)00366-0)
- Knust, E., & Bossinger, O. (2002). Composition and formation of intercellular junctions in epithelial cells. *Science*, *298*(5600), 1955-1959. <https://doi.org/10.1126/science.1072161>
- Krahn, M. P., Buckers, J., Kastrup, L., & Wodarz, A. (2010). Formation of a Bazooka-Stardust complex is essential for plasma membrane polarity in epithelia. *J Cell Biol*, *190*(5), 751-760. <https://doi.org/10.1083/jcb.201006029>
- Kristo, I., Bajusz, C., Borsos, B. N., Pankotai, T., Dopie, J., Jankovics, F., Vartiainen, M. K., Erdelyi, M., & Vilmos, P. (2017). The actin binding cytoskeletal protein Moesin is involved in nuclear mRNA export. *Biochim Biophys Acta Mol Cell Res*, *1864*(10), 1589-1604. <https://doi.org/10.1016/j.bbamcr.2017.05.020>
- Kristo, I., Bajusz, I., Bajusz, C., Borkuti, P., & Vilmos, P. (2016). Actin, actin-binding proteins, and actin-related proteins in the nucleus. *Histochem Cell Biol*, *145*(4), 373-388. <https://doi.org/10.1007/s00418-015-1400-9>
- Kuleshov, M. V., Jones, M. R., Rouillard, A. D., Fernandez, N. F., Duan, Q., Wang, Z., Koplev, S., Jenkins, S. L., Jagodnik, K. M., Lachmann, A., McDermott, M. G., Monteiro, C. D., Gundersen, G. W., & Ma'ayan, A. (2016). Enrichr: a comprehensive gene set enrichment analysis web server 2016 update. *Nucleic Acids Res*, *44*(W1), W90-97. <https://doi.org/10.1093/nar/gkw377>
- Kurochkina, N., & Guha, U. (2013). SH3 domains: modules of protein-protein interactions. *Biophys Rev*, *5*(1), 29-39. <https://doi.org/10.1007/s12551-012-0081-z>
- Lang, C. F., & Munro, E. (2017). The PAR proteins: from molecular circuits to dynamic self-stabilizing cell polarity. *Development*, *144*(19), 3405-3416. <https://doi.org/10.1242/dev.139063>
- Laprise, P., Beronja, S., Silva-Gagliardi, N. F., Pellikka, M., Jensen, A. M., McGlade, C. J., & Tepass, U. (2006). The FERM protein Yurt is a negative regulatory component of the Crumbs complex that controls epithelial polarity and apical membrane size. *Dev Cell*, *11*(3), 363-374. <https://doi.org/10.1016/j.devcel.2006.06.001>
- Lawrence, P. A., & Casal, J. (2018). Planar cell polarity: two genetic systems use one mechanism to read gradients. *Development*, *145*(23). <https://doi.org/10.1242/dev.168229>
- Lawrence, P. A., Struhl, G., & Casal, J. (2007). Planar cell polarity: one or two pathways? *Nat Rev Genet*, *8*(7), 555-563. <https://doi.org/10.1038/nrg2125>
- Lee, J. Y., & Harland, R. M. (2010). Endocytosis is required for efficient apical constriction during *Xenopus* gastrulation. *Curr Biol*, *20*(3), 253-258. <https://doi.org/10.1016/j.cub.2009.12.021>
- Lee, S., Zhou, L., Kim, J., Kalbfleisch, S., & Schock, F. (2008). Lasp anchors the *Drosophila* male stem cell niche and mediates spermatid individualization. *Mech Dev*, *125*(9-10), 768-776. <https://doi.org/10.1016/j.mod.2008.06.012>
- Lehmann, R., & Nüsslein-Volhard, C. (1986). Abdominal segmentation, pole cell formation, and embryonic polarity require the localized activity of oskar, a maternal gene in *drosophila*. *Cell*, *47*(1), 141-152. [https://doi.org/10.1016/0092-8674\(86\)90375-2](https://doi.org/10.1016/0092-8674(86)90375-2)
- Lens, S. M. A., & Medema, R. H. (2019). Cytokinesis defects and cancer. *Nat Rev Cancer*, *19*(1), 32-45. <https://doi.org/10.1038/s41568-018-0084-6>
- Lepage, S. E., & Bruce, A. E. (2014). Dynamin-dependent maintenance of epithelial integrity is essential for zebrafish epiboly. *Bioarchitecture*, *4*(1), 31-34. <https://doi.org/10.4161/bioa.28178>

- Leptin, M. (1999). Gastrulation in *Drosophila*: the logic and the cellular mechanisms. *EMBO J*, *18*(12), 3187-3192. <https://doi.org/10.1093/emboj/18.12.3187>
- Lim, J., & Thiery, J. P. (2012). Epithelial-mesenchymal transitions: insights from development. *Development*, *139*(19), 3471-3486. <https://doi.org/10.1242/dev.071209>
- Liu, X., Yuan, H., Zhou, J., Wang, Q., Qi, X., Bernal, C., Avella, D., Kaifi, J. T., Kimchi, E. T., Timothy, P., Cheng, K., Miao, Y., Jiang, K., & Li, G. (2021). LMO7 as an Unrecognized Factor Promoting Pancreatic Cancer Progression and Metastasis. *Front Cell Dev Biol*, *9*, 647387. <https://doi.org/10.3389/fcell.2021.647387>
- Macara, I. G. (2004). Parsing the polarity code. *Nat Rev Mol Cell Biol*, *5*(3), 220-231. <https://doi.org/10.1038/nrm1332>
- Machnicka, B., Grochowalska, R., Boguslawska, D. M., Sikorski, A. F., & Lecomte, M. C. (2012). Spectrin-based skeleton as an actor in cell signaling. *Cell Mol Life Sci*, *69*(2), 191-201. <https://doi.org/10.1007/s00018-011-0804-5>
- Maddox, A. S., Lewellyn, L., Desai, A., & Oegema, K. (2007). Anillin and the septins promote asymmetric ingression of the cytokinetic furrow. *Dev Cell*, *12*(5), 827-835. <https://doi.org/10.1016/j.devcel.2007.02.018>
- Manning, A. J., & Rogers, S. L. (2014). The Fog signaling pathway: insights into signaling in morphogenesis. *Dev Biol*, *394*(1), 6-14. <https://doi.org/10.1016/j.ydbio.2014.08.003>
- Mannix, K. M., Starble, R. M., Kaufman, R. S., & Cooley, L. (2019). Proximity labeling reveals novel interactomes in live *Drosophila* tissue. <https://doi.org/10.1101/542795>
- Martin, A. C., Kaschube, M., & Wieschaus, E. F. (2009). Pulsed contractions of an actin-myosin network drive apical constriction. *Nature*, *457*(7228), 495-499. <https://doi.org/10.1038/nature07522>
- Mason, F. M., Tworoger, M., & Martin, A. C. (2013). Apical domain polarization localizes actin-myosin activity to drive ratchet-like apical constriction. *Nat Cell Biol*, *15*(8), 926-936. <https://doi.org/10.1038/ncb2796>
- Matakatsu, H., & Blair, S. S. (2004). Interactions between Fat and Dachous and the regulation of planar cell polarity in the *Drosophila* wing. *Development*, *131*(15), 3785-3794. <https://doi.org/10.1242/dev.01254>
- Matis, M., Russler-Germain, D. A., Hu, Q., Tomlin, C. J., & Axelrod, J. D. (2014). Microtubules provide directional information for core PCP function. *Elife*, *3*, e02893. <https://doi.org/10.7554/eLife.02893>
- Matsuda, M., Chu, C. W., & Sokol, S. Y. (2022). Lmo7 recruits myosin II heavy chain to regulate actomyosin contractility and apical domain size in *Xenopus* ectoderm. *Development*, *149*(10). <https://doi.org/10.1242/dev.200236>
- Matsui, T., Maeda, M., Doi, Y., Yonemura, S., Amano, M., Kaibuchi, K., Tsukita, S., & Tsukita, S. (1998). Rho-kinase phosphorylates COOH-terminal threonines of ezrin/radixin/moesin (ERM) proteins and regulates their head-to-tail association. *J Cell Biol*, *140*(3), 647-657. <https://doi.org/10.1083/jcb.140.3.647>
- Matter, K. (2000). Epithelial polarity: sorting out the sorters. *Curr Biol*, *10*(1), R39-42. [https://doi.org/10.1016/s0960-9822\(99\)00256-0](https://doi.org/10.1016/s0960-9822(99)00256-0)
- McCartney, B. M., & Fehon, R. G. (1996). Distinct cellular and subcellular patterns of expression imply distinct functions for the *Drosophila* homologues of moesin and the neurofibromatosis 2 tumor suppressor, merlin. *J Cell Biol*, *133*(4), 843-852. <https://doi.org/10.1083/jcb.133.4.843>
- Medina, E., Williams, J., Klipfell, E., Zarnescu, D., Thomas, C. M., & Le Bivic, A. (2002). Crumbs interacts with moesin and beta(Heavy)-spectrin in the apical membrane skeleton of *Drosophila*. *J Cell Biol*, *158*(5), 941-951. <https://doi.org/10.1083/jcb.200203080>

- Metral, S., Machnicka, B., Bigot, S., Colin, Y., Dhermy, D., & Lecomte, M. C. (2009). AlphaII-spectrin is critical for cell adhesion and cell cycle. *J Biol Chem*, *284*(4), 2409-2418. <https://doi.org/10.1074/jbc.M801324200>
- Miao, H., & Blankenship, J. T. (2020). The pulse of morphogenesis: actomyosin dynamics and regulation in epithelia. *Development*, *147*(17). <https://doi.org/10.1242/dev.186502>
- Milas, A., & Telley, I. A. (2022). Polarity Events in the *Drosophila melanogaster* Oocyte. *Front Cell Dev Biol*, *10*, 895876. <https://doi.org/10.3389/fcell.2022.895876>
- Morais-de-Sa, E., Mirouse, V., & St Johnston, D. (2010). aPKC phosphorylation of Bazooka defines the apical/lateral border in *Drosophila* epithelial cells. *Cell*, *141*(3), 509-523. <https://doi.org/10.1016/j.cell.2010.02.040>
- Mull, A., Kim, G., & Holaska, J. M. (2015). LMO7-null mice exhibit phenotypes consistent with emery-dreifuss muscular dystrophy. *Muscle Nerve*, *51*(2), 222-228. <https://doi.org/10.1002/mus.24286>
- Müller, H. A., & Bossinger, O. (2003). Molecular networks controlling epithelial cell polarity in development. *Mech Dev*, *120*(11), 1231-1256. <https://doi.org/10.1016/j.mod.2003.06.001>
- Müller, H. A., & Wieschaus, E. (1996). armadillo, bazooka, and stardust Are Critical for Early Stages in Formation of the zonula adherens and Maintenance of the Polarized Blastoderm Epithelium in *Drosophila*. *The Journal of Cell Biology*, *134*(1), 149-163. <https://doi.org/10.1083/jcb.134.1.149>
- Nakamura, H., Hori, K., Tanaka-Okamoto, M., Higashiyama, M., Itoh, Y., Inoue, M., Morinaka, S., & Miyoshi, J. (2011). Decreased expression of LMO7 and its clinicopathological significance in human lung adenocarcinoma. *Exp Ther Med*, *2*(6), 1053-1057. <https://doi.org/10.3892/etm.2011.329>
- Neufeld, T. P., & Rubin, G. M. (1994). The *Drosophila* peanut gene is required for cytokinesis and encodes a protein similar to yeast putative bud neck filament proteins. *Cell*, *77*(3), 371-379. [https://doi.org/10.1016/0092-8674\(94\)90152-X](https://doi.org/10.1016/0092-8674(94)90152-X)
- Neuman-Silberberg, F. S., & Schupbach, T. (1993). The *Drosophila* dorsoventral patterning gene gurken produces a dorsally localized RNA and encodes a TGF alpha-like protein. *Cell*, *75*(1), 165-174. <https://www.ncbi.nlm.nih.gov/pubmed/7691414>
- Neuman, S., Kaban, A., Volk, T., Yaffe, D., & Nudel, U. (2001). The dystrophin / utrophin homologues in *Drosophila* and in sea urchin. *Gene*, *263*(1-2), 17-29. [https://doi.org/10.1016/s0378-1119\(00\)00584-9](https://doi.org/10.1016/s0378-1119(00)00584-9)
- Nishimura, T., & Takeichi, M. (2008). Shroom3-mediated recruitment of Rho kinases to the apical cell junctions regulates epithelial and neuroepithelial planar remodeling. *Development*, *135*(8), 1493-1502. <https://doi.org/10.1242/dev.019646>
- Oegema, K., Savoian, M. S., Mitchison, T. J., & Field, C. M. (2000). Functional Analysis of a Human Homologue of the *Drosophila* Actin Binding Protein Anillin Suggests a Role in Cytokinesis. *The Journal of Cell Biology*, *150*(3), 539-552. <https://doi.org/10.1083/jcb.150.3.539>
- Ooshio, T., Irie, K., Morimoto, K., Fukuhara, A., Imai, T., & Takai, Y. (2004). Involvement of LMO7 in the association of two cell-cell adhesion molecules, nectin and E-cadherin, through afadin and alpha-actinin in epithelial cells. *J Biol Chem*, *279*(30), 31365-31373. <https://doi.org/10.1074/jbc.M401957200>
- Pare, A. C., & Zallen, J. A. (2020). Cellular, molecular, and biophysical control of epithelial cell intercalation. *Curr Top Dev Biol*, *136*, 167-193. <https://doi.org/10.1016/bs.ctdb.2019.11.014>
- Pascual, J., Castresana, J., & Saraste, M. (1997). Evolution of the spectrin repeat. *BioEssays*, *19*(9), 811-817. <https://doi.org/10.1002/bies.950190911>

- Pedelacq, J. D., Cabantous, S., Tran, T., Terwilliger, T. C., & Waldo, G. S. (2006). Engineering and characterization of a superfolder green fluorescent protein. *Nat Biotechnol*, *24*(1), 79-88. <https://doi.org/10.1038/nbt1172>
- Peek, I. (2019). Functional and structural characterization of the Drosophila gene smallish during epithelial morphogenesis. *Doctoral thesis, University of Cologne*. <https://kups.ub.uni-koeln.de/9502/>
- Percipalle, P., & Vartiainen, M. (2019). Cytoskeletal proteins in the cell nucleus: a special nuclear actin perspective. *Mol Biol Cell*, *30*(15), 1781-1785. <https://doi.org/10.1091/mbc.E18-10-0645>
- Perez-Vale, K. Z., & Peifer, M. (2020). Orchestrating morphogenesis: building the body plan by cell shape changes and movements. *Development*, *147*(17). <https://doi.org/10.1242/dev.191049>
- Petersen, C. P., & Reddien, P. W. (2009). Wnt signaling and the polarity of the primary body axis. *Cell*, *139*(6), 1056-1068. <https://doi.org/10.1016/j.cell.2009.11.035>
- Pignoni, F., & Zipursky, S. L. (1997). Induction of Drosophila eye development by decapentaplegic. *Development*, *124*(2), 271-278. <https://doi.org/10.1242/dev.124.2.271>
- Pilot, F., & Lecuit, T. (2005). Compartmentalized morphogenesis in epithelia: from cell to tissue shape. *Dev Dyn*, *232*(3), 685-694. <https://doi.org/10.1002/dvdy.20334>
- Plant, P. J., Fawcett, J. P., Lin, D. C., Holdorf, A. D., Binns, K., Kulkarni, S., & Pawson, T. (2003). A polarity complex of mPar-6 and atypical PKC binds, phosphorylates and regulates mammalian Lgl. *Nat Cell Biol*, *5*(4), 301-308. <https://doi.org/10.1038/ncb948>
- Poernbacher, I., Crossman, S., Kurth, J., Nojima, H., Baena-Lopez, A., Alexandre, C., & Vincent, J. P. (2019). Lessons in genome engineering: opportunities, tools and pitfalls. *bioRxiv*. <https://doi.org/10.1101/710871>
- Polesello, C., Delon, I., Valenti, P., Ferrer, P., & Payre, F. (2002). Dmoesin controls actin-based cell shape and polarity during Drosophila melanogaster oogenesis. *Nat Cell Biol*, *4*(10), 782-789. <https://doi.org/10.1038/ncb856>
- Pouille, P. A., Ahmadi, P., Brunet, A. C., & Farge, E. (2009). Mechanical signals trigger Myosin II redistribution and mesoderm invagination in Drosophila embryos. *Sci Signal*, *2*(66), ra16. <https://doi.org/10.1126/scisignal.2000098>
- Ragkousi, K., & Gibson, M. C. (2014). Cell division and the maintenance of epithelial order. *J Cell Biol*, *207*(2), 181-188. <https://doi.org/10.1083/jcb.201408044>
- Razzell, W., Bustillo, M. E., & Zallen, J. A. (2018). The force-sensitive protein Ajuba regulates cell adhesion during epithelial morphogenesis. *J Cell Biol*, *217*(10), 3715-3730. <https://doi.org/10.1083/jcb.201801171>
- Rehfeld, A., Nylander, M., & Karnov, K. (2017). Epithelial Tissue. In: *Compendium of Histology*. Springer, Cham. [https://doi.org/10.1007/978-3-319-41873-5\\_5](https://doi.org/10.1007/978-3-319-41873-5_5)
- Robinson, B. S., Huang, J., Hong, Y., & Moberg, K. H. (2010). Crumbs regulates Salvador/Warts/Hippo signaling in Drosophila via the FERM-domain protein Expanded. *Curr Biol*, *20*(7), 582-590. <https://doi.org/10.1016/j.cub.2010.03.019>
- Rodriguez-Boulan, E., & Macara, I. G. (2014). Organization and execution of the epithelial polarity programme. *Nat Rev Mol Cell Biol*, *15*(4), 225-242. <https://doi.org/10.1038/nrm3775>
- Rørth, P. (1998). Gal4 in the Drosophila female germline. *Mechanisms of Development*, *78*, 113-118. [https://doi.org/10.1016/s0925-4773\(98\)00157-9](https://doi.org/10.1016/s0925-4773(98)00157-9)
- Roth, S., Neuman-Silberberg, F. S., Barcelo, G., & Schüpbach, T. (1995). cornichon and the EGF receptor signaling process are necessary for both anterior-posterior and dorsal-ventral pattern formation in Drosophila. *Cell*, *81*(6), 967-978. [https://doi.org/10.1016/0092-8674\(95\)90016-0](https://doi.org/10.1016/0092-8674(95)90016-0)

- Roth, S., Stein, D., & Nusslein-Volhard, C. (1989). A gradient of nuclear localization of the dorsal protein determines dorsoventral pattern in the *Drosophila* embryo. *Cell*, *59*(6), 1189-1202. [https://doi.org/10.1016/0092-8674\(89\)90774-5](https://doi.org/10.1016/0092-8674(89)90774-5)
- Salis, P., Payre, F., Valenti, P., Bazellieres, E., Le Bivic, A., & Mottola, G. (2017). Crumbs, Moesin and Yurt regulate junctional stability and dynamics for a proper morphogenesis of the *Drosophila* pupal wing epithelium. *Sci Rep*, *7*(1), 16778. <https://doi.org/10.1038/s41598-017-15272-1>
- Sawyer, J. K., Choi, W., Jung, K. C., He, L., Harris, N. J., & Peifer, M. (2011). A contractile actomyosin network linked to adherens junctions by Canoe/afadin helps drive convergent extension. *Mol Biol Cell*, *22*(14), 2491-2508. <https://doi.org/10.1091/mbc.E11-05-0411>
- Sawyer, J. M., Harrell, J. R., Shemer, G., Sullivan-Brown, J., Roh-Johnson, M., & Goldstein, B. (2010). Apical constriction: a cell shape change that can drive morphogenesis. *Dev Biol*, *341*(1), 5-19. <https://doi.org/10.1016/j.ydbio.2009.09.009>
- Schejter, E. D., & Wieschaus, E. (1993). Functional elements of the cytoskeleton in the early *Drosophila* embryo. *Annu Rev Cell Biol*, *9*, 67-99. <https://doi.org/10.1146/annurev.cb.09.110193.000435>
- Schimizzi, G. V., & Longmore, G. D. (2015). Ajuba proteins. *Curr Biol*, *25*(11), R445-446. <https://doi.org/10.1016/j.cub.2015.02.034>
- Sharma, M., Castro-Piedras, I., Simmons, G. E., Jr., & Pruitt, K. (2018). Dishevelled: A masterful conductor of complex Wnt signals. *Cell Signal*, *47*, 52-64. <https://doi.org/10.1016/j.cellsig.2018.03.004>
- Shimada, Y., Yonemura, S., Ohkura, H., Strutt, D., & Uemura, T. (2006). Polarized transport of Frizzled along the planar microtubule arrays in *Drosophila* wing epithelium. *Dev Cell*, *10*(2), 209-222. <https://doi.org/10.1016/j.devcel.2005.11.016>
- Sidor, C., Stevens, T. J., Jin, L., Boulanger, J., & Roper, K. (2020). Rho-Kinase Planar Polarization at Tissue Boundaries Depends on Phospho-regulation of Membrane Residence Time. *Dev Cell*, *52*(3), 364-378 e367. <https://doi.org/10.1016/j.devcel.2019.12.003>
- Simões, S. M., Blankenship, J. T., Weitz, O., Farrell, D. L., Tamada, M., Fernandez-Gonzalez, R., & Zallen, J. A. (2010). Rho-kinase directs Bazooka/Par-3 planar polarity during *Drosophila* axis elongation. *Dev Cell*, *19*(3), 377-388. <https://doi.org/10.1016/j.devcel.2010.08.011>
- Simões, S. M., Mainieri, A., & Zallen, J. A. (2014). Rho GTPase and Shroom direct planar polarized actomyosin contractility during convergent extension. *J Cell Biol*, *204*(4), 575-589. <https://doi.org/10.1083/jcb.201307070>
- Simon, M. A. (2004). Planar cell polarity in the *Drosophila* eye is directed by graded Four-jointed and Dachshous expression. *Development*, *131*(24), 6175-6184. <https://doi.org/10.1242/dev.01550>
- Simon, M. A., Xu, A., Ishikawa, H. O., & Irvine, K. D. (2010). Modulation of fat:dachshous binding by the cadherin domain kinase four-jointed. *Curr Biol*, *20*(9), 811-817. <https://doi.org/10.1016/j.cub.2010.04.016>
- Sit, S. T., & Manser, E. (2011). Rho GTPases and their role in organizing the actin cytoskeleton. *J Cell Sci*, *124*(Pt 5), 679-683. <https://doi.org/10.1242/jcs.064964>
- Sjoblom, B., Salmazo, A., & Djinovic-Carugo, K. (2008). Alpha-actinin structure and regulation. *Cell Mol Life Sci*, *65*(17), 2688-2701. <https://doi.org/10.1007/s00018-008-8080-8>
- Sokac, A. M., & Wieschaus, E. (2008a). Local actin-dependent endocytosis is zygotically controlled to initiate *Drosophila* cellularization. *Dev Cell*, *14*(5), 775-786. <https://doi.org/10.1016/j.devcel.2008.02.014>
- Sokac, A. M., & Wieschaus, E. (2008b). Zygotically controlled F-actin establishes cortical compartments to stabilize furrows during *Drosophila* cellularization. *J Cell Sci*, *121*(11), 1815-1824. <https://doi.org/10.1242/jcs.025171>

- Sokol, S. Y. (2015). Spatial and temporal aspects of Wnt signaling and planar cell polarity during vertebrate embryonic development. *Semin Cell Dev Biol*, *42*, 78-85. <https://doi.org/10.1016/j.semcdb.2015.05.002>
- Sotillos, S., Diaz-Meco, M. T., Caminero, E., Moscat, J., & Campuzano, S. (2004). DaPKC-dependent phosphorylation of Crumbs is required for epithelial cell polarity in *Drosophila*. *J Cell Biol*, *166*(4), 549-557. <https://doi.org/10.1083/jcb.200311031>
- Speck, O., Hughes, S. C., Noren, N. K., Kulikaukas, R. M., & Fehon, R. G. (2003). Moesin functions antagonistically to the Rho pathway to maintain epithelial integrity. *Nature*, *421*, 83-87. <https://doi.org/10.1038/nature01295>
- Straight, A. F., Field, C. M., & Mitchison, T. J. (2005). Anillin binds nonmuscle myosin II and regulates the contractile ring. *Mol Biol Cell*, *16*(1), 193-201. <https://doi.org/10.1091/mbc.e04-08-0758>
- Strutt, D. (2001). Asymmetric localization of frizzled and the establishment of cell polarity in the *Drosophila* wing. *Molecular Cell*, *7*(2), 367-375. [https://doi.org/10.1016/s1097-2765\(01\)00184-8](https://doi.org/10.1016/s1097-2765(01)00184-8)
- Strutt, H., Warrington, S. J., & Strutt, D. (2011). Dynamics of core planar polarity protein turnover and stable assembly into discrete membrane subdomains. *Dev Cell*, *20*(4), 511-525. <https://doi.org/10.1016/j.devcel.2011.03.018>
- Suyama, R., Jenny, A., Curado, S., Pellis-van Berkel, W., & Ephrussi, A. (2009). The actin-binding protein Lasp promotes Oskar accumulation at the posterior pole of the *Drosophila* embryo. *Development*, *136*(1), 95-105. <https://doi.org/10.1242/dev.027698>
- Sweeton, D., Parks, S., Costa, M., & Wieschaus, E. (1991). Gastrulation in *Drosophila*: the formation of the ventral furrow and posterior midgut invaginations. *Development*, *112*(3), 775-789. <https://doi.org/10.1242/dev.112.3.775>
- Tan, J. L., Ravid, S., & Spudich, J. A. (1992). Control of nonmuscle myosin by phosphorylation. *Annu. Rev. Biochem.*, *61*, 721-759. <https://doi.org/10.1146/annurev.bi.61.070192.003445>
- Tanaka-Okamoto, M., Hori, K., Ishizaki, H., Hosoi, A., Itoh, Y., Wei, M., Wanibuchi, H., Mizoguchi, A., Nakamura, H., & Miyoshi, J. (2009). Increased susceptibility to spontaneous lung cancer in mice lacking LIM-domain only 7. *Cancer Sci*, *100*(4), 608-616. <https://doi.org/10.1111/j.1349-7006.2009.01091.x>
- Taylor, M. J., Lampe, M., & Merrifield, C. J. (2012). A feedback loop between dynamin and actin recruitment during clathrin-mediated endocytosis. *PLoS Biol*, *10*(4), e1001302. <https://doi.org/10.1371/journal.pbio.1001302>
- Thomas, G. H., Newbern, E. C., Korte, C. C., Bales, M. A., Muse, S. V., Clark, A. G., & Kiehart, D. P. (1997). Intragenic duplication and divergence in the spectrin superfamily of proteins. *Mol. Biol. Evol.*, *14*(12), 1285-1295. <https://doi.org/10.1093/oxfordjournals.molbev.a025738>
- Torban, E., & Sokol, S. Y. (2021). Planar cell polarity pathway in kidney development, function and disease. *Nat Rev Nephrol*, *17*(6), 369-385. <https://doi.org/10.1038/s41581-021-00395-6>
- Tree, D. R., Shulman, J. M., Rousset, R., Scott, M. P., Gubb, D., & Axelrod, J. D. (2002). Prickle mediates feedback amplification to generate asymmetric planar cell polarity signaling. *Cell*, *109*(3), 371-381. [https://doi.org/10.1016/s0092-8674\(02\)00715-8](https://doi.org/10.1016/s0092-8674(02)00715-8)
- van der Plas, M. C., Pilgram, G. S., de Jong, A. W., Bansraj, M. R., Fradkin, L. G., & Noordermeer, J. N. (2007). *Drosophila* Dystrophin is required for integrity of the musculature. *Mech Dev*, *124*(7-8), 617-630. <https://doi.org/10.1016/j.mod.2007.04.003>
- van der Plas, M. C., Pilgram, G. S., Plomp, J. J., de Jong, A., Fradkin, L. G., & Noordermeer, J. N. (2006). Dystrophin is required for appropriate retrograde control of neurotransmitter release at the *Drosophila* neuromuscular junction. *J Neurosci*, *26*(1), 333-344. <https://doi.org/10.1523/JNEUROSCI.4069-05.2006>

- Varadi, M., Anyango, S., Deshpande, M., Nair, S., Natassia, C., Yordanova, G., Yuan, D., Stroe, O., Wood, G., Laydon, A., Zidek, A., Green, T., Tunyasuvunakool, K., Petersen, S., Jumper, J., Clancy, E., Green, R., Vora, A., Lutfi, M., . . . Velankar, S. (2022). AlphaFold Protein Structure Database: massively expanding the structural coverage of protein-sequence space with high-accuracy models. *Nucleic Acids Res*, *50*(D1), D439-D444. <https://doi.org/10.1093/nar/gkab1061>
- Vasquez, C. G., Heissler, S. M., Billington, N., Sellers, J. R., & Martin, A. C. (2016). Drosophila non-muscle myosin II motor activity determines the rate of tissue folding. *Elife*, *5*. <https://doi.org/10.7554/eLife.20828>
- Vasquez, C. G., Tworoger, M., & Martin, A. C. (2014). Dynamic myosin phosphorylation regulates contractile pulses and tissue integrity during epithelial morphogenesis. *J Cell Biol*, *206*(3), 435-450. <https://doi.org/10.1083/jcb.201402004>
- Veneti, Z., Clark, M. E., Karr, T. L., Savakis, C., & Bourtzis, K. (2004). Heads or tails: host-parasite interactions in the Drosophila-Wolbachia system. *Appl Environ Microbiol*, *70*(9), 5366-5372. <https://doi.org/10.1128/AEM.70.9.5366-5372.2004>
- Verdier, V., Guang Chao, C., & Settleman, J. (2006). Rho-kinase regulates tissue morphogenesis via non-muscle myosin and LIM-kinase during Drosophila development. *BMC Dev Biol*, *6*, 38. <https://doi.org/10.1186/1471-213X-6-38>
- Verdier, V., Johndrow, J. E., Betson, M., Chen, G. C., Hughes, D. A., Parkhurst, S. M., & Settleman, J. (2006). Drosophila Rho-kinase (DRok) is required for tissue morphogenesis in diverse compartments of the egg chamber during oogenesis. *Dev Biol*, *297*(2), 417-432. <https://doi.org/10.1016/j.ydbio.2006.05.016>
- Vicente-Manzanares, M., Ma, X., Adelstein, R. S., & Horwitz, A. R. (2009). Non-muscle myosin II takes centre stage in cell adhesion and migration. *Nat Rev Mol Cell Biol*, *10*(11), 778-790. <https://doi.org/10.1038/nrm2786>
- Walker, J. M. (2002). *The Protein Protocols Handbook*. (2 ed.). Humana Totowa, NJ. <https://doi.org/10.1385/1592591698>
- Watanabe, T., Hosoya, H., & Yonemura, S. (2007). Regulation of myosin II dynamics by phosphorylation and dephosphorylation of its light chain in epithelial cells. *Mol Biol Cell*, *18*(2), 605-616. <https://doi.org/10.1091/mbc.e06-07-0590>
- Wei, Z., Li, Y., Ye, F., & Zhang, M. (2015). Structural basis for the phosphorylation-regulated interaction between the cytoplasmic tail of cell polarity protein crumbs and the actin-binding protein moesin. *J Biol Chem*, *290*(18), 11384-11392. <https://doi.org/10.1074/jbc.M115.643791>
- Wodarz, A., & Nusse, R. (1998). Mechanisms of Wnt signaling in development. *Annu Rev Cell Dev Biol*, *14*, 59-88. <https://doi.org/10.1146/annurev.cellbio.14.1.59>
- Wodarz, A., Ramrath, A., Grimm, A., & Knust, E. (2000). Drosophila atypical protein kinase C associates with Bazooka and controls polarity of epithelia and neuroblasts. *J Cell Biol*, *150*(6), 1361-1374. <https://doi.org/10.1083/jcb.150.6.1361>
- Wong, L. L., & Adler, P. N. (1993). Tissue polarity genes of Drosophila regulate the subcellular location for prehair initiation in pupal wing cells. *J Cell Biol*, *123*(1), 209-221. <https://doi.org/10.1083/jcb.123.1.209>
- Yamanaka, T., & Ohno, S. (2008). Role of Lgl/Dlg/Scribble in the regulation of epithelial junction, polarity and growth. *Front Biosci*, *13*, 6693-6707. <https://doi.org/10.2741/3182>
- Young, P., Pesacreta, T. C., & Kiehart, D. P. (1991). Dynamic changes in the distribution of cytoplasmic myosin during Drosophila embryogenesis. *Development*, *111*(1), 1-14. <https://doi.org/10.1242/dev.111.1.1>

- Young, P. E., Richman, A. M., Ketchum, A. S., & Kiehart, D. P. (1993). Morphogenesis in *Drosophila* requires nonmuscle myosin heavy chain function. *Genes Dev*, 7(1), 29-41. <https://doi.org/10.1101/gad.7.1.29>
- Yu, H. H., & Zallen, J. A. (2020). Abl and Cdc42/Afadin mediate mechanotransduction at tricellular junctions. *Science*, 370(6520). <https://doi.org/10.1126/science.aba5528>
- Zahedi, B., Shen, W., Xu, X., Chen, X., Mahey, M., & Harden, N. (2008). Leading edge-secreted Dpp cooperates with ACK-dependent signaling from the amnioserosa to regulate myosin levels during dorsal closure. *Dev Dyn*, 237(10), 2936-2946. <https://doi.org/10.1002/dvdy.21722>
- Zalewski, J. K., Mo, J. H., Heber, S., Heroux, A., Gardner, R. G., Hildebrand, J. D., & VanDemark, A. P. (2016). Structure of the Shroom-Rho Kinase Complex Reveals a Binding Interface with Monomeric Shroom That Regulates Cell Morphology and Stimulates Kinase Activity. *J Biol Chem*, 291(49), 25364-25374. <https://doi.org/10.1074/jbc.M116.738559>
- Zallen, J. A. (2007). Planar polarity and tissue morphogenesis. *Cell*, 129(6), 1051-1063. <https://doi.org/10.1016/j.cell.2007.05.050>
- Zhang, B., Zhang, Y., & Liu, J. L. (2021). Highly effective proximate labeling in *Drosophila*. *G3 Genes/Genomes/Genetics*, 11(5). <https://doi.org/10.1093/g3journal/jkab077>

## Supplementary material

To determine the lethality rate of *smash*<sup>A35</sup> mutants, a lethality assay was performed. For this purpose, the following cross was set up:

F<sub>0</sub>: *smash*<sup>A35</sup>/TM6B x *smash*<sup>A35</sup>/TM6B

Following Mendelian rules, the genotypes in the offspring should be distributed as follows: 25 % *smash*<sup>A35</sup>/*smash*<sup>A35</sup>, 25 % TM6B/TM6B and 50 % *smash*<sup>A35</sup>/TM6B. Assuming that the *smash*<sup>A35</sup> mutation has no effect on viability, the expectation is that 75 % of embryos should hatch as larvae. 25 % should not hatch because of lethality factors on TM6B. Hatched larvae were used for further analysis. The portion of *Tubby*<sup>+</sup> (*Tb*<sup>+</sup>) and *Tubby* (*Tb*<sup>-</sup>) pupae and *Antp*<sup>+</sup> and *Antp*<sup>Hu</sup> adults was counted. Assuming that the *smash*<sup>A35</sup> mutation has no effect on viability, the expectation is that 66.7 % of larvae should be *Tb*<sup>-</sup> while 33.3 % should be *Tb*<sup>+</sup>. Accordingly, 66.7 % of adults should be *Antp*<sup>Hu</sup> and 33.3 % *Antp*<sup>+</sup>.

The following observations were made in the F<sub>1</sub> generation and the corresponding likelihoods were calculated:

| N° of embryos | Hatched                  | Not hatched               | Chi <sup>2</sup> test (p-value) |
|---------------|--------------------------|---------------------------|---------------------------------|
| 590           | 488 (82.7 %)             | 102 (17.3 %)              | 1.51854E-05                     |
| N° of pupae   | <i>Tb</i> <sup>+</sup>   | <i>Tb</i> <sup>-</sup>    | Chi <sup>2</sup> test (p-value) |
| 254           | 77 (30.31 %)             | 177 (69.69 %)             | 0.310549                        |
| N° of adults  | <i>Antp</i> <sup>+</sup> | <i>Antp</i> <sup>Hu</sup> | Chi <sup>2</sup> test (p-value) |
| 246           | 71 (28.86 %)             | 175 (71.14 %)             | 0.13710519                      |

Chi<sup>2</sup> test was performed to investigate whether the observed data is statistically significant different from the expected data. p-value < 0,05 means that the observed value is different from the expected value.

For Chi<sup>2</sup> test calculations, following expected likelihoods were used:

| N° of embryos | Hatched                  | Not hatched               |
|---------------|--------------------------|---------------------------|
| 590           | 443 (75 %)               | 147 (25 %)                |
| N° of pupae   | <i>Tb</i> <sup>+</sup>   | <i>Tb</i> <sup>-</sup>    |
| 254           | 85 (33.3 %)              | 169 (66.7 %)              |
| N° of adults  | <i>Antp</i> <sup>+</sup> | <i>Antp</i> <sup>Hu</sup> |
| 246           | 82 (33.3 %)              | 164 (66.7 %)              |

More embryos hatched as expected. The observed ratio of *Tb*<sup>+</sup> and *Tb*<sup>-</sup> pupae and *Antp*<sup>+</sup> and *Antp*<sup>Hu</sup> adult flies was not different from the expectation, suggesting no increased lethality in the F<sub>1</sub> generation.

To calculate the lethality rate of *smash*<sup>Δ35m/z</sup> mutants, the following cross was set up:

F<sub>1</sub>: *smash*<sup>Δ35</sup> × *smash*<sup>Δ35</sup>

The following observations were made in the F<sub>2</sub> generation:

| N° of embryos | Hatched    | Not hatched  |
|---------------|------------|--------------|
| 277           | 26 (9.4 %) | 251 (90.6 %) |

If the *smash*<sup>Δ35</sup> mutation would not affect viability, the theoretical likelihood for lethality is 0 %. In contrast to the expectation, the observed lethality is 90.6 %. Thus, *smash*<sup>Δ35m/z</sup> mutant embryos show a strong increase in lethality.

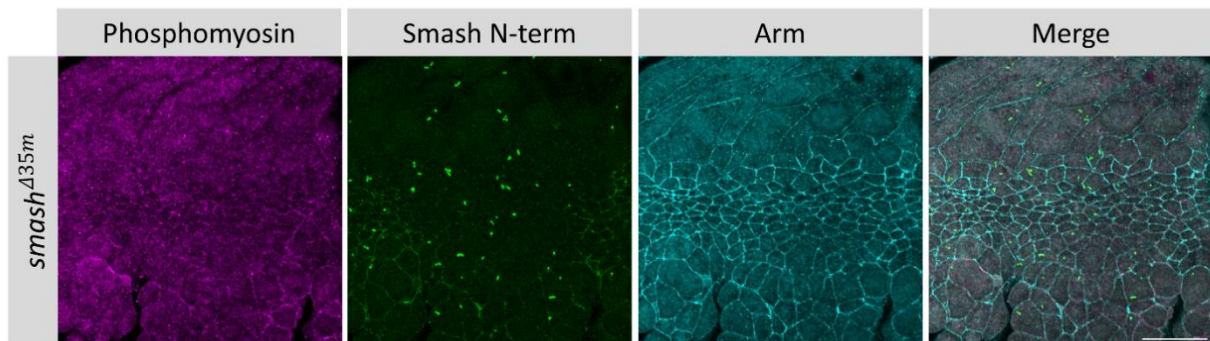


**Figure S 1: A weak Smash signal was detected in *smash*<sup>Δ35</sup> maternal mutant embryos.** Complete loss of Smash occurs only in *smash*<sup>Δ35</sup> maternal and zygotic mutants. The shown optical section was obtained from a stage 8 embryo, which is maternal mutant only. Homozygous *smash*<sup>Δ35</sup> mothers were mated with males that were heterozygous for the *smash*<sup>Δ35</sup> mutation, thus potentially providing a WT copy of Smash. The weak Smash expression coincides with a weak phosphomyosin signal. Antibodies used for IF staining are indicated above each panel. Scale bar: 20 μm.

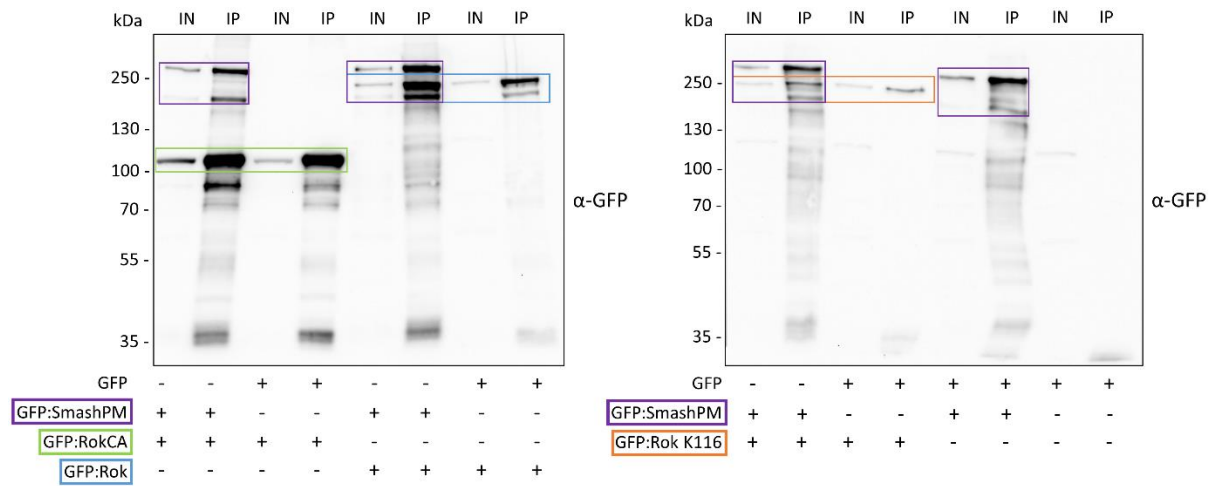


**Figure S 2: Detection of GFP fusion proteins used for the *in vitro* kinase assay.** Indicated proteins were expressed in S2 cells. Cell lysates were used to enrich GFP-tagged proteins for the kinase assay. The presence of GFP-tagged fusion proteins in input (IN) and immunoprecipitated (IP) samples was verified by Western blotting. Proteins were detected with an  $\alpha$ -GFP antibody. Predicted molecular weight of proteins: GFP:SmashPM = 197.8 kDa, GFP = 26.9 kDa, GFP:RokCA = 92.4 kDa, GFP:Rok = 189.2 kDa, GFP:Rok K116 = 189.2 kDa.

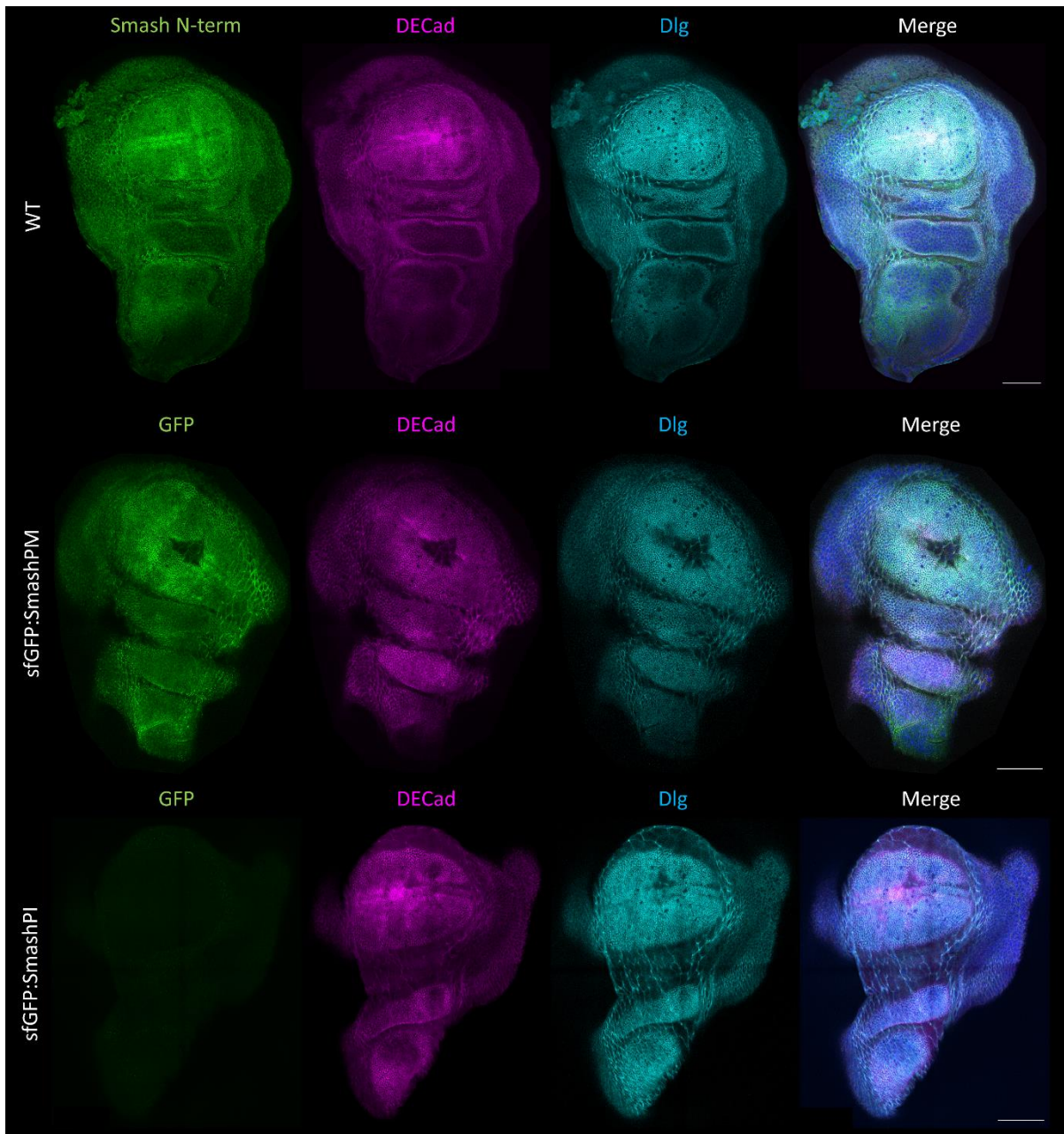


**Figure S 3: Expression pattern of endogenous SmashPM, sfGFP:SmashPM, and sfGFP:SmashPI in wing disc.** While sfGFP:SmashPM reflects the endogenous localization pattern of SmashPM, which was visualized with the antibody against the N-terminus of Smash, sfGFP:SmashPI is not expressed in wing discs. Used antibodies for IF staining are indicated above each panel. Scale bar: 50  $\mu$ m.

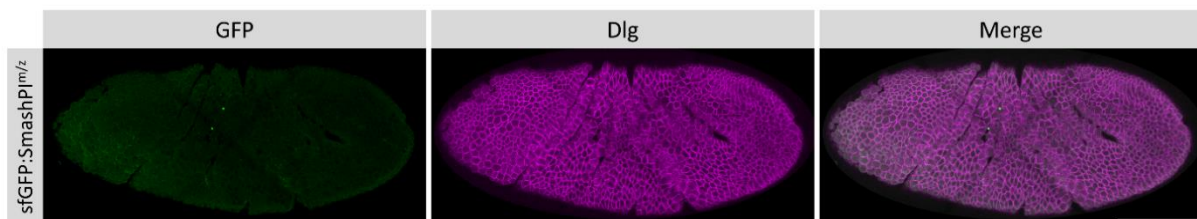


**Figure S 4: sfGFP:SmashPI<sup>m/z</sup> is not expressed in embryos.** A whole mount stage 8 embryo is shown. IF staining was performed using indicated antibodies. Scale bar: 100  $\mu$ m.

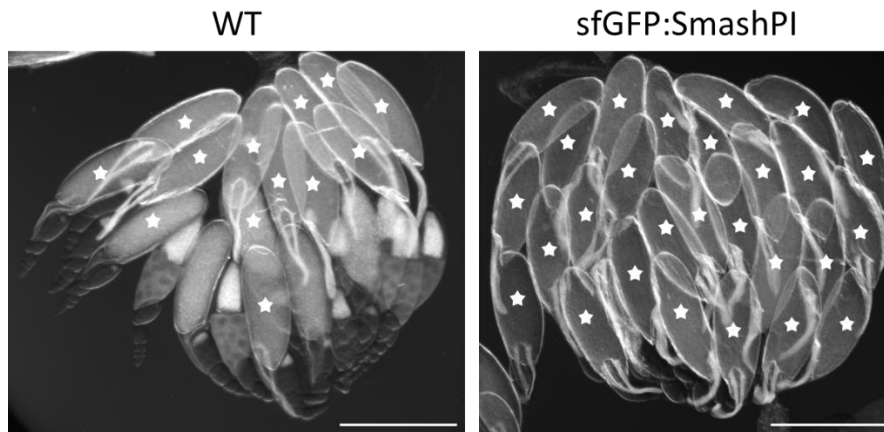


**Figure S 5: Comparison of WT and sfGFP:SmashPI ovarian morphology.** A characteristic example of a WT and a sfGFP:SmashPI ovary is shown. sfGFP:SmashPI ovaries showed an egg-retention phenotype (described in Beard et al. (2023)). The stars denote mature oocytes. Ovaries were dissected from 1 week old flies kept at 25 °C. Flies were fed with yeast paste. Images were taken by brightfield microscopy. Scale bar: 500  $\mu$ m.

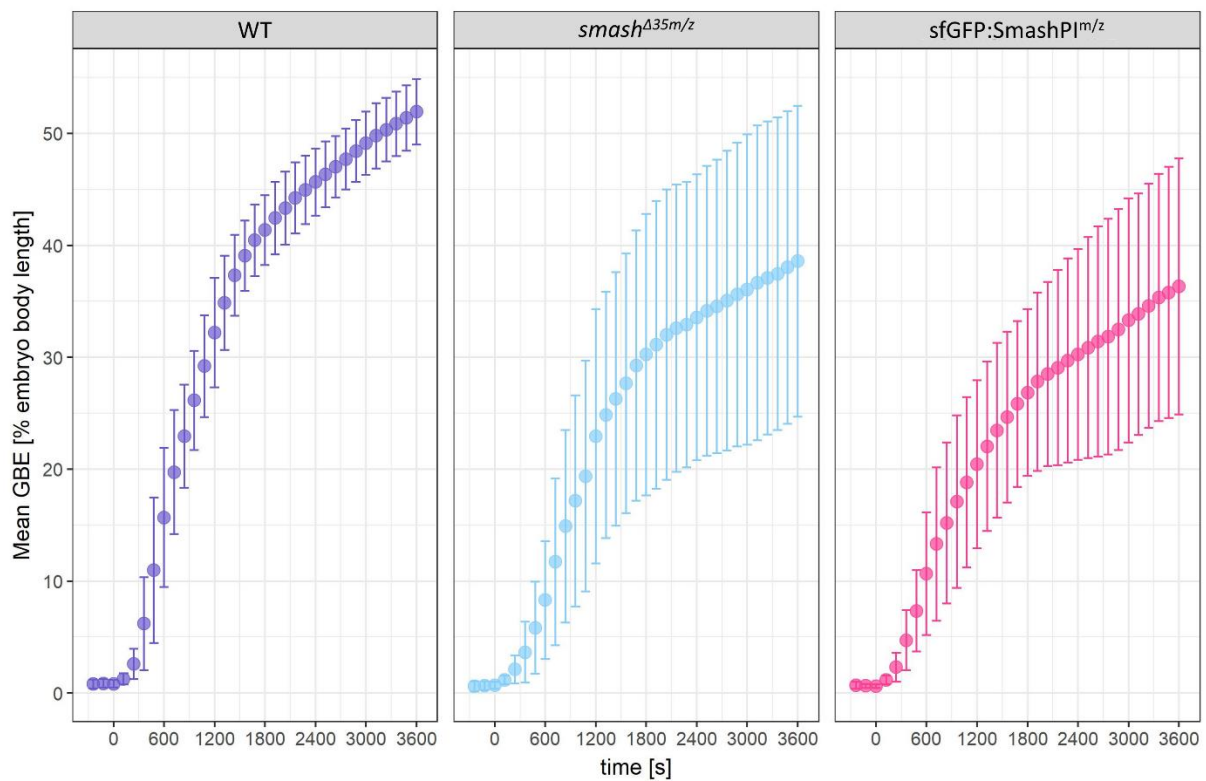


**Figure S 6: Mean GBE in WT, *smash* <sup>$\Delta$ 35m/z</sup>, and sfGFP:SmashPI<sup>m/z</sup> embryos.** Mean and error bars were generated based on the data shown in Figure 28. Corresponding statistics can be found in Table S 1.

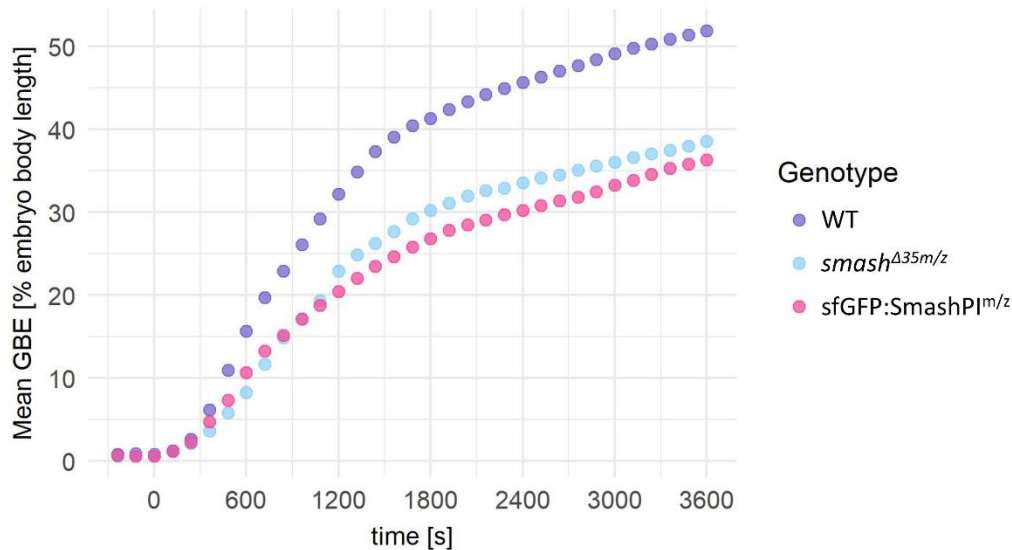


**Figure S 7: Direct comparison of mean GBE in WT, *smash*<sup>Δ35m/z</sup>, and sfGFP:SmashPI<sup>m/z</sup> embryos.** The mean was calculated based on the data shown in Figure 28. Corresponding statistics can be found in Table S 1.

**Table S 1: Statistical test to determine the significance of the differences between WT, *smash*<sup>Δ35m/z</sup>, and sfGFP:SmashPI<sup>m/z</sup> relative GBE.** SPSS software was used to calculate statistics. A nonparametric test based on a Kruskal-Wallis ANOVA was performed to test whether there is a statistically significant difference between samples. Pairwise comparison was performed to investigate which samples were different from each other. The p-value was adjusted by Bonferroni correction. The difference between samples was measured for each time point separately. The significance level is indicated with asterisks. '\*' p < 0.05, '\*\*' p < 0.01, '\*\*\*' p < 0.001, 'ns' not significant.

| Time | Pairwise comparison   | p-value adjusted | Significance level |
|------|---|------------------|--------------------|
| -240 | sfGFP:SmashPI <sup>m/z</sup> – <i>smash</i> <sup>Δ35m/z</sup> | 1                | ns                 |
|      | sfGFP:SmashPI <sup>m/z</sup> – WT                             | 0.359            | ns                 |
|      | <i>smash</i> <sup>Δ35m/z</sup> – WT                           | 0.835            | ns                 |
| -120 | sfGFP:SmashPI <sup>m/z</sup> – <i>smash</i> <sup>Δ35m/z</sup> | 1                | ns                 |
|      | sfGFP:SmashPI <sup>m/z</sup> – WT                             | 1                | ns                 |
|      | <i>smash</i> <sup>Δ35m/z</sup> – WT                           | 1                | ns                 |
| 0    | sfGFP:SmashPI <sup>m/z</sup> – <i>smash</i> <sup>Δ35m/z</sup> | 1                | ns                 |
|      | sfGFP:SmashPI <sup>m/z</sup> – WT                             | 0.239            | ns                 |
|      | <i>smash</i> <sup>Δ35m/z</sup> – WT                           | 1                | ns                 |
| 120  | sfGFP:SmashPI <sup>m/z</sup> – <i>smash</i> <sup>Δ35m/z</sup> | 1                | ns                 |
|      | sfGFP:SmashPI <sup>m/z</sup> – WT                             | 1                | ns                 |
|      | <i>smash</i> <sup>Δ35m/z</sup> – WT                           | 1                | ns                 |
| 240  | sfGFP:SmashPI <sup>m/z</sup> – <i>smash</i> <sup>Δ35m/z</sup> | 1                | ns                 |
|      | sfGFP:SmashPI <sup>m/z</sup> – WT                             | 1                | ns                 |
|      | <i>smash</i> <sup>Δ35m/z</sup> – WT                           | 1                | ns                 |
| 360  | sfGFP:SmashPI <sup>m/z</sup> – <i>smash</i> <sup>Δ35m/z</sup> | 0.875            | ns                 |
|      | sfGFP:SmashPI <sup>m/z</sup> – WT                             | 0.312            | ns                 |
|      | <i>smash</i> <sup>Δ35m/z</sup> – WT                           | 1                | ns                 |
| 480  | sfGFP:SmashPI <sup>m/z</sup> – <i>smash</i> <sup>Δ35m/z</sup> | 1                | ns                 |
|      | sfGFP:SmashPI <sup>m/z</sup> – WT                             | 0.122            | ns                 |
|      | <i>smash</i> <sup>Δ35m/z</sup> – WT                           | 0.392            | ns                 |

| Time | Pairwise comparison   | p-value adjusted | Significance level |
|------|---|------------------|--------------------|
| 600  | sfGFP:SmashPI <sup>m/z</sup> – <i>smash</i> <sup>Δ35m/z</sup> | 1                | ns                 |
|      | sfGFP:SmashPI <sup>m/z</sup> – WT                             | 0.044            | *                  |
|      | <i>smash</i> <sup>Δ35m/z</sup> – WT                           | 0.166            | ns                 |
| 720  | sfGFP:SmashPI <sup>m/z</sup> – <i>smash</i> <sup>Δ35m/z</sup> | 1                | ns                 |
|      | sfGFP:SmashPI <sup>m/z</sup> – WT                             | 0.042            | *                  |
|      | <i>smash</i> <sup>Δ35m/z</sup> – WT                           | 0.041            | *                  |
| 840  | sfGFP:SmashPI <sup>m/z</sup> – <i>smash</i> <sup>Δ35m/z</sup> | 1                |                    |
|      | sfGFP:SmashPI <sup>m/z</sup> – WT                             | 0.016            | *                  |
|      | <i>smash</i> <sup>Δ35m/z</sup> – WT                           | 0.088            | ns                 |
| 960  | sfGFP:SmashPI <sup>m/z</sup> – <i>smash</i> <sup>Δ35m/z</sup> | 1                | ns                 |
|      | sfGFP:SmashPI <sup>m/z</sup> – WT                             | 0.005            | **                 |
|      | <i>smash</i> <sup>Δ35m/z</sup> – WT                           | 0.062            | ns                 |
| 1080 | sfGFP:SmashPI <sup>m/z</sup> – <i>smash</i> <sup>Δ35m/z</sup> | 1                | ns                 |
|      | sfGFP:SmashPI <sup>m/z</sup> – WT                             | 0.002            | **                 |
|      | <i>smash</i> <sup>Δ35m/z</sup> – WT                           | 0.046            | *                  |
| 1200 | sfGFP:SmashPI <sup>m/z</sup> – <i>smash</i> <sup>Δ35m/z</sup> | 1                | ns                 |
|      | sfGFP:SmashPI <sup>m/z</sup> – WT                             | 0.001            | **                 |
|      | <i>smash</i> <sup>Δ35m/z</sup> – WT                           | 0.08             | ns                 |
| 1320 | sfGFP:SmashPI <sup>m/z</sup> – <i>smash</i> <sup>Δ35m/z</sup> | 1                | ns                 |
|      | sfGFP:SmashPI <sup>m/z</sup> – WT                             | 0                | ***                |
|      | <i>smash</i> <sup>Δ35m/z</sup> – WT                           | 0.042            | *                  |
| 1440 | sfGFP:SmashPI <sup>m/z</sup> – <i>smash</i> <sup>Δ35m/z</sup> | 1                | ns                 |
|      | sfGFP:SmashPI <sup>m/z</sup> – WT                             | 0                | ***                |
|      | <i>smash</i> <sup>Δ35m/z</sup> – WT                           | 0.044            | *                  |
| 1560 | sfGFP:SmashPI <sup>m/z</sup> – <i>smash</i> <sup>Δ35m/z</sup> | 1                | ns                 |
|      | sfGFP:SmashPI <sup>m/z</sup> – WT                             | 0                | ***                |
|      | <i>smash</i> <sup>Δ35m/z</sup> – WT                           | 0.025            | *                  |
| 1680 | sfGFP:SmashPI <sup>m/z</sup> – <i>smash</i> <sup>Δ35m/z</sup> | 1                | ns                 |
|      | sfGFP:SmashPI <sup>m/z</sup> – WT                             | 0                | ***                |
|      | <i>smash</i> <sup>Δ35m/z</sup> – WT                           | 0.024            | *                  |
| 1800 | sfGFP:SmashPI <sup>m/z</sup> – <i>smash</i> <sup>Δ35m/z</sup> | 0.83             | ns                 |
|      | sfGFP:SmashPI <sup>m/z</sup> – WT                             | 0                | ***                |
|      | <i>smash</i> <sup>Δ35m/z</sup> – WT                           | 0.039            | *                  |
| 1920 | sfGFP:SmashPI <sup>m/z</sup> – <i>smash</i> <sup>Δ35m/z</sup> | 0.97             | ns                 |
|      | sfGFP:SmashPI <sup>m/z</sup> – WT                             | 0                | ***                |
|      | <i>smash</i> <sup>Δ35m/z</sup> – WT                           | 0.032            | *                  |
| 2040 | sfGFP:SmashPI <sup>m/z</sup> – <i>smash</i> <sup>Δ35m/z</sup> | 0.852            | ns                 |
|      | sfGFP:SmashPI <sup>m/z</sup> – WT                             | 0                | ***                |
|      | <i>smash</i> <sup>Δ35m/z</sup> – WT                           | 0.04             | *                  |
| 2160 | sfGFP:SmashPI <sup>m/z</sup> – <i>smash</i> <sup>Δ35m/z</sup> | 0.97             | ns                 |
|      | sfGFP:SmashPI <sup>m/z</sup> – WT                             | 0                | ***                |
|      | <i>smash</i> <sup>Δ35m/z</sup> – WT                           | 0.039            | *                  |
| 2280 | sfGFP:SmashPI <sup>m/z</sup> – <i>smash</i> <sup>Δ35m/z</sup> | 1                | ns                 |
|      | sfGFP:SmashPI <sup>m/z</sup> – WT                             | 0                | ***                |
|      | <i>smash</i> <sup>Δ35m/z</sup> – WT                           | 0.019            | *                  |
| 2400 | sfGFP:SmashPI <sup>m/z</sup> – <i>smash</i> <sup>Δ35m/z</sup> | 1                | ns                 |
|      | sfGFP:SmashPI <sup>m/z</sup> – WT                             | 0                | ***                |
|      | <i>smash</i> <sup>Δ35m/z</sup> – WT                           | 0.02             | *                  |

| Time | Pairwise comparison   | p-value adjusted | Significance level |
|------|---|------------------|--------------------|
| 2520 | sfGFP:SmashPI <sup>m/z</sup> – <i>smash</i> <sup>Δ35m/z</sup> | 1                | ns                 |
|      | sfGFP:SmashPI <sup>m/z</sup> – WT                             | 0                | ***                |
|      | <i>smash</i> <sup>Δ35m/z</sup> – WT                           | 0.021            | *                  |
| 2640 | sfGFP:SmashPI <sup>m/z</sup> – <i>smash</i> <sup>Δ35m/z</sup> | 1                | ns                 |
|      | sfGFP:SmashPI <sup>m/z</sup> – WT                             | 0                | ***                |
|      | <i>smash</i> <sup>Δ35m/z</sup> – WT                           | 0.028            | *                  |
| 2760 | sfGFP:SmashPI <sup>m/z</sup> – <i>smash</i> <sup>Δ35m/z</sup> | 1                | ns                 |
|      | sfGFP:SmashPI <sup>m/z</sup> – WT                             | 0                | ***                |
|      | <i>smash</i> <sup>Δ35m/z</sup> – WT                           | 0.027            | *                  |
| 2880 | sfGFP:SmashPI <sup>m/z</sup> – <i>smash</i> <sup>Δ35m/z</sup> | 1                | ns                 |
|      | sfGFP:SmashPI <sup>m/z</sup> – WT                             | 0                | ***                |
|      | <i>smash</i> <sup>Δ35m/z</sup> – WT                           | 0.024            | *                  |
| 3000 | sfGFP:SmashPI <sup>m/z</sup> – <i>smash</i> <sup>Δ35m/z</sup> | 1                | ns                 |
|      | sfGFP:SmashPI <sup>m/z</sup> – WT                             | 0                | ***                |
|      | <i>smash</i> <sup>Δ35m/z</sup> – WT                           | 0.026            | *                  |
| 3120 | sfGFP:SmashPI <sup>m/z</sup> – <i>smash</i> <sup>Δ35m/z</sup> | 1                | ns                 |
|      | sfGFP:SmashPI <sup>m/z</sup> – WT                             | 0                | ***                |
|      | <i>smash</i> <sup>Δ35m/z</sup> – WT                           | 0.026            | *                  |
| 3240 | sfGFP:SmashPI <sup>m/z</sup> – <i>smash</i> <sup>Δ35m/z</sup> | 1                | ns                 |
|      | sfGFP:SmashPI <sup>m/z</sup> – WT                             | 0                | ***                |
|      | <i>smash</i> <sup>Δ35m/z</sup> – WT                           | 0.019            | *                  |
| 3360 | sfGFP:SmashPI <sup>m/z</sup> – <i>smash</i> <sup>Δ35m/z</sup> | 1                | ns                 |
|      | sfGFP:SmashPI <sup>m/z</sup> – WT                             | 0                | ***                |
|      | <i>smash</i> <sup>Δ35m/z</sup> – WT                           | 0.014            | *                  |
| 3480 | sfGFP:SmashPI <sup>m/z</sup> – <i>smash</i> <sup>Δ35m/z</sup> | 1                | ns                 |
|      | sfGFP:SmashPI <sup>m/z</sup> – WT                             | 0                | ***                |
|      | <i>smash</i> <sup>Δ35m/z</sup> – WT                           | 0.017            | *                  |
| 3600 | sfGFP:SmashPI <sup>m/z</sup> – <i>smash</i> <sup>Δ35m/z</sup> | 1                | ns                 |
|      | sfGFP:SmashPI <sup>m/z</sup> – WT                             | 0                | ***                |
|      | <i>smash</i> <sup>Δ35m/z</sup> – WT                           | 0.013            | *                  |

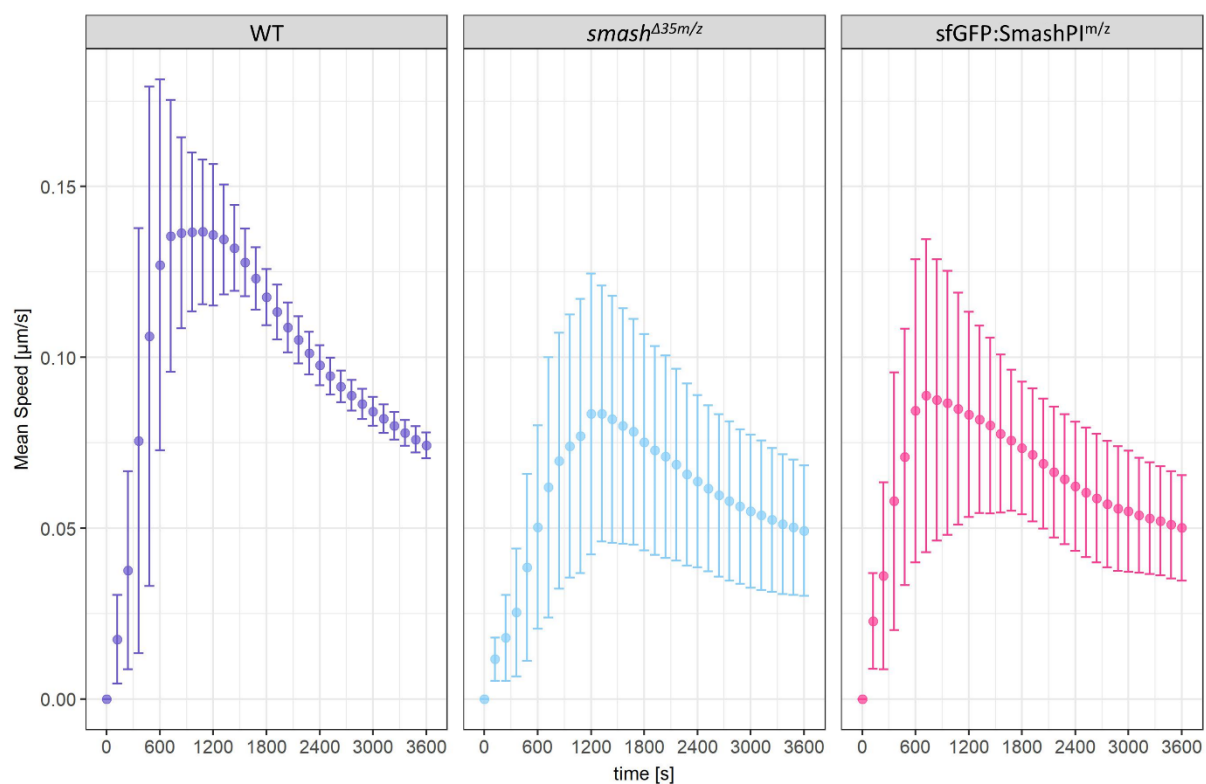


**Figure S 8: Mean GBE speed in WT,  $smash^{\Delta 35m/z}$ , and sfGFP:SmashPI<sup>m/z</sup> embryos.** Mean and error bars were generated based on the data shown in Figure 30. Corresponding statistics can be found in Table S 2.

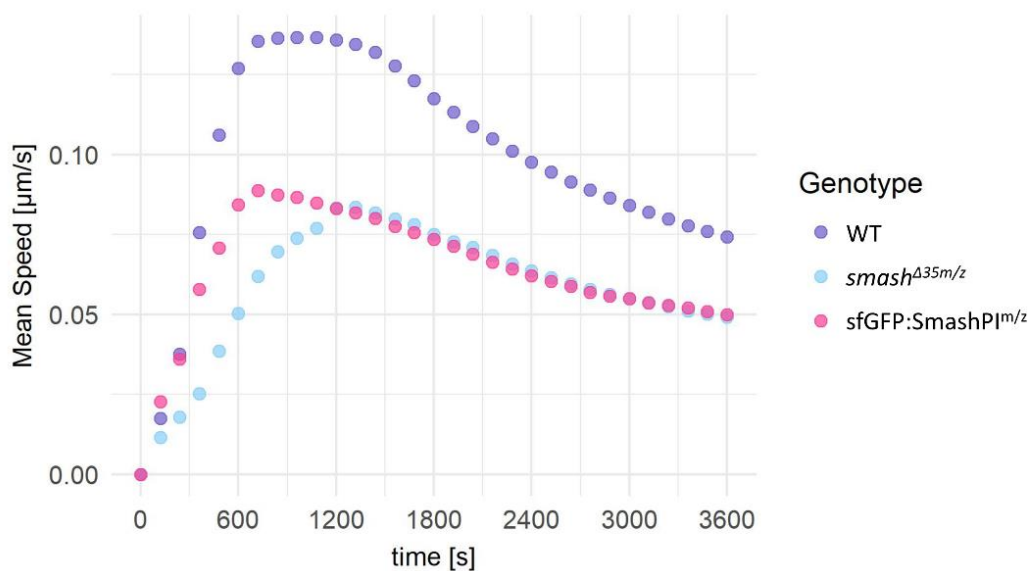


**Figure S 9: Direct comparison of mean GBE speed in WT,  $smash^{\Delta 35m/z}$ , and sfGFP:SmashPI<sup>m/z</sup> embryos.** The mean was calculated based on the data shown in Figure 30. Corresponding statistics can be found in Table S 2.

**Table S 2: Statistical test to determine the significance of the differences between WT, *smash*<sup>Δ35m/z</sup>, and sfGFP:SmashPI<sup>m/z</sup> GBE speed.** SPSS software was used to calculate statistics. A nonparametric test based on a Kruskal-Wallis ANOVA was performed to test whether there is a statistically significant difference between samples. Pairwise comparison was performed to investigate which samples were different from each other. The p-value was adjusted by Bonferroni correction. The difference between samples was measured for each time point separately. The significance level is indicated with asterisks. '\*' p < 0.05, '\*\*' p < 0.01, '\*\*\*' p < 0.001, 'ns' not significant.

| Time | Pairwise comparison   | p-value adjusted | Significance level |
|------|---|------------------|--------------------|
| 0    | sfGFP:SmashPI <sup>m/z</sup> – <i>smash</i> <sup>Δ35m/z</sup> | 1                | ns                 |
|      | sfGFP:SmashPI <sup>m/z</sup> – WT                             | 1                | ns                 |
|      | <i>smash</i> <sup>Δ35m/z</sup> – WT                           | 1                | ns                 |
| 120  | sfGFP:SmashPI <sup>m/z</sup> – <i>smash</i> <sup>Δ35m/z</sup> | 0.275            | ns                 |
|      | sfGFP:SmashPI <sup>m/z</sup> – WT                             | 1                | ns                 |
|      | <i>smash</i> <sup>Δ35m/z</sup> – WT                           | 0.454            | ns                 |
| 240  | sfGFP:SmashPI <sup>m/z</sup> – <i>smash</i> <sup>Δ35m/z</sup> | 0.364            | ns                 |
|      | sfGFP:SmashPI <sup>m/z</sup> – WT                             | 1                | ns                 |
|      | <i>smash</i> <sup>Δ35m/z</sup> – WT                           | 0.217            | ns                 |
| 360  | sfGFP:SmashPI <sup>m/z</sup> – <i>smash</i> <sup>Δ35m/z</sup> | 0.156            | ns                 |
|      | sfGFP:SmashPI <sup>m/z</sup> – WT                             | 1                | ns                 |
|      | <i>smash</i> <sup>Δ35m/z</sup> – WT                           | 0.038            | *                  |
| 480  | sfGFP:SmashPI <sup>m/z</sup> – <i>smash</i> <sup>Δ35m/z</sup> | 0.282            | ns                 |
|      | sfGFP:SmashPI <sup>m/z</sup> – WT                             | 0.94             | ns                 |
|      | <i>smash</i> <sup>Δ35m/z</sup> – WT                           | 0.032            | *                  |
| 600  | sfGFP:SmashPI <sup>m/z</sup> – <i>smash</i> <sup>Δ35m/z</sup> | 0.396            | ns                 |
|      | sfGFP:SmashPI <sup>m/z</sup> – WT                             | 0.233            | ns                 |
|      | <i>smash</i> <sup>Δ35m/z</sup> – WT                           | 0.009            | **                 |
| 720  | sfGFP:SmashPI <sup>m/z</sup> – <i>smash</i> <sup>Δ35m/z</sup> | 0.724            | ns                 |
|      | sfGFP:SmashPI <sup>m/z</sup> – WT                             | 0.057            | ns                 |
|      | <i>smash</i> <sup>Δ35m/z</sup> – WT                           | 0.006            | **                 |
| 840  | sfGFP:SmashPI <sup>m/z</sup> – <i>smash</i> <sup>Δ35m/z</sup> | 1                | ns                 |
|      | sfGFP:SmashPI <sup>m/z</sup> – WT                             | 0.009            | **                 |
|      | <i>smash</i> <sup>Δ35m/z</sup> – WT                           | 0.007            | **                 |
| 960  | sfGFP:SmashPI <sup>m/z</sup> – <i>smash</i> <sup>Δ35m/z</sup> | 1                | ns                 |
|      | sfGFP:SmashPI <sup>m/z</sup> – WT                             | 0.003            | **                 |
|      | <i>smash</i> <sup>Δ35m/z</sup> – WT                           | 0.007            | **                 |
| 1080 | sfGFP:SmashPI <sup>m/z</sup> – <i>smash</i> <sup>Δ35m/z</sup> | 1                | ns                 |
|      | sfGFP:SmashPI <sup>m/z</sup> – WT                             | 0.001            | **                 |
|      | <i>smash</i> <sup>Δ35m/z</sup> – WT                           | 0.009            | **                 |
| 1200 | sfGFP:SmashPI <sup>m/z</sup> – <i>smash</i> <sup>Δ35m/z</sup> | 1                | ns                 |
|      | sfGFP:SmashPI <sup>m/z</sup> – WT                             | 0                | ***                |
|      | <i>smash</i> <sup>Δ35m/z</sup> – WT                           | 0.012            | *                  |
| 1320 | sfGFP:SmashPI <sup>m/z</sup> – <i>smash</i> <sup>Δ35m/z</sup> | 1                | ns                 |
|      | sfGFP:SmashPI <sup>m/z</sup> – WT                             | 0                | ***                |
|      | <i>smash</i> <sup>Δ35m/z</sup> – WT                           | 0.004            | **                 |
| 1440 | sfGFP:SmashPI <sup>m/z</sup> – <i>smash</i> <sup>Δ35m/z</sup> | 1                | ns                 |
|      | sfGFP:SmashPI <sup>m/z</sup> – WT                             | 0                | ***                |
|      | <i>smash</i> <sup>Δ35m/z</sup> – WT                           | 0.002            | **                 |

| Time | Pairwise comparison   | p-value adjusted | Significance level |
|------|---|------------------|--------------------|
| 1560 | sfGFP:SmashPI <sup>m/z</sup> – <i>smash</i> <sup>Δ35m/z</sup> | 1                | ns                 |
|      | sfGFP:SmashPI <sup>m/z</sup> – WT                             | 0                | ***                |
|      | <i>smash</i> <sup>Δ35m/z</sup> – WT                           | 0.002            | **                 |
| 1680 | sfGFP:SmashPI <sup>m/z</sup> – <i>smash</i> <sup>Δ35m/z</sup> | 1                | ns                 |
|      | sfGFP:SmashPI <sup>m/z</sup> – WT                             | 0                | ***                |
|      | <i>smash</i> <sup>Δ35m/z</sup> – WT                           | 0.003            | **                 |
| 1800 | sfGFP:SmashPI <sup>m/z</sup> – <i>smash</i> <sup>Δ35m/z</sup> | 1                | ns                 |
|      | sfGFP:SmashPI <sup>m/z</sup> – WT                             | 0                | ***                |
|      | <i>smash</i> <sup>Δ35m/z</sup> – WT                           | 0.003            | **                 |
| 1920 | sfGFP:SmashPI <sup>m/z</sup> – <i>smash</i> <sup>Δ35m/z</sup> | 1                | ns                 |
|      | sfGFP:SmashPI <sup>m/z</sup> – WT                             | 0                | ***                |
|      | <i>smash</i> <sup>Δ35m/z</sup> – WT                           | 0.004            | **                 |
| 2040 | sfGFP:SmashPI <sup>m/z</sup> – <i>smash</i> <sup>Δ35m/z</sup> | 1                | ns                 |
|      | sfGFP:SmashPI <sup>m/z</sup> – WT                             | 0                | ***                |
|      | <i>smash</i> <sup>Δ35m/z</sup> – WT                           | 0.004            | **                 |
| 2160 | sfGFP:SmashPI <sup>m/z</sup> – <i>smash</i> <sup>Δ35m/z</sup> | 1                | ns                 |
|      | sfGFP:SmashPI <sup>m/z</sup> – WT                             | 0                | ***                |
|      | <i>smash</i> <sup>Δ35m/z</sup> – WT                           | 0.004            | **                 |
| 2280 | sfGFP:SmashPI <sup>m/z</sup> – <i>smash</i> <sup>Δ35m/z</sup> | 1                | ns                 |
|      | sfGFP:SmashPI <sup>m/z</sup> – WT                             | 0                | ***                |
|      | <i>smash</i> <sup>Δ35m/z</sup> – WT                           | 0.002            | **                 |
| 2400 | sfGFP:SmashPI <sup>m/z</sup> – <i>smash</i> <sup>Δ35m/z</sup> | 1                | ns                 |
|      | sfGFP:SmashPI <sup>m/z</sup> – WT                             | 0                | ***                |
|      | <i>smash</i> <sup>Δ35m/z</sup> – WT                           | 0.002            | **                 |
| 2520 | sfGFP:SmashPI <sup>m/z</sup> – <i>smash</i> <sup>Δ35m/z</sup> | 1                | ns                 |
|      | sfGFP:SmashPI <sup>m/z</sup> – WT                             | 0                | ***                |
|      | <i>smash</i> <sup>Δ35m/z</sup> – WT                           | 0.002            | **                 |
| 2640 | sfGFP:SmashPI <sup>m/z</sup> – <i>smash</i> <sup>Δ35m/z</sup> | 1                | ns                 |
|      | sfGFP:SmashPI <sup>m/z</sup> – WT                             | 0                | ***                |
|      | <i>smash</i> <sup>Δ35m/z</sup> – WT                           | 0.002            | **                 |
| 2760 | sfGFP:SmashPI <sup>m/z</sup> – <i>smash</i> <sup>Δ35m/z</sup> | 1                | ns                 |
|      | sfGFP:SmashPI <sup>m/z</sup> – WT                             | 0                | ***                |
|      | <i>smash</i> <sup>Δ35m/z</sup> – WT                           | 0.002            | **                 |
| 2880 | sfGFP:SmashPI <sup>m/z</sup> – <i>smash</i> <sup>Δ35m/z</sup> | 1                | ns                 |
|      | sfGFP:SmashPI <sup>m/z</sup> – WT                             | 0                | ***                |
|      | <i>smash</i> <sup>Δ35m/z</sup> – WT                           | 0.001            | **                 |
| 3000 | sfGFP:SmashPI <sup>m/z</sup> – <i>smash</i> <sup>Δ35m/z</sup> | 1                | ns                 |
|      | sfGFP:SmashPI <sup>m/z</sup> – WT                             | 0                | ***                |
|      | <i>smash</i> <sup>Δ35m/z</sup> – WT                           | 0.001            | **                 |
| 3120 | sfGFP:SmashPI <sup>m/z</sup> – <i>smash</i> <sup>Δ35m/z</sup> | 1                | ns                 |
|      | sfGFP:SmashPI <sup>m/z</sup> – WT                             | 0                | ***                |
|      | <i>smash</i> <sup>Δ35m/z</sup> – WT                           | 0.001            | **                 |
| 3240 | sfGFP:SmashPI <sup>m/z</sup> – <i>smash</i> <sup>Δ35m/z</sup> | 1                | ns                 |
|      | sfGFP:SmashPI <sup>m/z</sup> – WT                             | 0                | ***                |
|      | <i>smash</i> <sup>Δ35m/z</sup> – WT                           | 0.001            | **                 |
| 3360 | sfGFP:SmashPI <sup>m/z</sup> – <i>smash</i> <sup>Δ35m/z</sup> | 1                | ns                 |
|      | sfGFP:SmashPI <sup>m/z</sup> – WT                             | 0                | ***                |
|      | <i>smash</i> <sup>Δ35m/z</sup> – WT                           | 0.001            | **                 |

| Time | Pairwise comparison   | p-value adjusted | Significance level |
|------|---|------------------|--------------------|
| 3480 | sfGFP:SmashPI <sup>m/z</sup> – <i>smash</i> <sup>Δ35m/z</sup> | 1                | ns                 |
|      | sfGFP:SmashPI <sup>m/z</sup> – WT                             | 0                | ***                |
|      | <i>smash</i> <sup>Δ35m/z</sup> – WT                           | 0.001            | **                 |
| 3600 | sfGFP:SmashPI <sup>m/z</sup> – <i>smash</i> <sup>Δ35m/z</sup> | 1                | ns                 |
|      | sfGFP:SmashPI <sup>m/z</sup> – WT                             | 0                | ***                |
|      | <i>smash</i> <sup>Δ35m/z</sup> – WT                           | 0.001            | **                 |

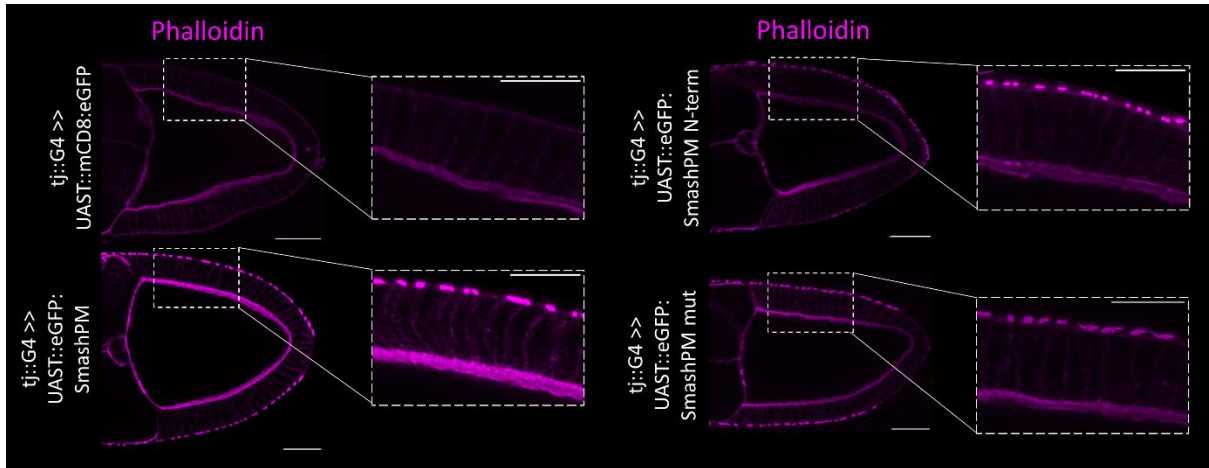


**Figure S 10: Close-up of phalloidin signal in ovaries overexpressing mCD8:eGFP, eGFP:SmashPM, eGFP:SmashPM N-term, and eGFP:SmashPM mut.** Overexpression was driven under the control of traffic jam (tj) Gal4. The phalloidin signal appeared as a double line since it was detected at the apical cortex of follicle cells and at the oocyte membrane in all samples. The respective genotypes are indicated on the left of each ovary. Scale bar: 30  $\mu$ m, scale bar close-up: 20  $\mu$ m.

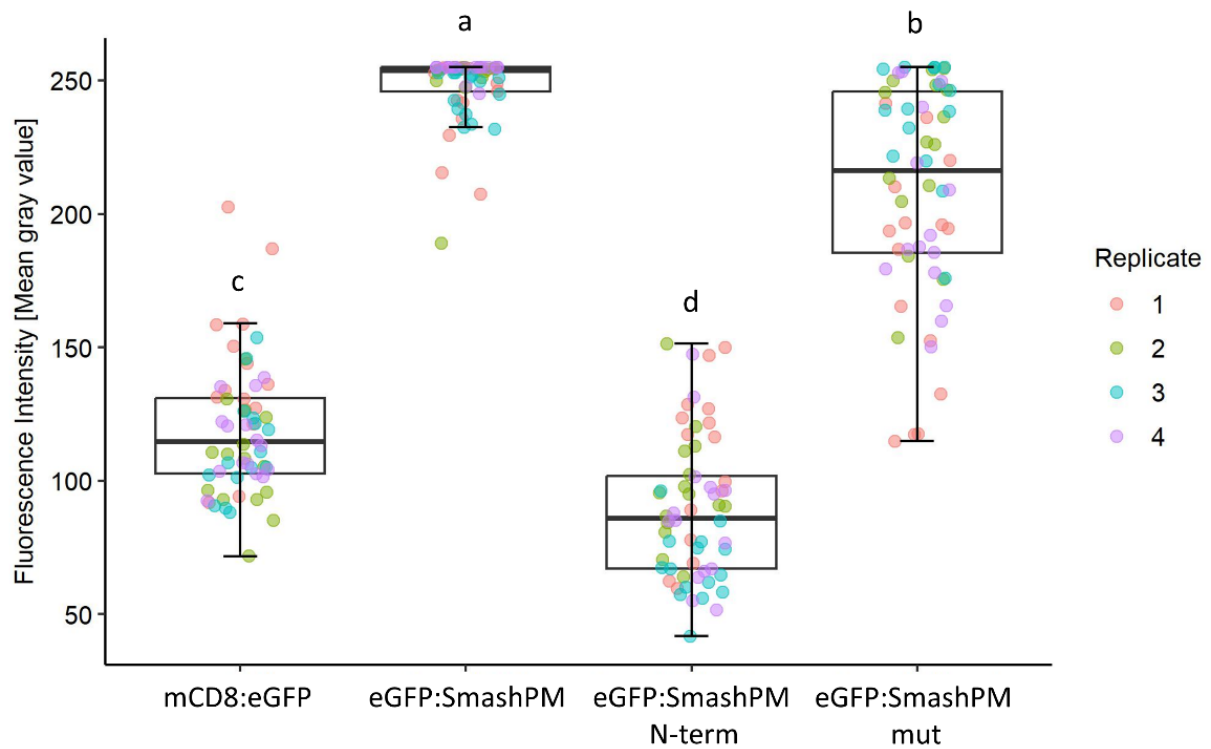


**Figure S 11: GFP intensity at the apical cell cortex of follicle cells.** mCD8:eGFP, eGFP:SmashPM, eGFP:SmashPM N-term, and eGFP:SmashPM mut overexpressing ovaries were examined. The straight-line tool in ImageJ was used for analysis. The mean gray value was used for calculations. The color code represents the replicate to which a data point belongs to.  $n = 60$  (4 replicates, 15 cells per replicate). A Kruskal-Wallis test and a post hoc Dunn test were performed to identify the statistically significant difference of two samples. Compact letter display (CLD) is used to visualize a statistically significant difference. Same letters mean that samples do not differ in a statistically significant manner from each other. For more details on the significance level, see Table S 3.

**Table S 3: Statistical test to determine the significance of the differences in GFP intensity at the apical cortex of follicle cells between mCD8:eGFP, eGFP:SmashPM, eGFP:SmashPM N-term, and eGFP:SmashPM mut overexpressing ovaries.** RStudio software was used to calculate statistics. A Kruskal-Wallis ANOVA was performed to test whether there is a statistically significant difference between samples. A post hoc Dunn test for pairwise comparison was performed. The p-value was adjusted by Bonferroni correction. The significance level is indicated with asterisks. '\*'  $p < 0.05$ , '\*\*'  $p < 0.01$ , '\*\*\*'  $p < 0.001$ , '\*\*\*\*'  $p < 0.0001$ , 'ns' not significant.

| Group 1             | Group 2             | p-value adjusted | Significance level |
|---------------------|---------------------|------------------|--------------------|
| mCD8:eGFP           | eGFP:SmashPM        | 2.095103E-20     | ****               |
| mCD8:eGFP           | eGFP:SmashPM N-term | 0.018737         | *                  |
| mCD8:eGFP           | eGFP:SmashPM mut    | 8.645022E-09     | ****               |
| eGFP:SmashPM        | eGFP:SmashPM N-term | 1.524782E-34     | ****               |
| eGFP:SmashPM        | eGFP:SmashPM mut    | 0.004103         | **                 |
| eGFP:SmashPM N-term | eGFP:SmashPM mut    | 1.279486E-18     | ****               |

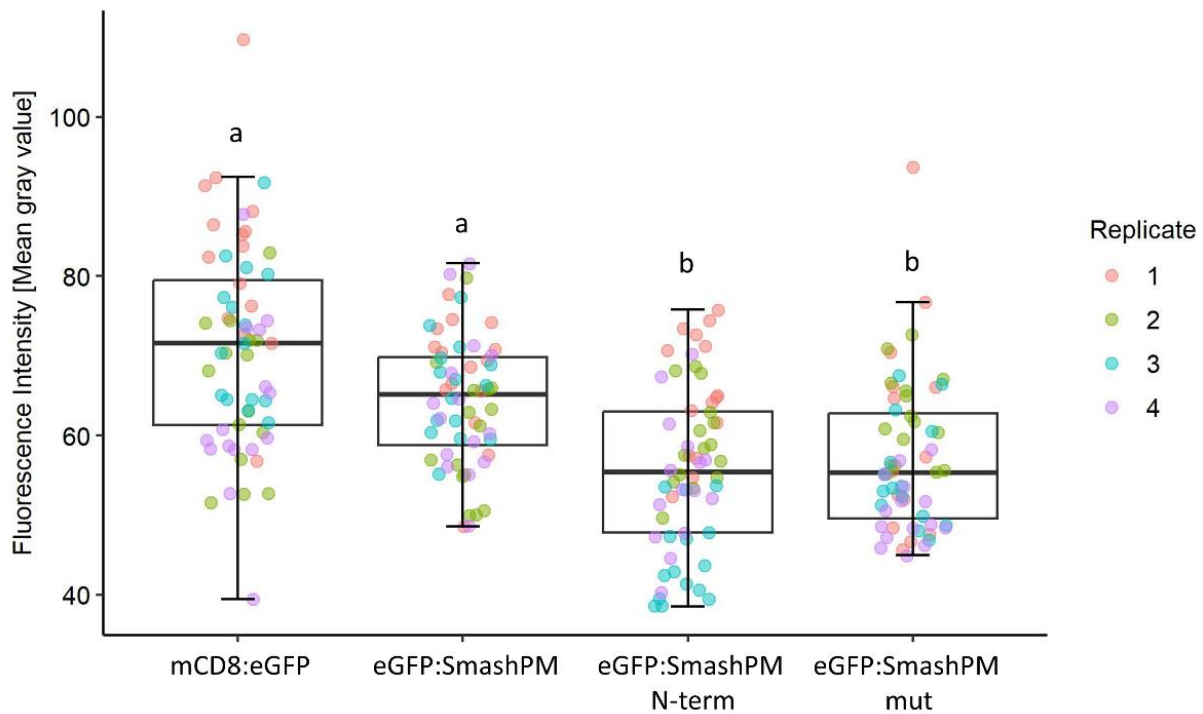


**Figure S 12: GFP intensity in the cytosol of follicle cells.** mCD8:eGFP, eGFP:SmashPM, eGFP:SmashPM N-term, and eGFP:SmashPM mut overexpressing ovaries were examined. The straight-line tool in ImageJ was used for analysis. The mean gray value was used for calculations. The color code represents the replicate to which a data point belongs to.  $n = 60$  (4 replicates, 15 cells per replicate). A Kruskal-Wallis test and a post hoc Dunn test were performed to identify the statistically significant difference of two samples. Compact letter display (CLD) is used to visualize a statistically significant difference. Same letters mean that samples do not differ in a statistically significant manner from each other. For more details on the significance level, see Table S 4.

**Table S 4: Statistical test to determine the significance of the differences in GFP intensity in the cytosol of follicle cells between mCD8:eGFP, eGFP:SmashPM, eGFP:SmashPM N-term, and eGFP:SmashPM mut overexpressing ovaries.** RStudio software was used to calculate statistics. A Kruskal-Wallis ANOVA was performed to test whether there is a statistically significant difference between samples. A post hoc Dunn test for pairwise comparison was performed. The p-value was adjusted by Bonferroni correction. The significance level is indicated with asterisks. '\*'  $p < 0.05$ , '\*\*'  $p < 0.01$ , '\*\*\*'  $p < 0.001$ , '\*\*\*\*'  $p < 0.0001$ , 'ns' not significant.

| Group 1             | Group 2             | p-value adjusted | Significance level |
|---------------------|---------------------|------------------|--------------------|
| mCD8:eGFP           | eGFP:SmashPM        | 0.141120         | ns                 |
| mCD8:eGFP           | eGFP:SmashPM N-term | 3.229900E-10     | ****               |
| mCD8:eGFP           | eGFP:SmashPM mut    | 4.858054E-10     | ****               |
| eGFP:SmashPM        | eGFP:SmashPM N-term | 0.000105         | ***                |
| eGFP:SmashPM        | eGFP:SmashPM mut    | 0.000138         | ***                |
| eGFP:SmashPM N-term | eGFP:SmashPM mut    | 1                | ns                 |

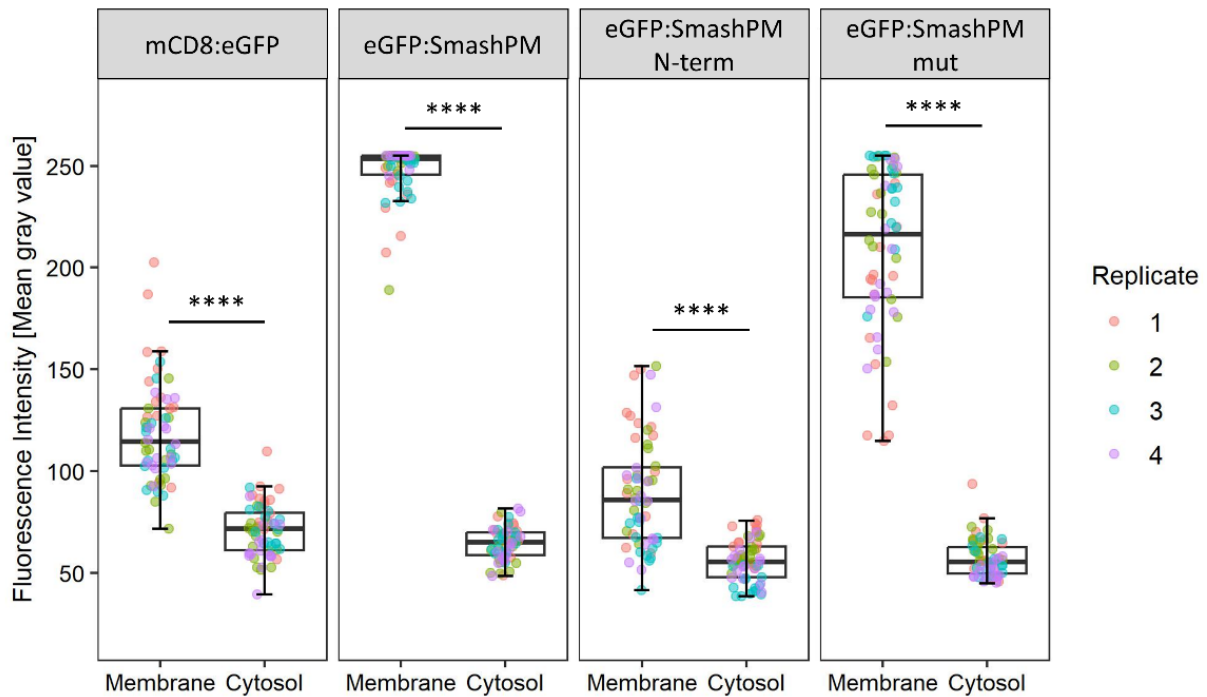


**Figure S 13: Comparison of GFP intensities at the apical cell cortex with GFP intensities in the cytosol of follicle cells.** mCD8:eGFP, eGFP:SmashPM, eGFP:SmashPM N-term, and eGFP:SmashPM mut overexpressing ovaries were examined. The straight-line tool in ImageJ was used for analysis. The mean gray value was used for calculations. The color code represents the replicate to which a data point belongs to.  $n = 60$  (4 replicates, 15 cells per replicate). A Kruskal-Wallis test and a post hoc Dunn test were performed to identify the statistically significant difference of two samples. The significance level is indicated with asterisks. '\*\*\*\*'  $p < 0.0001$ .

**Table S 5: Statistical test to determine the significance of the differences in GFP membrane/cytosol ratio mCD8:eGFP, eGFP:SmashPM, eGFP:SmashPM N-term, and eGFP:SmashPM mut overexpressing ovaries.** RStudio software was used to calculate statistics. A Kruskal-Wallis ANOVA was performed to test whether there is a statistically significant difference between samples. A post hoc Dunn test for pairwise comparison was performed. The p-value was adjusted by Bonferroni correction. The significance level is indicated with asterisks. '\*'  $p < 0.05$ , '\*\*'  $p < 0.01$ , '\*\*\*'  $p < 0.001$ , '\*\*\*\*'  $p < 0.0001$ , 'ns' not significant.

| Group 1             | Group 2             | p-value adjusted | Significance level |
|---------------------|---------------------|------------------|--------------------|
| mCD8:eGFP           | eGFP:SmashPM        | 3.230929E-20     | ****               |
| mCD8:eGFP           | eGFP:SmashPM N-term | 1                | ns                 |
| mCD8:eGFP           | eGFP:SmashPM mut    | 3.781492E-17     | ****               |
| eGFP:SmashPM        | eGFP:SmashPM N-term | 5.009187E-24     | ****               |
| eGFP:SmashPM        | eGFP:SmashPM mut    | 1                | ns                 |
| eGFP:SmashPM N-term | eGFP:SmashPM mut    | 1.152735E-20     | ****               |

**Table S 6: Statistical test to determine the significance of the differences in apical phalloidin intensity between mCD8:eGFP, eGFP:SmashPM, eGFP:SmashPM N-term, and eGFP:SmashPM mut overexpressing ovaries.** RStudio software was used to calculate statistics. A Kruskal-Wallis ANOVA was performed to test whether there is a statistically significant difference between samples. A post hoc Dunn test for pairwise comparison was performed. The p-value was adjusted by Bonferroni correction. The significance level is indicated with asterisks. *'\**  $p < 0.05$ , *'\*\*'*  $p < 0.01$ , *'\*\*\*'*  $p < 0.001$ , *'\*\*\*\*'*  $p < 0.0001$ , 'ns' not significant.

| Group 1             | Group 2             | p-value adjusted | Significance level |
|---------------------|---------------------|------------------|--------------------|
| mCD8:eGFP           | eGFP:SmashPM        | 1.518483E-27     | ****               |
| mCD8:eGFP           | eGFP:SmashPM N-term | 1.712987E-07     | ****               |
| mCD8:eGFP           | eGFP:SmashPM mut    | 1                | ns                 |
| eGFP:SmashPM        | eGFP:SmashPM N-term | 2.453029E-07     | ****               |
| eGFP:SmashPM        | eGFP:SmashPM mut    | 6.322484E-23     | ****               |
| eGFP:SmashPM N-term | eGFP:SmashPM mut    | 0.000032         | ****               |

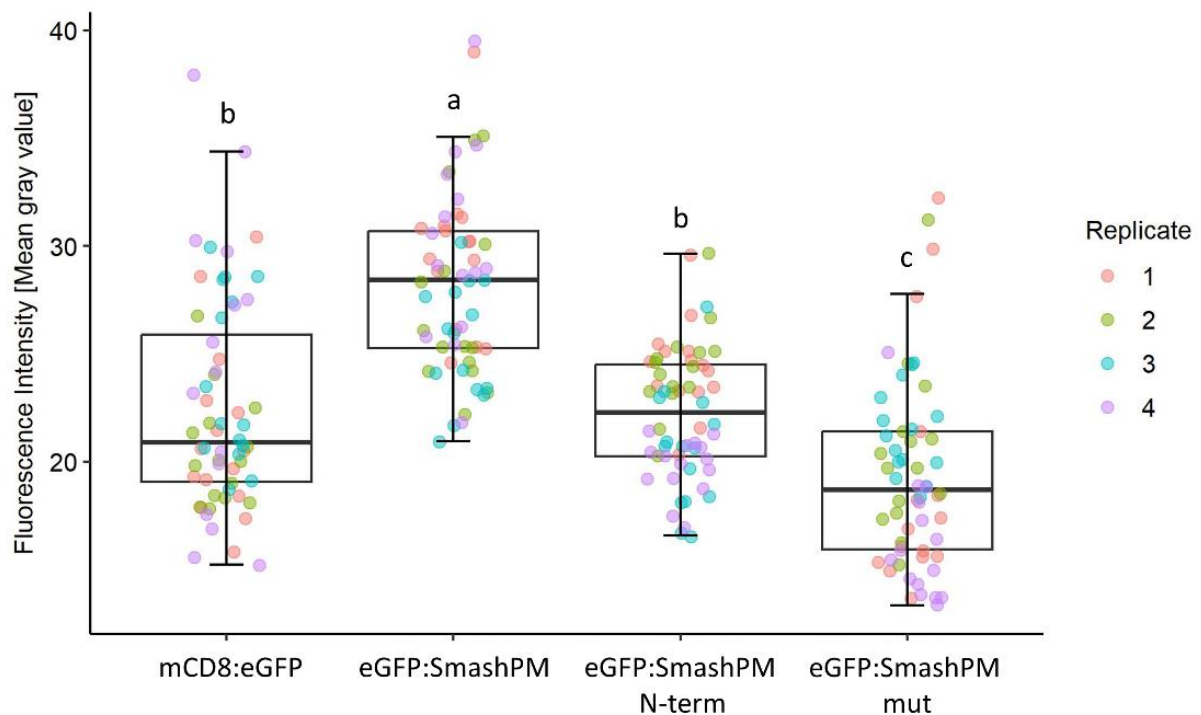


**Figure S 14: Phalloidin intensity in the cytosol of follicle cells.** mCD8:eGFP, eGFP:SmashPM, eGFP:SmashPM N-term, and eGFP:SmashPM mut overexpressing ovaries were examined. The straight-line tool in ImageJ was used for analysis. The mean gray value was used for calculations. The color code represents the replicate to which a data point belongs to.  $n = 60$  (4 replicates, 15 cells per replicate). A Kruskal-Wallis test and a post hoc Dunn test were performed to identify the statistically significant difference of two samples. Compact letter display (CLD) is used to visualize a statistically significant difference. Same letters mean that samples do not differ in a statistically significant manner from each other. For more details on the significance level, see Table S 7.

**Table S 7: Statistical test to determine the significance of the differences in cytosolic phalloidin intensity between mCD8:eGFP, eGFP:SmashPM, eGFP:SmashPM N-term, and eGFP:SmashPM mut overexpressing ovaries.** RStudio software was used to calculate statistics. A Kruskal-Wallis ANOVA was performed to test whether there is a statistically significant difference between samples. A post hoc Dunn test for pairwise comparison was performed. The p-value was adjusted by Bonferroni correction. The significance level is indicated with asterisks. '\*' p < 0.05, '\*\*' p < 0.01, '\*\*\*' p < 0.001, '\*\*\*\*' p < 0.0001, 'ns' not significant.

| Group 1             | Group 2             | p-value adjusted | Significance level |
|---------------------|---------------------|------------------|--------------------|
| mCD8:eGFP           | eGFP:SmashPM        | 5.017838E-09     | ****               |
| mCD8:eGFP           | eGFP:SmashPM N-term | 1                | ns                 |
| mCD8:eGFP           | eGFP:SmashPM mut    | 0.004983         | **                 |
| eGFP:SmashPM        | eGFP:SmashPM N-term | 2.199994E-08     | ****               |
| eGFP:SmashPM        | eGFP:SmashPM mut    | 1.521113E-20     | ****               |
| eGFP:SmashPM N-term | eGFP:SmashPM mut    | 0.002048         | **                 |

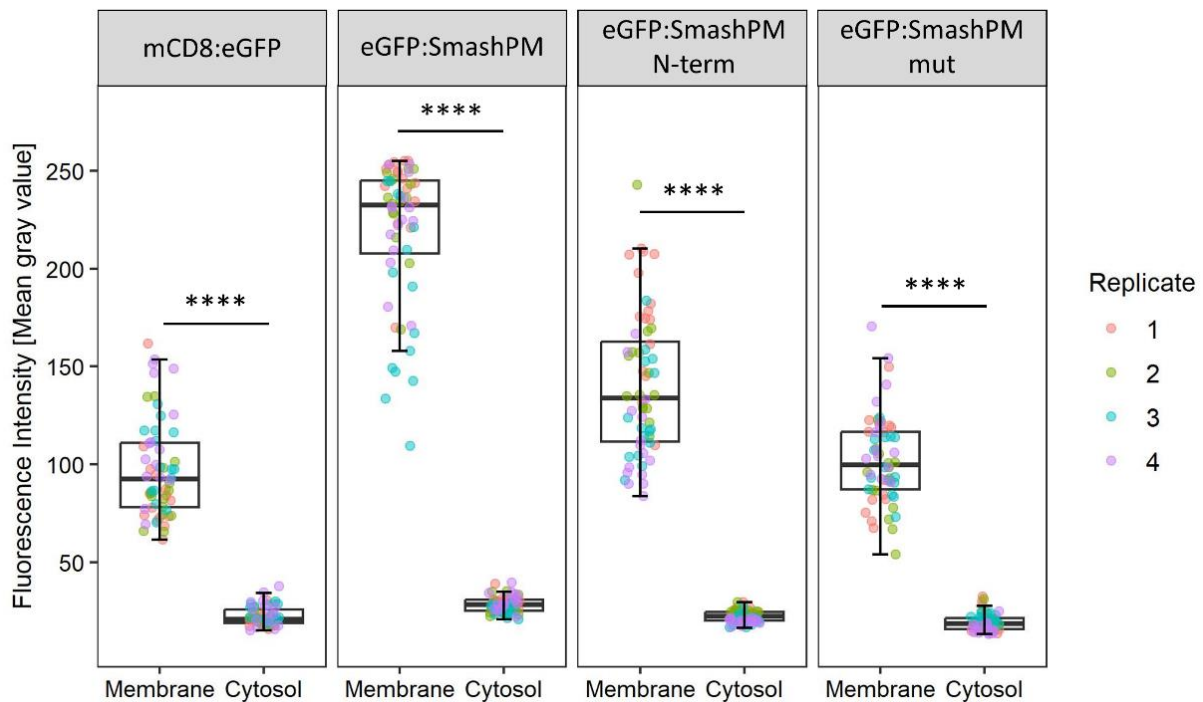


**Figure S 15: Comparison of phalloidin intensities at the apical cell cortex with phalloidin intensities in the cytosol of follicle cells.** mCD8:eGFP, eGFP:SmashPM, eGFP:SmashPM N-term, and eGFP:SmashPM mut overexpressing ovaries were examined. The straight-line tool in ImageJ was used for analysis. The mean gray value was used for calculations. The color code represents the replicate to which a data point belongs to. n = 60 (4 replicates, 15 cells per replicate). A Kruskal-Wallis test and a post hoc Dunn test were performed to identify the statistically significant difference of two samples. The significance level is indicated with asterisks. '\*\*\*\*' p < 0.0001.

**Table S 8: Statistical test to determine the significance of the differences in cell area between mCD8:eGFP, eGFP:SmashPM, eGFP:SmashPM N-term, and eGFP:SmashPM mut overexpressing ovaries.** RStudio software was used to calculate statistics. A Kruskal-Wallis ANOVA was performed to test whether there is a statistically significant difference between samples. A post hoc Dunn test for pairwise comparison was performed. The p-value was adjusted by Bonferroni correction. The significance level is indicated with asterisks. ‘\*’ p < 0.05, ‘\*\*’ p < 0.01, ‘\*\*\*’ p < 0.001, ‘\*\*\*\*’ p < 0.0001, 'ns' not significant.

| Group 1                        | Group 2                           | p-value adjusted | Significance level |
|--------------------------------|-----------------------------------|------------------|--------------------|
| mCD8:eGFP, GFP-negative        | mCD8:eGFP, GFP-positive           | 1                | ns                 |
| mCD8:eGFP, GFP-negative        | eGFP:SmashPM, GFP-negative        | 0.022882         | *                  |
| mCD8:eGFP, GFP-negative        | eGFP:SmashPM, GFP-positive        | 0.284078<br>E-14 | ****               |
| mCD8:eGFP, GFP-negative        | eGFP:SmashPM mut, GFP-negative    | 1                | ns                 |
| mCD8:eGFP, GFP-negative        | eGFP:SmashPM mut, GFP-positive    | 1                | ns                 |
| mCD8:eGFP, GFP-negative        | eGFP:SmashPM N-term, GFP-negative | 0.252454         | ns                 |
| mCD8:eGFP, GFP-negative        | eGFP:SmashPM N-term, GFP-positive | 1                | ns                 |
| mCD8:eGFP, GFP-positive        | eGFP:SmashPM, GFP-negative        | 0.260086         | ns                 |
| mCD8:eGFP, GFP-positive        | eGFP:SmashPM, GFP-positive        | 7.779187<br>E-17 | ****               |
| mCD8:eGFP, GFP-positive        | eGFP:SmashPM mut, GFP-negative    | 1                | ns                 |
| mCD8:eGFP, GFP-positive        | eGFP:SmashPM mut, GFP-positive    | 0.234809         | ns                 |
| mCD8:eGFP, GFP-positive        | eGFP:SmashPM N-term, GFP-negative | 1                | ns                 |
| mCD8:eGFP, GFP-positive        | eGFP:SmashPM N-term, GFP-positive | 0.388948         | ns                 |
| eGFP:SmashPM, GFP-negative     | eGFP:SmashPM, GFP-positive        | 2.879194<br>E-28 | ****               |
| eGFP:SmashPM, GFP-negative     | eGFP:SmashPM mut, GFP-negative    | 0.026615         | *                  |
| eGFP:SmashPM, GFP-negative     | eGFP:SmashPM mut, GFP-positive    | 4.561005<br>E-06 | ****               |
| eGFP:SmashPM, GFP-negative     | eGFP:SmashPM N-term, GFP-negative | 1                | ns                 |
| eGFP:SmashPM, GFP-negative     | eGFP:SmashPM N-term, GFP-positive | 0.000011         | ****               |
| eGFP:SmashPM, GFP-positive     | eGFP:SmashPM mut, GFP-negative    | 3.043530<br>E-14 | ****               |
| eGFP:SmashPM, GFP-positive     | eGFP:SmashPM mut, GFP-positive    | 3.281486<br>E-08 | ****               |
| eGFP:SmashPM, GFP-positive     | eGFP:SmashPM N-term, GFP-negative | 9.696492<br>E-25 | ****               |
| eGFP:SmashPM, GFP-positive     | eGFP:SmashPM N-term, GFP-positive | 1.077370<br>E-08 | ****               |
| eGFP:SmashPM mut, GFP-negative | eGFP:SmashPM mut, GFP-positive    | 1                | ns                 |

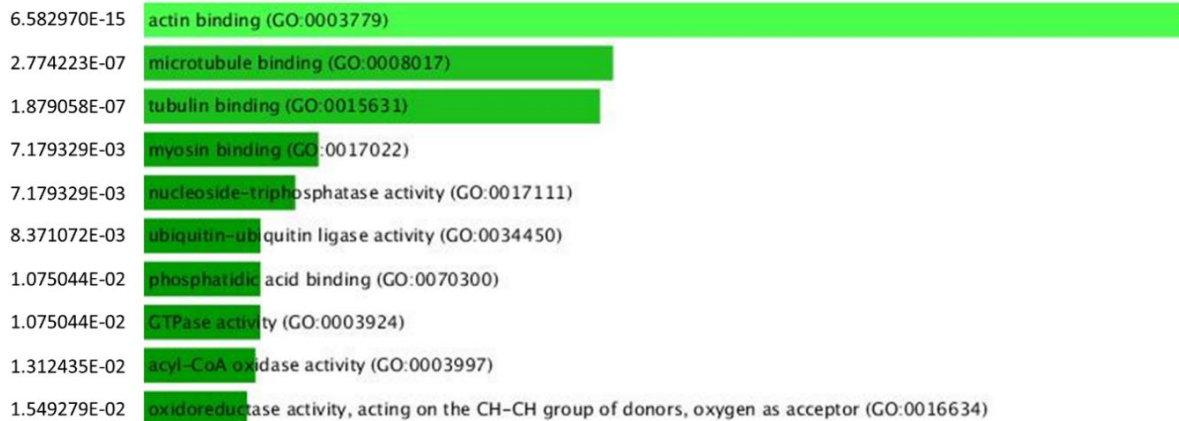
| Group 1                           | Group 2                           | p-value adjusted | Significance level |
|-----------------------------------|-----------------------------------|------------------|--------------------|
| eGFP:SmashPM mut, GFP-negative    | eGFP:SmashPM N-term, GFP-negative | 0.285316         | ns                 |
| eGFP:SmashPM mut, GFP-negative    | eGFP:SmashPM N-term, GFP-positive | 1                | ns                 |
| eGFP:SmashPM mut, GFP-positive    | eGFP:SmashPM N-term, GFP-negative | 0.000189         | ***                |
| eGFP:SmashPM mut, GFP-positive    | eGFP:SmashPM N-term, GFP-positive | 1                | ns                 |
| eGFP:SmashPM N-term, GFP-negative | eGFP:SmashPM N-term, GFP-positive | 0.000425         | ***                |

**Table S 9: List of input genes for GO term analysis.** Genes encoding proteins whose abundance was statistically significantly increased in eGFP:TurbolD:SmashPM expressing embryos compared to TurbolD:eGFP or eGFP:SmashPM expressing embryos were used as input genes for GO term analysis.

| Comparison                          | Input genes  |
|-------------------------------------|--|
| TurbolD:eGFP – eGFP:TurbolD:SmashPM | <i>zip, Actn, Dys, alpha-Spec, Lasp, tud, jub, PR2, His3, RpL37A, Cog3, pnut, RpS29, scra, Moe, CG9951, Top2, CG5009, Nup54, CG7065, dsh, hyd, shi, Adh</i>  |
| eGFP:SmashPM – eGFP:TurbolD:SmashPM | <i>Nup358, lig, Actn, Lasp, Nmt, CG11148, pAbp, Dys, Rpn11, Edc3, CG8635, Sir2, Nup50, MED6, betaCop, Argk, alpha-Spec, eIF3-S4-1, zip, eIF-4E, Trx-2, TER94, eIF3-S10, Atx2, Lsd-2, cup, bel, CG13900-RA, Nup54, Nup214, Vha55, eIF-3p66, FKBP59, CG5110, mask, Hsp70Bb, Rpt6, GlyP, CG3760, Ahcy13, Zw, sle, Cog3, Prosalph6, sqd, lap, CG6621, wupA, CG16742, Srp68, Sap47, SmB, Map205, Mtap, CIAPIN1, CG10336, RpA-70, rudhira, Prosalph1, Hrb27C, faf, Capr, RpLP1, egg, CtBP, me31B, larp, dgt6, Pp2B-14D, Ef1beta, jub, CG1458, HIP-R, gw, CG8858, sta, tud, Pen, mgr, eIF-2alpha, eIF-3p40, Clbn, dsh, Nlp, Hel25E, CG17683, Lam, pont, eIF-5A, eIF3-S5-1, Nup98-96, Vha68-2, Eno, Sod, Prosalph3, dgt5, CG1354, viaf, RnrL, Adh, scra, shi, Mtor, CG11505, Ptp61F, Moe, Hsc70-4, Nup62, Usp7, Rpn8, RanGAP, scu, RhoGAP92B, eIF-2gamma, eIF3-S6, Trxr-1, CG5009, wibg, Cyp1, enc, ras, RpS27A;Ubi-p63E, Rpn2, Aats-cys, Nurf-38, Rack1, Pkn, Jupiter, Aats-ala, PR2, CG2263, Gl, msps, eIF3-S8, Akap200, RpS19a, TppII, poe, Ef1alpha48D;Ef1alpha100E, pnut, Aats-glupro, RpLP0, RpS21, MED1, T-cp1, mit(1)15, Yp1</i> |

## GO term molecular function

### p-value ranking TurboID:eGFP – eGFP:TurboID:SmashPM



### p-value ranking eGFP:SmashPM – eGFP:TurboID:SmashPM

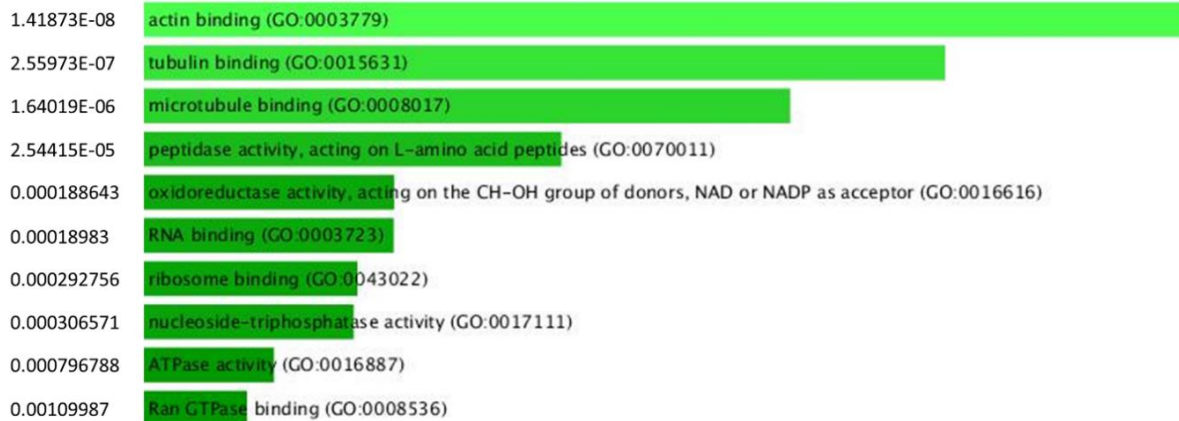


**Figure S 16: GO term analysis sorted by molecular function.** FlyEnrichr (Chen et al., 2013; Kuleshov et al., 2016) was used for GO term analysis. Input genes indicated in Table S 9 were used for analysis. Results are depicted as p-value ranking. The p-values are indicated on the left side of each bar. The length of the bar represents the significance of a specific term. The brighter the color, the more significant that term is. For more information, see Table S 10 & S 11.

**Table S 10: Go term molecular function TurboID:eGFP – eGFP:TurboID:SmashPM.** Additional information, such as how many and which of the input genes can be assigned to a GO term, are listed. The p-value and the adjusted p-value indicate the significance of a specific term. The p-value was used to generate the bar graph depicted in Figure S 16.

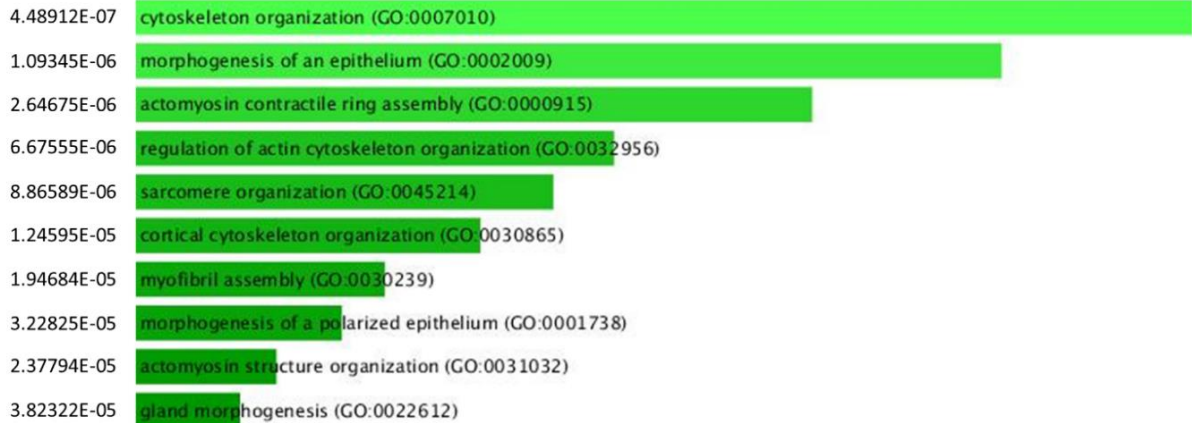
| Term  | Overlap | p-value      | p-value adjusted | Genes   |
|---|---------|--------------|------------------|---|
| actin binding (GO:0003779)  | 9/116   | 6.582970E-15 | 3.094E-13        | <i>Moe; Actn; shi; Lasp; jub; pnut; scra; alpha-Spec; Dys</i> |
| tubulin binding (GO:0015631)  | 5/120   | 2.774223E-07 | 4.34628E-06      | <i>Moe; shi; pnut; scra; alpha-Spec</i>                       |
| microtubule binding (GO:0008017)  | 5/111   | 1.879058E-07 | 4.34628E-06      | <i>Moe; shi; pnut; scra; alpha-Spec</i>                       |
| ubiquitin-ubiquitin ligase activity (GO:0034450)  | 1/6     | 7.179329E-03 | 0.042580236      | <i>hyd</i>  |
| phosphatidic acid binding (GO:0070300)  | 1/6     | 7.179329E-03 | 0.042580236      | <i>dsh</i>  |
| acyl-CoA oxidase activity (GO:0003997)  | 1/7     | 8.371072E-03 | 0.043715596      | <i>CG5009</i>   |
| oxidoreductase activity, acting on the CH-CH group of donors, oxygen as acceptor (GO:0016634) | 1/9     | 1.075044E-02 | 0.044060305      | <i>CG5009</i>   |
| four-way junction DNA binding (GO:0000400)  | 1/9     | 1.075044E-02 | 0.044060305      | <i>Top2</i>   |
| phosphatidylinositol-4,5-bisphosphate binding (GO:0005546)                                    | 1/11    | 1.312435E-02 | 0.044060305      | <i>Moe</i>  |
| myosin light chain binding (GO:0032027)   | 1/13    | 1.549279E-02 | 0.045510064      | <i>zip</i>  |

**Table S 11: Go term molecular function eGFP:SmashPM – eGFP:TurboID:SmashPM.** Additional information, such as how many and which of the input genes can be assigned to a GO term, are listed. The p-value and the adjusted p-value indicate the significance of a specific term. The p-value was used to generate the bar graph depicted in Figure S 16.

| Term   | Overlap | p-value    | p-value adjusted | Genes   |
|--|---------|------------|------------------|---|
| actin binding (GO:0003779)   | 10/116  | 1.4187E-08 | 1.87272E-06      | <i>Moe; Actn; shi; Lasp; jub; wupA; pnut; scra; alpha-Spec; Dys</i>           |
| tubulin binding (GO:0015631)   | 9/120   | 2.5597E-07 | 1.68942E-05      | <i>Jupiter; Moe; Map205; shi; pnut; mgr; scra; msps; alpha-Spec</i>           |
| microtubule binding (GO:0008017)   | 8/111   | 1.6402E-06 | 7.21682E-05      | <i>Jupiter; Moe; Map205; shi; pnut; scra; msps; alpha-Spec</i>                |
| peptidase activity, acting on L-amino acid peptides (GO:0070011)                                   | 6/79    | 2.5442E-05 | 0.00083957       | <i>TppII; Prosalpha1; Prosalpha3; Rpn2; Prosalpha6; Rpn11</i>                 |
| oxidoreductase activity, acting on the CH-OH group of donors, NAD or NADP as acceptor (GO:0016616) | 4/39    | 0.00018864 | 0.004176263      | <i>scu; Adh; ras; Zw</i>  |
| RNA binding (GO:0003723)   | 11/401  | 0.00018983 | 0.004176263      | <i>RanGAP; Nup98-96; me31B; Clbn; Hrb27C; sqd; Smb; pAbp; Capr; Edc3; cup</i> |
| ribosome binding (GO:0043022)  | 3/18    | 0.00029276 | 0.005058418      | <i>sta; RpS21; Rack1</i>  |
| nucleoside-triphosphatase activity (GO:0017111)  | 8/230   | 0.00030657 | 0.005058418      | <i>zip; CG1354; Hsc70-4; shi; Rpt6; pnut; TER94; Hsp70Bb</i>                  |
| ATPase activity (GO:0016887)   | 6/148   | 0.00079679 | 0.011686231      | <i>zip; CG1354; Hsc70-4; Rpt6; TER94; Hsp70Bb</i>                             |
| Ran GTPase binding (GO:0008536)  | 2/7     | 0.00109987 | 0.014009276      | <i>Nup358; Nup50</i>  |

## GO term biological process

### p-value ranking TurboID:eGFP – eGFP:TurboID:SmashPM



### p-value ranking eGFP:SmashPM – eGFP:TurboID:SmashPM

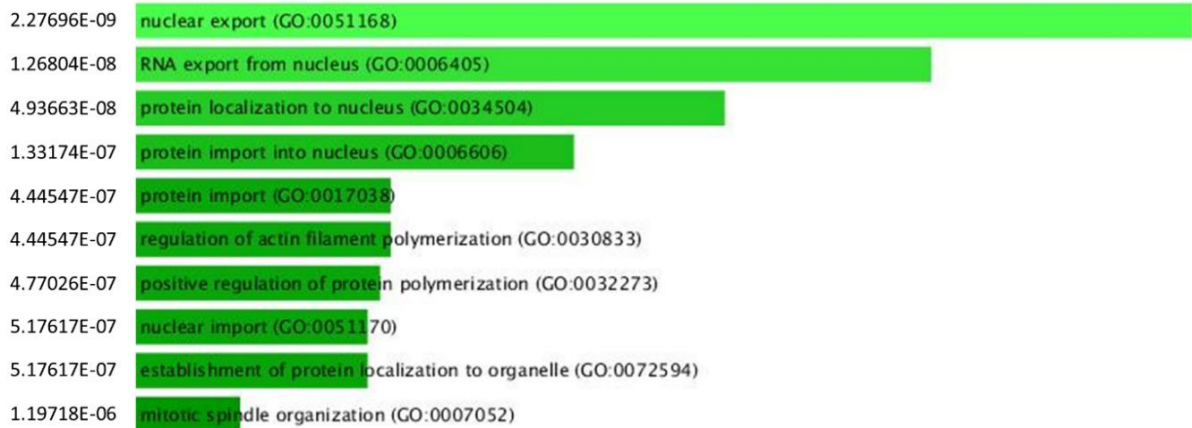


**Figure S 17: GO term analysis sorted by biological process.** FlyEnrichr (Chen et al., 2013; Kuleshov et al., 2016) was used for GO term analysis. Input genes indicated in Table S 9 were used for analysis. Results are depicted as p-value ranking. The p-values are indicated on the left side of each bar. The length of the bar represents the significance of a specific term. The brighter the color, the more significant that term is. For more information, see Table S 12 & S 13.

**Table S 12: Go term biological process TurboID:eGFP – eGFP:TurboID:SmashPM.** Additional information, such as how many and which of the input genes can be assigned to a GO term, are listed. The p-value and the adjusted p-value indicate the significance of a specific term. The p-value was used to generate the bar graph depicted in Figure S 17.

| Term   | Overlap | p-value     | p-value adjusted | Genes                       |
|--|---------|-------------|------------------|-----------------------------|
| cytoskeleton organization (GO:0007010)                     | 4/53    | 4.48912E-07 | 0.000146794      | <i>Moe; Actn; jub; scra</i> |
| morphogenesis of an epithelium (GO:0002009)                | 4/66    | 1.09345E-06 | 0.000178779      | <i>zip; Moe; shi; dsh</i>   |
| actomyosin contractile ring assembly (GO:0000915)          | 3/23    | 2.64675E-06 | 0.000288495      | <i>shi; pnut; scra</i>      |
| regulation of actin cytoskeleton organization (GO:0032956) | 3/31    | 6.67555E-06 | 0.000545726      | <i>Moe; shi; dsh</i>        |
| sarcomere organization (GO:0045214)                        | 3/34    | 8.86589E-06 | 0.000579829      | <i>zip; Actn; Lasp</i>      |
| cortical cytoskeleton organization (GO:0030865)            | 3/38    | 1.24595E-05 | 0.000679041      | <i>Moe; shi; scra</i>       |
| myofibril assembly (GO:0030239)                            | 3/44    | 1.94684E-05 | 0.000909451      | <i>zip; Actn; Lasp</i>      |
| morphogenesis of a polarized epithelium (GO:0001738)       | 3/47    | 2.37794E-05 | 0.000971984      | <i>zip; shi; dsh</i>        |
| actomyosin structure organization (GO:0031032)             | 3/52    | 3.22825E-05 | 0.001048368      | <i>zip; Actn; Lasp</i>      |
| gland morphogenesis (GO:0022612)                           | 3/55    | 3.82322E-05 | 0.001048368      | <i>zip; shi; dsh</i>        |

**Table S 13: Go term biological process eGFP:SmashPM – eGFP:TurboID:SmashPM.** Additional information, such as how many and which of the input genes can be assigned to a GO term, are listed. The p-value and the adjusted p-value indicate the significance of a specific term. The p-value was used to generate the bar graph depicted in Figure S 17.

| Term  | Overlap | p-value     | p-value adjusted | Genes   |
|---|---------|-------------|------------------|---|
| nuclear export (GO:0051168)                                     | 7/31    | 2.27696E-09 | 1.74415E-06      | <i>RanGAP; Nup98-96; Moe; Nup214; Clbn; sqd; Nup62</i>    |
| RNA export from nucleus (GO:0006405)                            | 7/39    | 1.26804E-08 | 4.85658E-06      | <i>sta; Nup98-96; Moe; Nup214; sqd; Nup62; Hel25E</i>     |
| protein localization to nucleus (GO:0034504)                    | 7/47    | 4.93663E-08 | 1.26049E-05      | <i>Nup98-96; Nup214; Nup358; Nup50; Nup62; Lam; Nup54</i> |
| protein import into nucleus (GO:0006606)                        | 7/54    | 1.33174E-07 | 2.55028E-05      | <i>Nup98-96; Nup214; Nup358; Nup50; Nup62; Pen; Nup54</i> |
| protein import (GO:0017038)                                     | 6/40    | 4.44547E-07 | 4.40549E-05      | <i>Nup98-96; Nup214; Nup358; Nup50; Nup62; Nup54</i>      |
| regulation of actin filament polymerization (GO:0030833)        | 6/40    | 4.44547E-07 | 4.40549E-05      | <i>Atx2; Nup98-96; shi; RhoGAP92B; Lam; Rack1</i>         |
| positive regulation of protein polymerization (GO:0032273)      | 5/22    | 4.77026E-07 | 4.40549E-05      | <i>Nup98-96; Jupiter; shi; Lam; Rack1</i>                 |
| nuclear import (GO:0051170)                                     | 6/41    | 5.17617E-07 | 4.40549E-05      | <i>Nup98-96; Nup214; Nup358; Nup50; Nup62; Nup54</i>      |
| establishment of protein localization to organelle (GO:0072594) | 6/41    | 5.17617E-07 | 4.40549E-05      | <i>Nup98-96; Nup214; Nup358; Nup50; Nup62; Nup54</i>      |
| mitotic spindle organization (GO:0007052)                       | 7/74    | 1.19718E-06 | 9.17039E-05      | <i>pont; mgr; msps; dgt6; dgt5; TER94; Mtor</i>           |

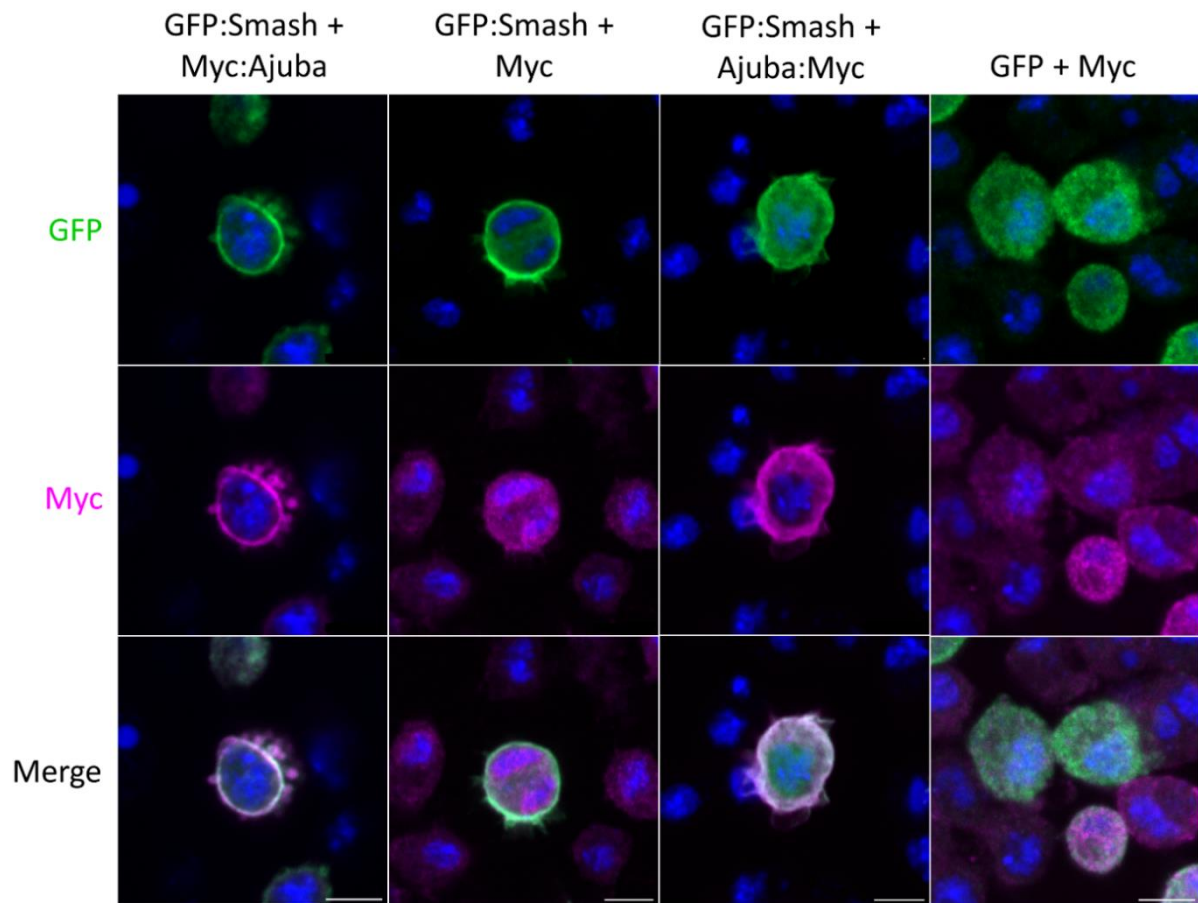


**Figure S 18: GFP:Smash and Myc:Ajuba co-localize in S2 cells.** Indicated proteins were co-expressed in S2 cells. IF staining was performed using indicated antibodies. Scale bar: 5  $\mu$ m.

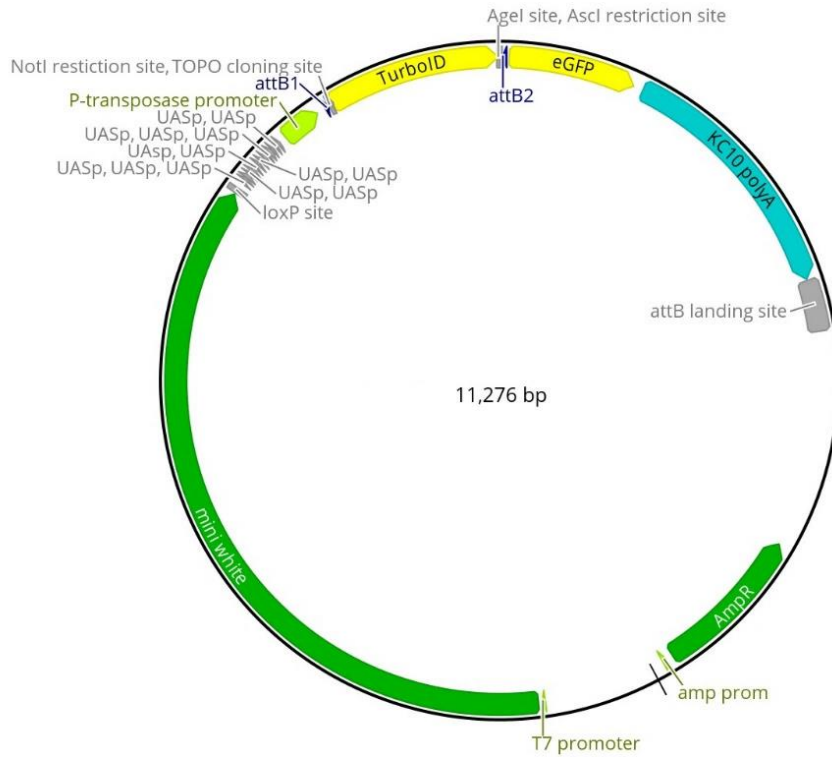


**Figure S 19: Plasmid map of pUASP-attB-eGFP-rfA\_TurboID.** Sequences are annotated. The size of the vector is indicated in base pairs (bp). The map was generated in Geneious Prime.

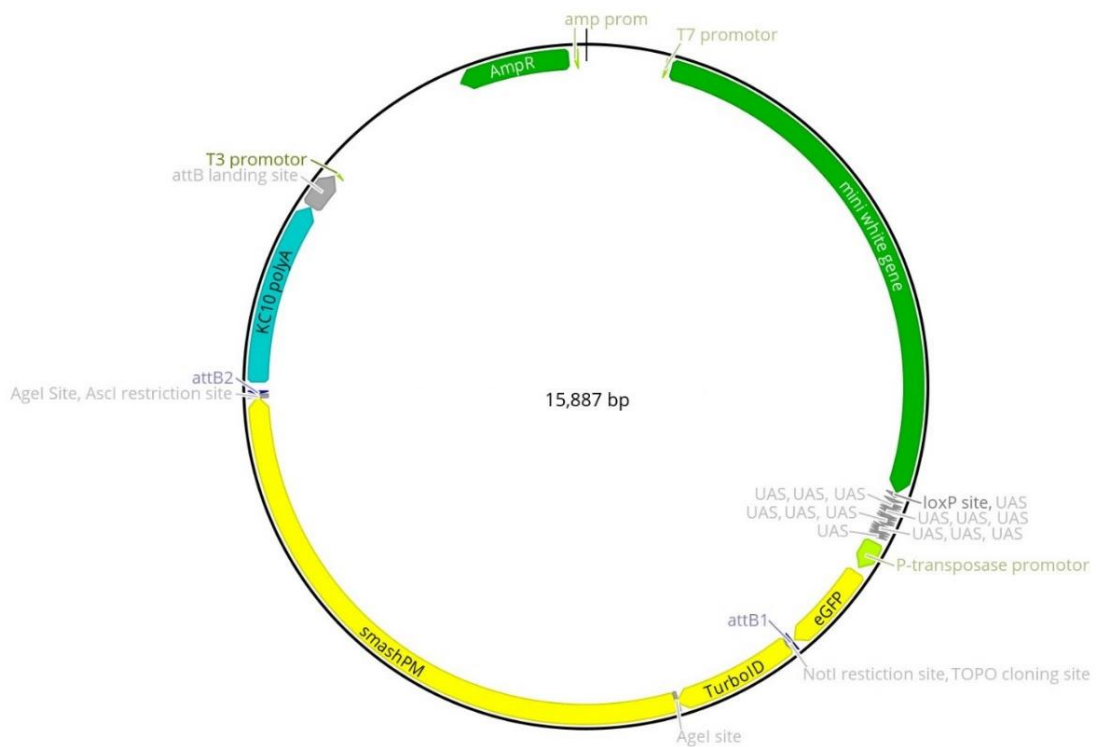


**Figure S 20: Plasmid map of pUASP-attB-eGFP-rfA\_TurboID:SmashPM.** The size of the vector is indicated in base pairs (bp). The map was generated in Geneious Prime.



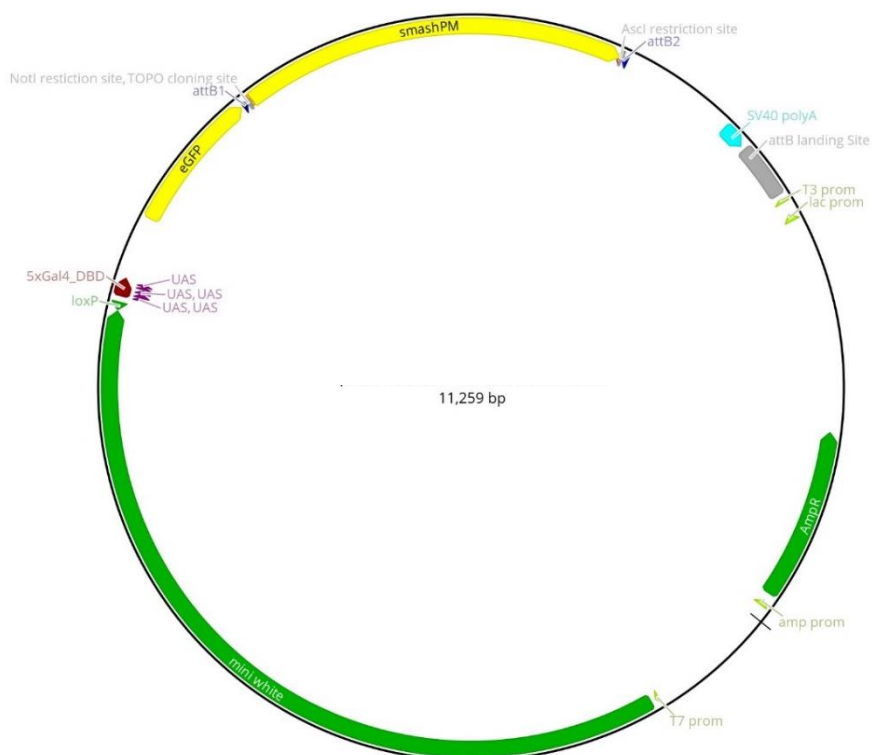


**Figure S 23: Plasmid map of pUAST-attB-eGFP-rfA\_SmashPM N-term.** Sequences are annotated. The size of the vector is indicated in base pairs (bp). The map was generated in Geneious Prime.

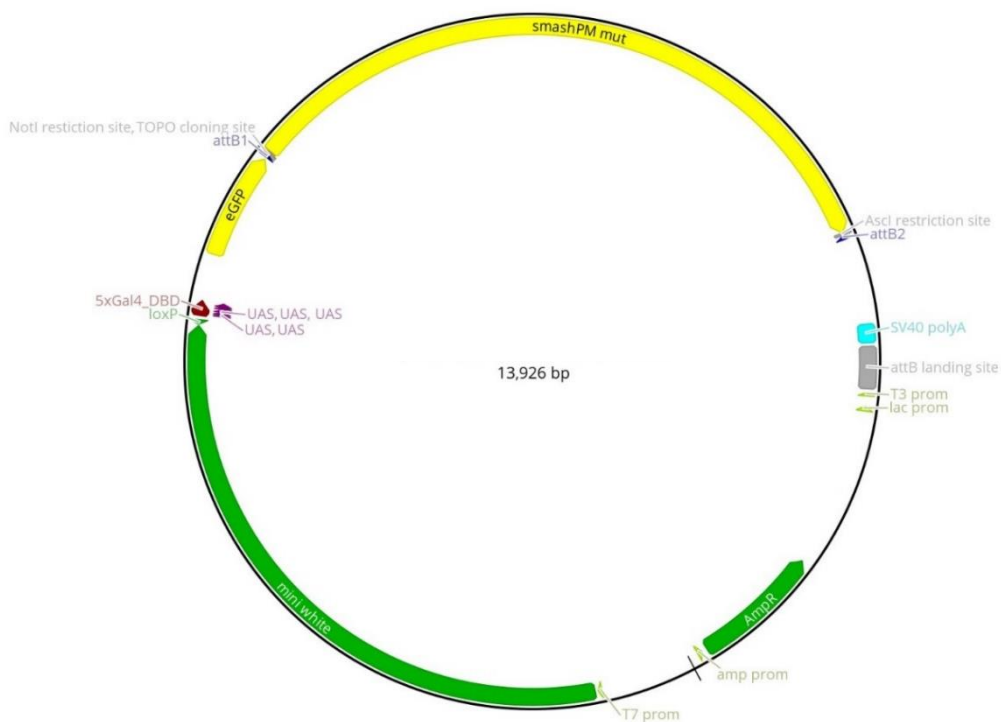


**Figure S 24: Plasmid map of pUAST-attB-eGFP-rfA\_SmashPM mut.** Sequences are annotated. The size of the vector is indicated in base pairs (bp). The map was generated in Geneious Prime.

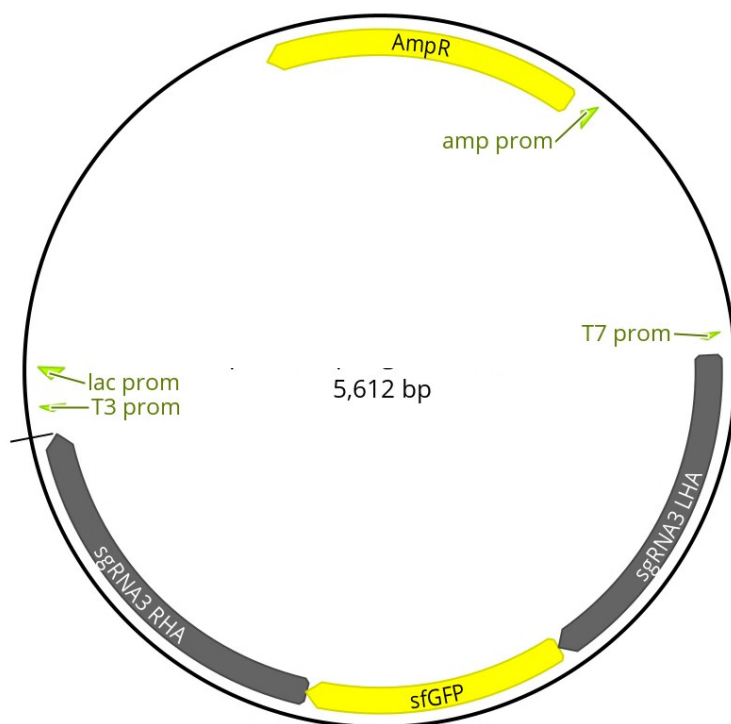


**Figure S 25: Plasmid map of pBluescript\_sgRNA3\_sfGFP.** Sequences are annotated. The size of the vector is indicated in base pairs (bp). The map was generated in Geneious Prime.

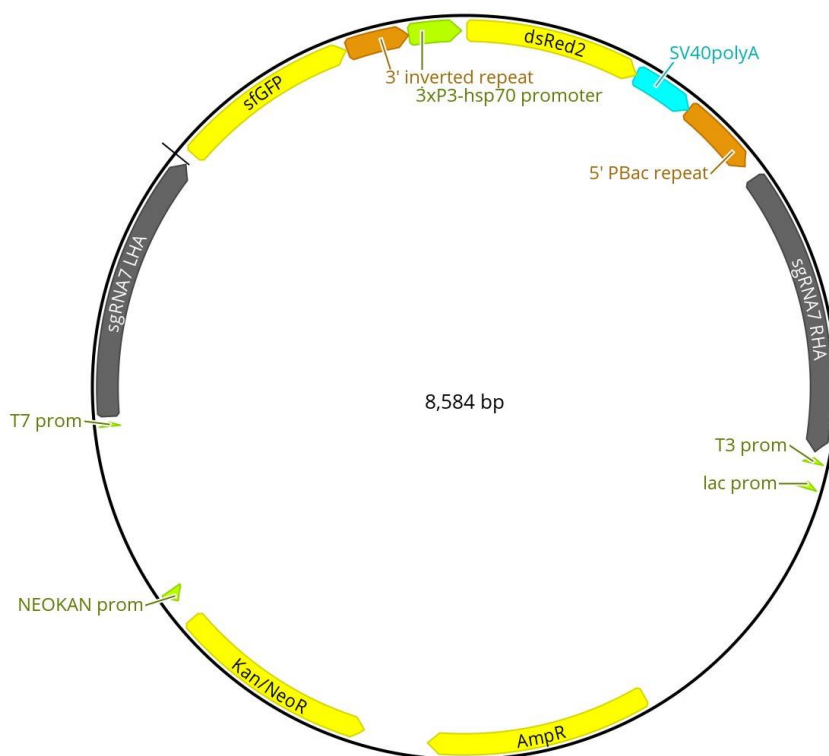


**Figure S 26: Plasmid map of pScareless-sfGFP-dsRed\_HA\_sgRNA7.** Sequences are annotated. The size of the vector is indicated in base pairs (bp). The map was generated in Geneious Prime.

## Acknowledgements

First, I would like to thank Prof. Dr. Andreas Wodarz for giving me the opportunity to become part of his working group. Thank you for your advice and support, for fruitful discussions and for giving me the chance to realize my own ideas in this project.

I would also like to thank Prof. Dr. Siegfried Roth and Dr. Astrid Schauss for being a part of my thesis advisory committee. Thank you for the inspiring exchange and your helpful comments.

Thanks to Prof. Dr. Steffen Lemke for inviting me to his lab in Heidelberg to show me the tricks to perform good live imaging. Thanks to Dr. Girish Kale for his enthusiastic on-site support.

My thanks go to the CECAD Imaging Facility for providing me with a microscope during the time when our own microscope was broken. Special thanks go to Dr. Christian Jüngst for his great on-site support.

I would also like to acknowledge the CECAD Proteomics Facility for processing and analyzing my samples. Thank you to Dr. Stefan Müller and Dr. Prerana Wagle for your technical support.

Thanks to Stella Eun Cho (Jianjun Sun Lab, University of Connecticut) for sharing her unpublished work with me.

I am grateful for the time I had in the lab and would like to thank all those who made this possible.

Special thanks to our technician Lisa, who accompanied me in my project from beginning on. Thank you for your professional suggestions and your active support in all fly matters. Thanks to our former technician Monique for her support in cloning and cell culture. My thanks also to Tim and Petra who took over these tasks from Monique. Thank you to Christian for his IT support. Thank you to Ferdi for helping in all kinds of matters. A big thank you goes to Jolanta for her support in tissue dissection and IF staining. Thank you for wonderfully crazy, but also serious conversations in every way.

Thanks to Klaus, Julia C., Markus, and Olaf for all your professional suggestions and for being great colleagues. Special thanks to Markus and Olaf for proof-reading my thesis.

Big thanks to my PhD colleagues Julia G., Jiyu, Hong, and Nikolaj for being such great fellow sufferers. Thanks for all the professional and private exchanges and fun times we had together.

My thanks also go to all students who have contributed to my work.

Thank you to my dearest friend Vanessa for being by my side since the first day of our studies. Together we go through thick and thin!

Thanks to my family, who has accompanied and supported me throughout my life.

Finally, I would like to thank my boyfriend, Sebastian. Thank you for your tireless encouragement, your support, your understanding, and your constant willingness to discuss.

## Erklärung zur Dissertation

gemäß der Promotionsordnung vom 12. März 2020

Hiermit versichere ich an Eides statt, dass ich die vorliegende Dissertation selbstständig und ohne die Benutzung anderer als der angegebenen Hilfsmittel und Literatur angefertigt habe. Alle Stellen, die wörtlich oder sinngemäß aus veröffentlichten und nicht veröffentlichten Werken dem Wortlaut oder dem Sinn nach entnommen wurden, sind als solche kenntlich gemacht. Ich versichere an Eides statt, dass diese Dissertation noch keiner anderen Fakultät oder Universität zur Prüfung vorgelegen hat; dass sie - abgesehen von unten angegebenen Teilpublikationen und eingebundenen Artikeln und Manuskripten - noch nicht veröffentlicht worden ist sowie, dass ich eine Veröffentlichung der Dissertation vor Abschluss der Promotion nicht ohne Genehmigung des Promotionsausschusses vornehmen werde. Die Bestimmungen dieser Ordnung sind mir bekannt. Darüber hinaus erkläre ich hiermit, dass ich die Ordnung zur Sicherung guter wissenschaftlicher Praxis und zum Umgang mit wissenschaftlichem Fehlverhalten der Universität zu Köln gelesen und sie bei der Durchführung der Dissertation zugrundeliegenden Arbeiten und der schriftlich verfassten Dissertation beachtet habe und verpflichte mich hiermit, die dort genannten Vorgaben bei allen wissenschaftlichen Tätigkeiten zu beachten und umzusetzen. Ich versichere, dass die eingereichte elektronische Fassung der eingereichten Druckfassung vollständig entspricht.

Teilpublikationen: keine

20.10.2023, Patrizia Kroll